

Geochemical, Sedimentological and Mineralogical
Study of Sediments along Coastal Areas of Abu Dhabi,
United Arab Emirates (UAE): Implications for
Provenance, Depositional Environment, Heavy Minerals
and Radiogenic Elements Contamination

by

Saeed Rashed AlRashdi



A thesis submitted in fulfilment of the requirement for the degree of

UNIVERSITY of the

Doctor of Philosophy in Natural Sciences

Department of Earth Sciences, Faculty of Natural Sciences, University of the Western Cape

Supervisor: Dr. Abdi Mohamoud Siad

Co-Supervisor: Dr. Fares Howari

**University of the Western Cape, Department of Earth Sciences, P/Bag X17,
Robert Sobukwe Road, Bellville, 7535, South Africa**

June 2017

Geochemical, Sedimentological and Mineralogical Study of Sediments along Coastal Areas of Abu Dhabi, United Arab Emirates (UAE): Implications for Provenance, Depositional Environment, Heavy Minerals and Radiogenic Elements Contamination

Keywords

Abu Dhabi

United Arab Emirates

uranium

thorium

soils

industrial

geochemical

inductively coupled plasma mass spectroscopy

(ICP-MS)

X-ray diffraction(XRD)spectrometry

X-ray fluorescence (XRF) spectrometry



Abstract

Geochemical, Sedimentological and Mineralogical Study of Sediments Along Coastal Areas of Abu Dhabi, United Arab Emirates (UAE): Implications for Provenance, Depositional Environment, Heavy Minerals and Radiogenic Elements Contamination

Saeed Rashed AlRashdi

PhD Thesis, Department of Earth Sciences, University of the Western Cape

This study describes sedimentological, geochemical and mineralogical results of the beach sediments of Abu Dhabi in the United Arab Emirates in order to understand the provenance, depositional environment and the level of contamination. Fifty-seven beach sand samples were collected for grain size, geochemical and mineralogical analyses using inductively coupled plasma mass spectroscopy (ICP-MS), X-ray fluorescence (XRF) and using X-ray diffraction (XRD).

The grain size analysis revealed that samples of the study area range from 2.63 (pebble size) to 2.39 mm (fine sands). The statistical analysis revealed that the sand was characteristically fine-grained, and moderately well sorted to extremely poorly sorted. The sand distribution is strongly coarse and leptokurtic in nature. An abundance of the medium to fine sand shows the prevalence of a comparatively moderate- to low-energy condition in the study area. A linear discriminant analysis of the samples indicates an Aeolian, shallow marine deposition environment and less influence of a fluvial process (7%).

Scatter plots and multivariate statistical techniques, including factor, cluster and discriminant analyses, were used to classify, characterize and infer the provenance of the beach sediment of the coastal area of Abu Dhabi. A cluster analysis produced a dendrogram with two major beach sand types, namely terrigenous and marine-derived carbonate sand. Each sand type was further subdivided into two and was characterized through discriminant analysis. The terrigenous sand type was subdivided into aluminosilicate, characterized by SiO₂, Al₂O₃, K₂O and TiO₂, and heavy mineral-rich aluminosilicate, with a high content of Fe₂O₃, Cr₂O₃, MgO and MnO. The marine sand

type was subdivided into biogenic marine carbonate with a high content of CaO and LOI, and halite-rich, biogenic carbonate marine sand with Na₂O, in addition to CaO and LOI. Scatter-plots of the CaO against major compounds, like SiO₂ and Al₂O₃, Fe₂O₃ and MgO, produced similar results. A factor analysis produced five factors dominated by similar groups, i.e. marine-derived carbonate sand and terrigenous beach sand. U, Sr and as are highly correlated with CaO and LOI, suggesting possible marine sources, while the remaining heavy metals, including Th, have terrigenous origin.

The geoaccumulation index (I_{geo}), enrichment factor (EF) and Dutch guidelines showed no pollution with radiogenic elements and heavy metals in the coastal areas of Abu Dhabi. Mineralogically, the sediment is dominated by carbonate minerals and quartz.

June 2017



Abbreviations and Acronyms

AD	Abu Dhabi
Al ₂ O ₃	Aluminium Oxides
As	Arsenic
Ba	Barium
0°C	Degree Celsius
CA	Cluster Analysis
CaO	Calcium Oxides
Cd	Cadmium
Cm	Centimetres
Co	Cobalt
Cr ₂ O ₃	Chromium Oxides
Cu	Copper
DEM	Digital Elevation Model
FA	Factor Analysis
Fe ₂ O ₃	Iron Oxides
HCl	Hydrochloric acid
Hg	Mercury

HNO ₃	Nitric acid
IDW	Inverse Distance Weighted
ICP-MS	Inductively Coupled Plasma – Mass Spectroscopy
Igeo	Index of Geo-accumulation
Km	Kilometres
K ₂ O	Potassium Oxides
LOI	Loss on Ignition
m	Meter
MnO	Manganese Oxides
Mo	Molybdenum
Na ₂ O	Sodium Oxides
Ni	Nickel
Pb	Lead
P ₂ O ₄	Phosphorus Oxides
R	Correlation coefficient
UAE	United Arab Emirates
U	Uranium
Sb	Antimony



UNIVERSITY of the
WESTERN CAPE

SiO ₂	Silicon Oxides
SKI	Skewness
TiO ₂	Titanium Oxides
Th	Thorium
Wt.	Weight
XRD	X-Ray Diffraction spectrometry
XRF	X-Ray Fluorescence spectrometry
Zn	Zinc



UNIVERSITY *of the*
WESTERN CAPE

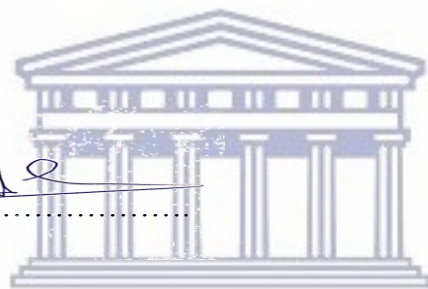
Declaration

I declare that *Geochemical, Sedimentological, and Mineralogical Study of Sediments along Coastal Areas of Abu Dhabi, United Arab Emirates (UAE): Implications for Provenance, Depositional Environment, Heavy Minerals and Radiogenic Elements Contamination* is my own work that has not been submitted before for any scientific degree or examination in any other university or institute, and that all the sources I have used or quoted have been indicated and acknowledged as complete references.

Saeed AlRashdi

June 2017

Signed:



UNIVERSITY of the
WESTERN CAPE

Acknowledgements

I would like to acknowledge the Academic Education Ministry in UAE for considering this thesis, and the Abu Dhabi Environment Agency, the Geology Department at the College of Science, UAE University, and the UAE Embassy in South Africa for supporting this work. Furthermore, I would like to express my gratitude to the many people who encouraged and supported me academically, as well as to my family and friends. Special thanks and appreciation go to my supervisor, Dr. Abdi M. Siad. I would also like to thank my co-supervisor, Dr. F. Howari, for his support throughout my studies, and, above all, Allah the Almighty, without Whom the present study would not have seen the light or been possible.

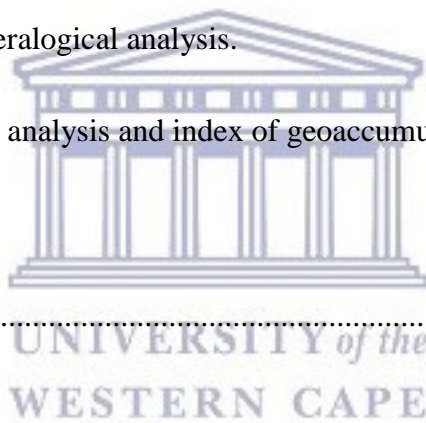


Table of Contents

Keywords	2
Abstract	3
Abbreviations and Acronyms	5
Declaration	8
Acknowledgements	9
Table of Contents	10
Chapter I.....	18
1.0 Introduction	18
1.1 General outline	18
1.2 General setting of the study area	19
1.3 Background of the coastline complex	20
1.4 Regional geological and geomorphologic setting	26
1.5 Climatology and oceanography	31
1.6 The sedimentary facies	35
1.7 Mangrove swamp	36
1.8 Indurated cemented crusts (Hardgrounds)	38
1.9 Distribution of cyanobacterial mats south of Abu Dhabi	40
1.10 Uranium, thorium and heavy metals	41



1.11	Purpose and scope	45
Chapter II.....		48
2.0	Methodology	48
2.1	Location of the soil sampling	48
2.2	Collecting samples	50
2.3	Sample data preparation techniques and analysis	50
2.4	Sedimentology	56
2.5	Mineralogical analysis	58
2.6	Geochemistry and mineralogical analysis.	58
2.7	Enrichment factor (EF) analysis and index of geoaccumulation (Igeo)	65
2.8	Spatial analysis	68
Chapter III.....		71
3.0	Results	71
3.1	Sedimentology and depositional environment	71
3.2	Geochemistry	81
3.3	Mineralogy	127
Chapter IV.....		129
4.0	Discussion	129
4.1	Grain-size distribution	129
4.2	Bivariant scatter graphs of grain size parameters	130



4.3	Determination of the mechanisms and environments of deposition	130
4.4	Pollutant indicators	131
4.5	Mineralogical and analysis of the beach sand	138
Chapter V		139
5.0	Conclusion and Recommendation	139
5.1	Summary and conclusion	139
5.2	Recommendation	140
References		141
Appendices		159



List of Figures

Figure 1.1 A map of the study area's location.	20
Figure 1.2 Structure map of the study area showing oil and gas fields and Zeugen landform (Simplified from EAD, 2012).	21
Figure 1.3 Geological map of the study area (Simplified from EAD, 2012).	22
Figure 1.4 General sedimentary facies along the waterfront regions of Abu Dhabi, demonstrating the territories specified in the content (Modified from Kendall and Skipwith, 1969a, b).	24
Figure 1.5 Sedimentary facies of Ras Ghanada, eastern Abu Dhabi Island (Modified from Baltzer et al., 1994).	25
Figure 1.6 Schematic interrelationships between chief stratigraphic developments, UAE (After Steve and Richard, 2006)	27
Figure 1.7 Temperatures, sea levels and terrace heights in the Arabian Gulf area during the Pleistocene–Holocene (compiled from Fairbridge, 1961; Kessler, 1973; Al Asfour)	29
Figure 1.8 Facies variations associated with carbonate tidal flat accumulation (Shinn, 1983)	30
Figure 1.9 Sedimentary facies dissemination of Khor al Bazam, western Abu Dhabi.(Modified from Alsharhan and Kendall, 2003).	36
Figure 1.10 Sedimentary facies conveyance around Abu Dhabi Island and adjoining islands (Modified from Kenig et al., 1991).	37
Figure 1.11 Sedimentary facies delineating the Al Dhabaiya Peninsula, western Abu Dhabi (Modified from Alsharhan and Kendall, 2003).	38
Figure 1.12 Sedimentary facies delineating the southern shore of the SW Khor al Bazam south of Al Qanatir Island, western Abu Dhabi.	39

Figure 1.13 Distribution of evaporites and algal mats in southwest Abu Dhabi Island and along the southern shore of the SW Khor Al Bazam (Modified from Kendall and Skipwith, 1968).....	40
Figure 1.14. Zonation of algal morphology along the Abu Dhabi waterfront range (Modified from Kendall and Skipwith, 1968).	41
Figure 2.1 Location map of sampling sites at the study area.	49
Figure 2.2 Precision control scatterplot for V at 10% precision	54
Figure 2.3 Precision control scatterplot for Rb at 10% precision	55
Figure 2.4 Precision control scatterplot for Zr at 10% precision	55
Figure 2.5 Precision control scatterplot for U at 10% precision	56
Figure 3.1 Trilinear plot sieve analysis after Folk (1974).....	71
Figure 3.2 Shows the mean size of the collected samples from the study area.	72
Figure 3.3 Classification of average cumulative curves according to sorting values	75
Figure 3.4 Sector Plot showing the bivariant relationship between Grain size (ϕ) and Sorting.	77
Figure 3.5 Sector Plot showing the bivariant relationship between Skewness and Sorting....	77
Figure 3.6 Sector Plot showing the bivariant relationship between Skewness and Kurtosis.	78
Figure 3.7 Relationship between the discriminant functions Y1 and Y2 showing estimated environments.	80
Figure 3.8. Relationship between the discriminant functions Y2 and Y3 showing estimated environments.	81
Figure 3.9 Aluminum oxides (Al_2O_3) class distribution in the study area.	83

Figure 3.10 Calcium oxide (CaO) class distribution in the study area.	87
Figure 3.11 Iron oxides (Fe ₂ O ₃) class distribution in the study area.....	88
Figure 3.12 Silicon oxides (SiO ₄) class distribution in the study area.....	90
Figure 3.13 Loss On Ignition (LOI) class distribution in the study area.	92
Figure 3.14 Map of Abu Dhabi showing the Arsenic (As) concentration of the areas from which the samples were collected, as indicated with dots, along with their numbers. ...	95
Figure 3.15 Map of Abu Dhabi showing the Cadmium's (Cd) concentration of the areas from which the samples were collected, as indicated with dots, along with their numbers.	96
Figure 3.16 Map of Abu Dhabi showing the Cobalt (Co) concentration of the areas from which the samples were collected, as indicated with dots, along with their numbers. ...	98
Figure 3.17 Map of Abu Dhabi showing the Copper (Cu) concentration of the areas from which the samples were collected, as indicated with dots, along with their numbers. .	100
Figure 3.18 Map of Abu Dhabi showing the lead (Pb) concentration of the areas from which the samples were collected, as indicated with dots, along with their numbers. .	102
Figure 3.19 A comparison of the maximum level of each metal (in ppm) with the limit set by the Dutch uidelines for each metal.	103
Figure 3.20 Map of Abu Dhabi showing the resulting EF values of Ca/Al of the areas from which the samples were collected.	104
Figure 3.21 Map of Abu Dhabi showing the resulting EF values of Fe/Al of the areas from which the samples were collected.	105
Figure 3.22 Map of Abu Dhabi showing the resulting EF values of K/Al of the areas from which the samples were collected.	105

Figure 3.23 Map of Abu Dhabi showing the resulting EF values of Mg/Al of the areas from which the samples were collected.	106
Figure 3.24 Map of Abu Dhabi showing the resulting EF values of Na/Al of the areas from which the samples were collected.	106
Figure 3.25 Map of Abu Dhabi showing the resulting EF values of Ti/Al of the areas from which the samples were collected.	107
Figure 3.26 GIS map of Geo-accumulation index (Igeo) values of Strontium in study area	110
Figure 3.27 GIS map of Geo-accumulation index (Igeo) values of Lead in study area.....	110
Figure 3.28 GIS map of Geo-accumulation index (Igeo) values of Chromium in study area.	111
Figure 3.29 GIS map of Geo-accumulation index (Igeo) values of Arsenic in study area. ...	112
Figure 3.30a Contents of major elements against Al ₂ O ₃ contents for all samples.....	114
Figure 3.30b Minor and trace elements – Al ₂ O ₃ variation in beach sand samples from Abu Dhabi, United Arab Emirates.....	115
Figure 3.31 The relationship between the CaO for biogenic carbonate, SiO ₂ for quartz sand and Al ₂ O ₃ for silt/clay in the beach sediments of Abu Dhabi samples.	116
Figure 3.32 Dendrogram showing cluster result for the beach sand of Abu Dhabi, United Arab Emirates.....	118
Figure 3.33 Two-function discriminant plot showing the abundance of elements in each beach sand type.	121
Figure 3.34 Scatter plot of SiO ₂ and Fe ₂ O ₃	122

List of Tables

Table 1. 1 Heavy metal fixations in surface residue from various regions in the UAE.....	45
Table 2.1 Geochemical composition of beach sand collected from Abu Dhabi (UAE)	67
Table 2.2 Enrichment factor categories, after Birch (2003).....	67
Table 2.3 Index of geo-accumulation class with associated sand/sediment quality	68
Table 3.1 Size percentage values of the samples from the study area.	74
Table 3.2 Summary of the environment, using the discriminate functions of the collected samples	80
Table 3.3 XRF analysis of the major elements, expressed as weight percent oxide.....	84
Table 3.4 Sampling name and the trace elements concentration, which has been done by inductively coupled plasma (ICP) analyses.	85
Table 3.5 Descriptive statistics of the geochemical data for beach sand.	86
Table 3.6 Concentration elements ppm of Abu Dhabi beach standard their crustal abundance	94
Table 3.7 EF values and geoaccumulation index (I_{geo}) from Abu Dhabi beach sand samples and minor.....	108
Table 3.8 The calculated results of I_{geo} values according to Muller scale (Muller, 1981)	109
Table 3.9a Three-discriminant group function.....	119
Table 3.9b Function at group centroid	120
Table 3.10. Factor analysis results: Total variance	125
Table 3.11 Factor analysis result: Rotated Component Matrix.....	125
Table 3.12 The mineralogical composition of the 12 beach sand samples from Abu Dhabi.....	125

Chapter I

1.0 Introduction

1.1 General outline

Soil is a natural growing medium for plants, as it is rich in humus and organic matter. Different factors affect the type of soil, including weather, climate, fertilisers, humus parent material, agriculture, human activities, biological and bacterial activity and pH. Biological activity has a minor effect on soil in arid areas, or on soil with low organic matter, as is the case in the UAE.

Coastal soils offer important information on chemical and mineralogical accumulation; moreover, these soils shed light on the geology of the origin rocks (Reinson, 1992; Barnhardt et al., 1997). In addition, coastal soils provide information on the energetic conditions of transport and the deposition of suspended and dissolved loads (Sahu, 1964; Pickrill, 1986; Kelley, 1987; Carter et al., 1990). This thesis explains the particle sources of coastal soil and how it has been related to adjacent coastal rocks and precipitation. Other coastal soil could be of biogenic or cosmic sources (Storlazzi, C.D. and Field, M.E., 2000). The interaction of both marine and terrestrial processes gives coastal soils their textural and compositional characteristics. The period over which these marine and terrestrial processes take place, along with their magnitude, influences, to some extent, the dominant characteristics of coastal soil deposits (Pickrill, 1986).

Research and studies on the origins and genesis of the mineral phase in coastal systems, especially carbonates, have focused on examples from different parts of the world, such as, the Bahamas and the Caribbean Sea (Boardman, 1978; Crevello and Schlager, 1980). The formation of sabkhas in Abu Dhabi has been explained by Alsharhan and Kendall (2003), who described the carbonate and evaporates of Abu Dhabi. El-Sammak (2001) investigated the oil characteristics and metallic concentrations, as well. Few studies applied multiple analytical techniques for the sake of the investigation of UAE coastal soil.

1.2 General setting of the study area

The coastline along the Arabian Gulf is characterized by a mixed clastic-carbonate-evaporate sediment. The coastal sediments may contain soil horizons and regular carbonate-clastic-evaporate sediments are infertile, sandy and composed of minerals, such as quartz and carbonates. The size of the particles in the sandy-soil reduces the water-holding capacity of the soil, which, together with weather factors, such as wind, may exacerbate erosion. The soil contains high concentrations of sodium chloride and tends to be poorly drained along the coast.

A survey was carried out by the Environment Agency of Abu Dhabi in the study area, to identify and map the soil of the region, as well as to determine the suitability of the soil for different uses and to assist with land management planning. The regolith consists of extensive dune systems and sand sheets. Surface runoff is also common, along with low water holding, low fertility and high infiltration. The degradation of the soil leads to reduced production capacity in terms of agriculture and other services, which affects food security and environmental quality.

1.2.1 Location of the study area

The UAE lies between $22^{\circ} 50'$ and $26^{\circ} 00'$ North and between $51^{\circ} 00'$ and $56^{\circ} 25'$ East. The coast of the United Arab Emirates stretches along the southern boundary of the Arabian Gulf. The coast is around 900 km long, 350 km wide, has a minimum depth of 35 m and a maximum depth of 100 m of the Strait of Hormuz (Purser and Seibold, 1973). The UAE is in southwest Asia, bordering the Gulf of Oman and the Arabian Gulf, between Oman and Saudi Arabia; it is a dynamic transit point for the world's crude oil, strategically located close to the Strait of Hormuz.

The study area is in the Abu Dhabi Emirate (Fig.1.1), which includes Abu Dhabi City, the capital of the UAE. Abu Dhabi lies N $24^{\circ} 28' 0.2202''$, E $54^{\circ} 21' 59.976''$. Abu Dhabi accounts for 87% (67,340 km²) of the UAE's total area, with an estimated population (nationals and non-nationals) of 2.33 million (in mid-2012) per Statistics Centre Abu Dhabi (SCAD). In 2013, the UAE's GDP was 1.087 trillion AED, per the

National Bureau of Statistics (NBS), while Abu Dhabi's GDP was 953.2 billion, per SCAD (i.e. 88% of UAE's GDP).

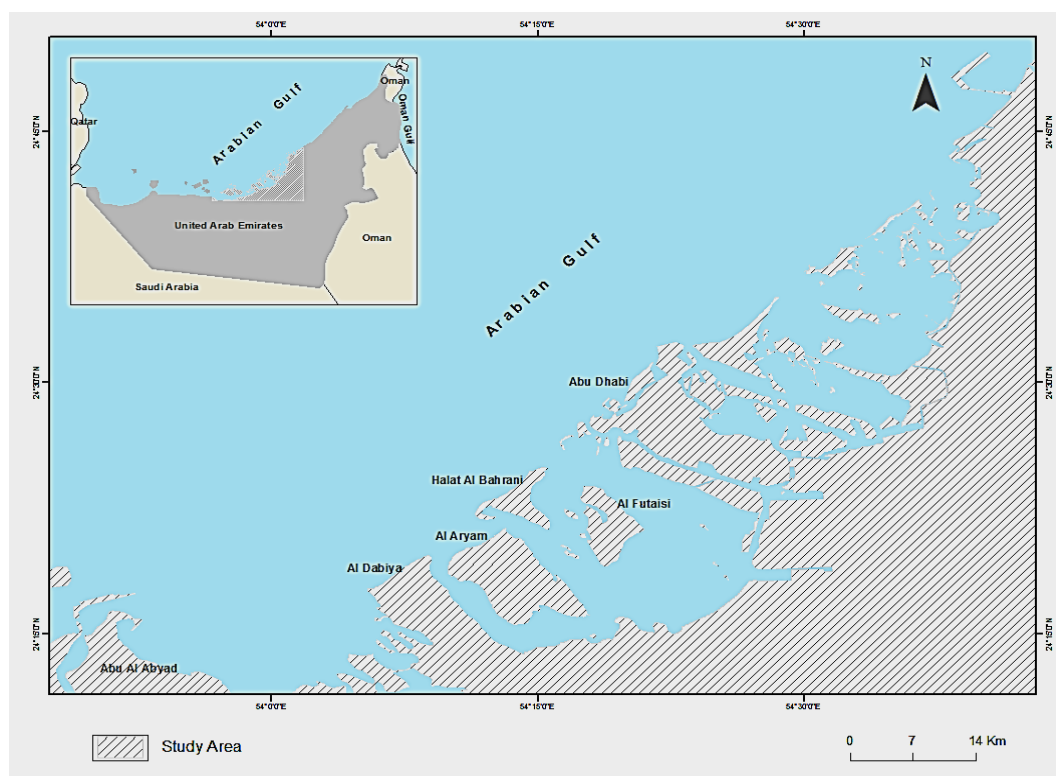


Figure 1.1. A map of the study area's location.

Anticlines and synclines are often associated with oil fields. Anticlines (arch-shaped rock formations) form natural hydrocarbon traps, commonly associated with oil and gas fields. Synclines (trough-shaped rock layers) usually occur with underground water supplies. Umm Ad Dalkh and Zubbaya are the offshore oil fields, while Jarn Yafour, Rumaitha and Shanayel are the onshore oilfields (Fig. 1.2).

1.3 Background of the coastline complex

Holocene sediments along the coast of the United Arab Emirates accumulated on Neogene sedimentary rocks (Fig.1.3). The substrate of the Miocene period consists of a sequence of marls, sandstone and limestone, and evaporation occurred towards the south, dipping gently (Alsharhan and Kendall, 2003). The rocks along the coast crop out as a low northeast-southwest escarpment, with a height of more than 35m, paralleling the United Arab Emirates. The orientation of the valleys and the ridges of the escarpments comparable to that of the local lagoons and islands, signifying a

combination of a structural mechanism and the prevalent north-west wind. Distinguishing between the impact of the wind and structural controls is problematic. Neogene rocks are composed of Quaternary Carbonate called miliolite limestone (Kinsman, 1964; Kirkham, 1997).

During the last major glacial eustatic change, sediments were deposited in the Arabian Gulf. These sediments, now cemented and endurated, were largely Aeolian origin. They currently line the internal margins of the present-day sabkhas, or salt flats, and occasionally their festoon cross-beds are well-exposed as wind-deflated surfaces (Kirkham, 1998). The rock sediments permeate much of the Holocene carbonate evaporate complex and form the headlands and core barrier island.

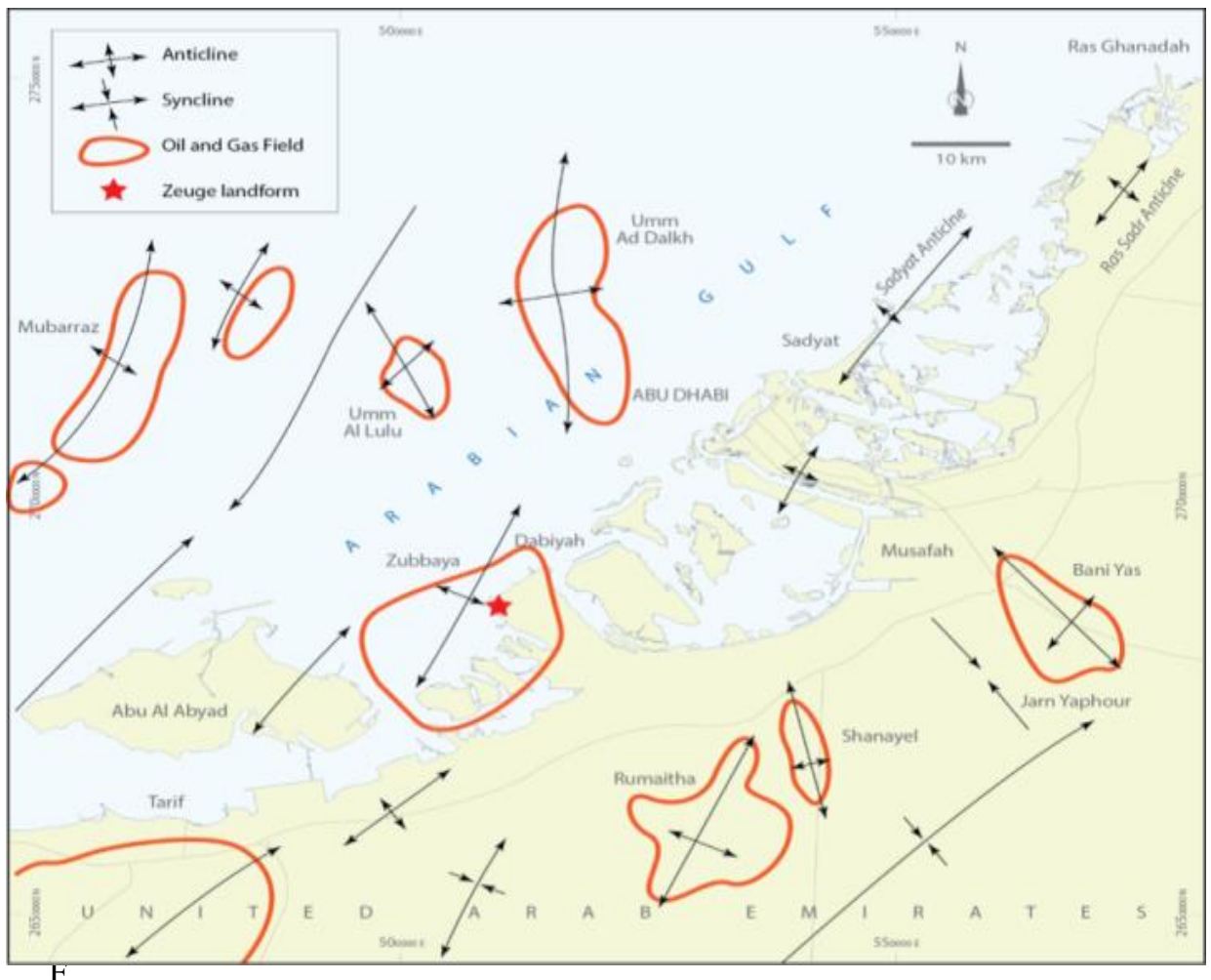


Figure 1.2. Structure map of the study area showing oil and gas fields and Zeuge landform (Simplified from EAD, 2012).

The shape of the coast between Abu Dhabi and Ras Al-Khaimah is a curve linear, and is slanted by shamal winds, which are associated with surface currents and waves. The coast is largely composed of skeletal carbonate sands, due to the tempestuous beaches, which are fringed by the dunes of the coast. A series of sub-parallel spots near Umm Al Quwain, Ras Al Khaimah and Sharjah enable the coastline to prograde seaward for 5 km to 10 km within the last 3000 years (Alsharhan and Kendall, 2003). Channels terminate seaward and split into small tidal deltas, shaped by pelleted carbonate sands. The absence of an offshore barrier means that the deep waters impinge directly onto the shore, creating a ramp-type carbonate shelf a region of maximum water agitation; this region is an effective location for longshore transport (Purser and Seibold, 1973).

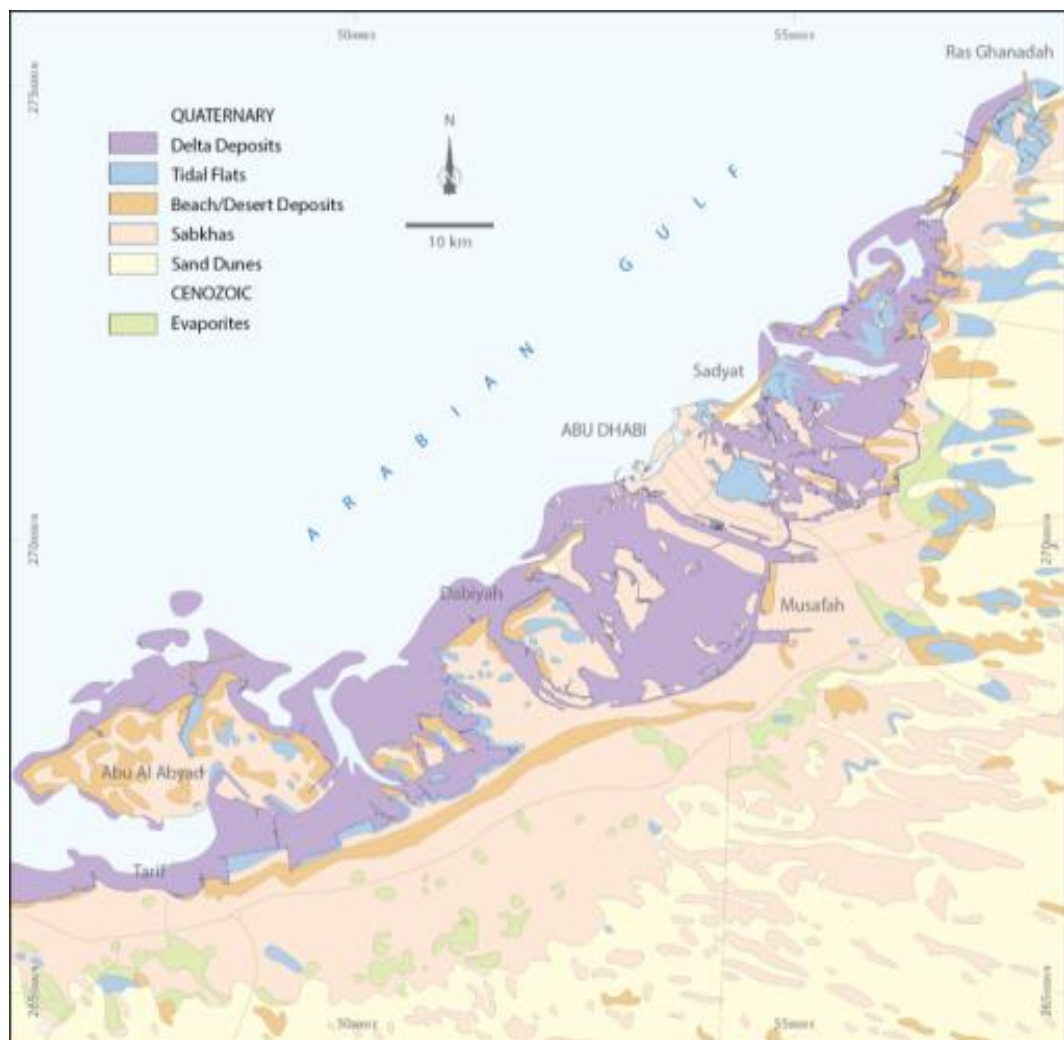


Figure 1.3. Geological map of the study area (Simplified from EAD, 2012).

Grid sediments fill frameworks along the Abu Dhabi coast (Fig. 1.4). These frameworks incorporate a proximately shut tidal pond, linked to the Arabian Gulf by slender channels, and were created by a long sabkha constituting the supratidal part of the lagoons (Baltzer *et al.*, 1994). The barrier island is spread at the southwest along the shore of the United Arab Emirates; these islands, which form part of this study, incorporate Abu Dhabi, Al Sadiyat, Al Qanatir, Abu Al Abyad and Marawwah (Fig.1.4). These various and far-reaching islands, as well as the landmass of Al Dhabaiya, are nucleated around Aeolian, calcareous sands from the Pleistocene period, and marine residue; the miliolite is hoisted around 2m to 4m above the sea level (Kirkham, 1998; Alsharhan and Kendall, 2003). The aggregations of the Holocene dregs on the previously mentioned island are a blend of both marine and Aeolian carbonates that reach 2 m above the sea level. The coastline of Abu Dhabi splits into two sections at Al Dhabaiya, and west of this peninsula the boundary islands are isolated from each other, linking up at the eastern ranges. At the edge of the ocean oolitic sands and skeletal grain stones were generally formed by high-energy shoals, shoreline obstructions, tidal deltas and channels. These channels are the site of the gathering of well-rubbed mollusks, echinoids, foraminifera and corals (Alsharhan and Kendall, 2003). Exactly at the north of the focal segments of the above-mentioned islands, irregular reefs occurred (Evans *et al.*, 1964).

UNIVERSITY of the
WESTERN CAPE

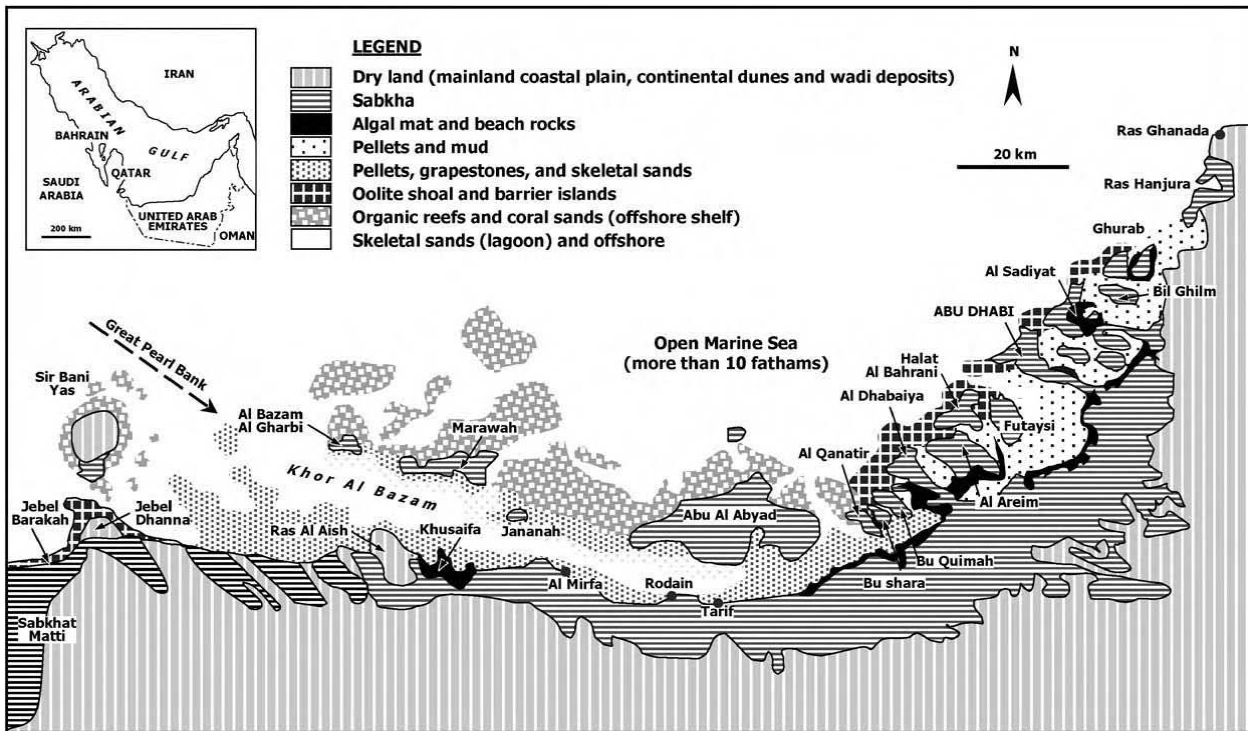


Figure 1.4. General sedimentary facies along the waterfront regions of Abu Dhabi demonstrate the territories specified in the content (Modified from Kendall and Skipwith, 1969a, b).

Trenches cutting in the beach-front sabkhas indicate that shoaling-upward cycles (Fig.1.5) generally comprise of a subtidal/intertidal succession overlain by supratidal facies. The coral reefs are additionally growing along the seaward of the tidal diverts and in the offshore parts of the tidal ponds, where the water provides enough circulation to enable coral growth. At the south of the peninsula, there are some confined tidal ponds and the development of tidal grounds towards the edges of the drift and landwards of the boundary islands. The residue of the tidal ponds is controlled by time and mudstones with scattered skeletal grains.

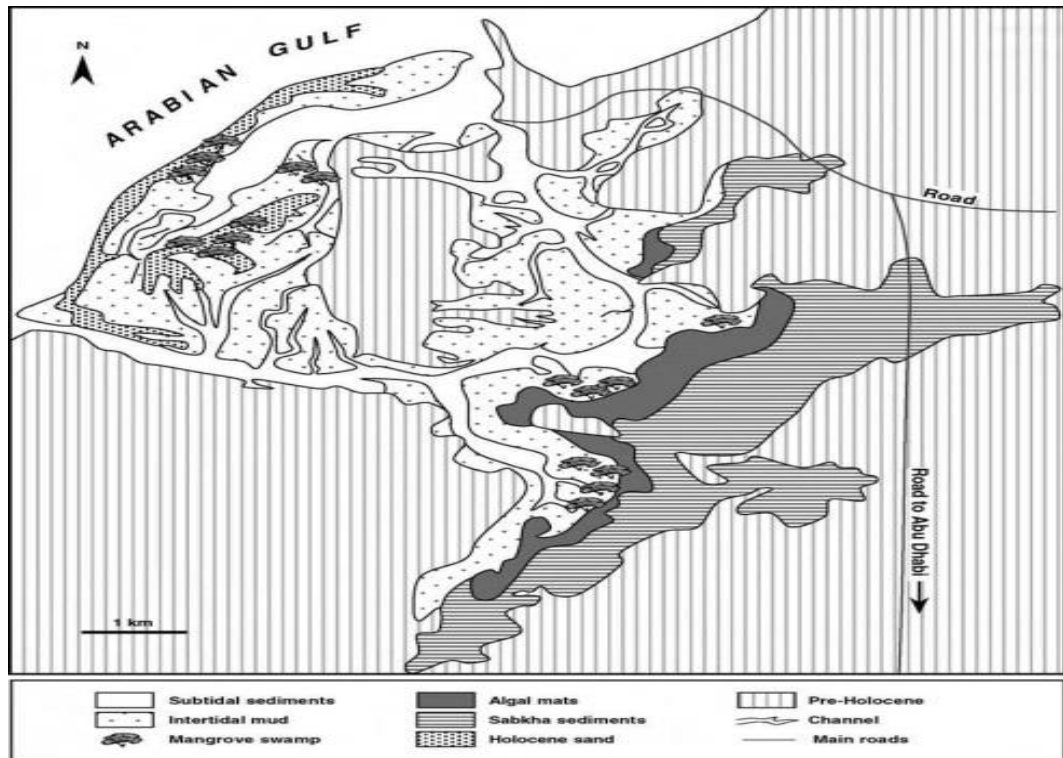


Figure 1.5. Sedimentary facies of Ras Ghanada, eastern Abu Dhabi Island
(Modified from Baltzer et al., 1994).

Carbonates and occur in the sections of the tidal ponds close to the sea, where faecal pellets are produced. Low-tide activity plays some part in the expanding level of saltiness, where, at low tide, the broad part of the tidal pond floor uncovers, resulting in the dissipation of intertidal waters and prompting a high level of salinity.

On the other hand, this increased salinity and the decreased levels in echinoids, corals and algae growth prompts an expansion in gastropods and imperforate foraminifera (Alsharhan and Kendall, 2003). In the intertidal waters, the mangrove swamp grows and accumulates lime mud and forms mangrove peats. Abu Dhabi drift has enough assurance from the overwhelming north-northwest twist, as well as the landward mangroves; additionally, microbial mats dominate the salt marshes of the drift. At the point when the tide brings on the diurnal flooding, there are next to no dregs retained on the mats; yet lime mud and sand can be transported onto the surfaces of the mats due to the events of the storm. These flats pass landward into the supratidal zone of the sabkha (Evans *et al.*, 1964a, b; Butler *et al.*, 1982; Kirkham, 1997; Alsharhan and Kendall, 2003).

The sabkha is level and inclines towards the drift; its surface extends over the beach-front, given the early Holocene high-energy shoreline, which is defined by bioclastic sand, rich in cerithidea gastropods. Finally, a geological understanding of the conditions of the ground and significant geohazards is very important to develop this study. At the same time, the enormous quantities of raw materials are indicative of the importance of understanding local industries and sustainable mineral resources. For the purposes of this study, it is also important to highlight the Neogene and Quaternary deposits, because they underlie most of the Abu Dhabi soil.

1.4 Regional geological and geomorphologic setting

The eastern Arabian Peninsula (empty quarter) from Kuwait to the north and the emirate of Abu Dhabi to the east has been characterized by the Late Cretaceous-Quaternary rocks, containing a significant thickness of carbonate, calcitic and other types of sedimentary rocks, which are for the most part in moderately tectonically conditions. The Arabian Shield contains Precambrian rocks and it is overlain by rocks as old as Cambrian, through the forward geological periods (Alsharhan and Kendall, 2003). The previously mentioned rocks have been influenced by the disfigurements linked to the ongoing aggressive, anti-clockwise movement of the Arabian Plate towards the Eurasian Plate, because of the increase in strata dips in the United Arab Emirates, which are generally shallow (Alsharhan, 1989).

The geographical history of the district was overwhelmed by an event that ended in the abduction of the Oman-UAE Semail Ophiolite onto the eastern mainland edge of the Arabian Platform in the Late Cretaceous period 96 million (Ma) years ago. The shallow water stage limestones were set down contemporaneously at the edge of the Neo-Tethys sea.

The foreland and basin development has extended from the north to the south between the Abu Dhabi coastlines and the present mountain front, because of the Arabian platform margin and crustal flexure. During the Miocene epoch, about 23 to 5 Ma, a compressive event took place due to the reestablishment of the north-eastern part of the Arabian Plate, which resulted in the arrangement of the Zagros Mountains. Additionally, this compressive event resulted in the Hajar Mountains rising to no less than 3 km.

Searle, 1980, said that the Hajar Mountains were around 1,500 m more noteworthy than the present stature of the ophiolite outcrops. Thus, the ocean withdrew from a large portion of the foreland basin, and the earthly environment was set up where the streams spilled out of the elevated Hajar Mountains, while the bajada was formed more than 100 km along the mountain front.

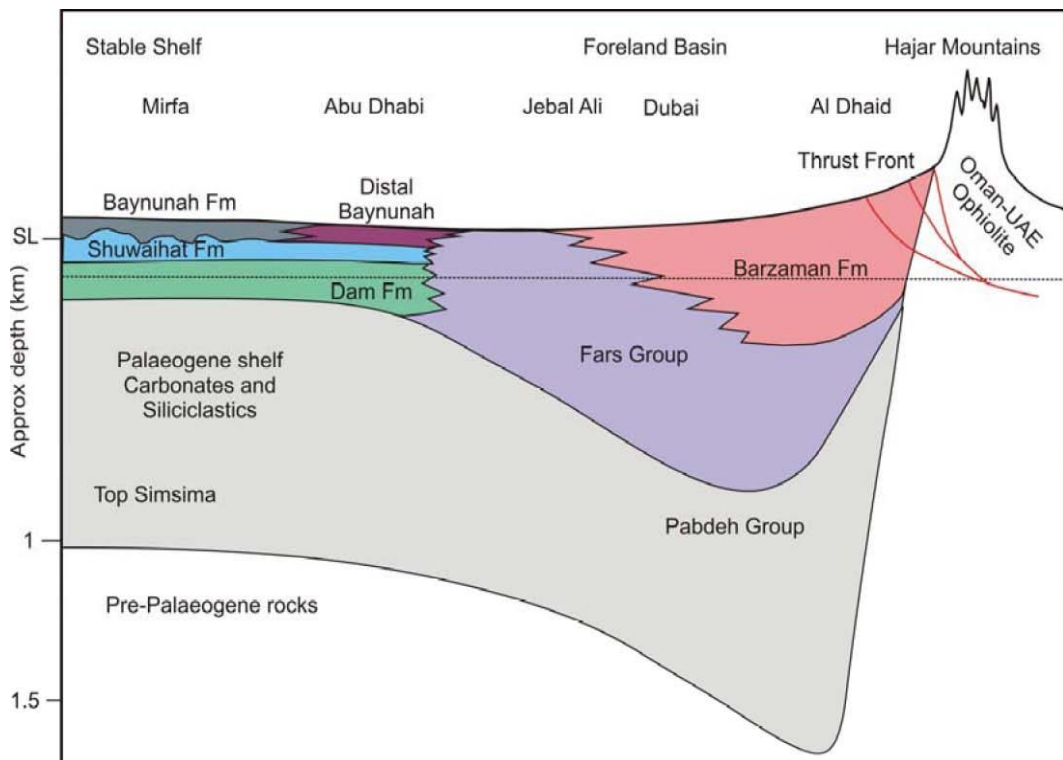
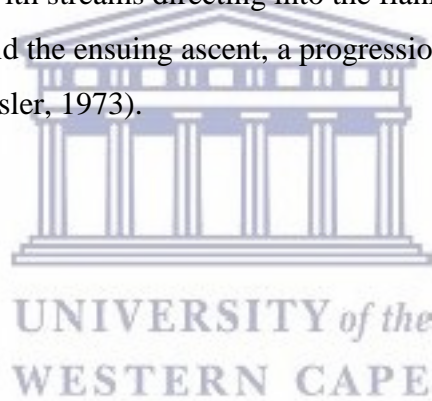


Figure 1. 6. Schematic interrelationships between main stratigraphic developments, UAE (After Steve, M., Richard, E., Jason, M., Andrew, F., & Leon, L. 2012).

A fluvial framework was set up in the west of the Hajar Mountains. The foundation bed deposited in the late Miocene to Pliocene times. This bed was formed eastwards, depleting streams and keeping a grouping of fluvial siliciclastic stores (Baynunah Formation) which drop out along the drift, west of Abu Dhabi. The depletion of these streams towards the eastern zone of Saudi Arabia had been tilted up, after the rafting of the Red Sea, around 20 Ma. These fluvial systems debauched into a restricted basin located along the Abu Dhabi coastline, where thin limestone, sabkha deposits and evaporate-rich mudstones of Miocene age also occur. Figure 1.6 outlines the surmised stratigraphic connections between main stratigraphic developments, UAE and the fundamental developments experienced in the district.

The hot and humid climate of the later Miocene period, along with its rainfall, led to the amount of clastic residue in these alluvial fans (Abdel Fattah MA, Shahid SA, 2007) in Abu Dhabi and Qatar. The marine limestone and sabkha sandstones of the Dam and Shuwaihat formations were set down on the Cratonic side of the foreland bowl. The Arabian Gulf is semi-encased in delicately halting bathymetry and a long hub that isolated it into two regions, defined by contrasting structural histories, which are: a) the steady foreland Arabia, influenced by Late Pliocene to Pleistocene collapsing sediments and salt diapirism, and (b) the unstable Iranian Tertiary fold belt (Kassler, 1973). The Arabian Gulf is asymmetric, with its more profound pivot closer to the Iranian side of the Zagros Mountains (Purser and Seibold, 1973). The Arabian Gulf has been overwhelmed by the Pliocene-Pleistocene tectonics (Fig.1.7) through Quaternary disintegration, and has adjusted with the help of these structures (Kassler, 1973). For illustration, the ocean level fell 120m during the Pleistocene age, leaving the Arabian Gulf totally uncovered, with streams directing into the flanks (Weijermars, 1999). Amid this great sea level fall and the ensuing ascent, a progression of stages was cut into the pre-existing surface (Kassler, 1973).



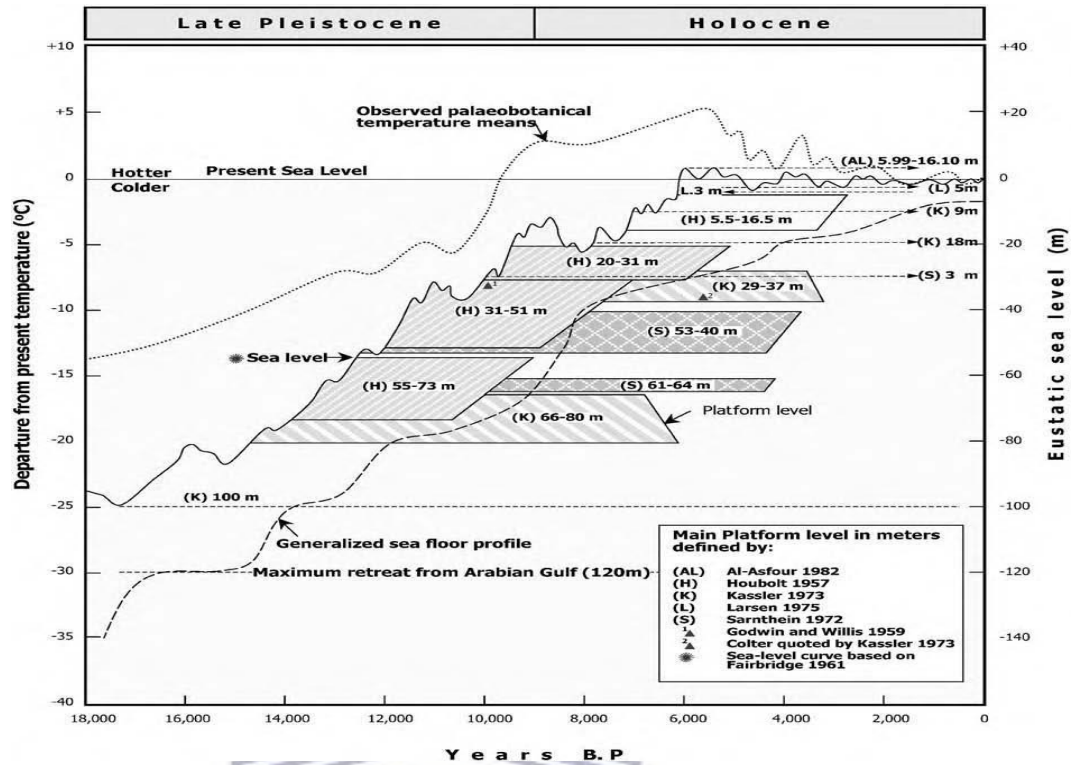


Figure 1.7. Temperatures, sea levels and terrace heights in the Arabian Gulf area during the Pleistocene-Holocene period (compiled from Fairbridge, 1961; Kassler, 1973; Al Asfour 1982).

The Arabian Gulf is found in the low latitudes, controlled by different elements, including an arid climate, the impact of low or high wave vitality, the drifted introduction of the northwest shamal winds, and the nearness or nonappearance of seaward obstructions (Wangor and Togt, 1973). Toward the northwest, the Arabian Gulf is being filled by the Shatt Al Arab delta at the conversion of the Tigris, Euphrates and Karun water ways (Purser and Seibold, 1973).

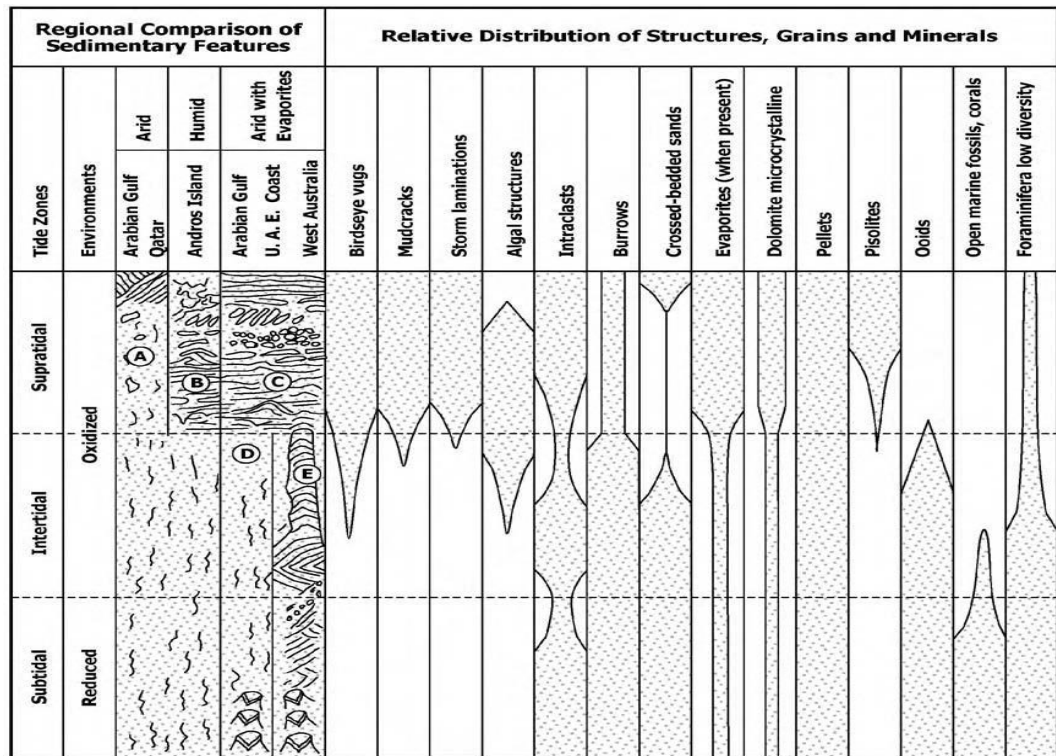


Figure 1.8. Facies variations associated with carbonate tidal flat accumulation (Shinn, 1983).

Conversely, the Iranian shoreline is rough, with estuaries and seaside fields connected with streams that take in the Zagros Mountains (Purser and Seibold, 1973; Alsharhan and Kendall, 2003) and is the site of terrigenous sedimentation and some carbonates. The vitality of the setting, which comprises bioclastic and oolitic sands, pulls the residue of the southern Arabian drift seaward. The vast majority of the Arabian Gulf, deeper than 20 m, has low to direct vitality conditions (Fig.1.3) and this is where fine-grained argillaceous and micrite sand dregs amass (Houbolt, 1957; Purser and Seibold, 1973; Alsharhan and Kendall, 2003).

Fig.1.8. Facies variations associated with carbonate tidal flat accumulation (Shinn, 1983). The sequence on tidal flats (Fig.1.8) around the Qatar Peninsula is shown at (A). Note the lack of a well-developed algal mat or anhydrite zone due to slightly higher rainfall than on the Abu Dhabi Coast. The drawing at (B) shows sedimentary structures, such as soil clasts, current-deposited intraclasts, minor algal heads and domes, mud polygons and mud cracks, developed in humid climates, such as at Andros Island in the Bahamas. The drawing at (C) shows the sedimentary features associated with arid tidal

flats, such as on the Abu Dhabi Coast in the Arabian Gulf or in the Shark Bay region, western Australia. Note that the major characteristic of the last case is the presence of nodular, or chicken wire, anhydrite. The intertidal zones can range from oxidized muds to (D) coral reefs to (E) rippled cross-bedded sands, containing large, club-shaped algal structures. The right-hand section tracks the relative abundance of the various characteristic sedimentary structures, grains, minerals and fossils.

The focal part of the United Arab Emirates, especially the western part of the coast near the Arabian Gulf, is described as a clastic carbonate/ complex, while the beachfront regions of the Gulf of Oman is defined by siliciclastic/minor carbonate sands and neighbouring sabkhas. There is a broad arrangement of tidal ponds and boundary islands in Abu Dhabi. The western part of Abu Dhabi, on the southern shore of the Khor Al Bazam, is a prolonged tidal pond that structures a persistent, open assemblage of water(Fig.1.4) whose western part is associated with the Arabian Gulf.

A shallower bank shapes the northern edge and has broad sandy shores and coral banks, which the tidal channels cut through (Alsharhan and Kendall, 2003). The quantitative examination of surface residue along numerous transects of the Arabian Gulf shoreline of Abu Dhabi (Lokier *et al*, 2013) has established that siliciclastic grains are normally sourced from disintegration of outcrops of the Ghayathi Formation and by means of the Aeolian transport of terrigenous silt, which is regularly obtained from the north and northeast. Anthropogenic exercises, such as development, channel digging and land recovery, are adding to noteworthy amounts of siliciclastic and evaporate residue to this carbonate depositional setting. The nearness of evaporate in the foreshore silt of four transects is especially credited to anthropogenic exercises.

1.5 Climatology and oceanography

The climate of the study area is hot and humid in the summer and moderate with slight rainfall in the winter. The average temperature in the coastal site of Abu Dhabi is higher than 43⁰C, with a duration between May and September. The average temperature is 14⁰C between October and April (Ministry of Agriculture and Fisheries, 2001). Where the Arabian Gulf is surrounded by land, it extreme variations in sand

influx in to the sea; therefore, the United Arab Emirates has an arid sub-tropical continental climate (Purser and Seibold, 1973; Alsharhan and Kendall,2003).

Given the climate of the region, the desert of Abu Dhabi is highly prone to crosswinds and degradation, increased salinization, waterlogging, human land use practices and overgrazing. The narrow Strait of Hormuz plays some role in the widely varying water temperature and salinity; this is a direct result of restraint in the trading of marine water into the bay. The summer temperature is high, due to the fact that the Arabian Gulf is close to the Tropic of Cancer during the summer season, when the air temperature is commonly in the range of 45°C to 50°C. By contrast, during winter, the air temperature is as low as 0°C. The combination of strong winds, high temperatures and low precipitation brings about noteworthy dissipation and high salinity (Kendall and Skipwith,1969a). The high temperature, combined with the aridity of the United Arab Emirates drift, by one means or another, clarifies the vast measure of carbonate and evaporates in the nation's waterfront fields (Alsharhan and Kendall, 2003). Counter-clockwise flow samples of the Arabian Gulf are driven by thick streams. Salinities in the Gulf are marginally higher than in the Indian Ocean, which is linked to the Strait of Hormuz (Sheppard *et al.*, 1992). Lightning bolts strike surface water in the Gulf of Oman and dull bolts are denser over the deeper water stream. The records show a sabkha surface temperature of more than 40°C in the winter months and not higher than 50°C in summer season months (Kinsman, 1964; Bulter, 1965). The Arabian Gulf water temperature tends to increase far from its coastal line, especially in the shallow waterfront ranges and tidal ponds (Purser and Seibold, 1973). The records demonstrate the same contrasts and variety in the water temperature; in the scope of 23°C to 24°C in the close shore and 22°C to 36°C in the close tidal ponds (Evans *et al.*, 1969). These temperatures can reach as high as 40°C in summer and as low as 15°C in the winter season. The average beach-front precipitation in the United Arab Emirates is under 40mm. Rainfall occurs during harvest time, winter and spring. The records allude to the rain creating vaporous changes in the evaporate minerals (Butler, 1965). Records indicate little impact on the silt and ground waters, although these might be affected by street developments, enormous landfills and the water system of neighbourhood activities. Silt collection tends to result in unadulterated carbonate on the Arabian side of the bay, because of the absence of fluvial sources (Purser and Seibold, 1973). In the

southern Arabian Gulf, where the study area has been located, the rate of evaporation has been evaluated to be as much as 124cm/year (Privett, 1959). Sugden (1963) recorded higher summer salinities for some zones of the southern part of the Arabian Gulf. Salinities of the Arabian Gulf suggest that these react to the hydrographic barrier made by the maritime upwelling at the Strait of Hormuz, which keeps the Indian Ocean from entering where the activity of water is counter-clockwise and has been driven by the thickness of the stream (Emery 1956; Hartman *et al.*, 1971; Sheppard *et al.*, 1992). The salinity range is 37‰, close to the Strait of Hormuz, in contrast with the Arabian drift tidal ponds, where the salinity is more than 65‰ (Bathurst, 1975). Because of the high rates of dissipation, the precipitation and fluvial input have offered no compensation for this salination.

The water close to the shore has a salinity ranging from 42.7 ‰ to 44.5 ‰ (Evans *et al.*, 1969) compared to an average salinity of 60 ‰ to 70 ‰ in the United Arab Emirates in the lagoon areas and embayment's (Alsharhan and Kendall, 2003). The seaside water salinity in the United Arab Emirates is changed with the condition of the tide (Kinsman, 1964). The more limited the dissemination, the more prominent the salinity variety. The normal components that present in the marine water have kept up a consistent rate, where the calcium is extraordinary in the light of the fact that it is drained in the internal tidal ponds; the drainage is especially found in the summer season (Evans *et al.*, 1969; Alsharhan and Kendall, 2003). The water at the coast and in the lagoons, has shown lower sulphate and nitrate concentrations, whereas it showed higher concentrations of silicate in the open seawater. Some seasonal changes have taken place in winter in the coastal and lagoon water; these changes have a negative impact, leading to a higher concentration of phosphate. The concentration of silicate increases in summer, while there is no seasonal variation in the concentration of nitrate (Evans *et al.*, 1969). The Shamal is the most grounded northwest wind, which blows in winter; this prolonged wind, together with the spring tides, brings about flooding of the broad segments of the waterfront plain. The Shamals convey residue onto the supratidal level and straighten seaside rises; they start intertidal spits and shoreline edges of the highest point of the intertidal level. The Shamals transport residue landward and start super swells (Alsharhan and Kendall, 2003). The prevailing wind-bearing has been consistent through the Holocene and Quaternary periods (Kinsman, 1964; Kirkham, 1997); for this

reason, the region's wind-blown miliolite residue from the Pleistocene period has cross-bedding that perpetually plunges southeast. The northwest Shamal winds have created waves of 2.5 m; however, these waves have been disseminated on the sea bank along its northern flank, before reaching the Khor Al Bazam tidal ponds, west of the study range. In the south of Khor Al Bazam, these waves at times surpass 1m, but they rely on the viability of the tide and tidal streams in these tidal ponds and to the lee of the northern shores that rush it (Alsharhan and Kendall, 2003). The impact of these waves leads to the creation of sand bars, sand waves and scour marks. The development of material towards the east is hindered by headlands, where the shore is driven because of the southeast-coordinated waves (Kirkham, 1997). These waves break at a slant, in line with the shape of the shore. Towards the east of Abu Al Abyad Island, there is almost no longshore float inside the reef and channel region. Furthermore, dregs are created by the reef because of wave and tidal activity. Amid the activity of silt transport, the most vital means are waves and currents in the shallow regions of the Arabian ports of the bowl (Purser and Seibold, 1973). Along the United Arab Emirates drift, the upper east-inclining Shamal winds drive wave action, with tidal deltas accepting the vast majority of wave vitality (Evans *et al.*, 1969; Alsharhan and Kendall, 2003). Turbulence occurs in the tidal ponds, brought on by wave vitality; in so doing, winnowing the dregs that have not been secured by islands or banks. Tidal streams have been adjusted around the hub of the Arabian Gulf. The tides are blended in diurnal cycles, going from 2.5m seawards of the island to around 1m in the ensured tidal ponds.

On the eastern shore of Abu Dhabi, the range of the tide is about 1.5 m (Evans, 1970), so the prolongation of the winds may cause the tide to rise several meters, causing the coastal areas to be flooded. Evans *et al.* (1969) have reported the measurement of tidal speed at three locations:

1. On the eastern coast of Abu Dhabi, it measured 0.25 m/s at the ocean surface and 0.15 m/s on the ocean depths, streaming around to the shore.
2. Within the tidal deltas, 0.65 m/s at the ocean surface, and 0.4 m/s at the ocean depth.

3. In the minor southern tidal ponds, 0.25m/s at the surface and 0.2 m/s at the ocean floor (Evans *et al.*, 1969; Alsharhan and Kenggdall, 2003). Figure 4 demonstrates the general sedimentary facies along the beach front territories of Abu Dhabi (Modified from Kendall and Skipwith, 1992a, b).

On the western coast of Abu Dhabi, tidal streams with high speeds are contracted by channels framing the deltas, which frequently have a breadth of up to 8km². Seawards of the sea bank, tidal development has an east/west bearing. However, inside the Khor Al Bazam, on the western outskirts of the study area, there is a period of unmistakable abatement in tidal range southward over the tidal pond, towards the northern passage of the ocean (Kinsman, 1964a).

1.6 The sedimentary facies

On the western side of the Al Dhabaiya Peninsula, which is the western part of the study zone, the Khor Al Bazam tidal pond is located, and the coral reefs develop along the vast majority of the sea bank, towards the north of the Khor Al Bazam, and oolites are confined to a couple of waterfront strips. On the eastern side of the Al Dhabaiya Peninsula, the coral reefs are limited to little fixes and oolites accumulate on the entombing/island tidal deltas (Evans *et al.*, 1964a, b). The setting of this island is not the same as the secured tidal ponds beach front pads south of the island of Abu Dhabi; so, that the west of the Al Dhabaiya Peninsula is a 40 km-long cyanobacteria (microbial laminations), around 2 km wide northward crosswise, over sands and sandy micrites. On the western end of Khor Al Bazam west end, an accumulation of carbonate mud is found in a thin belt of deep water south of the sea bank. On the north end of the Khor Al Bazam, this belt is confronted by an intertidal stage (Kendall and Skipwith, 1969b). Nine localities of sedimentary facies were identified inside the tidal pond of the Khor Al Bazam and its nearby territories (Figs 1.4 and 1.9). These nine regions included:

1. An oolitic sand facies
2. Coral and coralline algal facies
3. Grape stone and pellet facies
4. A mud and pellet facies (Alsharhan and Kendall, 2003) at Khusaiffa region
5. A molluscan sand facies

6. A mangrove swamp facies
7. An algal mat facies
8. An evaporate facies
9. An Aeolian facies

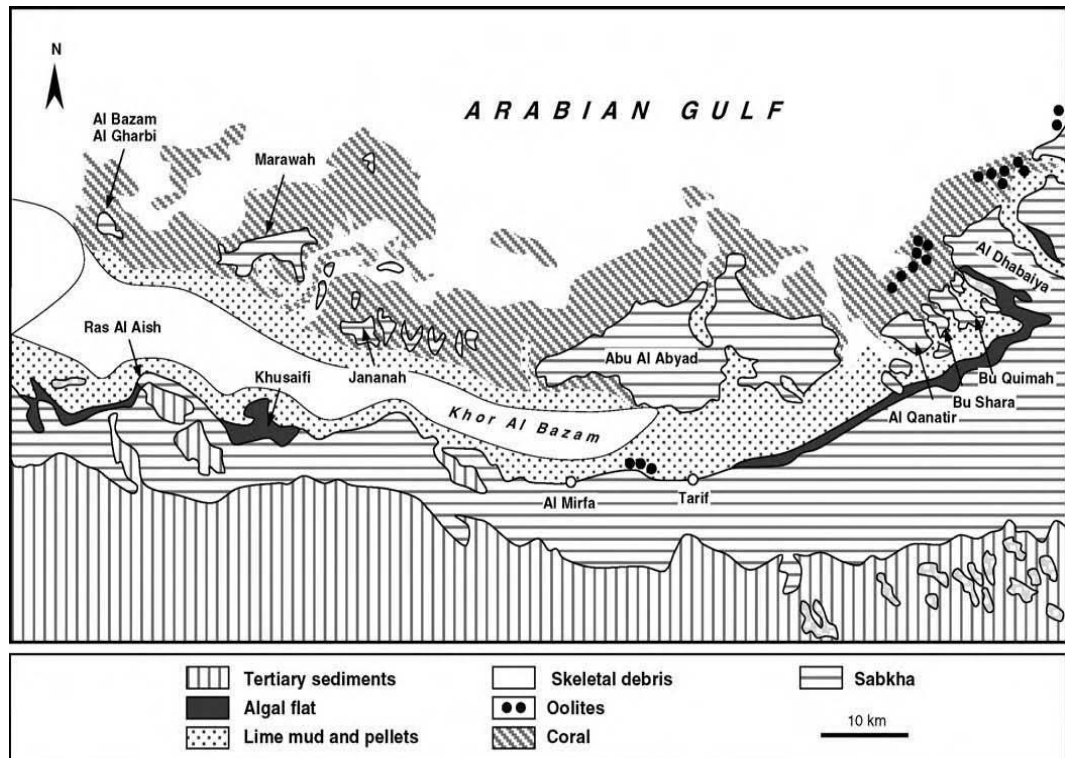


Figure 1.9. Sedimentary facies distribution of Khor Al Bazam, western Abu Dhabi. (Modified from Alsharhan and Kendall, 2003).

1.7 Mangrove swamp

The Al Dhabaiya Peninsula drift (south-western) is a typical mangrove development field, and extends from the neighbourhood framework (Figs 1.10 and 1.11). The drift followed a progression of Pleistocene outcrops, so that, around and between them, cyanobacteria pads and tidal channels were lined with stands of the grey mangrove (*Avicennia marina*). This mangrove-rich zone is a framework of jutting roots (pneumatophores). In the study area, *Avicennia marina* is the only mangrove that is shielded from turbulent wave activity. Uniquely, *Avicennia marina* is found in shallow, secured zones in the United Arab Emirates, where mangroves will line the banks of rivulets, depleting algal pads. Mangroves develop in a way that their roots and lower trunks are secured amid the high tide. At the edges of the channels, bigger mangroves

develop due to a superior exchange of tide, and this reduces in stature and dissemination inland. View the Niger delta for comparison (Allen,1965). The mangrove swamps at the south-western bank of the Al Dhabaiya Peninsula, the western section of the study area, have these trademark frameworks in the progradation. One such trademark is the exchange from mangrove line tidal squeaks horizontally to tunnelling crab level. Some *Salicornia* spp. can be observed colorizing nearby highs into gypsiferous cementation, framing the indurated, solidified outside layer around the shrubberies of the *Salicornia* spp, stretching out over the tunnelling crab flats (Alsharhan and Kendall, 2003). Usually, zones of mud brooks are found here. While it is conceivable to navigate mangrove-lined brooks, this took place after tunnelling crab pads turned to *Salicornia* spp, and gypsum over a restricted belt of algal flats.

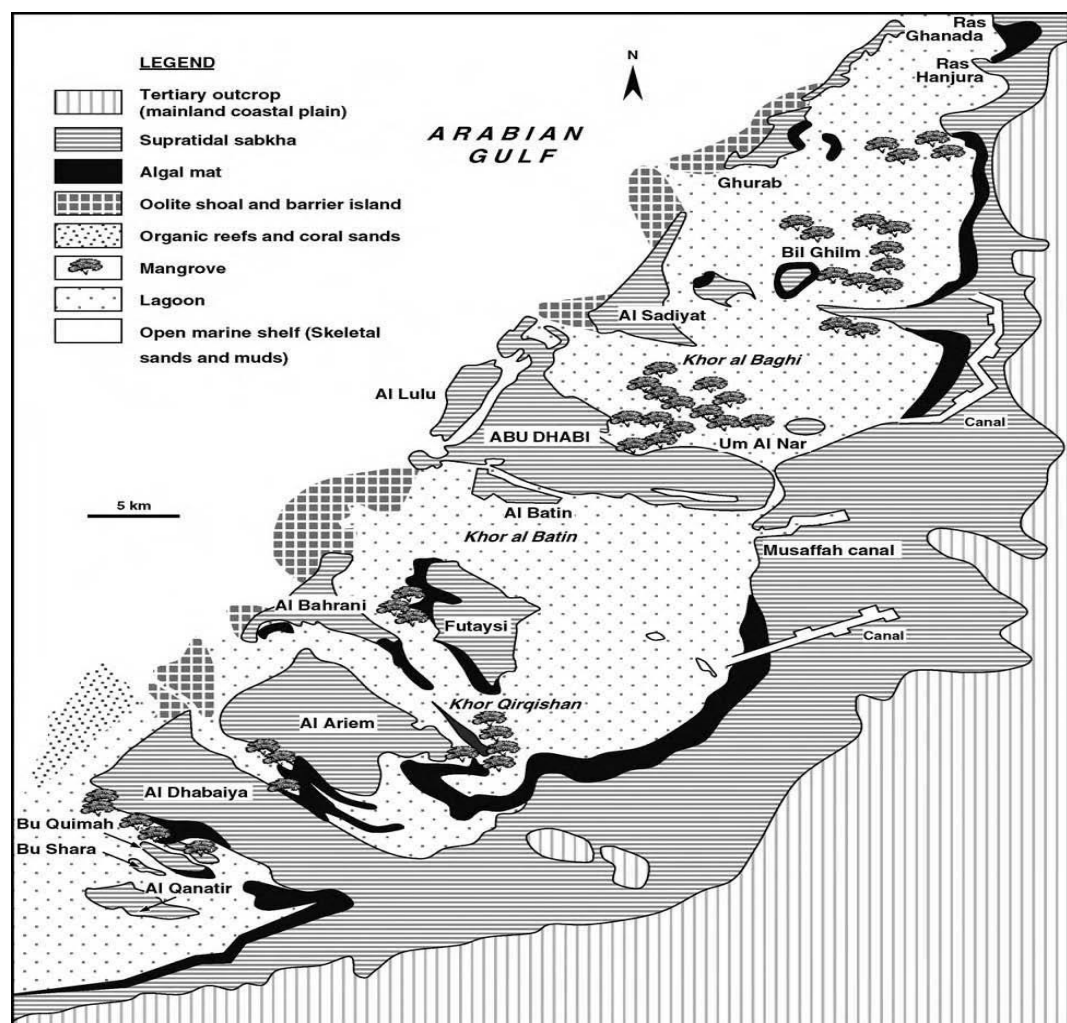


Figure 1.10. Sedimentary facies conveyance around Abu Dhabi Island and adjoining islands (Modified from Kenig *et al.*, 1989).

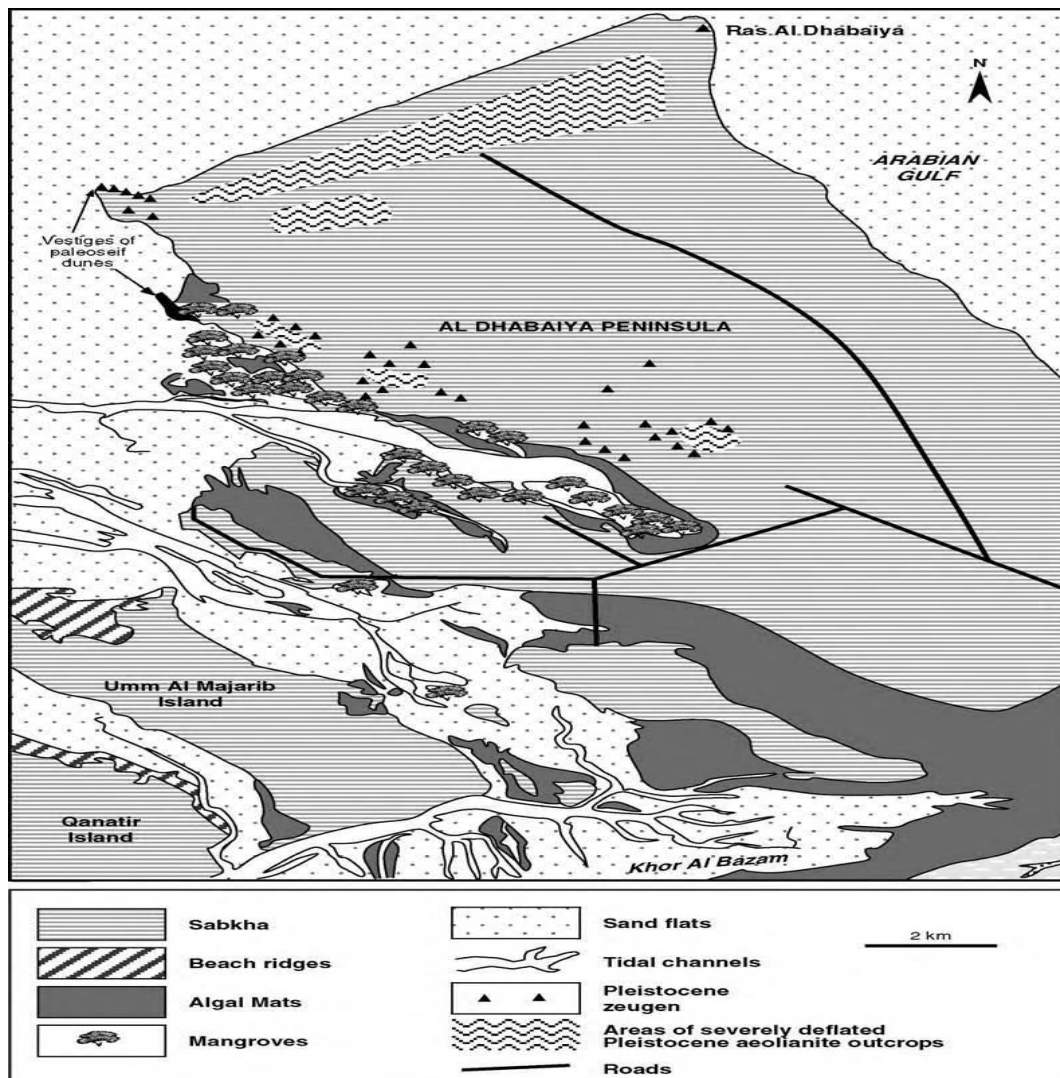


Figure 1. 11. Sedimentary facies delineate the Al Dhabeiya Peninsula, western Abu Dhabi (Modified from Alsharhan and Kendall, 2003).

1.8 Indurated cemented crusts (Hardgrounds)

Along the Abu Dhabi drift, and less commonly at Al Dhabeiya, indurated established coverings and shoreline rocks occurred; their segments are grains, concrete, textured and early diagenetic impacts (Kendall and Skipwith, 1969a; White *et al.*, 1998). Mud passes horizontally into the sands, which are usually solidified, and shape broadly along the side of the ceaseless, indurated solidified endurlated portions of the port (Alsharhan and Kendall, 2003). To the offshore lie the intertidal sand and mud pads, with indurated-solidified outside layers. Towards the ocean, cyanobacterial mats frame super polygonal saucers because of residue, and concrete-filled splits at the saucer edges. The distance across of the indurated-solidified outside layers, which is frequently clasped into megapolygonal, is 2 m to 3 m. The edge of this mega – polygonal (Fig.1.12,

1.13) sometimes project over the contiguous sands and are made by a square finished – surface of cyanobacterial mats. The dregs layers cover the polygons frequently, where their indurated solidified hulls surfaces are completely uncovered (Kendall and Warren, 1987). The development of extensive mega – polygons happened through the persistent procedure of diurnal warm extension and compression split falling and cementation and the development of thin outside layers. The mega – polygons are 1 to 2m in width. Blue-green algae growth secured these outside layers ordinarily, likewise some established blue-green algae occur with micrite, this is on the under surfaces of the polygons (Kendall et al., 1994). Magnesium calcite is the major cementing factor for the most concrete connected with landward outside on the algal pads, the overlying algal peats are eroded by the activity of wave and current, the shoreline unstable is covered with thick micrite bond layers that occasionally form into thick spiral stringy aragonite-cemented gravel (Kendall et al., 1994; Alsharhan and Kendall, 2003).

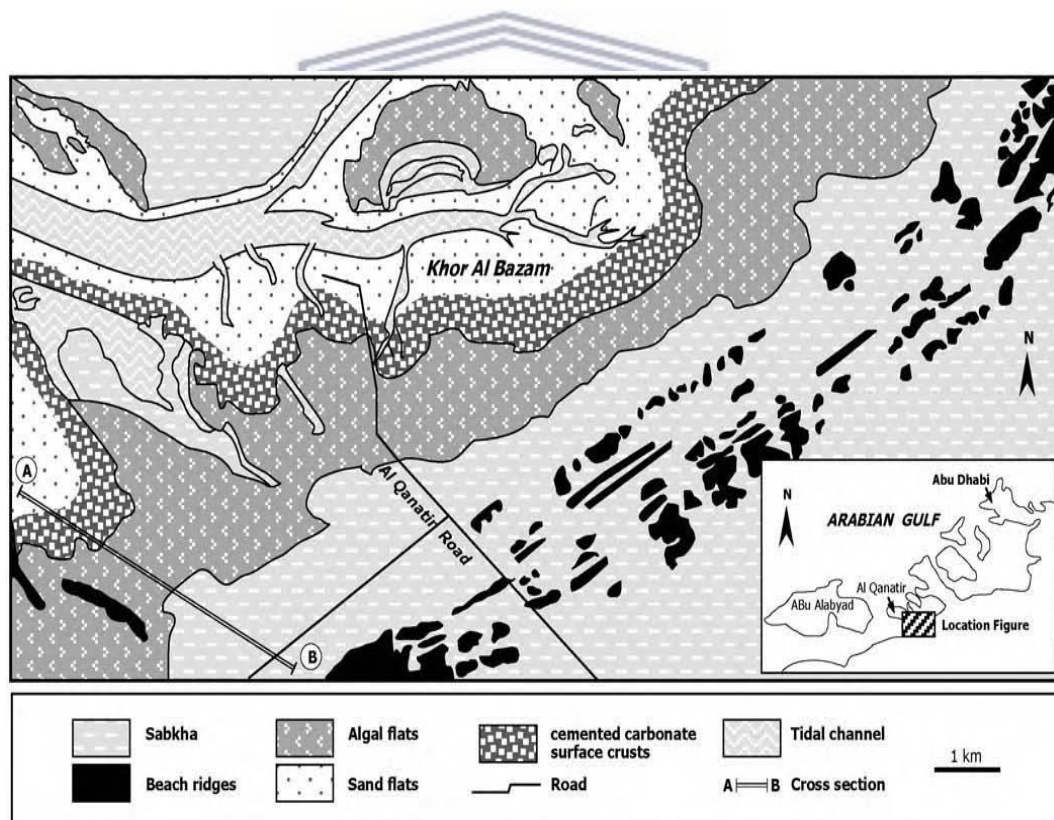


Figure 1. 12. Sedimentary facies delineate the southern shore of the SW Khor Al Bazam, south of Al Qanatir Island, western Abu Dhabi (Modified from Kenig *et al.*, 1989).

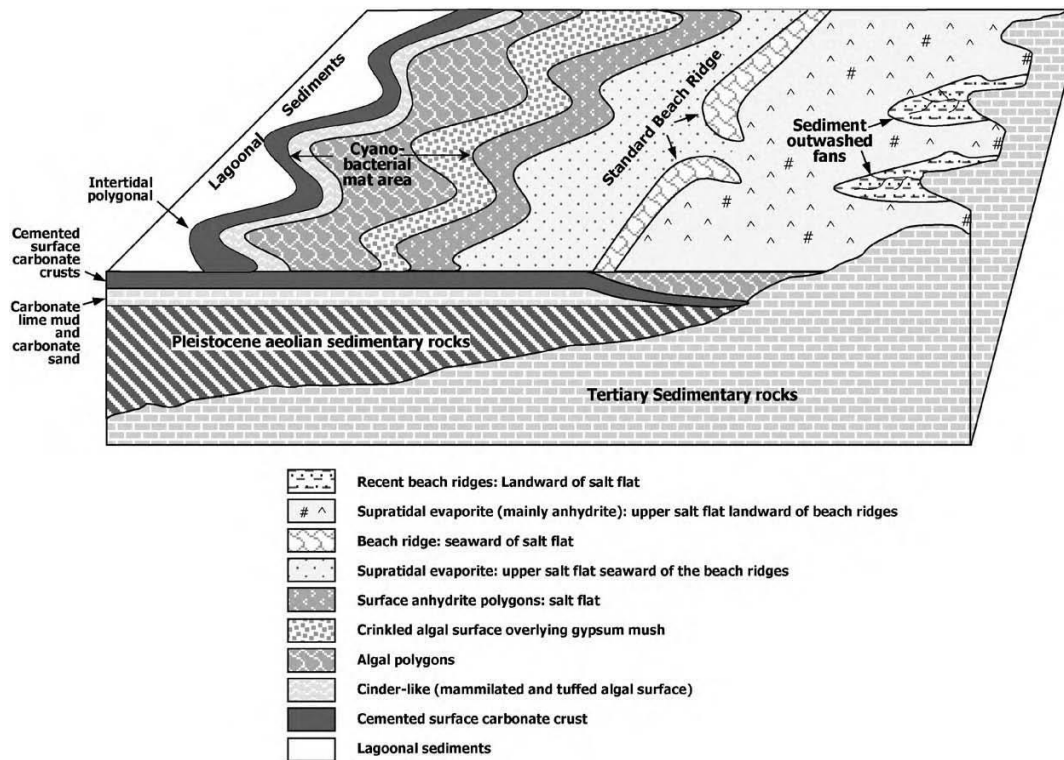


Figure 1.13. Distribution of evaporates and algal mats in southwest Abu Dhabi Island and along the southern shore of the SW Khor Al Bazam (Modified from Kendall and Skipwith, 1968).

1.9 Distribution of cyanobacterial mats south of Abu Dhabi

The south of Abu Dhabi and the eastern Khor Al Bazam coastal lagoons (Fig.1.13) are characterized by wide and long tidal flats, where cyanobacterial mats form part of the seaward edge of the prograding coastal plain, with an average width of about 2 km and underlain by some 5 cm to 30 cm of the compacted part. The tidal flats take the remains of cyanobacteria (Alsharhan and Kendall, 2003). Based upon gross surface morphology of the cyanobacterial mats, Kendall and Skipwith (1968) subdivided the mats into zones (Fig.1.13). The morphologic variations in zones probably represent differences in the microbial species that form the mats, as they are modified by environmental conditions; this can be expressed in general terms, from seaward to landward, as zone-mammillated mats. Figure 1.14 explains the zonation of algal morphology along the Abu Dhabi coastal area: (1) lagoonal carbonate sands and/or

muds; (2) poorly laminated, algal-rich carbonate muds; (3) algal mats formed into cinders; (4) carbonate-indurated, cemented crusts; (5) lagoonal sediments with gypsum crystal; (6) polygonal zone, algal peat with gypsum crystal; (7) polygonal zone algal peat; (8) anhydrite nodules and layers in matrix of windblown carbonate and quartz; (9) halite crust formed into compressional polygons.

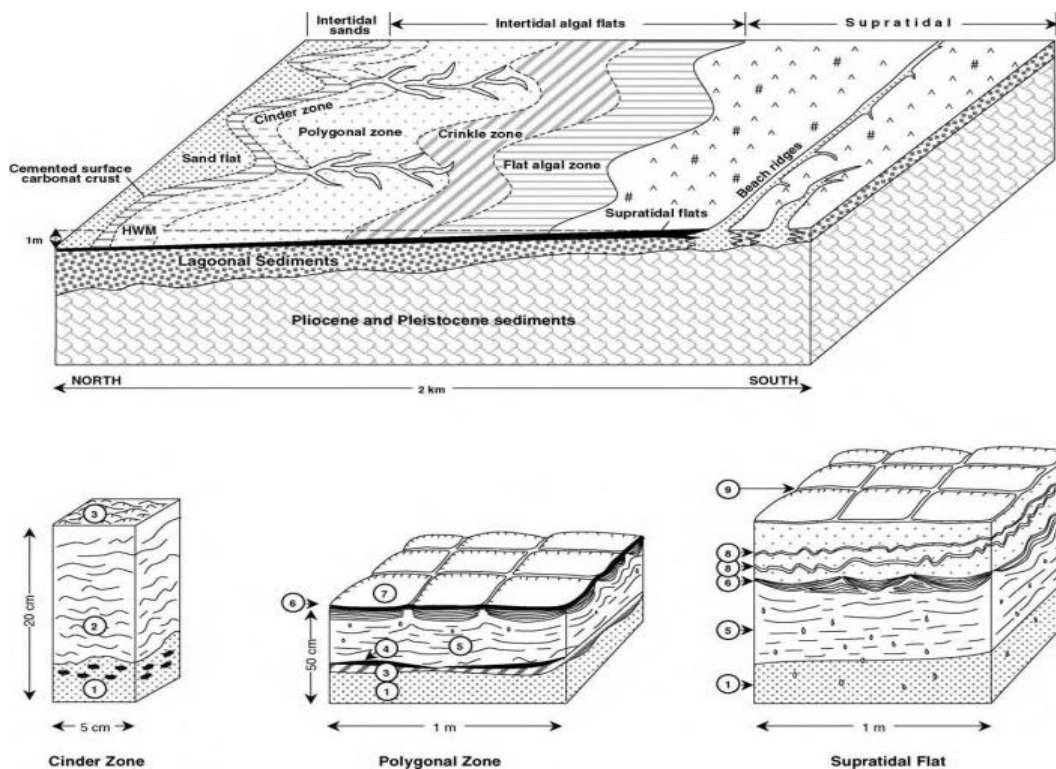


Figure 1.14. Zonation of algal morphology along the Abu Dhabi waterfront range (Modified from Kendall and Skipwith, 1968).

1.10 Uranium, thorium and heavy metals

Soils represent ideal media for both uranium and thorium sinking, compared with other environmental components of the United Arab Emirates. It is important to know more about soil and the above-mentioned radionuclides (uranium and thorium). The complex nature of the soil stands as a part of the difficulty facing the soil information preparation (Forstner and Wittmar, 1993; Adriano *et al.*, 1996). Numerous variables influence the focus levels of uranium and thorium in soil, i.e. Surface, sorts, structure, redox response, adsorption/retention; as well as physical transport and human activity (Ahumada *et al.* (1999); Howari and Banat, 2001). Studies demonstrate that uranium and

thorium come from various sources, such as from various modern sources, such as mining, smelters, restorative waste and various sources (Adeyumo, 1994; Namasivayan, 1994; Stephan *et al.*, 1999; Kamon *et al.*, 2000; Ract *et al.*, 2003). Uranium and thorium studies are vital, in the light of the fact that changes in ecological conditions and component accessibility may occur, causing harm to creatures and plants. Uranium remains one of the radionuclides that could indicate human activity in the soil. Examples of anthropogenic impact on soil include accidents, such as, the Fukushima nuclear power plant disaster, caused by seismic tremors; other examples include nuclear weapon testing (Çevik *et al.*, 2004). Likewise, we need to consider different human activities, for example, mining, transportation and reprocessing of uranium (Mahur *et al.*, 2008; Singh *et al.*, 2009). What is more, soil with low levels of radioactive waste has been covered for transfer (Gavrilescu *et al.*, 2009). The presence of radionuclides in soil, such as uranium, can be dissolved in liquids, or solutions, or react to ions, forming complexes with soil organics. Uranium could also precipitate as a pure, or other, mixed solids. Radionuclide can be transferred into the water or other natural resources, causing environmental pollution and posing risks to human health. Uranium can lead to serious damage to the environment, such as in the case of mining and milling, when there is improper disposal of radioactive nuclides. Waste disposal after uranium prospecting, as well as other activities, can be traced back to World War II (IAEA, 2004).

Heavy metals may be associated with soil components either as pure or mixed precipitates, or through ions exchange to form complexes (of different strengths) with soil organics (Kersten M, *et al.*, 2003). These metals can be transferred into the water, or other natural resources, creating environmental pollution and threats to human health. Heavy metals can be extremely harmful to the environment, as they induce high toxicity in animals and plants, especially if they were disposed of improperly.

While the vast majority of the substantial metals are vital for life at low concentrations, several of them are extremely lethal at high fixations. A few overwhelming metals, for example, lead, mercury, cadmium and arsenic, can bring about turmoil in the focal neurological framework, harm the cerebrum, failure in the kidney and liver, and malignancy (Paul B. Tchounwou, Clement G. Yedjou, Anita K. Patlolla, and Dwayne J. Sutton (2012). The aforementioned metals can bring about mental

deficiencies and miscarriages; they can likewise bring about serious harm to the bones. For instance, in 1978, the use of lead in paint was banned, as it is exceedingly toxic, even in concentrations as low as 10 µg/L. The quantity of metal uptake, toxicity and bioaccumulation varies according to the organism, the temperature and the pH of the medium, the turbidity, the amount of dissolved oxygen and the concentrations of other metals in solution (Mortimer, 2000). In the 1950s in Japan, 44 people died, and many children were born with defects, because of consuming fish from the Minamata Bay, in which mercury-containing waste from a chemical plant had been dumped. The level of mercury accumulation in the fish had reached 100ppm (P. Atkins and J. de Paula.2002). In Iraq, in 1972, 6,000 individuals were debilitated and 500 died after having eaten bread that was produced using wheat treated with methyl mercury fungicides (Bakir F., Damluji, S.F., Amin-Zaki L., (July 1973)). In the 1950s, effluent from a zinc mine was discharged in the Zintsu River in northern Japan. This river was relied on to irrigate rice fields. Residents who had eaten the rice had had the Ca^{2+} in their bones replaced with Cd^{2+} . Their bones became very fragile and they suffered from bone breakage, vomiting, liver damage and kidney failure (Scientific Opinion of the Panel on Contaminants in the Food Chain on a request from the European Commission on cadmium in food.2009). The components lead, mercury and cadmium have been grouped by the natural assurance organization (EPA) among the 25 most dangerous chemicals in the USA. These heavy metals are toxic because their cations have a high complexing affinity (Cox, 2004). The more water-soluble or volatile the complex is, the greater the impact on the environment. Safe practices for expulsion of unpredictable mixes before burning is vital. Heavy metals tend to accumulate in animals and plants (Melville, F. and M. Burchett, 2002.) and sea grasses (Prangea J.A. and Dennison W.C., 2000), causing biomagnifications and thus changes in morphology, physiology, biochemistry, behaviour and reproduction (Muller, 1969). For example, heavy metals can act as inhibitors for enzymes, due to the formation of mercaptides together with the sulfhydryl group, which are compounds responsible for the catalytic activity of enzymes (Vallee, B. L., and Wacker, W. E. C., 1970).

Metals and metalloids present in the earth's crust find their way to the soil through igneous, sedimentary and metamorphic rock cycles. Anthropogenic activities, including industrial and municipal waste products; urban and agricultural run-off, are the main

sources of metal contamination (Wei, W., Liu, M. & Jordan, F., 2002). The metal concentrations in the soil is highly controlled by the transport and deposition of soil. The size of soil grains also affects the affinity of the metal for the soil, which increases with finer grains (Harbison, 1986). Other factors, such as precipitation, adsorption and absorption, also affect, the contamination of heavy metals in soil. The concentration levels of heavy metals in soil are affected by factors such as texture, type, composition, redox reactions, in addition to physical transport and human activities (Ahumada *et al.*, 1999; Howari and Banat, 2001). Heavy metals find their way to soil from different point and non-point sources, such as mining, smelters and medical waste (Adejumo J., 1994; Namasivayan, 1994; Kamon *et al.*, 2000; Ract *et al.*, 2003). Anthropogenic activities, including nuclear weapons tests, nuclear power plant accidents such as the Fukushima disaster (Çevik *et al.*, 2004) cause pollution. The nature of the Arabian Gulf dregs has been examined in the entire district, including by the Regional Organization for the Protection of the Marine Environment (Hunter, 1986). In 1998, the International Atomic Energy Agency (IAEA) studied the impact of contaminants on the environment (IAEA, 1999). This overview secured a considerable measure of areas in Saudi Arabia, Kuwait, Qatar and the United Arab Emirates. In several locations on the coast of the United Arab Emirates, marine sediments were examined for the contamination of heavy metals, the organic matter contents and the size of the grains (Abu-Hilal and Khordagui, 1993). The concentrations of heavy metals, organic matter and mineralogical composition of Ras Al-Khaimah sediments was studied by El-Sammak (2001), and properties of sediments along Abu Dhabi and Dubai were studied by Al-Qubaisi (2001). AlRashdi et al. (2015) investigated the concentrations of heavy metals along the coastal area of Abu Dhabi. The Regional Organization for the Protection of the Marine Environment (ROPME) knows about the substantial use in the Arabian Gulf of conduits concerning oil tanker movement and transportation activities. In the past two decades, one of the major sources of pollution that left an environmental impact in the Gulf region was the war in 1991 in Kuwait. Some samples collected from Kuwait contained higher levels of several metals such as cadmium, vanadium, lead, copper and nickel, compared to 1985 to 1991 (Kureishy, 1993; Bou-Olayan *et al.*, 1995). In 1998, a study of metal contamination was conducted in the United Arab Emirates (Banat *et al.*, 1998). In the light of a study by Basaham and Al-Lihaibi (1993), Fowler *et al.* (1993); the mean estimations of substantial metal concentrations (mg/kg or ppm) in unpolluted marine dregs in the UAE

were: 2.5, 2.9, 0.96, 18.9, 4.2, 127, 4,800 and 20.7ppm for zinc, lead, cadmium, nickel, copper, manganese, vanadium, respectively. The numbers are fundamentally the same as we have in our study. Points of interest of metal concentrations in various zones of the UAE appear in Table 1.1.

Table 1.1 Heavy metal fixations in surface residue from various regions in the UAE (El-Sammak (2001). Al-Qubaisi (2001), Kureishy, 1993; Bou-Olayan et al., 1995, Banat et al., 1998, Basaham and Al-Lihaibi (1993), Fowler et al. (1993), Bou-Olayan et al., 1995).

Area	Metal studied and determined concentration (mg/kg)											
	Al	V	Cr	Mn	Fe	Co	Ni	Cu	As	Cd	Hg	Pb
Jebel Ali	8530	10.4	31.7	96.6	2740	1.16	8.3	1.92	1.9	0.05	0.0022	2.10
Abu Dhabi	2570	4.6	17.6	32.9	874	0.34	2.0	1.99	1.3	0.02	0.001	0.78
Al Marfa	21000	23.1	37.6	225	5820	2.61	15.5	3.58	2.7	0.11	0.0015	2.93
Al Ruweis	26000	35.5	171	358	8940	2.40	8.6	2.62	2.20	0.11	0.0013	5.88
Akkah Head	534	4.5	83.5	60.3	4020	6.13	139	0.64	0.7	0.05	0.0006	0.69
Akkah Beach	2680	18.2	303	360	29600	45.2	1010	3.31	9.6	0.09	0.0009	1.30

1.11 Purpose and scope

1.11.1 Research problem

Many countries surrounding the United Arab Emirates (UAE) have nuclear activities. The Arabian Gulf Area in general stands as a theatre of many regional conflicts, where the test of nuclear weapons and the transportation of radioactive nuclides take place. Iran is one of the Gulf countries that has some nuclear reactors for peaceful purposes. Pakistan and India, which are neighbouring countries to the Arabian Gulf, are members of the international nuclear club. Reports indicate that some of the countries in the region, e.g. Iraq, contaminated the environment by using depleted uranium (DU) during the last two decades from several activities related to the Gulf War. Approximately 321 tons of DU munitions were deployed during the 1991 Gulf War (Bleise *et al.* 2003). This study is intended to determine the concentration of uranium, thorium and overwhelming metals in soil in the waterfront region of Abu Dhabi. These actual concentrations will set up the foundation for uranium, thorium and

substantial metals fixations, as well as uncover any potential irregularities. These actual concentrations are likewise vital to evaluate any pollution for natural and security applications. The aim of this study is to characterize the focus and dissemination of tainting, determine the present type of pollution, and identify the procedures that influence this position.

1.11.2 Aims and objectives

1.11.2.1 Aim

The general aim of this thesis is to survey shoreline dregs, utilizing sedimentological, mineralogical, geochemical, multivariate, factual and spatial investigation systems, to comprehend the variations among shorelines, as well as the provenance and dispersion of substantial metals, including radioactive components, like uranium and thorium, and their level of pollution in the coastal sediments of Abu Dhabi.

1.11.2.2 Objectives

To achieve the above aim, the following objectives have been identified:

- Characterization and classification of beach sediments of the study area, using conventional bivariate scatterplots and discriminant functions (Sahu, 1964) to interpret the environments and mechanism of sediment deposition.
- Univariate and bivariate statistical analyses of the beach sand.
- Enrichment factor and geoaccumulation index analysis to understand the level of enrichment of heavy metals and radioactive elements, like uranium and thorium.
- Classification and characterization of beach sediments of the study area, using multivariate statistics.
- Comparison of bivariate scatterplots and discriminant functions (Sahu, 1964) and multivariate statistical interpretation methods.
- Mapping the spatial distribution of sample locations, heavy metal and radioactive element concentrations, enrichment factor and geoaccumulation index results and statistical analysis results of the beach sediments using ArcGIS 10.

The proceeding sections will discuss and outline the introduction, study area background information, literature and methods employed in the thesis, results, their detailed explanation, and the conclusions and recommendations arrived at from the results.



UNIVERSITY *of the*
WESTERN CAPE

Chapter II

2.0 Methodology

This chapter will cover the methodology and literature associated with acquiring, preparing and interpreting data used for the evaluation of the soil of the study area.

Methods described and discussed in this chapter include:

- coastal sediments sampling, data management and analysis
- inductively coupled plasma –mass spectroscopy (ICP-MS) analysis
- X-ray fluorescence (XRF) spectrometry analysis
- X-ray diffraction (XRD) spectrometry analysis
- enrichment factor analysis and index of geoaccumulation (Igeo)
- sieve analysis and soil type diagram classification
- Factor analysis
- Cluster analysis
- Discriminant analysis

2.1 Location of the soil sampling

Fifty-seven sampling sites have been selected in the study area around Abu Dhabi city, the capital of the United Arab Emirates (Fig.2.1).

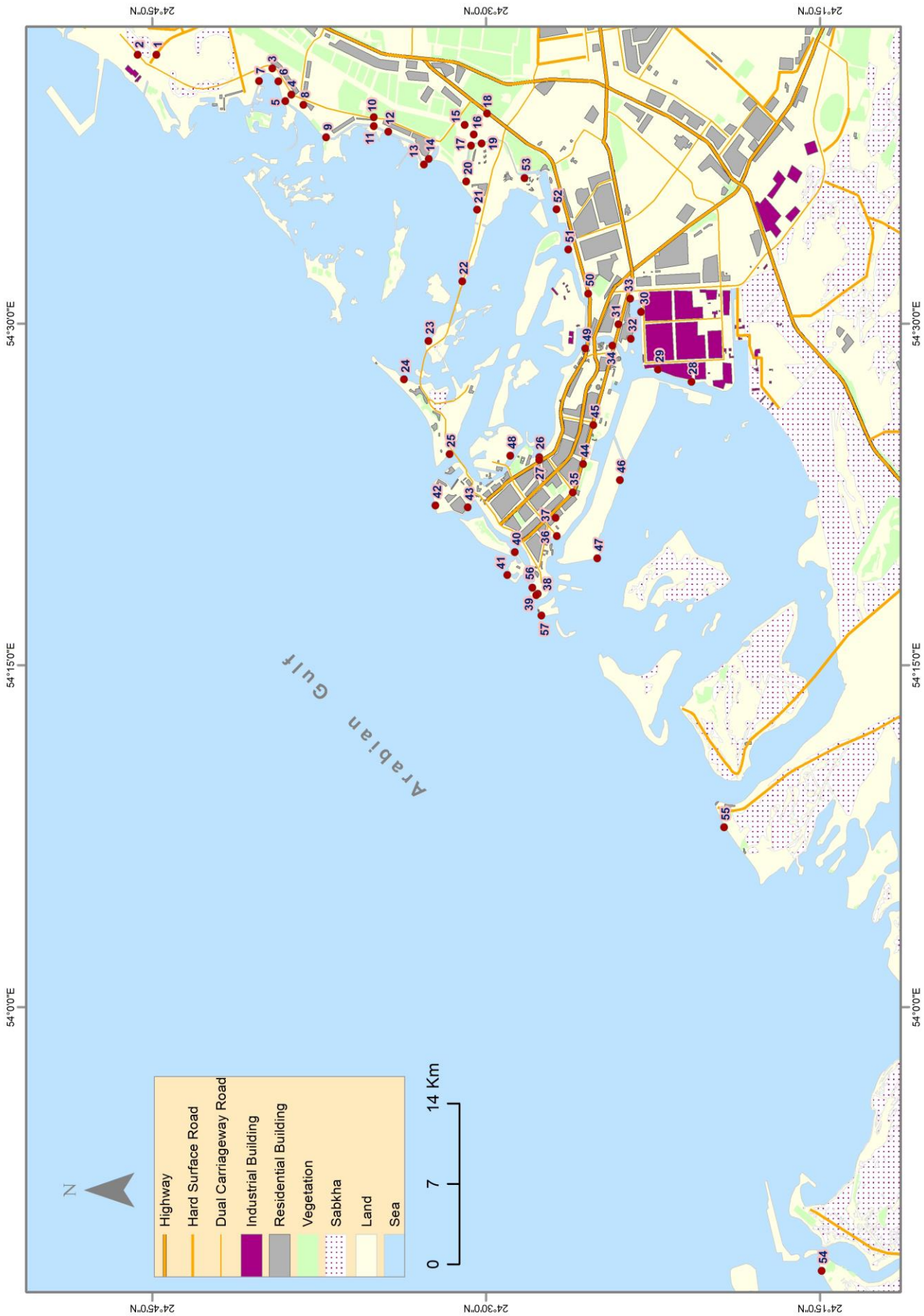


Figure 2.1. Location map of sampling sites in the study area.

2.2 Collecting samples

Samples were gathered from the beachfront, locales under the conditions of 10 cm to 15 cm long and 5.5 cm in breadth, using the dirt specimens taken after the 1981 EPA/CE-81-1 convention (Plumb, 1981). The gathered samples were taken in polyethylene packs and transported in a test holder, three to four hours after accumulation, for different investigations. Examinations were done by the Acme Labs, Canada; XRD and XRF Lab, Geology Division, College of Science, UAE University, United Arab Emirates, and Central Analytical Facilities, Stellenbosch University, South Africa.

2.3 Sample data preparation techniques and analysis

2.3.1 Sieve analysis and soil type – diagram classification

Fifty-seven samples were analysed for sieve analysis, using ASTM sieves. Part of the samples were dried using a dry oven, while others were used as reference samples; 100 gm, representing the original dry sample, was taken using a John splitter and poured into a set of sieves, arranged from coarse to fine as follows: 4, 2, 1, 0.5, 0.25, 0.125, 0.062 mm and pan. The set of sieves was fixed on a mechanical shaker. The samples were shaken for about 15 minutes. The retained weights were recorded in a form sheet used for this purpose, using a sensitive balance. The weight percentages and cumulative weight percentages were calculated for all samples and were then plotted on a ternary figure (shown in the results chapter). All samples were analysed at the geology workshop lab, Geology Department, UAE University.

2.3.2 X-ray fluorescence (XRF) spectrometry analysis

Samples were pounded into a fine powder (grain size estimate $<70 \mu\text{m}$) with a jaw crusher and processed in a tungsten-carbide Zibb process before the arrangement of an intertwined circle for major and follow components examination. The jaw crusher and plant are cleaned with clean, uncontaminated quartz between two tests to prevent cross-pollution. Glass plates were set up for XRF investigation, utilizing 10g of high virtue follow component and rare earth without element flux ($\text{LiBO}_2 = 32.83\%$, $\text{Li}_2\text{B}_4\text{O}_7 = 66.67\%$, $\text{LiI} = 0.50\%$) blended with 1g of the powder test. Entire shake significant

component organizations were dictated by XRF spectrometry on a PAN expository Axios Wave Length Dispersive spectrometer at the Central Analytical Facilities, Stellenbosch University, South Africa. The spectrometer is fitted with a Rh tube, with the accompanying breaking down precious stones: LIF200, LIF220, PE 002, Ge 111 and PX1. The instrument is fitted with a gas-stream relative counter and a glitter locator. The gas-stream corresponding counter uses a 90% Argon-10% methane blend of gas. Significant components were dissected on a melded glass plate at 50 kV and 50 mA tube working conditions. Network impacts in the samples were adjusted for by applying hypothetical alpha elements and measured line cover variables to the crude powers measured with the Super QPAN investigative programming. The convergence of the control guidelines, which were utilized as part of the alignment strategies for real component examinations, fit the scope of grouping of the specimens. Among these guidelines were NIM-G (Granite from the Council for Mineral Technology, South Africa) and BE-N (Basalt from the International Working Group). XRF was completed to the significant components examination of basic shake or soil (on intertwined dot) and real component on squeezed pellet.

X-ray fluorescence (XRF) is the emanation of trademark “auxiliary” (or fluorescent) X-ray material that has been energized by assaulting with high-vitality X-rays or gamma rays, broadly utilized for essential examination and substance examination, particularly in the examination of metals. On presentation of materials to short-wave length X-rays or to gamma rays, ionization of their particles may happen. The wave length of this fluorescent radiation is then ascertained from Planck's law:

The fluorescent radiation can be dissected either by sorting the energies of the photons (vitality dispersive investigation) or by isolating the wave lengths of the radiation (wave length-dispersive examination). The force of every trade mark radiation is straight forwardly identified with the measure of every component in the material. The aforementioned principle is the premise of a capable system in analytical chemistry.

The device used is PAN analytical Axiosm AX-Metals wave length dispersive XRF spectrometer. PAN alytical's Super Q software, was used.

2.3.3 X-ray diffraction (XRD) spectrometry analysis

An XRD analysis took place at iThemba Labs, Old Faure Road, Faure, 7131, South Africa. The XRD analysis definitely enhanced our understanding of the beach sands of Abu Dhabi. XRD analysis depends on valuable obstruction of monochromatic X-beams and a crystalline sample. The XRD strategy is portrayed in Ph. Eur 2.9.33. XRD analysis brings about a diffract ogram, demonstrating the force as a component of the diffraction points. Positive ID of a material utilizing XRD analysis depends on agreement between the diffraction points of a reference material and the specimen being referred to, to full fill Bragg's law ($n\lambda=2d \sin \theta$). This law relates the wavelength of electromagnetic radiation to the diffraction edge and the cross-section dividing a crystalline example. The trademark X-beam diffraction design normally gives a one-of-a-kind "unique finger impression" of the precious stones introduced in the specimen. Proper interpretation allows this fingerprint to identify the crystalline form.

The device used was Bruker AXS GmbH – D8 ADVANCE. Vertical theta-theta goniometer in powder XRD setting; most minimal stride measure (2θ) = 0.0002o; flat example transporter; nine-position numerous phase with programmed test changer; altered opening framework. One-dimensional identifier (Lynx Eye sort) was utilized. Copper target X-beam tube was utilized, with nickel $K\beta$ channel or with bended graphite monochromator (default setting) or molybdenum target tube – if vast dispersing vector reaches are required. DIFFRAC plus BASIC programming bundle for subjective and semi-quantitative stage investigations was utilized.

Fig's from 2.2 to 2.5 is a scatter diagram of the data, based on four groups created through cluster analysis. The four groups can be separated with CaO and SiO₂, as per the scatter plot. Based on this diagram managed us to select three (3) samples from each group. The XRD analysis had been done for the 12 samples as follows:

Group 1: samples 28, 29, 56

Group 2: samples 8, 39, 57

Group 3: samples 3, 46, 52

Group 4: samples 10, 50, 55

2.3.4 Inductively coupled plasma (ICP) analysis

Analysis were set up by assimilation, with a changed Aqua Regina arrangement of a balance of concentrated HCl, HNO₃, and DI H₂O, for one hour in a high-temperature water shower. Tests were made up to volume with diluted HCl, then from every specimen parts of 0.5g, 15g or 30g were dissected (Geochemical Aqua Regina Digestion). Also, lithochemical entire Rock Fusion was connected to prepare specimens by blending with LiBo₂/LiB₂O₇ in a flux pot and melding in a heater. The cooled dab is broken down in ACS review nitric corrosive. Miscalculation is ruled by touching off a specimen split, then measuring the weight reduction. Carbon and sulphur are controlled by leco strategy (Group 2A).

According to our targets, to study uranium, thorium and heavy metals footprints, depending on the determination of their concentration, and achieving high accuracy, inductivity coupled plasma-mass spectrometer was applied.

The ICP-MS techniques have been chosen for many reasons, such as low limits detection, high accuracy and high speed of analysis.

The instrument used was the ELAN 6100 inductivity coupled plasma mass spectrometer, Perkin Elmer SCIEX, USA. The instrument can be viewed as a system consisting of three major components (ELAN 6100, Hardware Guide, 2000). Sample analyses were carried out by the Acme Labs, Canada.

2.3.5 Data validation

Figures 2.2,2.3,2.4 and 2.5 below show an estimated analytical (precision) error of 10% for Zr, V, U and Rb for samples DH10 and 56 in the geochemical data (see Appendix A). With the specific end goal to decide the heterogeneity of the testing material and the explanatory exactness, replications were conducted against the first test for major and follow component information. The results show that the data for V and Rb are precise for both samples as there is not much difference between the original and the duplicate, while for U and Zr, one sample plots outside the control lines, indicating

some degree of contamination during preparation of that specific sample.

Notwithstanding this heterogeneity of a few samples, this information can be utilized with an exceptional degree of certainty. Comparable results between the original and the duplicate indicate that analytical variability controls precision.

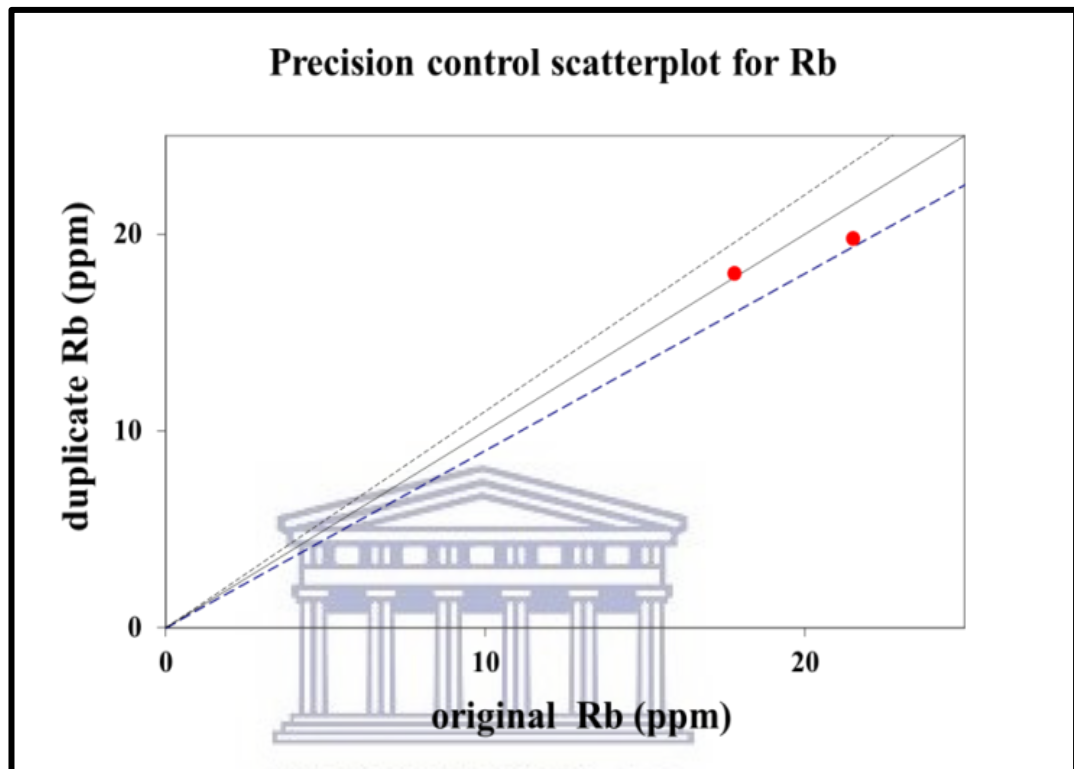


Figure 2.2. Precision control scatterplot for V at 10% precision.

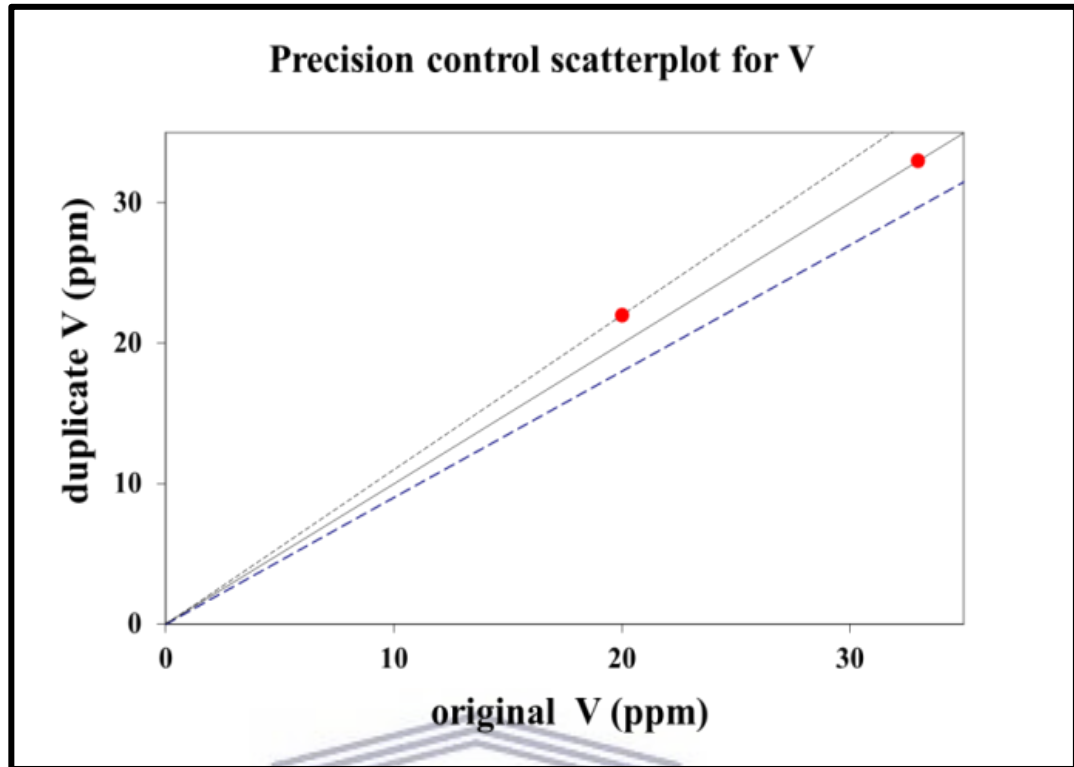


Figure 2.3. Precision control scatterplot for Rb at 10% precision.

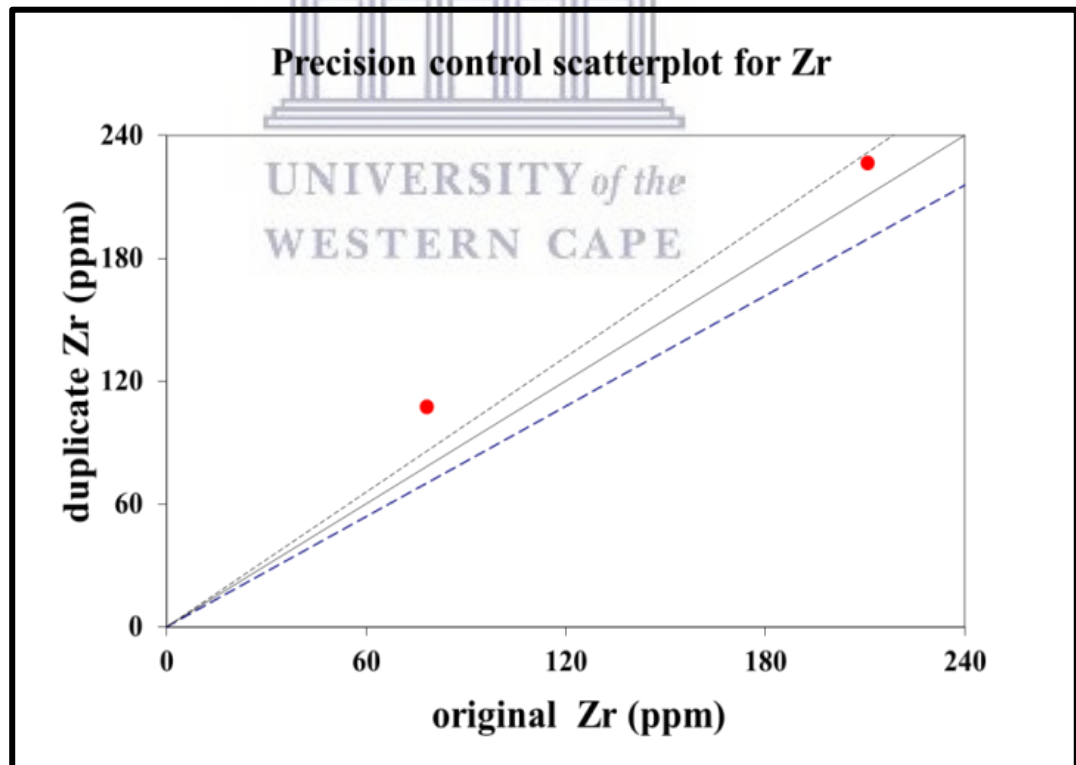


Figure 2.4. Precision control scatterplot for Zr at 10% precision.

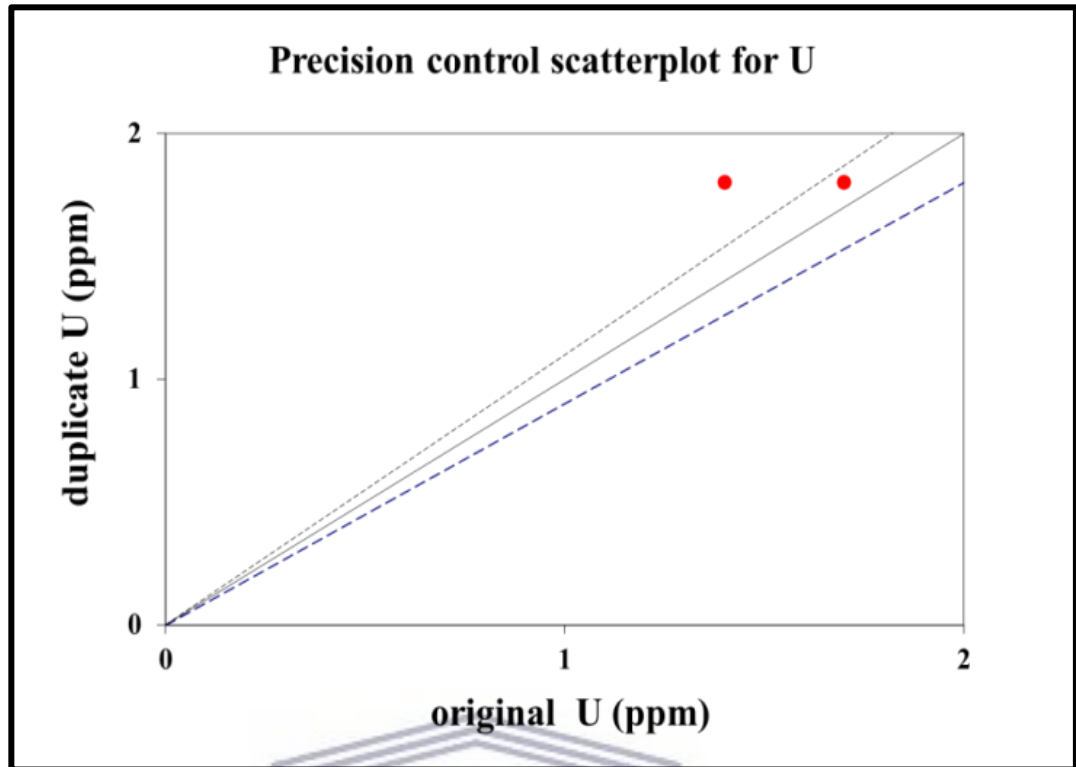


Figure 2.5. Precision control scatterplot for U at 10% precision.

2.4 Sedimentology

2.4.1 Grain size analysis

The primary motivation behind the sieve analysis of shoreline soil is to determine and comprehend their granulometric attributes and textural properties. There are several techniques for the size analysis of soil: the most widely used are sieve analysis, the one used for sand and gravel, which has been discussed in section 2.3.1.

The weight percentages and cumulative weight percentages were calculated for each sieve, using the following equation (Ibe, K.K. S. I. Ibeneme, Y. E. Obioha, I. O. Eze, I. L. Ibeneme, H. O. Israe, B. O. Ubechu, C. O. Nlemadim (2013)):

$$\text{Weight \%} = (\text{weight retained}/\text{total weight}) * 100,$$

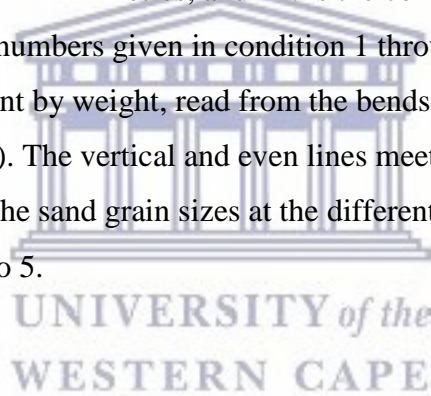
Where the Cumulative weight % for the 1st = 1st Wt. %

2ndWt. % = the 1st +2nd

3rd Wt. % =Sum. Of 1st +2nd+3rd

Wt. %etc.

The device used was the Fritsch mechanical shaker, together with ASTM Sieves. The ternary diagram shows the plotting of the grain size analysis for the 57 samples (After Folk 1974). The sand test portion held in every sifter was weighed and changed over into its total recurrence rate. The sample total rate qualities were then used to plot the relating total recurrence bends, shown in Fig. 2.2 and Fig. 2.3. Fig. 2.4 is a superimposed aggregate recurrence bend of the considerable number of tests considered in this analysis. The previously mentioned bends (Fig. 2.2 to Fig. 2.5), and condition 1 through condition 5 were then used to ascertain the measurable parameters. (D) is the grain diameter, measured in millimetres, and LN is the common logarithm of the base 2.7182818. The outright numbers given in condition 1 through condition 5 indicate to the total recurrence percent by weight, read from the bends at specific grain estimate units, measured in Phi (~). The vertical and even lines meeting the bends in Fig. 2.2 through Fig.2.5 indicate the sand grain sizes at the different total recurrence percent, indicated in condition 1 to 5.



The median (M_d)

$$M_d = \varphi_{50} \quad (\text{Equation 1})$$

The mean (M_z)

$$M_z = \frac{\varphi_{16} + \varphi_{50} + \varphi_{84}}{3} \quad (\text{Equation 2})$$

The graphic standard deviation (Sorting) (σ_1)

$$\sigma_1 = \frac{\varphi_{84} - \varphi_{16}}{4} + \frac{\varphi_{95} - \varphi_5}{6.6} \quad (\text{Equation 3})$$

The graphic skewness(SK_1)

$$S_{k1} = \frac{\varphi_{16} + \varphi_{16} - 2\varphi_{50}}{2(\varphi_{84} - \varphi_{16})} + \frac{\varphi_{50} + \varphi_{95} - 2\varphi_{50}}{2(\varphi_{95} - \varphi_{50})} \quad (\text{Equation 4})$$

The graphic kurtosis (KG_1)

$$K_G = \frac{\varphi_{95} - \varphi_5}{2.44(\varphi_{75} - \varphi_{25})} \quad (\text{Equation 5})$$

(Ibe, *et al.* (2013))

2.5 Mineralogical analysis

The mineralogical structure analysis of 12 shoreline sand specimens was done utilizing the Bruker AXA D8 Advance X-ray diffraction spectrometry (XRD) machine, in bolted coupled mode at Ithemba Labs. These 12 tests were chosen in view of the diverse structure and provenance of the specimen.

For every sample, 1.2 g of powder was stored in the focal point of the specimen holder, which comprised a 20-mm corning glass (tube voltage: 40 Kv, tube current: 40mA, sediment framework: V20 variable opening). The powder was easily straightened into a plate state of 15 mm width and 1mm thickness by method, for round movement of a magnifying instrument glass slide, until the zero level for a proper sample height was accomplished.

2.6 Geochemistry and mineralogical analysis.

2.6.1 Major oxides

The real oxides of materials of generally contrasting organization, for example, silicates, carbonates, sulphates and phosphates, are resolved quickly at levels from under 0.01% to 100%. The convergences of a few oxides (wt. %) in the shoreline tests are given in the result section.

2.6.1.1 Follow elements and radioactive elements

All fifty-seven samples collected from the study area were analysed by using inductively coupled plasma mass spectroscopy (ICP-MS), to determine the convergence of uranium, thorium and metals in them.

2.6.2 Univariate analysis

Geochemical variables of beach sediment samples were analysed using IBM SPSS statistics (IBM, 2012). This software was significant for determining the descriptive statistics for beach sand samples that provide information on the minimum, maximum, mean, and standard deviation. The first step of the univariate data analysis was to examine the frequency distribution of the data set, using frequency histograms, as well as, a statistical summary table with the minimum, maximum, mean, and standard deviation. Another common approach that was used to address the skewness of the data was to transform the geochemical data to a normal distribution pattern using a simple lognormal (\log_{10}) transformation, in order to see if the data would still be normally distributed.

2.6.3 Bivariate analysis

2.6.3.1 Correlation analysis

Correlation analysis produces a relationship from an arrangement of factors and shows them as a grid. This sort of investigation lends quality and gives an indication of the relationship between two factors. Twenty-six noteworthy, minor and follow components from the shoreline sand tests were examined for their interrelation, utilizing the bivariate connections strategy, with the Pearson correlation coefficient and a two-fold trial of noteworthiness, utilizing SPSS 21® [IBM Corp. IBM SPSS, 2012].

Additionally, scatter plots of CaO , Al_2O_3 and SiO_2 , against all major and trace elements, were studied. A ternary diagram of the three major components, i.e., CaO , SiO_2 and Al_2O_3 was plotted to discover the dominant sediment types.

2.6.4 Multivariate analysis

2.6.4.1 Factor analysis

Considering the investigation is a multivariate factual system, that takes into consideration various factors between connected samples. This investigation decreased into smaller measurements called elements, with minimal loss of data (Suk and Lee, 1999). Given the multivariate factual technique, the investigation delivers the general relationship between factors by indicating multivariate examples that may characterize the initial information. With element examination, the arrangements of factors having solid relations with each other are identified with fundamental components called basic variables. The primary regular variable is connected to the eigenvalue, having the most noteworthy commitment to the covariance relationship. The second basic component, orthogonal to begin with, has the second most noteworthy commitment to the relationship. Understanding the variables yields knowledge of the fundamental procedures, which may represent the circulation of geochemical tests.

An important part of the investigation strategy was utilized as extraction technique to change the arrangement of observed reliant factors into an orthogonal arrangement of factors, called main segments (Matalas and Reihner, 1967). The subsequent primary parts represented the fluctuation of the observed factors in a manner that the principal segment represented however much as could reasonably be expected of the difference and the succeeding segments, which clarified the remaining change, not represented by the previous segment in a comparable way.

The underlying element loadings acquired by the foremost part of the examination are, ordinarily, too exaggerated to unveil the fundamental structure of the observed factors, as a result of certain scientific conditions, for example, the fluctuation and properties of the key segment. To uncover this structure better, the basic variable connected with the underlying arrangement of loadings was directly changed into another arrangement of normal components, connected with another arrangement of loadings, by element revolution (Suk and Lee, 1999). Kaiser's plan, called the Varimax pivot, was utilized to create an arrangement of loadings with the end goal that the

fluctuation of the square of the loadings turns into the most extreme. In this examination, the element scores were obtained through relapse strategy (Johnson and Wichern, 1992).

The question around how many factors ought to be rotated is a common one faced during factor analysis. One method of selecting the number of factors is by using their eigenvalues. The common guideline is that only factors whose eigenvalues are greater than one are selected. Afifi and Clarke (1990) expressed that this technique created approximately one component for each three to five factors and looked to evaluate accurately the quantity of elements if the communalities were high and the quantity of factors was not great. Cattell (1978) argued that this method severely underestimated the number of factors in large matrices and supported the use of the scree plot method. This method involves creating a scree plot against the eigenvalues and selecting the point where the slope changes as the cut-off point for deciding the number of factors.

Figure scores are regularly obtained in two ways: the weighted minimum squares strategy and the relapse technique. The latter was utilized as part of the theory, in order to ascertain the variable scores.

2.6.4.2 Cluster analysis

In analysis, placing items in fairly homogenous gatherings in a way that the connection between gatherings is uncovered is called “arrangement” (Davis, 1979). Group examination is an exploratory technique for information mining, sorted into order. The essential point of group investigation is the gathering of an accumulation of various articles or substances into subsets, to such an extent that the items inside every subset have the same measurable relationship, yet the articles in one subset are not quite the same as those in another (Pirkle *et al.*, 1984).

Gathering the comparable examples on which numerous estimations have been made, and measuring the level of closeness between the gatherings, has been alluring in some geological studies. Group examination, a strategy created by analysts as a technique for looking for connections in an information set, has presumably been a standout amongst the most valuable measurable apparatuses accessible to geologists (Prayet *et al.*, 1966).

In this study, group investigation has been utilized to comprehend the dispersion of shoreline residue tests. A decent result of group examination would bring about various groups. Tests in a group are fundamentally the same as each other, though tests in various bunches are not the same as those in alternate groups. The after-effects of the bunch investigation can be effortlessly comprehended and translated, as they are shown as two-dimensional in multi-level outline called a dendogram (Templ *et al.*, 2008).

Cluster analysis requires a two-step process. First, a similarity analysis should be done between all samples and the results should be shown in a symmetric matrix called a similarity (or dissimilarity) matrix; then most similar items are clustered first and then the collective results of linking similar samples and sample clusters are shown on dendograms.

Cluster analysis is a clear and intelligent examination that does a couple by-match correlation between tests, items or factors. There are two approaches to cluster analysis to choose from, depending on whether you want to link samples or variables.

R-mode analysis is used to see which variables are more often co-occur. Q-mode analysis is used to see which samples are most similar or dissimilar (Pray, 1966). In this study, Q-mode analysis is chosen to group beach sediment samples, based on their geochemical characteristics.

2.6.4.3 Clustering methods

A huge number of various bunching techniques exist. The aim of these techniques is to gather perceptions into groups. On the off chance that every perception is dispensed into only one bunch, this is called parceling. Apportioning will bring about a pre-characterized number of groups, utilized by an agent. Then again, it is additionally conceivable to develop a chain of command of parcels, which is called various-levelled bunching. Various-levelled strategies and apportioning techniques are the most well-known bunching techniques and will be examined in detail beneath.

2.6.4.4 Hierarchical methods

Progressive techniques begin by treating N items to be grouped as N bunches independently; at the end of the day, every protest is at first considered as a bunch. The $(n-1)/2$ separations or similitudes among the N items are analysed and, by gathering the two closest or comparable protests together, new groups are developed. This system of treating N items is rehased until all N articles are in one group (Pirkle *et al.*, 1984). Removal in group investigation has nothing to do with geographic separation between two perceptions. It is a measure of similitude or divergence between perceptions in the multivariate space, characterized by entered factors (Templ *et al.*, 2008). An agglomerative calculation begins with every perception having its own class. At that point, at every progression of the calculation, most comparable classes are consolidated. Toward the end of the procedure there is a stand-out bunch, which contains all perceptions. A separation, or closeness lattice, is a contribution to the clear majority of the progressive bunching calculations. A group comes about for progressive strategies, represented by a dendogram (Temple *et al.*, 2008).

2.6.4.5 Partitioning methods

Differently various-levelled bunching techniques, apportioning strategies begin with an underlying division of the information, pre-characterized by the client. After that, by utilizing different iterative plans, a gathering is resolved that upgrades a measure, mirroring the homogeneity of the groups (Pirkle *et al.*, 1984). K-means is the most prominent apportioning calculation. K-means expects to minimize the normal, squared separation between the perceptions and their group centroids.

2.6.4.6 Discriminant analysis

Discriminant Analysis (DA) utilizes an arrangement of methods to separate gatherings of information and to allot new perceptions into the current gatherings. DA perceives the most critical parameters in charge of separating gatherings or bunches (at least two) from a substantial dataset, and, in this way, realizes huge dimensionality or information lessening.

For this study, the groups (or clusters) provided from cluster analysis were combined as dependent variables, with their respective geochemical data as independent variables, into discriminant analysis (linear and stepwise). The main aim was to characterize these clusters by identifying the variables that differentiate between them, and to develop functions to calculate new variables as a measure of the difference between them (Soldić-Aleksić, 2001). The above technique used the Wilk's Lambda method of classification.

2.6.4.7 Linear discriminant analysis

Most geochemical factors are measured on a consistent proportion scale. In any case, their definitive capacity for the agent is as a guide to changing them to all-out factors, which may have as few as two values in the entire information set.

These factors can be managed by utilizing discriminant analysis. This analysis method is connected to conditions where there are pre-characterized "preparing sets" speaking to classes, which contrast in some vital, detectable and critical trademark. From the multivariate perceptions that make up these preparation sets, a progression of discriminant capacities is determined, one for every characterized class. Arranging the capacities on a solitary sample delivers a progression of lists, known as discriminant scores. The class whose discriminant score is most noteworthy is the one to which that example would be distributed. The discriminant capacities are characterized as:

$D_j = a_{j1}X_1 + a_{j2}X_2 \dots \dots \dots - t - a_{jp}X_p$, where X_1, X_2 and X_p are the discriminant factors, a_{j1}, a_{j2} and a_{jp} are the discriminant work coefficients, D_j =the discriminant score of the projection through the information, along which the populaces demonstrate the best detachment (Alperen *et al.* (2016)).

The strategy is helpful in two-aggregate conditions where appropriate preparing sets are accessible and it is important to separate and order "terrigenous" and "marine", or "defiled" and "uncontaminated", "very mineralized" and "less mineralized" tests, as shown by Clausen and Harpoth (1983), where these attributes are not specifically discernible in routine specimen. The system is likewise fitting where more than two gatherings are recognized (for instance, when various geochemical factors are available

inside broken-up constituents of the groundwater, which is the truth of shoreline residue science).

The technique is also appropriate where more than two groups are identified (for example, when multiple geochemical variables are present within dissolved constituents of the groundwater, which is the reality of beach sediment chemistry).

The use of discriminant analysis in this thesis is aimed at understanding the geochemistry of the beach sediment along the Abu Dhabi coastline and to determine the source of sediment in the study area.

2.6.4.8 Stepwise discriminant analysis

The quantitative and subjective impact of the factors on the right arrangement rate of the aggregate populace and the individual gatherings was analysed in a stepwise discriminant examination. At the point of utilizing the strategy, factors are chosen through a measurable test to choose the request in which they are incorporated (entered/expelled) in the examination. At every progression, the component that created the best arrangement was entered; along these lines, it was conceivable to test:

The geochemical factors are expected to depict the individual elemental results in the study zone, with some particular geochemical facies, and to determine which factors have the best and the smallest significance in the grouping, as well as the impact of individual factors on the depiction of the individual gatherings.

2.7 Enrichment factor (EF) analysis and index of geoaccumulation (Igeo)

2.7.1 Enrichment factor analysis

In the present study, the enrichment factor (EF) is utilized to evaluate the level of tainting and the conceivable anthropogenic effect on the shoreline sand of Abu Dhabi. To distinguish up normal metal concentration, the geochemical standardization of the metal information to a traditionalist component, for example, Al, Fe, or Si, is utilized. The EF system is utilized as part of the territory of environmentally-pressurizing

elements, such as canned products, residue, soil and strong squanders, to decide the level of alteration (Pekey, 2006).

A few studies have effectively utilized Al and Fe to standardize metal contaminants (Leal-Acosta *et al.*, 2013; Schiff and Weisberg, 1999; BaptistaNeto *et al.*, 2000; Mucha *et al.*, 2003; Conrad and Chisholm-Brause, 2004; Cevik *et al.*, 2009; Meza-Figueroa *et al.*, 2009; Bhuiyanet *al.*, 2010; Esen *et al.*, 2010). In the present study, the advancement variables for components were computed utilizing the Earth's crustal normal (Taylor, 1964) with Al as the normalizing component (Salomons and Förstner, 1984):

$EF = (\text{element}/Al)_{\text{sample}} / (\text{element}/Al)_{\text{background}}$, where EF is the enrichment factor and $(\text{element}/Al)_{\text{sample}}$ is the ratio between trace element and aluminium content in a sediment sample, and $(\text{element}/Al)_{\text{crust}}$ is the ratio between trace element and aluminium average abundance in the continental crust (Taylor, 1964).

The background concentrations of Fe, Cr, Sr, Cu, Zn, Pb, Hg, Cr, Cd, Th, U and Al in the average crustal abundance obtained from Taylor (1964) are used in this study (Table 2.1). Birch (2003) divided contamination into different categories based on EF, as shown in Table 2.2.

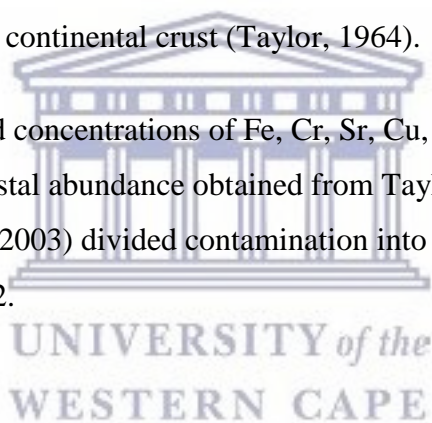


Table 2.1. Geochemical composition of beach sand collected from Abu Dhabi.

Variable	Mean	St. Deviation	Minimum	Maximum	Average crustal abundance Taylor, ppm (1964).
Al	2.23	1.09	0.36	4.42	8.23%
Fe	0.89	0.42	0.22	2.15	5.60
As	2.85	0.78	1.40	5.10	1.8
Cd	0.12	0.05	0.10	0.30	0.2
Co	4.31	2.05	0.40	12.90	25
Cr	272.48	182.17	0.001	752.62	102
Cu	4.04	1.72	1.80	13.50	55
Hg	0.02	0.01	0.01	0.04	80
Ni	29.94	22.80	3.50	118.20	75
Pb	2.26	1.56	0.90	10.40	14
Sr	2434.02	1563.41	560.90	7243.60	370
Th	1.37	0.50	0.20	2.50	9.6
U	2.34	0.84	1.30	4.60	2.7
V	29.05	9.53	9.00	47.00	85
Zn	9.00	5.79	2.00	35.00	70
Zr	91.14	61.86	11.60	300.10	-

Table 2.2. Enrichment factor categories, after Birch (2003)

Enrichment Factor (EF)	Categories
<1	No Enrichment
1 – 3	Minor enrichment
3 – 5	Moderate Enrichment
5 – 10	Moderate sever enrichment
10 – 25	Severe enrichment
25 – 50	Very severe enrichment
>50	Extremely severe enrichment

2.7.2 Index of Geo-accumulation (Igeo)

To comprehend the current ecological status and the degree of metal pollution concerning regular habitat, different methodologies ought to be likewise connected. A typical foundation to assess the overwhelming metal contamination in shoreline sand is the geoaccumulation file (Igeo) in Table 2.3, which was initially characterized by Muller

(1969) to decide metal defilement in dregs, by contrasting current fixations and pre-industrial levels, and can be computed by the accompanying condition:

$I_{geo} = \log_2 (C_n/1.5*B_n)$, where C_n is the deliberate convergence of component N in the shoreline sand test and B_n is the geochemical foundation for the component N, which is either specifically measured in pre-human progress silt of the territory, or taken from the writing (normal crustal plenitude). The component 1.5 relates to the conceivable variety of the foundation values that are the result of lithogenic varieties. Muller (1981) proposed seven evaluations or classes of the geo-amassing list. Distinctive geo-aggregation file classes, alongside the related dregs quality, are given in the relevant table. The most astounding class (class 6) reflects 64-overlay improvement over the foundation values (Singh *et al.*, 1997).

Table 2.3. Index of geo-accumulation class with associated sand/sediment quality.

Igeo	Igeo class	Sediment Quality
0 – 0	0	Unpolluted
0 – 1	1	Unpolluted to moderately polluted
1 – 2	2	Moderately polluted
2 – 3	3	Moderately polluted to highly polluted
3 – 4	4	Highly polluted
4 – 5	5	Highly polluted to very highly polluted
5 – 6	>5	Very highly polluted

2.8 Spatial analysis

2.8.1 Spatial data preparation

Information arrangement was done utilizing the ArcCatalog10.1, ArcMap 10.1 and the spatial analyst expansion of ArcGIS 10.1 from ESRI®. Test-point information was foreign, made into ArcMap, utilizing the scope and longitude arrangements captured by utilizing a hand-held GPS instrument, as part of the field work and anticipated utilizing of the WGS_1984_UTM_Zone_39 and 40 N anticipated organized framework. With the end goal of elucidation of sample information and factual examination of the factors, diverse maps were made, utilizing distinctive sources. Every one of the distinctive

sources was anticipated by utilizing the previously mentioned facilitation framework, with the WGS_1984 datum.

The soil review of the Abu Dhabi Emirate, actualized by the Environment Agency- Abu Dhabi vector information (EAD,2002), was utilized for showing nearby land cover and land use data of the study region. These vector files were analysed in ArcMap 10.0 and the area of interest was extracted, using the results of sampling points. Some of the land cover attributes of these vector files were edited to simplify the display of legends created for land use maps.

2.8.2 Spatial data presentation

Data presentation was done using the spatial analyst module of ArcGIS 10.0 from ESRI®. Based on the spatial distribution of the sample's location, univariate and multivariate statistical analysis encompassing the following were created for interpretation purposes: different maps displaying heavy metals, thorium and uranium concentrations, factor score results, geo-accumulation and enrichment factor, as compared and related to geology and land use. The spatial distribution of the XRF results was shown using proportional symbology in ArcMap to indicate the exact concentration values using symbol sizes. This display method was used for enhancing the actual concentration differences of the elements in the different sample locations. The overwhelming metal fixations of thorium and uranium were demonstrated utilizing graduated images, as part of a request to show the relative estimations of their focus, because of the extensive scope of these particles. Similarly, the factor score results, geoaccumulation and enrichment factor were also represented and shown using the same methodology as the heavy metals thorium and uranium. IDW interpolation explicitly implements the assumption that things that are close to one another are more alike than those that are farther apart. This assumption about the relationship between distance and similarity is based on Tobler's First Law of Geography, which states, "Everything is related to everything else, but near things are more related than distant things." Tobler's law was used to predict values for unmeasured locations in the study area, by using the measured values closest to these locations.

In inverse distance weighted (IDW) interpolation, weights are computed by taking the inverse of the distance from an observation's location to the location of the point being estimated. In this interpolation, the optimal power (p) was raised to three, in order to model a cubed geometry that gives better interpolation, compared to lower powers. This power controls the hugeness of encompassing focuses on the added esteem, where a higher power brings about less impact from inaccessible focuses and it is controlled by minimizing the root mean square expectation mistake (RMSPE) through a factual strategy known as cross-validation. The computed weights are proportional to the inverse distance (λ_i) raised to the power value (p). A variable search radius with the 12 nearest sample points and the default value of the map's diagonal extent length (in map units) was used to perform the interpolation. A polyline feature derived from the topography feature of the study area was utilized as an obstruction, in order to break or limit the search for input sample points beyond 900m elevation, excluding areas like the Nuweveld Mountains and above 900m altitudes of some of the dolerite outcrops.

The interpolation uses the following equation in measuring the unknown values from the known measurements.

$z(x) = \frac{\sum_i w_i z_i}{\sum_i w_i}$ where $z(x)$ (Hugo Raguet *et al.* (2013)) is the unknown or unmeasured value; z_i is the known measurements; w_i is the weight of the measured value; x is the point of interest; i runs from 1 to n (number of data points). The weights can be defined using various methods and the option most employed is computing them, using the inverse of the distance raised to a power. In this method, the power was raised to three and the weights were computed in ArcGIS, as in this equation.

$$w_i = 1 \div d_i^3$$

Where d is the distance from x_i to x .

Chapter III

3.0 Results

The following chapters present and discuss the sedimentological, geochemical, mineralogical and the multivariate statistical results of the beach sediments of Abu Dhabi, respectively. As mentioned in the introduction chapter, this study aims to classify these sediments, to determine their provenance and possibly their depositional environments, and lastly to assess their heavy metal and radiogenic element contents.

3.1 Sedimentology and depositional environment

Grain size analysis was carried out to construct histograms and cumulative curves and interpret the grain-size frequency distribution in the studied beach samples. Moreover, the cumulative curves were used to calculate the grain-size statistical parameters, such as mean size (M_z), inclusive standard deviation (σ_I), skewness (S_{ki}) and kurtosis (K_G) after Folk and Ward (1957).

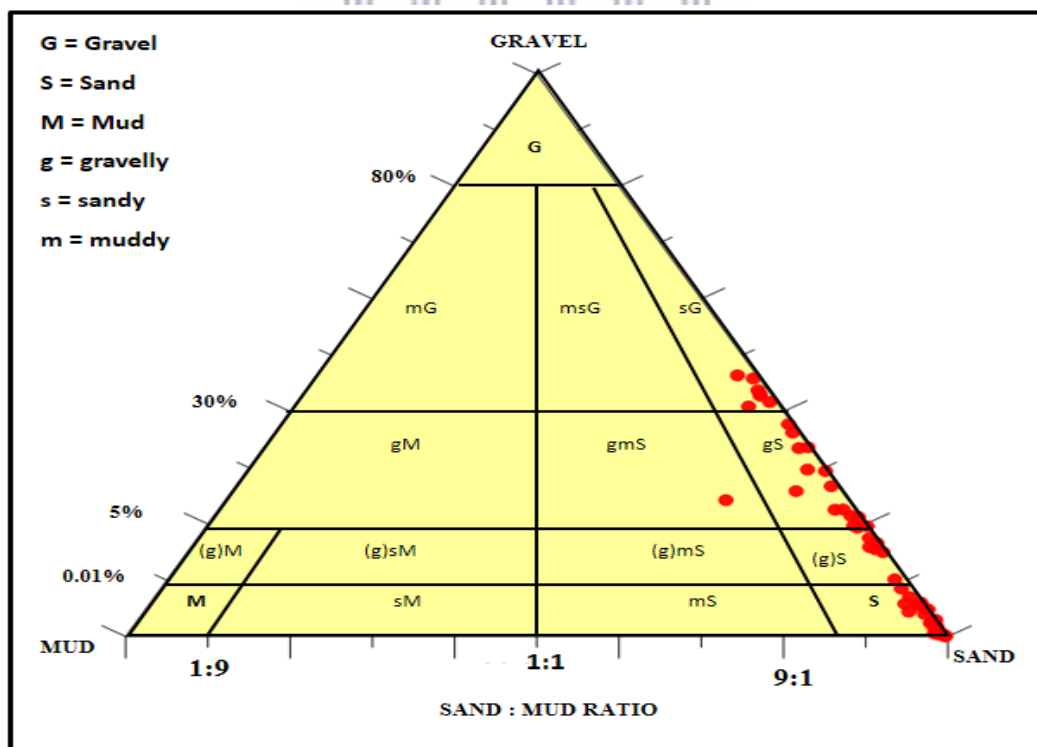


Figure 3.1. Trilinear plot sieve analysis of the samples.

3.1.1 Mean size (Mz)

The parameter reflects the overall average size of the beach samples, which is influenced by the beach samples source, mode of transportation and environment of deposition (Udden 1914; Folk, 1966). The measured values of mean size in the coastal samples of the study area (Table A1 in Appendix A and Figure 3.2) range between -2.63 (pebble size) to 2.39 (fine sand) with an average value of -0.12 (coarse sand) (AlRashdi and Siad, 2016 b). Table 3.1 and Figure 3.1 show that most the samples (56.14%) are medium and coarse sand size.

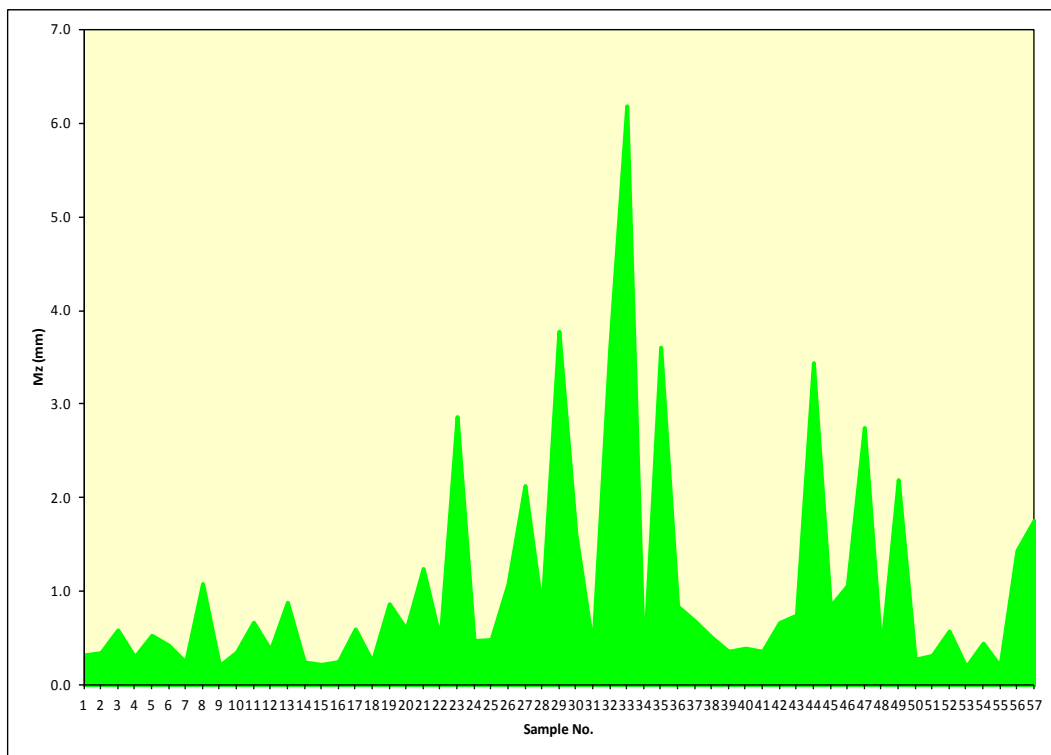


Figure 3.2. shows the mean size of the collected samples from the study area.

3.1.2 Inclusive standard deviation (σI)

The inclusive standard deviation is a measure of the uniformity of grain-size distribution within the beach samples. The standard deviation depends on the size range in the source rock, extent of weathering, distance of transportation and the energy variation of the depositing medium (Folk & Ward, 1957; Amaral and Prayor, 1977). The standard deviation of the coastal samples along the study area in Table A1(Appendix A) ranges between 0.51 (moderately well sorted) to 6.53 (extremely poorly sorted), Figure 3.3. The average value of σI is 1 Φ (poorly sorted). The frequency distribution of the beach samples among the sorting classes (Table 3.1)

reveals that the moderately and very poorly sorted samples are equally distributed (70.18%) and higher than the poorly sorted samples (17.54%). On the other hand, the very poorly and extremely poorly sorted classes are equal and less abundant (12.28%).

3.1.3 Skewness (Ski)

According to the parameters of geological processes (Folk, 1966), the lowest value of skewness in the beach samples is -0.86 (very coarse, skewed), while the highest value is 0.1 (near symmetrical). The average value of Ski -0.38 falls into the coarse skewness class (negative). Table A1 (Appendix A) and Table 3.1 show that the coarse, skewed beach samples are the most strongly coarse/skewed (54.39%). Meanwhile, the near symmetrical and coarsely skewed sediments are equally abundant (43.86 % for each). The less abundant skewness class is the fine skewed (1.75%).

3.1.4 Kurtosis (K_G)

This parameter measures the normality of grain size distribution, using the ratio of sorting in the central part of the curve to that in its extremities (Folk, 1966). The beach samples show kurtosis values ranging from 6.75 (extremely leptokurtic) to 0.80 (platykurtic) with an average value of 3.77. Table A1 (Appendix A) represents the very leptokurtic class. According to the kurtosis scale, 33.33% of the samples have mesokurtic curves of distribution and 28.07% of the samples have leptokurtic curves. The very platykurtic and platykurtic samples are equally abundant (36.85%). The rest of the samples have extremely leptokurtic curves (Table 3.1)

Table 3.1. Size percentage values of the samples from the study area.

Parameter	Description	Percentage of Samples
Mean	Pebble	1.75
	Granule	14.04
	Very Coarse Sand	12.28
	Coarse Sand	26.32
	Medium Sand	29.82
	Fine Sand	15.79
Sorting	very well sorted	0.00
	well sorted	0.00
	moderately well sorted	0.00
	Moderately Sorted	31.58
	Poorly Sorted	17.54
	Very Poorly Sorted	38.60
	Extremely Poorly Sorted	12.28
Skewness	strongly fine-skewed	0.00
	Fine Skewed	1.75
	Nearly Symmetrical	8.77
	Coarsely Skewed	35.09
	Strongly Coarse – Skewed	54.39
Kurtosis	Very Platykurtic	22.81
	Platykurtic	14.04
	Mesokurtic	33.33
	Leptokurtic	28.07
	very leptokurtic	0.00
	Extremely Leptokurtic	1.75

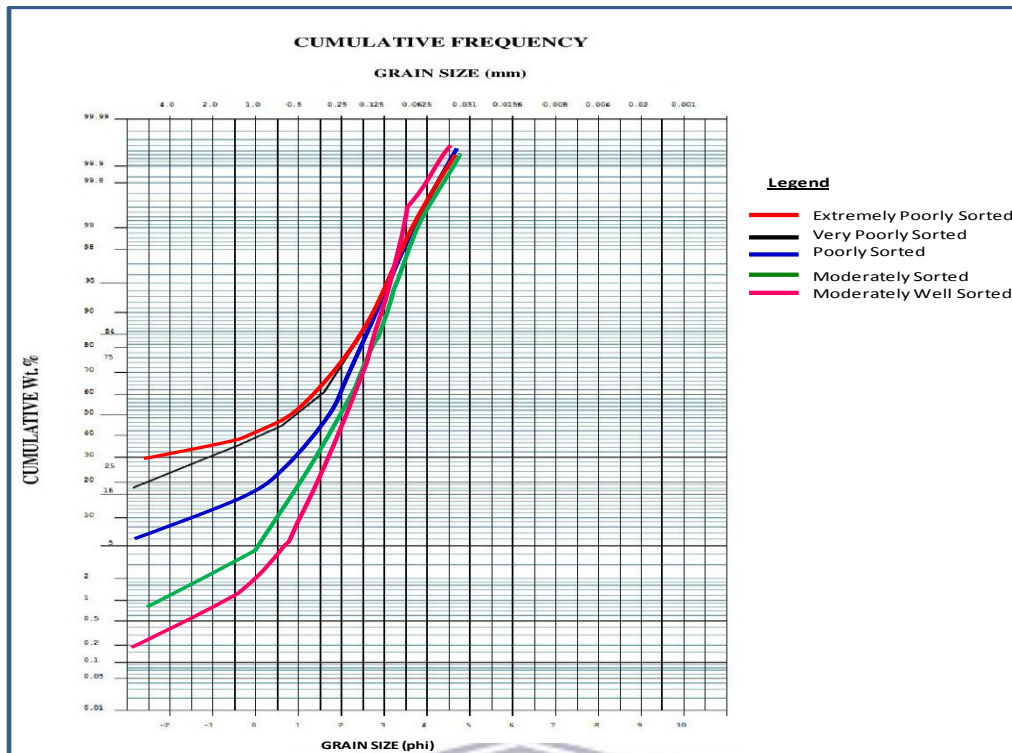


Figure 3.3. Classification of average cumulative curves, according to sorting values as the following: Extremely poorly sorted (29, 32, 33, 35, 44, 47, 57); Very poorly sorted (3, 8, 13, 17, 19, 20, 21, 22, 23, 26, 27, 28, 30, 36, 37, 42, 43, 45, 46, 49, 52, 56); Poorly sorted (4, 6, 10, 12, 18, 25, 31, 38, 39, 51); Moderately sorted (1, 2, 5, 7, 11, 15, 24, 34, 48, 50, 54); Moderately well sorted (9, 14, 16, 40, 41, 53, 55).

3.1.5 Bivariate scatter graphs of grain size parameters

Attempts to discriminate between different depositional settings, via bivariate plots, are based on the assumption that these statistical parameters reliably reflect differences in the fluid-flow mechanisms of sediment transportation and deposition (Sutherland and Lee, 1994). There is some covariance between mean grain size and sorting (Tucker, 1990). Griffiths (1967) explained that both mean grain size and sorting are hydraulically controlled, so that in all sedimentary environments the best sorted sediments have mean grain size in the fine sand size range. This energy-related universal relationship has been confirmed by many subsequent studies (Tucker, 1990 and AlRashdi and Siad, 2016 a). There is an obvious general trend for the sorting values to increase (i.e. for progressively poorer sorting) as mean grain size increases.

Plotting of skewness against kurtosis is a powerful tool for interpreting the genesis of sediment, by quantifying the degree of normality of its size distribution (Folk, 1974).

Tucker (1990) said that among the relatively fine-grained unimodal deposits from many parts of the world, beach sands are well sorted and negatively skewed, while river sands are less well sorted and usually positively skewed. Dune sand typically has positive skewness, but is finer grained than beach sand. Generally, most beach sediments are slightly negatively skewed because of the presence of a small proportion of coarse grains (coarse “tail”) (Folk, 1974). Friedman (1962) showed that most sands are leptokurtic and either positively or negatively skewed, which could be explained by the fact that most sands consist of two populations; one predominant, and the other very subordinate, coarse (leading to negative skewness), or fine (leading to positive skewness).

Figure 3.4 shows the relationship between mean grain size (ϕ) and sorting for the collected samples. Sediments of the collected samples are mostly within the medium to coarse sand range, and few samples are within fine sand, but also mainly lie in the range of moderately to poorly sorted sediments.

The relationship between skewness and sorting of the collected samples range mainly from moderately to poorly sorted sediments, and most of the samples have negative skewness values, with few samples near symmetrical (Figure 3.5). Coarse fractions may be due to the presence of shell fragments and rock fragments. It is clear from plotting the relationship between skewness and kurtosis that most of the sediments from the collected samples lay within the negative skewness and kurtosis range from the mesokurtic to leptokurtic field, with few samples platykurtic (Figure 3.6). This relationship between skewness and kurtosis suggests the dominance of a sand population with the presence of a subordinate population of coarse-grained particles.

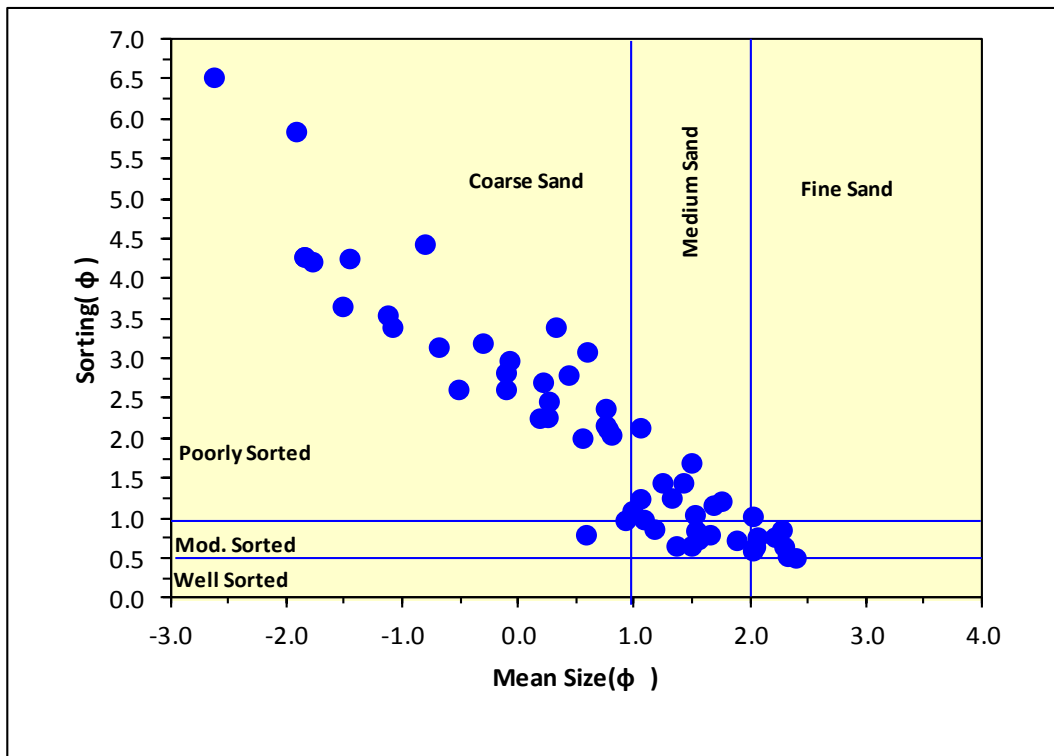


Figure 3.4. Sector plot showing the bivariate relationship between grain size (ϕ) and sorting.

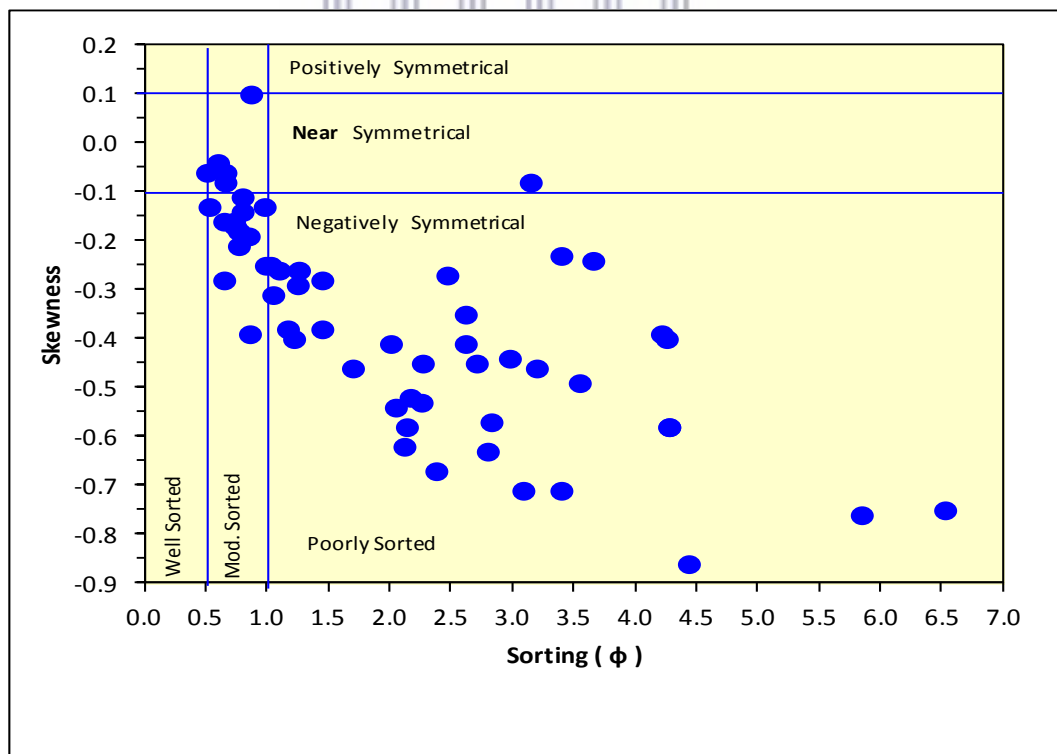


Figure 3.5. Sector plot showing the bivariate relationship between skewness and sorting.

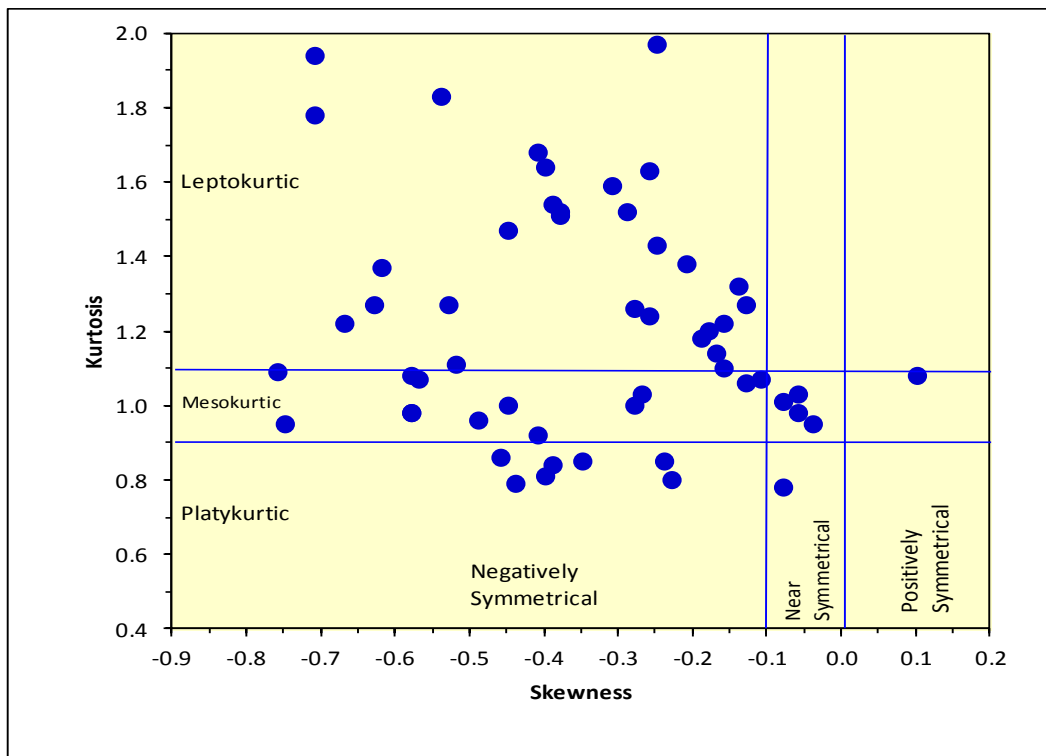


Figure 3.6. Sector plot showing the bivariate relationship between skewness and kurtosis.

3.1.6 Determination of the mechanisms and environments of deposition

In this section, the discriminate functions proposed by Sahu (1964) was applied to the sediment grain size data from the collected sediment sample environments in order to test the ability of these methods to characterize depositional setting. The following discriminate functions were used in the present work:

For the discrimination between Aeolian processes and littoral (intertidal zone) environments, the following equation was used:

$$Y1 = -3.5688MZ + 3.7016\delta I2\delta I - 2.0766SKI + 3.1135KG, \text{ where:}$$

Mz is the grain size mean;

δI is inclusive graphic standard deviation (sorting);

SKI, is the skewness, and

KG is the graphic kurtosis.

When Y1, is less than -2.7411, Aeolian deposition is indicated; whereas if it is greater than -2.7411, a beach environment is suggested. On the basis of Y1, values came from calculation for the present study, most of them as beach sediments. The collected sediment samples are identified as Aeolian deposits (5.3%) and 94.7% as beach deposits (Table 3.2).

For the discrimination between beach (back-shore) and shallow agitated marine environments (subtidal environment), the following equation was used: $Y2 = 16.6534Mz + 65.7091 \delta I2 + 18.1071SKI + 18.5043KG$.

If the value of Y2 is less than 65.3650, beach deposition is suggested; whereas if it is greater than 65.3650, a shallow, agitated marine environment is likely. Values of Y2 calculated for the present sediments, indicate that the collected sediment samples are derived mainly (100 %) from agitated marine environments and beach 0.0 % (Table 3.2).

For the discrimination between shallow marine and fluvial environments, the following equation was used: $Y3 = 0.2852Mz - 8.7604 \delta I2 - 4.8932SKI + 0.0482KG$.

If $Y3 < -7.419$, the sample is identified as a fluvial (deltaic) deposit; if greater than -7,419, the sample is identified as a shallow marine deposit. The collected sediment samples show about 68.4% fluvial and 31.6% shallow marine (Table 3.2).

Plotting of the three discriminate functions (Y1, Y2 and Y3) as bivariate scatter plots has the potential to improve the success rate and refinement of the discrimination method in relation to the deposition environment. Figure 3.7 shows the scatter graph of Y1 against Y2. Based on the classification of depositional environments, using the discriminate function values of Y1 and Y2, the graphs can be divided into four fields: Aeolian processes/littoral environment, beach and littoral environment, beach environment/shallow, marine agitated deposition and Aeolian process/shallow agitated marine environment. Most of the sediment samples plot within the beach/shallow, agitated marine field; few samples plot in the Aeolian/shallow agitated marine environment.

Table 3.2. Summary of the environment, using the discriminate functions of the collected samples

Samples	Area	Y1 (%)		Y2 (%)		Y3 (%)	
		Aeolian	Beach	Beach	Agitated	Fluvial	Shallow Marine
Number of samples	57	3	54	0	57	39	18
Percentage of samples	57	5.3	94.7	0.0	100.0	68.4	31.6

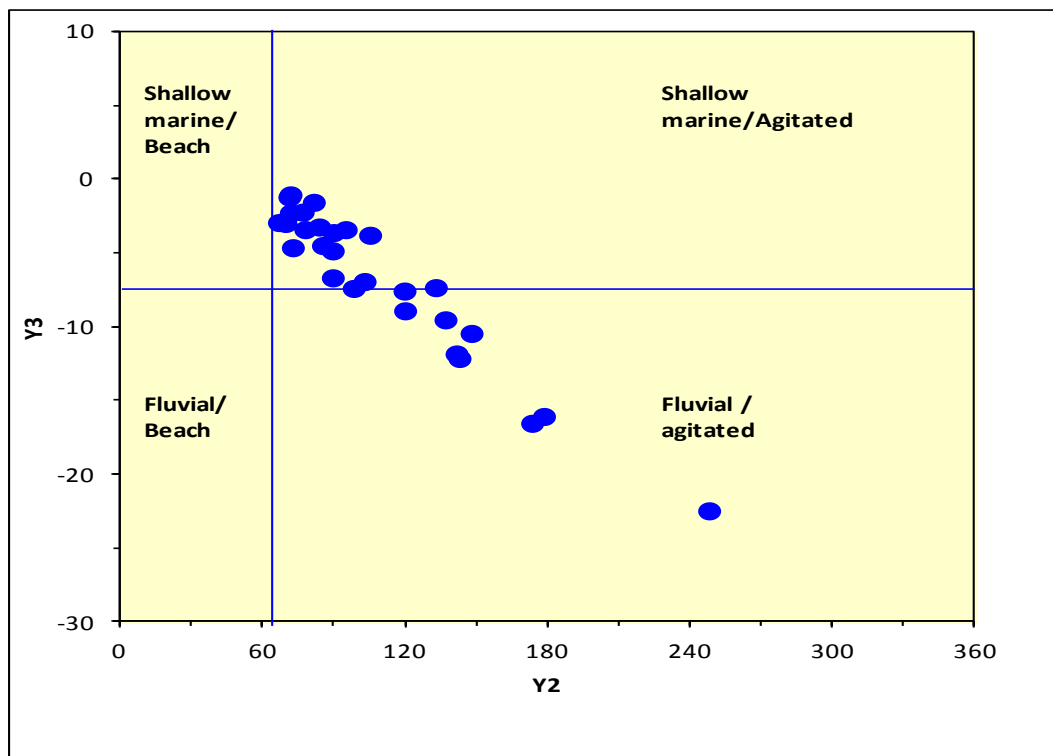


Figure 3.7. Relationship between the discriminate functions, Y1 and Y2, showing estimated environments.

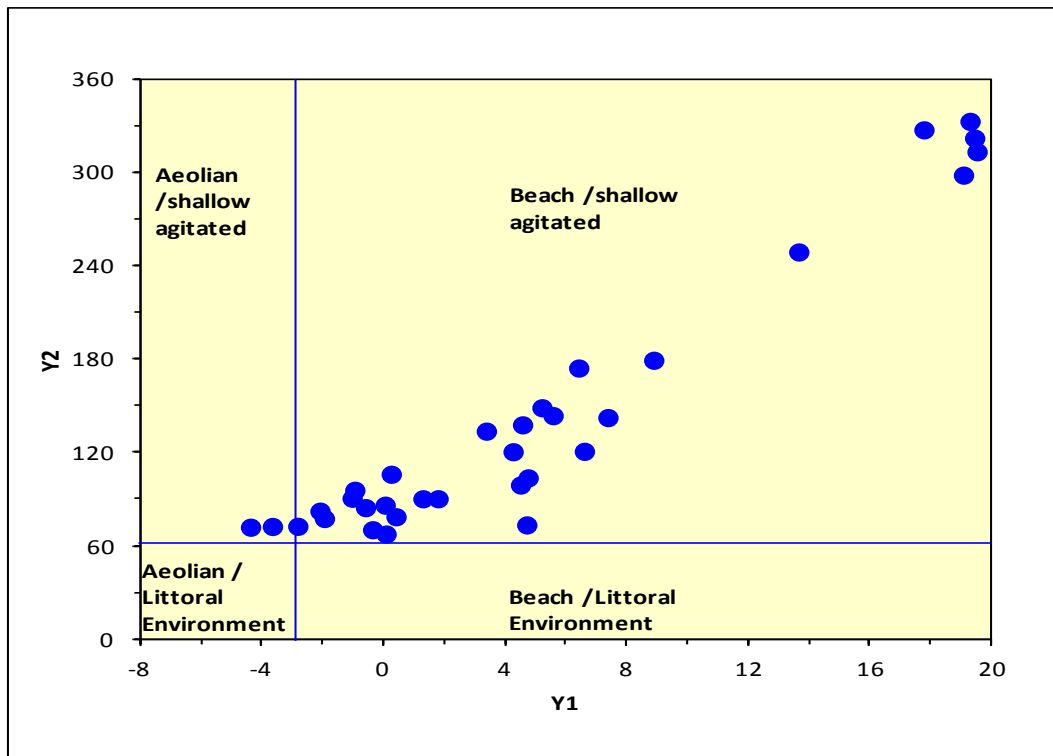


Figure 3.8. Relationship between the discriminate functions, Y2 and Y3, showing estimated environments.

A graphic plot of Y2 vs. Y3 allows four fields of depositional environments (based on the classification proposed by Sahu (1964) to be distinguished. Group I represent fluvial/beach deposits, Group II represents fluvial/shallow, agitated marine environment, Group III shallow marine/beach deposits, Group IV shallow marine agitated deposits. Most of the collected samples from the sediment samples lie in the shallow marine to fluvial environments (Figure 3.8).

3.2 Geochemistry

The analysis of the beach sand was done using XRF and ICP-MS. The major element in the percentage was analysed using XRF (figure B.1. Appendix B. show the average percent distribution of all oxides in the studied samples and B.2. show the average percent distribution of oxides in basalt, syenite, granodiorite and granite) and the results were summarized in Table

3.3, while the minor and trace elements in parts per million were analysed using ICP-MS; the results are summarized in Table 3.4.

3.2.1 Univariate statistics

All variables of the data set from the beach sand samples were tested for normality, as it is a prerequisite before performing any multivariate statistical analysis (Fig. B24; Appendix B). Reimann and Filzmoser (2000) interpreted the strong skewness in data sets as resulting from more than one population or process that affects the normal distribution of geochemical variables. The element distributions show a minor skewed pattern, have outliers and originate from more than just one process (Fig. B24; Appendix B). It has always been believed that regional geochemical data sets almost never follow a normal distribution and that in most cases a data transformation (e.g. logit, square root or range) will not result in a normal distribution (Reimann and Filzmoser, 1999). Almost all the variables show abnormal distribution and, when transformed in log, does not show normal distribution; therefore, the original data was used with the assumption that the studied data show a normal or a lognormal distribution. Table 3.5 below shows the mean, minimum, maximum, standard deviation, untransformed data for major and trace elements. The minimum, maximum, standard deviation, untransformed data for each beach sand sample is given in Appendix A. Additionally, the spatial distribution of the major and trace elements will be studied.

The mean, standard deviation, minimum and maximum values generated from the analysis of the 57 beach sand samples are presented in Table 3.5. The majority of the samples are dominated by CaO and SiO₂, ranging between 22.81 to 50.97 and 2.66 to 48.35 in wt. %, respectively; Sr and Cr ranging between 560.90 to 7243.60 and 0.001 to 752.62, respectively, dominate the trace elements. The standard deviation of the beach sand chemical composition showed that the sand in the beach area is not uniform. The variation could be attributed to the difference in their sources.

3.2.1.1 Aluminium oxides (Al₂O₃)

The aluminium oxides indicate a range of 0.36 to 4.42, with seven samples having Al₂O₃ of 0 <-1; 32 samples having 1 <-3 and 15 samples having >3 (Figure 3.9). The highest values of

4.42 occur in samples 19, 34 and 55; while the lowest values of 0.36, 0.49 and 0.62 occur in sample 57, 24 and 32, respectively, with an overall average percent of 2.28.

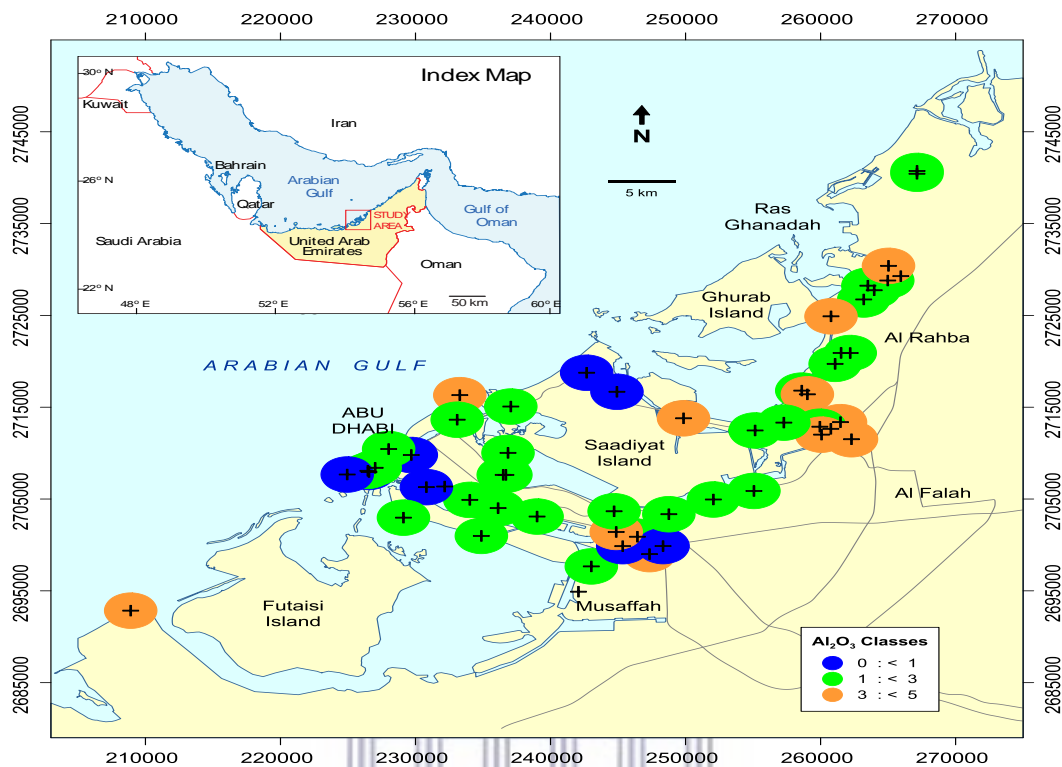


Figure 3.9. Aluminium oxide (Al_2O_3) class distribution in the study area.

3.2.1.2 Calcium oxide (CaO)

The calcium oxides indicate a range of 22 to 51, with 10 samples having CaO of <30; 29 samples having 30 to <40 and 16 samples having >40 (Figure 3.10). The highest values of 50.97, 49.65 and 48.71 occur in samples 57, 32 and 24, respectively; while the lowest values of 22.81, 23.09 and 23.84 occur in samples 30, 10 and 33, respectively, with an overall average percent of 36.58.

Table 3.3 XRF analysis of the major elements, expressed as weight percent oxide

Sample	Al ₂ O ₃	CaO	Cr ₂ O ₃	Fe ₂ O ₃	K ₂ O	MgO	MnO	Na ₂ O	P ₂ O ₅	SiO ₂	TiO ₂	L.O.I
1	2.41	29.37	0.05	1.13	0.55	3.3	0.01	0.95	0.04	31.84	0.11	27.13
2	1.11	48.63	0.01	0.38	0.2	2.07	0	0.91	0.06	9.01	0.06	36.83
3	2.13	36.82	0.03	0.67	0.44	1.94	0.01	3.73	0.05	16.81	0.12	38.25
4	2.91	31.71	0.04	1.02	0.55	2.49	0.02	1.27	0.05	26.49	0.14	28.22
5	2.72	37.37	0.06	0.99	0.45	1.92	0.02	1.25	0.06	22.61	0.2	33.33
6	1.25	37.79	0.01	0.45	0.32	2.79	0	4.9	0.04	8.01	0.08	44.8
7	3.28	31.72	0.05	1.15	0.63	2.23	0.03	1.13	0.05	31.86	0.18	27.71
8	1.77	41.34	0.02	0.58	0.34	1.79	0.01	2.24	0.04	14.03	0.1	38.3
9	3.75	31.2	0.04	1.1	0.65	2.33	0.03	1.75	0.06	30.96	0.2	28.4
10	2.43	23.09	0.04	0.82	0.73	2.01	0.01	1.24	0.04	48.36	0.11	21.44
11	0.47	48.89	0.02	0.28	0.1	1.05	0	0.76	0.04	3.89	0.04	42.29
12	2.25	38.64	0.05	0.82	0.4	2.64	0.01	1.56	0.05	18.12	0.15	35.22
13	1.61	38.14	0.06	1.47	0.24	4.83	0.02	1.25	0.03	17.82	0.09	34.47
14	3.44	32.19	0.04	1.02	0.6	1.94	0.02	1.57	0.06	30.81	0.18	28.42
15	3.82	28.39	0.02	1.03	0.76	2.27	0.03	2.08	0.05	38.64	0.15	22.7
16	3.14	32.82	0.02	0.89	0.6	1.73	0.02	1.58	0.06	30.55	0.15	28.99
17	2.54	36.08	0.02	0.73	0.45	3.87	0.02	1.43	0.03	20.03	0.13	34.34
18	3.39	30.87	0.06	1.37	0.58	2.93	0.03	1.08	0.05	32.25	0.18	27.06
19	4.42	26.11	0.02	1.19	0.81	2.25	0.03	2.11	0.06	38.71	0.21	24.92
20	1.72	36.79	0.02	0.67	0.4	2.56	0.01	3.92	0.05	13.74	0.11	37.55
21	2.67	37.04	0.03	0.69	0.46	1.81	0.02	1.83	0.04	21.41	0.14	34.05
22	3.17	34.3	0.03	0.92	0.55	2.46	0.02	1.5	0.05	25.15	0.18	31.39
23	0.94	48.52	0.02	0.43	0.15	1.7	0	0.32	0.03	6.68	0.09	40.07
24	0.49	48.71	0	0.22	0.12	0.85	0	1.45	0.04	3.58	0.04	43.59
25	2.35	32.7	0.07	1.31	0.48	3.97	0.02	0.96	0.05	28.68	0.11	29.23
26	1.39	42.71	0.02	0.55	0.28	1.8	0.01	1.2	0.09	12.4	0.08	39.02
27	2.84	30.45	0.08	1.42	0.5	5.33	0.03	1.05	0.04	26.48	0.16	28.86
28	3.39	30.45	0.05	1.24	0.65	2.81	0.03	1.35	0.06	31.94	0.19	27.69
29	2.7	31.51	0.07	1.56	0.46	5.41	0.03	0.91	0.05	26.07	0.16	28.97
30	3.48	22.81	0.07	1.56	0.63	6.04	0.03	1.5	0.06	28.64	0.2	23.66
31	2.93	33.73	0.05	1.03	0.52	3	0.02	1.3	0.06	23.84	0.2	30.57
32	0.62	49.65	0.01	0.29	0.11	1.22	0	0.67	0.05	4.56	0.05	41.96
33	0.85	42.49	0.01	0.48	0.24	3.32	0.01	4.03	0.03	4.07	0.05	44.14
34	4.31	23.84	0.03	1.16	0.93	2.9	0.03	1.86	0.05	42.29	0.19	22.58
35	1.02	43.13	0.06	0.8	0.21	3	0.01	1.13	0.05	11.51	0.07	38.78
36	0.85	47.58	0.01	0.33	0.17	1.3	0	0.84	0.06	7.25	0.06	40.92
37	1.2	37.28	0.04	1.06	0.3	4.28	0.01	0.84	0.04	21.29	0.07	40
38	0.7	48.23	0.02	0.32	0.13	1.4	0	0.65	0.05	6.52	0.05	42.02
39	1.35	45.53	0.02	0.44	0.24	1.6	0.01	0.97	0.05	10.53	0.1	38.9
40	0.73	48.65	0	0.24	0.13	1.01	0	0.76	0.05	6.24	0.05	41.26
41	1.28	41.19	0.06	0.72	0.29	2.09	0.01	0.93	0.05	17.28	0.1	35.65
42	3.76	33.42	0.03	1.27	0.48	3.54	0.03	1.48	0.05	25.44	0.18	30
43	2.12	34.18	0.02	0.84	0.56	2.28	0.01	1.05	0.04	28.82	0.1	30.19
44	2.1	34.62	0.09	1.77	0.38	5.58	0.02	0.95	0.05	23.01	0.14	31.37
45	2.22	38.5	0.03	0.81	0.4	2.3	0.02	0.99	0.06	19.27	0.14	33.83
46	2.48	38.33	0.01	0.9	0.47	2.66	0.02	1.64	0.05	18.01	0.15	35.17
47	1.9	42.33	0.01	0.81	0.37	2.25	0.01	1.25	0.05	13.68	0.11	37.71
48	1.49	40.53	0.05	0.55	0.38	1.47	0.01	0.93	0.05	18.62	0.11	35.41
49	2.39	35.02	0.1	2.15	0.25	6.92	0.03	0.81	0.05	20.89	0.13	30.33
50	2.78	27.72	0.09	0.98	0.65	1.81	0.02	0.83	0.05	40.68	0.21	23.93
51	2.99	34.32	0.08	1.11	0.54	2.01	0.02	1.14	0.06	27.61	0.23	29.63
52	1.81	40.77	0.05	0.74	0.35	1.78	0.01	0.86	0.06	18.22	0.12	34.77
53	3.41	31.79	0.08	1.1	0.61	2.48	0.03	2.19	0.06	29.12	0.27	29.85
54	1.25	43.7	0.05	0.48	0.25	2.22	0.01	0.94	0.08	11.95	0.12	38.38
55	4.33	26.53	0.03	1.1	0.78	2.73	0.03	2.34	0.06	37.21	0.23	25.53
56	1.72	36.28	0.11	1.08	0.41	3.3	0.01	0.78	0.04	24.17	0.12	31.7
57	0.36	50.97	0.01	0.23	0.09	0.8	0	0.82	0.05	2.66	0.03	43.35

Table 3.4 Sampling name and the trace elements concentration, which has been done by inductively coupled plasma (ICP) analyses and table A.4 in Appendix for the rest of elements.

Sample	Sb ppm	Ba ppm	Co ppm	Cu ppm	Pb ppm	Zn ppm	Ni ppm	As ppm	Cd ppm	Hg ppm	Mo ppm
1	0.1	201	6.4	13.5	2.2	17	86.8	2.9	<0.1	<0.01	0.5
2	<0.1	68	2.6	2.1	1.1	4	8.5	2.5	<0.1	0.01	0.8
3	0.2	134	4.1	3.3	1.5	6	24.6	3.2	<0.1	0.02	2.6
4	<0.1	157	4.7	3.6	1.9	12	29.8	2.7	0.1	<0.01	0.6
5	0.1	136	5.5	3.7	2.1	7	19.3	5	0.1	<0.01	0.3
6	<0.1	90	2.8	3.2	1.1	4	20.9	4	<0.1	0.01	6.2
7	0.1	185	5.2	3.4	1.3	4	15	3.1	0.1	0.02	5
8	0.1	92	2.5	3.9	1.8	7	27.5	2.3	0.1	<0.01	0.4
9	<0.1	159	5.3	4.3	1.9	9	22.6	2.6	<0.1	<0.01	0.3
10	0.1	190	3.2	3.3	1.5	7	42.5	2.3	<0.1	0.02	0.5
11	<0.1	74	5	6.5	6.2	21	73.5	2.8	<0.1	0.01	0.2
12	<0.1	109	2.9	3	1.3	5	25.3	3.3	<0.1	0.01	0.5
13	<0.1	125	3.9	3.7	1.5	7	37.3	2.8	<0.1	0.02	0.2
14	0.1	156	4.6	4	1.7	8	20.5	2.7	<0.1	<0.01	0.2
15	<0.1	179	4.6	3.8	1.5	8	34.5	1.8	<0.1	0.01	0.8
16	<0.1	197	4.1	3.5	1.5	7	19	2.5	<0.1	<0.01	0.6
17	0.1	124	3.2	3	1	5	18.3	3.7	<0.1	<0.01	0.2
18	<0.1	161	5	4	2	7	38.7	2.8	0.1	<0.01	0.6
19	<0.1	168	4.7	4.8	1.8	9	25.2	2.6	0.1	0.01	0.5
20	0.1	115	3.1	3.9	1.6	6	14.8	2.7	0.2	<0.01	4.2
21	0.2	131	3.7	3.1	1.1	6	17.3	3.7	0.3	0.04	1.1
22	0.2	123	3.7	3.6	1.6	7	21.6	4.4	<0.1	0.02	0.6
23	<0.1	89	3.5	4.1	1.9	7	18.4	3.5	<0.1	<0.01	0.3
24	0.1	46	1.4	2.5	1.2	5	9.6	5.1	<0.1	0.04	0.3
25	<0.1	70	1.3	4.1	2	6	18.6	4	0.1	<0.01	0.3
26	<0.1	99	2.2	5	4	14	26.5	2.4	<0.1	0.03	0.6
27	<0.1	176	12.9	4.3	1.5	11	118	2.2	0.1	0.02	1
28	0.1	179	4.4	5.7	2.9	13	23.7	2.6	0.1	<0.01	0.9
29	0.1	161	5.6	4.1	1.8	11	34.3	2.2	<0.1	<0.01	0.5
30	0.1	227	9.7	7.6	4.2	25	82.2	2.8	<0.1	0.02	2.7
31	0.2	141	5.1	4.3	1.8	8	30.6	3.1	0.2	0.02	1.7
32	<0.1	184	6.7	3.9	2.1	8	66.4	3.1	0.1	<0.01	0.7
33	0.1	35	1.9	2.3	1.8	3	13.1	4.2	<0.1	0.02	1.1
34	<0.1	199	4.1	4.3	3.2	17	26.3	2.9	0.2	0.02	0.6
35	<0.1	136	4.5	4.8	2.9	9	31.3	1.9	<0.1	0.02	0.5
36	0.1	62	1.9	3.2	3.4	6	13.9	2.3	<0.1	0.03	0.4
37	<0.1	122	5.3	5.5	2.4	35	78.1	2.6	<0.1	<0.01	0.2
38	<0.1	68	3.2	2.3	1.1	3	37.1	3.2	<0.1	0.02	0.2
39	0.2	68	1.1	2.5	1	3	6.1	2.7	<0.1	<0.01	0.4
40	<0.1	28	0.4	2.2	0.9	2	3.5	1.4	<0.1	<0.01	<0.1
41	<0.1	139	4.6	3.2	3.1	7	33.2	2.3	<0.1	<0.01	0.5
42	0.1	183	4	6.9	2.2	12	19.1	2.9	0.1	<0.01	1.4
43	0.1	180	4.7	5.6	5.1	20	45.3	2.3	0.1	<0.01	0.7
44	0.1	166	6.5	4.7	3.9	11	57.1	2.1	<0.1	0.02	0.6
45	0.1	210	3.9	4.4	1.6	8	18	2.6	0.1	<0.01	0.5
46	0.2	128	3.2	4.3	1.8	9	15.8	3.9	0.1	0.02	0.9
47	0.2	120	2.8	3.5	1.6	7	11.4	4	<0.1	<0.01	0.2
48	<0.1	139	4	2.3	1.4	4	17.3	2.2	<0.1	<0.01	0.1
49	0.1	150	7	5.2	5.3	12	44.9	2.5	0.1	0.02	0.5
50	<0.1	190	4.8	3.5	2.2	7	17.8	2.9	0.1	0.01	0.3
51	0.1	149	5.6	4.3	2.1	9	21.9	1.6	0.1	<0.01	0.4
52	<0.1	165	4.2	3.5	1.6	7	19.3	2.3	0.1	<0.01	0.4
53	0.1	141	6.6	3.1	1.5	6	11.6	3	<0.1	<0.01	0.3
54	<0.1	117	5	2.7	1.5	6	9.3	1.8	<0.1	<0.01	0.3
55	0.1	396	3.9	4.1	1.6	9	15.9	2.2	<0.1	<0.01	0.3
56	0.2	173	7.2	3.5	10.4	14	61.6	2.6	0.1	0.02	0.3
57	<0.1	77	1.8	1.8	2.5	4	5.4	2.4	<0.1	<0.01	0.2

Table 3.5 Descriptive statistics of the geochemical data for beach sand.

Variable	Mean	St. Deviation	Minimum	Maximum
Al ₂ O ₃	2.23	1.09	0.36	4.42
CaO	36.97	7.31	22.81	50.97
Fe ₂ O ₃	0.89	0.42	0.22	2.15
K ₂ O	0.43	0.2	0.09	0.93
MgO	2.64	1.31	0.8	6.92
MnO	0.02	0.01	0.001	0.03
Na ₂ O	1.43	0.88	0.32	4.9
P ₂ O ₅	0.05	0.01	0.03	0.09
SiO ₂	21.23	11.09	2.66	48.36
TiO ₂	0.13	0.06	0.03	0.27
LOI	33.42	6.24	21.44	44.8
As	2.85	0.78	1.4	5.1
Ba	140.12	58.34	28	396
Co	4.31	2.05	0.4	12.9
Cr	272.48	182.17	0.001	752.62
Cu	4.04	1.72	1.8	13.5
Nb	2.99	1.2	0.7	6.1
Ni	29.94	22.8	3.5	118.2
Pb	2.26	1.56	0.9	10.4
Rb	14.88	5.13	3	24.2
Sr	2434.02	1563.41	560.9	7243.6
Th	1.37	0.5	0.2	2.5
U	2.34	0.84	1.3	4.6
V	29.05	9.53	9	47
Zn	9	5.79	2	35
Zr	91.14	61.86	11.6	300.1

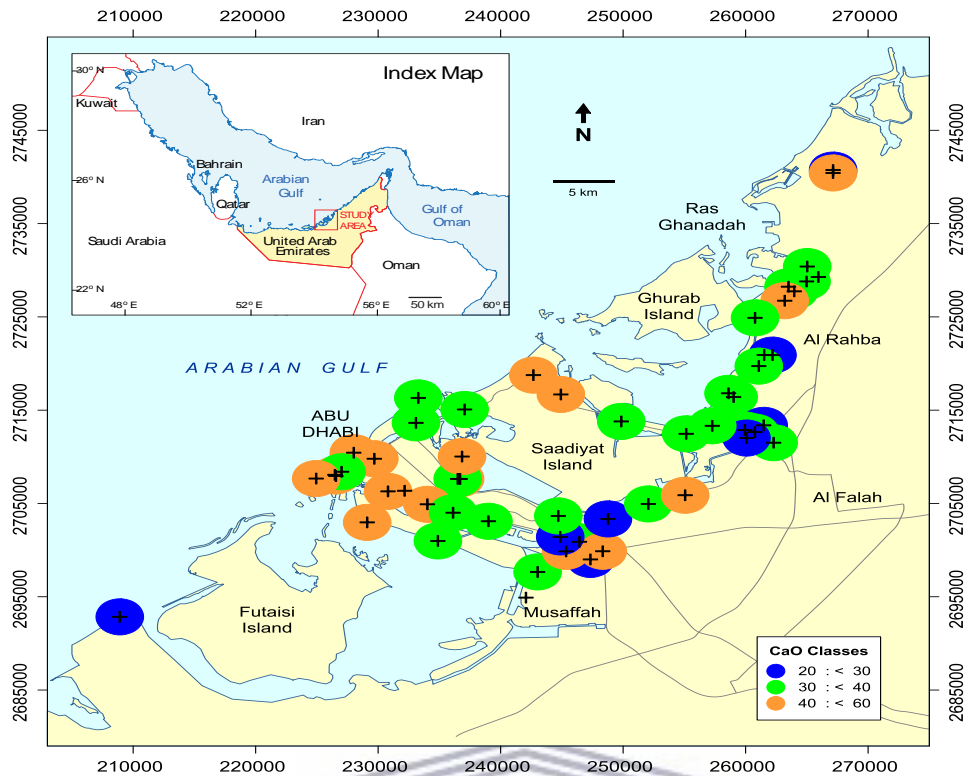


Figure 3.10. Calcium oxide (CaO) class distribution in the study area.

3.2.1.3 Chromium oxides (Cr_2O_3)

The chromium oxides indicate a range of 0.01 to 0.11, with 22 samples having Cr_2O_3 of <0.03 , 18 samples having $0.03-<0.06$ and 15 samples having >0.06 (Figure B.25.). The highest values of 0.11, 0.1 and 0.09 occur in samples 56, 49 and 50, 44, respectively, while the lowest value of 0.01 occurs in sample 2, 32, 33, 36, 46, 47 and 57, with an overall average percent of 0.04.

3.2.1.4 Iron oxides (Fe_2O_3)

The iron oxides indicate a range of 0.22-2.15, with 10 samples having Fe_2O_3 of <0.5 , 23 samples having $0.5 < 1$ and 22 samples having >1 (Figure 3.11). The highest values of 2.15, 1.77 and 1.56 occur in samples 49, 44 and 29, 30, respectively, while the lowest values of 0.22, 0.23 and 0.29 occur in samples 24, 57 and 32, respectively, with an overall average percent of 0.9.

3.2.1.5 Potassium oxides (K₂O)

The potassium oxides indicate a range of 0.09 to 0.93, with 16 samples having K₂O of <0.3, 28 samples having 0.3 to <0.6 and 11 samples having >0.6 (Figure B.26). The highest values of 0.93, 0.81 and 0.78 occur in samples 34, 19 and 55, respectively, while the lowest values of 0.09, 0.11 and 0.12 occur in samples 57, 32 and 24, respectively, with an overall average percent of 0.43.

3.2.1.6 Magnesium oxides (MgO)

The magnesium oxides indicate a range of 0.8 to 6.92, with 19 samples having MgO of <2, 30 samples having 2 to <4 and 6 samples having >4 (Figure B.27). The highest values of 6.92, 6.04 and 5.41 occur in samples 49, 30 and 29, respectively, while the lowest values of 0.8, 0.85 and 0.01 occur in samples 57, 24 and 40, respectively, with an overall average percent of 2.63.

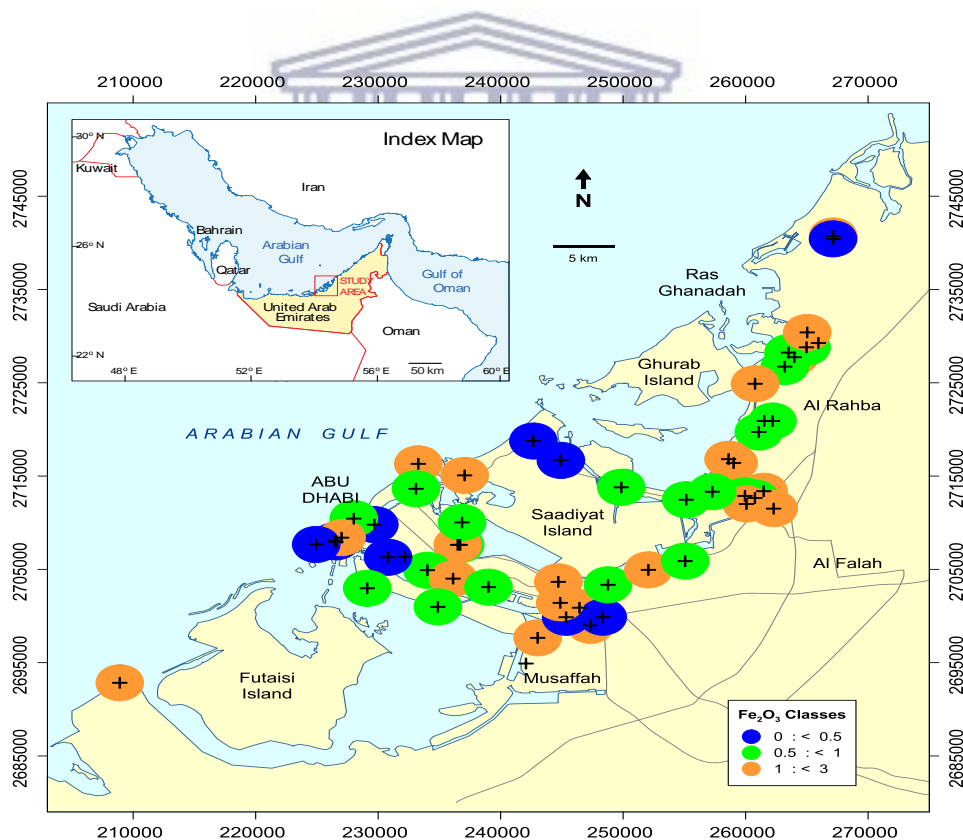


Figure 3.11. Iron oxides (Fe₂O₃) class distribution in the study area.

3.2.1.8 Manganese oxides (MnO)

The manganese oxides indicate a range of 0.01 to 0.03, with 7 samples having MnO of <0.01, 20 samples having 0.01 to <0.02 and 28 samples having >0.02 (Figure B.28). The highest value of 0.03 occurs in 13 samples, while the lowest value of 0.01 occurs in 15 samples, and 7 samples have a value of 0, with an overall average percent of 0.02.

3.2.1.9 Sodium oxides (Na₂O)

The sodium oxides indicate a range of 0.32 to 4.03, with 19 samples having Na₂O of <2, 30 samples having 2 to <4 and 6 samples having >4 (Figure B.29). The highest values of 4.03, 3.92 and 3.85 occur in samples 33, 20 and 6, respectively, while the lowest values of 0.32, 0.65 and 0.78 occur in samples 23, 38 and 56, respectively, with an overall average percent of 1.4.

3.2.1.10 Phosphorus oxides (P₂O₅)

The phosphorus oxides indicate a range of 0.03 to 0.09, with 19 samples having P₂O₅ of <2, 30 samples having 2 to <4 and 6 samples having >4 (Figure B.30). The highest value of 0.09 occurs in 26, while the lowest value of 0.03 occurs in samples 13, 17, 23 and 33, with an overall average percent of 0.05.

3.2.1.11 Silicon oxides (SiO₄)

The silicon oxides indicate a range of 2.66 to 48.36, with 14 samples having SiO₄ of <15, 29 samples having 15 to <30 and 12 samples having >30 (Figure 3.12). The highest values of 48.36, 42.29 and 40.68 occur in samples 10, 34 and 50, respectively, while the lowest values of 2.66, 3.58 and 4.07 occur in samples 57, 24 and 33, respectively, with an overall average percent of 21.63.

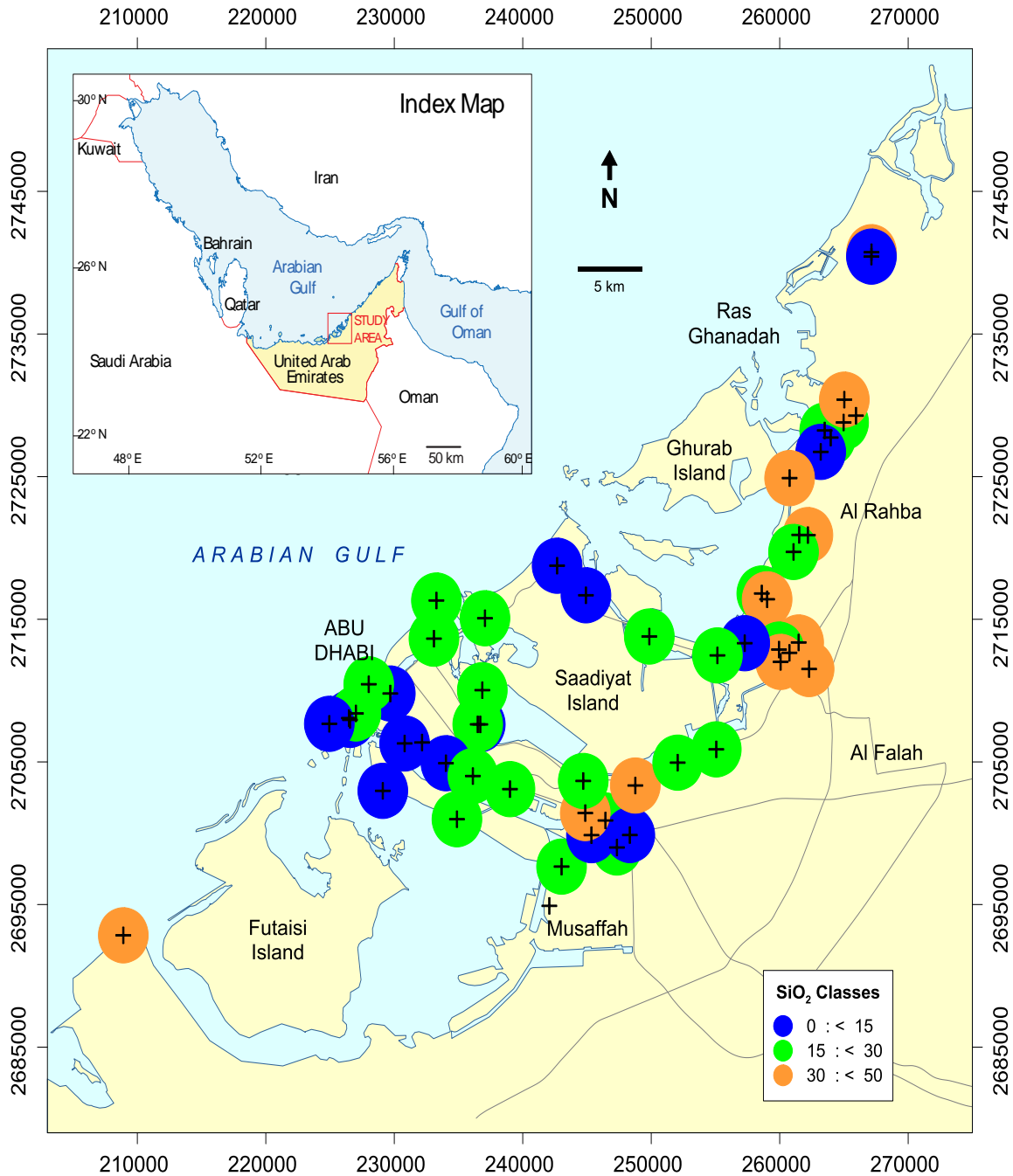


Figure 3.12. Silicon oxides (SiO_4) class distribution in the study area.

3.2.1.12 Titanium oxides (TiO_2)

The titanium oxides indicate a range of 0.03 to 0.27, with 14 samples having TiO_2 of <15 , 29 samples having 15 to <30 and 12 samples having >30 (Figure B.31). The highest values of 0.27, 0.21 and 0.2 occur in samples 53, 19 and 9, respectively, while the lowest values of 0.03,

0.04 and 0.05 occur in samples 57, 24 and 32, 33, 38, 40, respectively, with an overall average percent of 0.13.

3.2.1.13 Loss on ignition (LOI)

This includes volatile material, such as the oxides of C, S, H, and N, some of which are from organic material. The LOI indicates a range of 21.44 to 44.14, with 14 samples having TiO_2 of <15, 29 samples having 15 to <30 and 12 samples having >30 (Figure 3. 13). The highest values of 44.14, 43.59 and 43.35 occur in samples 33, 24 and 57, respectively, while the lowest values of 21.44, 22.58 and 22.7 occur in samples 10, 34 and 15, respectively, with an overall average percent of 33.07. Figure 3.32 illustrates the average distribution of all oxides in the studied sample, which can be summarized as the following: the highest values of 36.85 for CaO, 33.07 for LOI and 21.63 for SiO_2 , while the lowest values of 0.02, 0.04 and 0.05 for MnO, Cr_2O_3 and P_2O_5 , respectively.



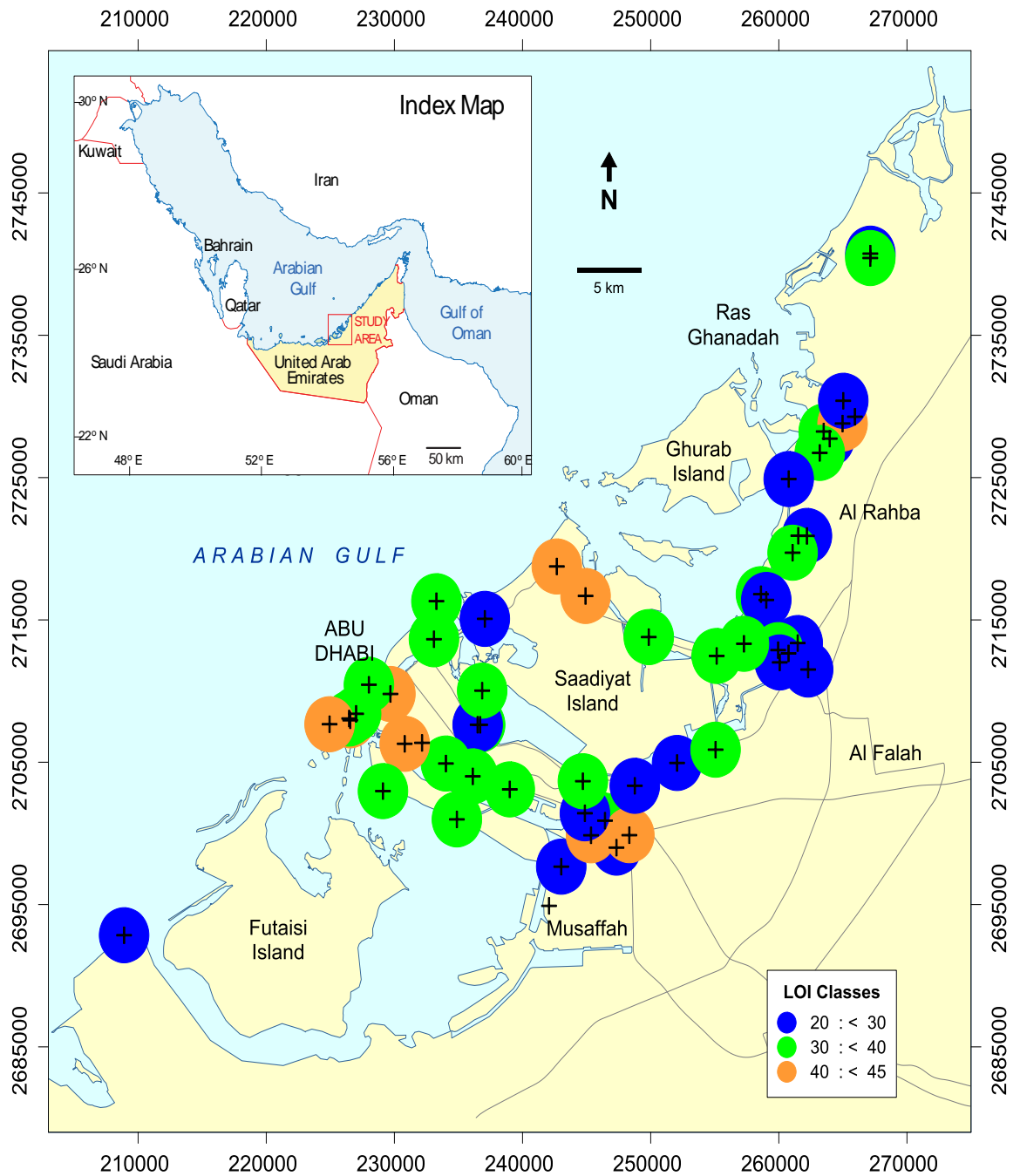


Figure 3.13. Loss on Ignition (LOI) class distribution in the study area.

3.2.2 Trace elements distribution and comparison with Dutch guidelines

According to our objectives to study uranium, thorium and heavy metal footprints, depending on the determination of their concentration, and achieving high accuracy, the inductively coupled plasma mass spectrometer was applied (Table 3.4).

According to Table 3.4, strontium is the most abundant trace element, with an average value of 2434 ppm, and a maximum of 7243 ppm. Barium values range from 28 ppm to 396 ppm, with a mean value of 140 ppm; zircon ranges 11 to 300 ppm, with an average of 91 ppm and rubidium has an average value of 15 ppm, ranging from 3 to 24 ppm.

Among the remaining trace elements, only Ni, Y, Zn, Cu, V, Co, U, Th, Mo, Pb and Nb were present in moderate concentrations. Nickel values ranged from 3.5 to 118.2 ppm (average 29.9 ppm); Y from 1.6 to 10 ppm (average 6.4 ppm); and Zn from 2 to 35 ppm (average 9 ppm). copper (2 to 14 ppm; average 4), vanadium (9 to 47 ppm, average 29 ppm), lead (0.9 to 10.4 ppm; average 2.3 ppm), thorium (0.2 to 2.5; average 1.4 ppm), niobium (0.7 to 6.1 ppm; average 3 ppm) and cobalt (0.4 to 13 ppm, average 4 ppm) contents were somewhat lower than this group. Among the remaining trace elements, concentrations of as are relatively high (1.4-5.1 ppm), uranium (1.3-4.6 ppm, average 2.3 ppm), exceeding the value in average upper continental crust of 4.6.

3.2.2.1 Antimony (Sb)

The level of antimony does not exceed 0.2 ppm in eight samples (3, 21, 22, 31, 39, 46, 47 and 56). The rest of the samples have 0.1 ppm of Sb or less (figure B.32. Appendix B). In all samples, the level of antimony is well below the limit suggested by the Dutch guidelines (15 ppm) (Lijzen et al., 2001) (Table 3.6).

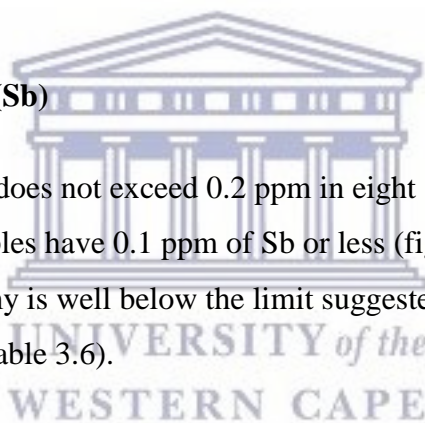


Table 3.6 Concentration of elements (in ppm) of samples collected from Abu Dhabi beach. The standards are their respective crustal abundances.

Variable	Mean	St. Deviation	Minimum	Maximum	ACA. (Taylor, 1964)
Al	2.23	1.09	0.36	4.42	8.23%
Fe	0.89	0.42	0.22	2.15	5.60
As	2.85	0.78	1.40	5.10	1.8
Cd	0.12	0.05	0.10	0.30	0.2
Co	4.31	2.05	0.40	12.90	25
Cr	272.48	182.17	0.001	752.62	102
Cu	4.04	1.72	1.80	13.50	55
Hg	0.02	0.01	0.01	0.04	80
Ni	29.94	22.80	3.50	118.20	75
Pb	2.26	1.56	0.90	10.40	14
Sr	2434.02	1563.41	560.90	7243.60	370
Th	1.37	0.50	0.20	2.50	9.6
U	2.34	0.84	1.30	4.60	2.7
V	29.05	9.53	9.00	47.00	85
Zn	9.00	5.79	2.00	35.00	70
Zr	91.14	61.86	11.60	300.10	97

3.2.2.2 Arsenic (As)

The level of contamination with arsenic in Abu Dhabi is almost negligible. While the safe limit of As, based on the Dutch guidelines (Lijzen et al., 2001), is 55 ppm, the maximum concentration of As in AD is 5.1 ppm (sample 24) and the minimum value is 1.4 ppm (sample 40). The majority of the samples (28 samples) (Figure 3.14) have As in the range of 2.5 to 3.3 ppm.

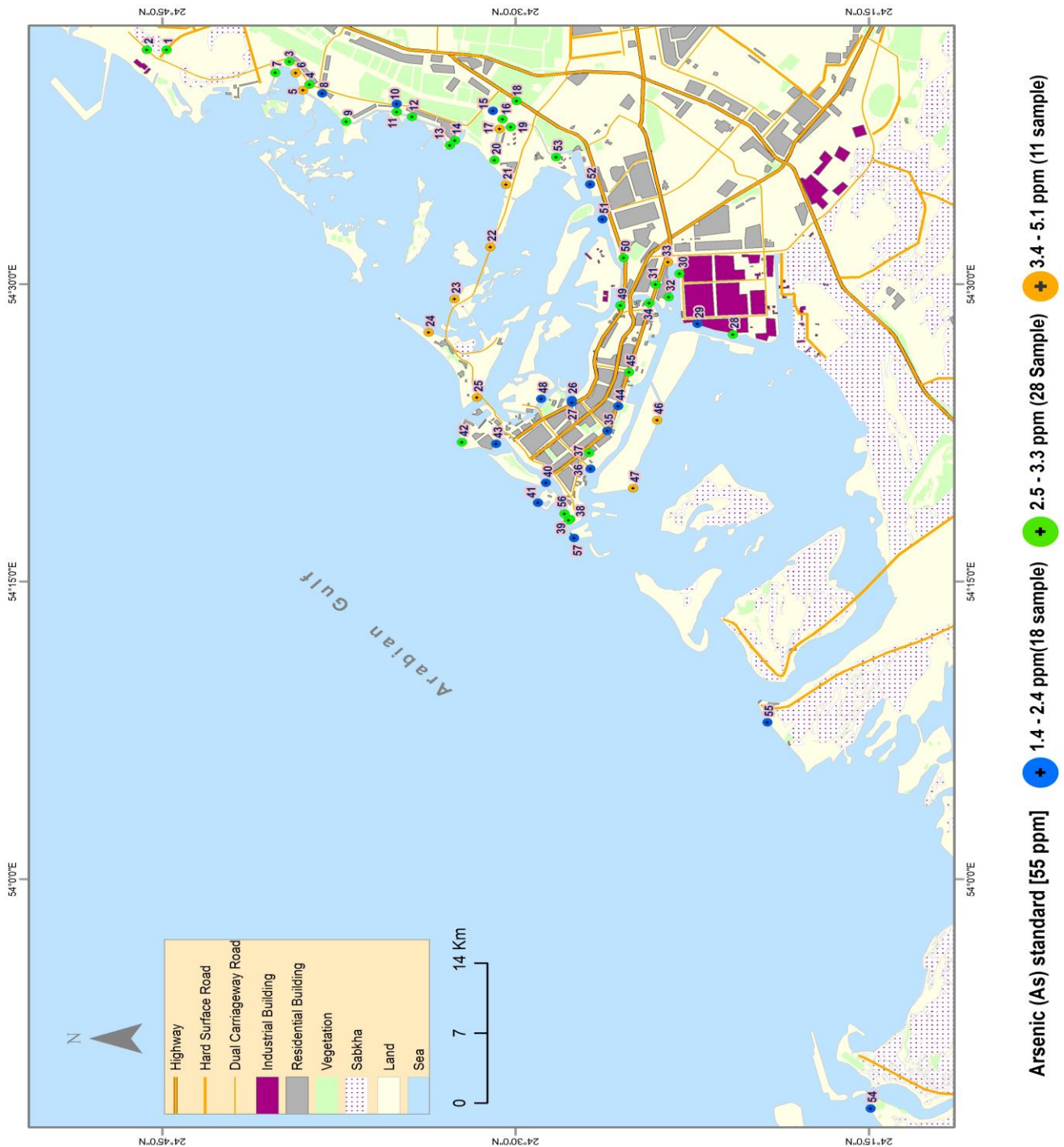


Figure 3.14. Map of Abu Dhabi showing the arsenic (As) concentration of the areas from which the samples were collected, as indicated with dots, along with their numbers.

3.2.2.3 Barium (Ba)

Barium (Ba) is present in concentrations ranging from 28 to 396 ppm. The highest value is less than 65% of the limit set by the Dutch guidelines (625 ppm). Fourteen samples have less than 100 ppm of Ba, 38 samples have Ba ranging from 100 to less than 200 ppm and 4 samples have more than 200 ppm of Ba (Figure B.34). The highest values of 396 ppm, 227 ppm and 210

ppm are in samples 55, 30 and 45, respectively, while the lowest values of 22 ppm, 35 ppm and 46 ppm are in samples 40, 33 and 24, respectively, with an overall average of 140 ppm.

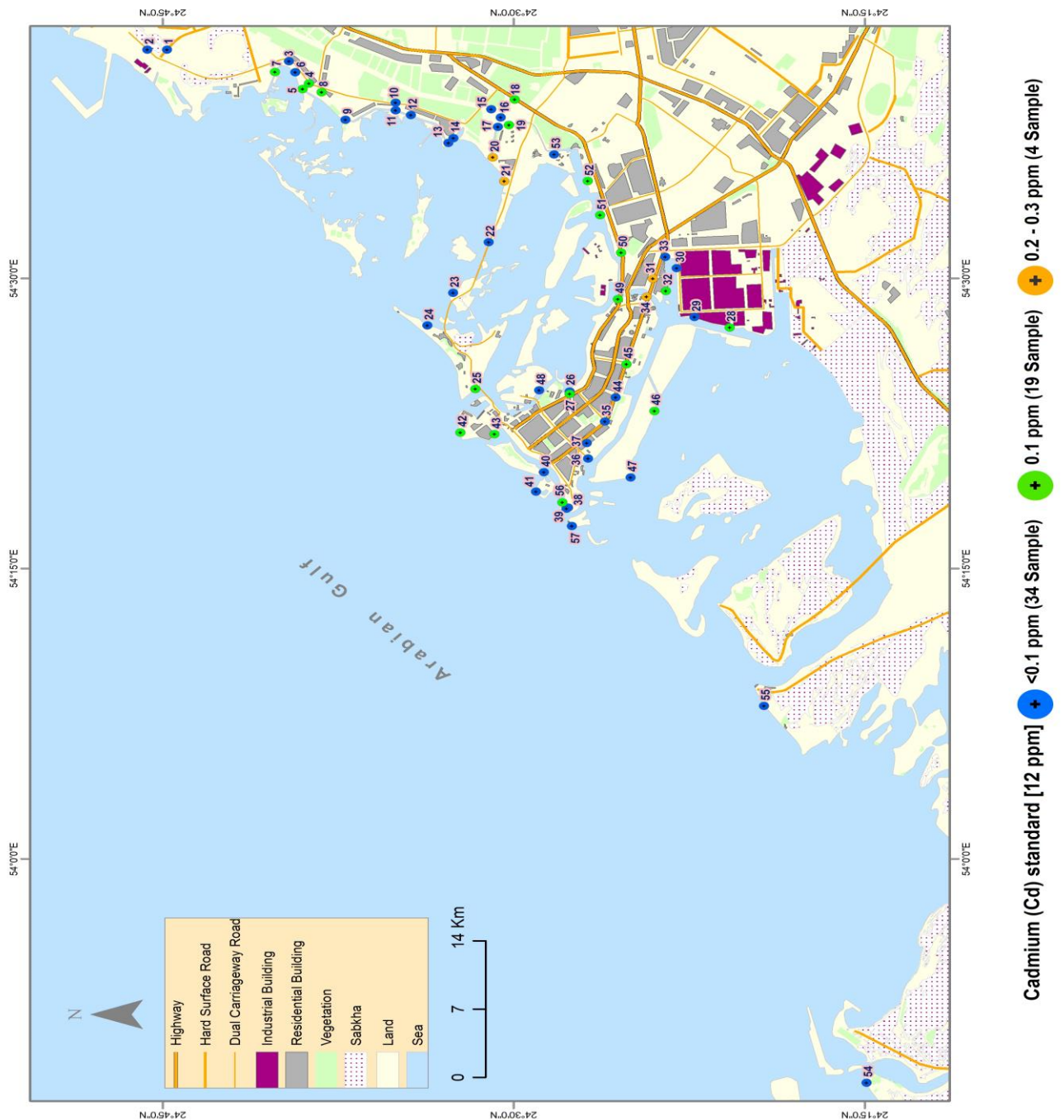


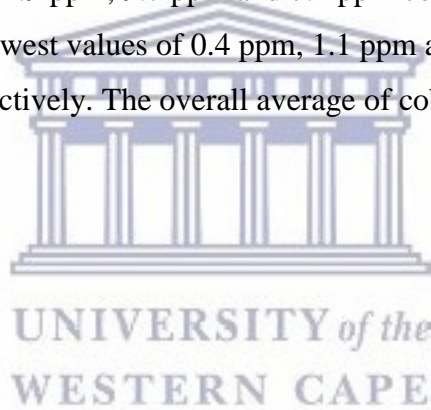
Figure 3.15. Map of Abu Dhabi showing the cadmium (Cd) concentration of the areas from which the samples were collected, as indicated with dots, along with their numbers.

3.2.2.4 Cadmium (Cd)

The safe limit of cadmium concentration in soil, according to the Dutch guidelines, is 12 ppm. The Cd concentration in the soil samples in this study ranges from less than 0.1 ppm to 0.3 ppm. Thirty-four samples have Cd concentration of less than 0.1 ppm. The highest value of 0,3ppm is in sample 21 (Figure 3.16). The results clearly suggest that the soil in Abu Dhabi is not contaminated with a toxic level of cadmium.

3.2.2.5 Cobalt (Co)

The contamination of cobalt in the Abu Dhabi coastal line is less than 5% of the safe limit suggested by the Dutch guidelines (240 ppm). Cobalt is distributed in a range of 0.4 to 12.9 ppm. The highest values of 12.9 ppm, 9.7 ppm and 7.2 ppm correspond to samples 27, 30 and 56, respectively, while the lowest values of 0.4 ppm, 1.1 ppm and 1.3 ppm correspond to samples 40, 39 and 25, respectively. The overall average of cobalt in all samples is 4.3 ppm (Figure 3.17).



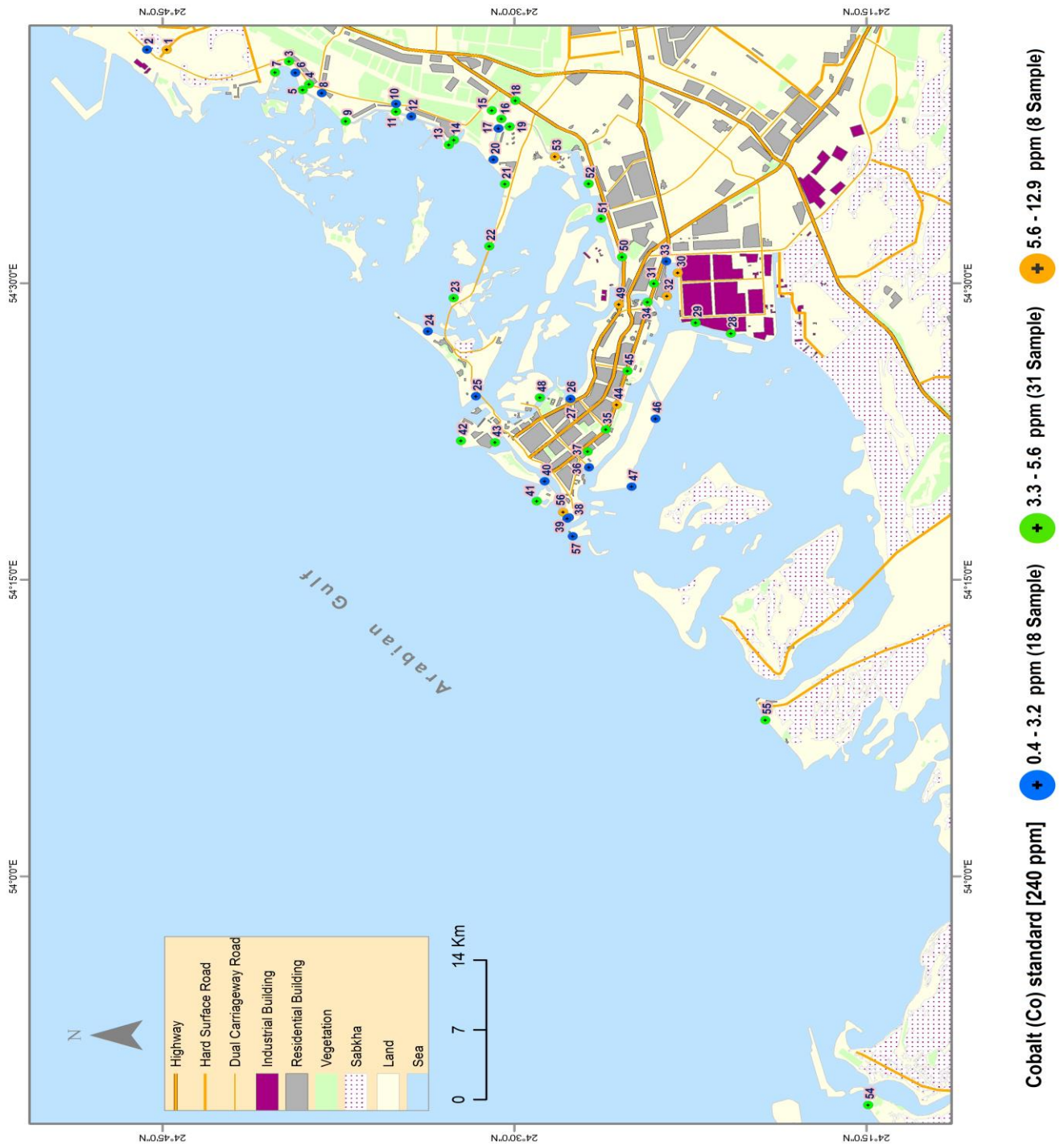


Figure 3.16. Map of Abu Dhabi showing the cobalt (Co) concentration of the areas from which the samples were collected, as indicated with dots, along with their numbers

3.2.2.6 Copper (Cu)

The maximum contamination of copper in Abu Dhabi does not exceed the 7% safe limit set by the Dutch guidelines (190 ppm). This level of copper indicates that the area is very safe, as copper and all the metals discussed earlier are present in very low concentrations, well below the safe limit of the Dutch guidelines. Cu is present in the samples in a range of 1.8 ppm to 13.5 ppm. Nine of the samples collected have Cu in less than 3 ppm, 39 samples have Cu in 3 to 5 ppm and 9 samples have Cu in less than 5 ppm. The highest values of 13.5 ppm, 7.6 ppm and 6.5ppmare in samples 1, 30 and 11, respectively, while the lowest values of 1.8ppm, 2.1 ppm and 2.2 ppm are in samples 57, 2 and 40, respectively (Figure 3.18). The overall average of copper concentration in the soil of the samples collected along the coastal line of AD is 4 ppm.



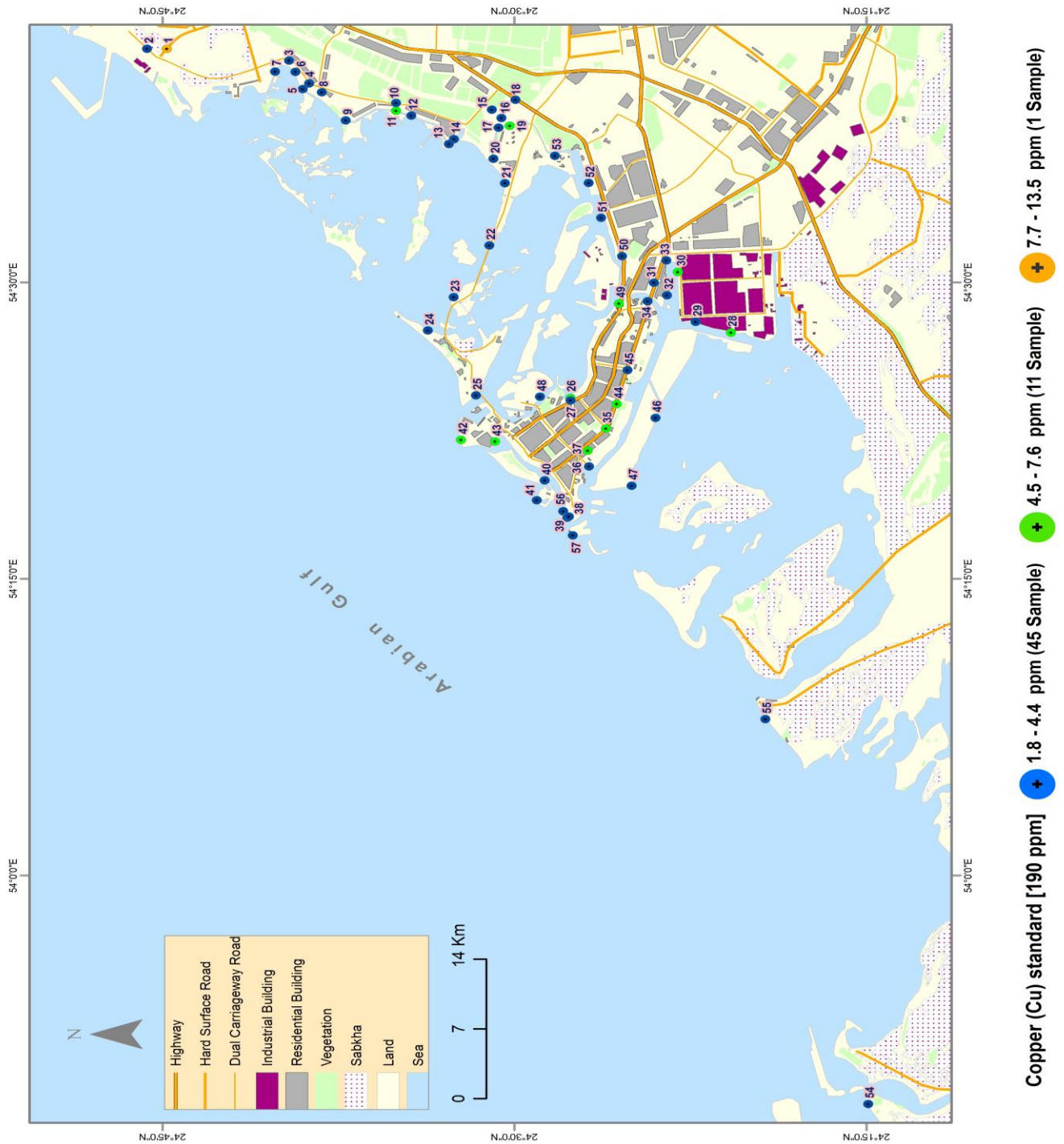


Figure 3.17. Map of Abu Dhabi showing the copper (Cu) concentration of the areas from which the samples were collected, as indicated with dots, along with their numbers.

3.2.2.7 Mercury (Hg)

While the Dutch guideline limit is 10ppm, the mercury concentration in the samples from Abu Dhabi ranges from less than 0.01 to 0.04 ppm (figure B.33. Appendix B).

3.2.2.8 Lead (Pb)

Lead is present in the samples studied in a range of 0.9 to 10.4 ppm, which is below the Dutch guideline limit of 530ppm. The highest values of 10.4 ppm, 6.2 ppm and 5.3 ppm are in samples 56, 11 and 49, respectively, while the lowest values of 0.9 ppm, 1 ppm and 1.1 ppm are in samples 40, 17 and 2, 6, 21, 32, respectively on average, lead is present in the coastal line of AD in a concentration of 2.3 ppm (figure 3.18).

3.2.2.9 Molybdenum (Mo)

The concentration of molybdenum in the samples collected ranges from less than 0.1 to 6.2 ppm. The Dutch guideline limit (200 ppm) far exceeds the concentration, with 46 samples having a concentration of Mo less than 1 ppm, and 11 samples having a concentration of 1 to 6.2 ppm (figure B.35. Appendix B). The highest values of 6.2ppm is in sample 6.

3.2.2.10 Nickel (Ni)

The nickel concentration ranges between 3.5 and 118.2 ppm, which is below the Dutch guideline limit of (210 ppm). The highest value reaches 56% of the limit by the Dutch guidelines. The highest values of 118.2, 86.8 and 82.2 ppm are in samples 27, 1 and 30, respectively, while the lowest values of 3.5, 5.4 and 8.5 ppm are in samples 40, 57 and 2, respectively. The overall average is 29.9 ppm (figure B.36. Appendix B).

3.2.2.11 Zinc (Zn)

The range of zinc concentration in the area covered by this study ranges from 2 to 35 ppm, which is well below the Dutch guideline (Lijzen et al., 2001) limit of 720 ppm. Only 15 samples have a concentration greater than 10 ppm. The highest values of 35, 25 and 21 ppm are in samples 37, 30 and 11, respectively. The overall average is 9 ppm (figure B.37. Appendix B).

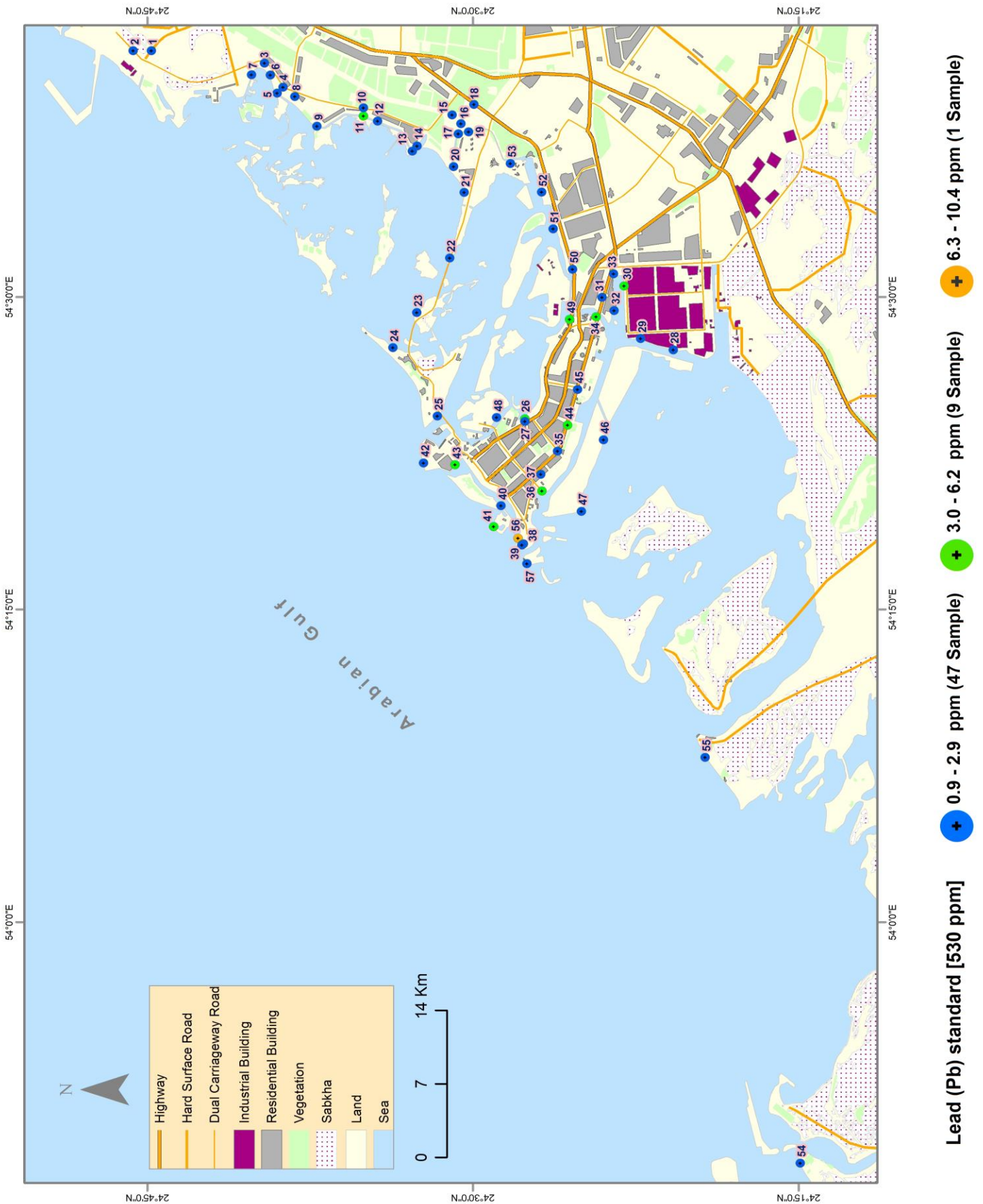


Figure 3.18. Map of Abu Dhabi showing the lead (Pb) concentration of the areas from which the samples were collected, as indicated with dots, along with their numbers.

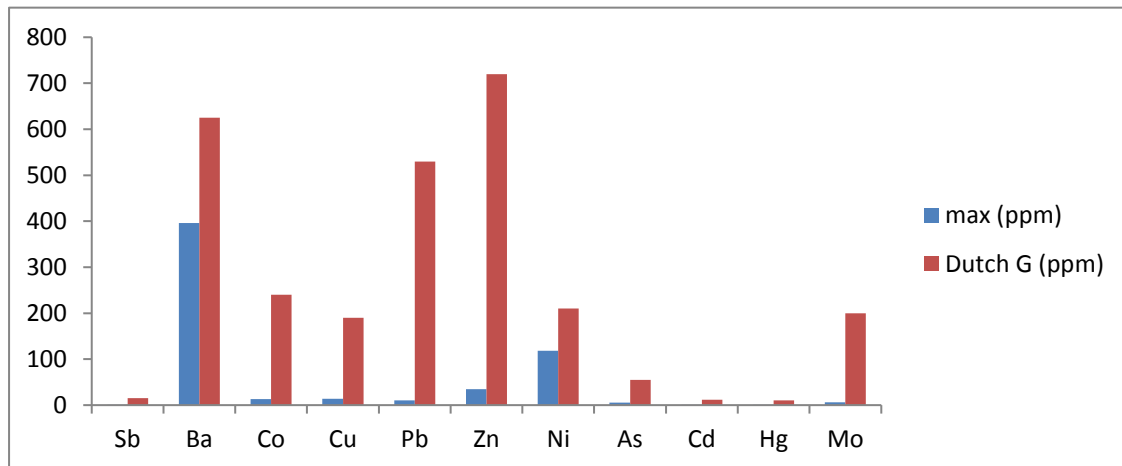


Figure 3.19. A comparison of the maximum level of each metal (in ppm) with the limit set by the Dutch guidelines (Lijzen et al., 2001) for each metal.

3.2.3 Enrichment Factor (EF) analysis and index of geoaccumulation (Igeo)

The resulting EF values, on average, show higher enrichment values for As, Cr, Sr and U concentration from Abu Dhabi beach sand samples and minor or no enrichment for metals like, Co, Cu, Pb, Zn, Ni, V. With the exception of Co, Th and Zn, all the metals do show samples with severe enrichment, in comparison to their average crustal abundance, as shown in GIS maps in (Figures 3.20 to 3.25).

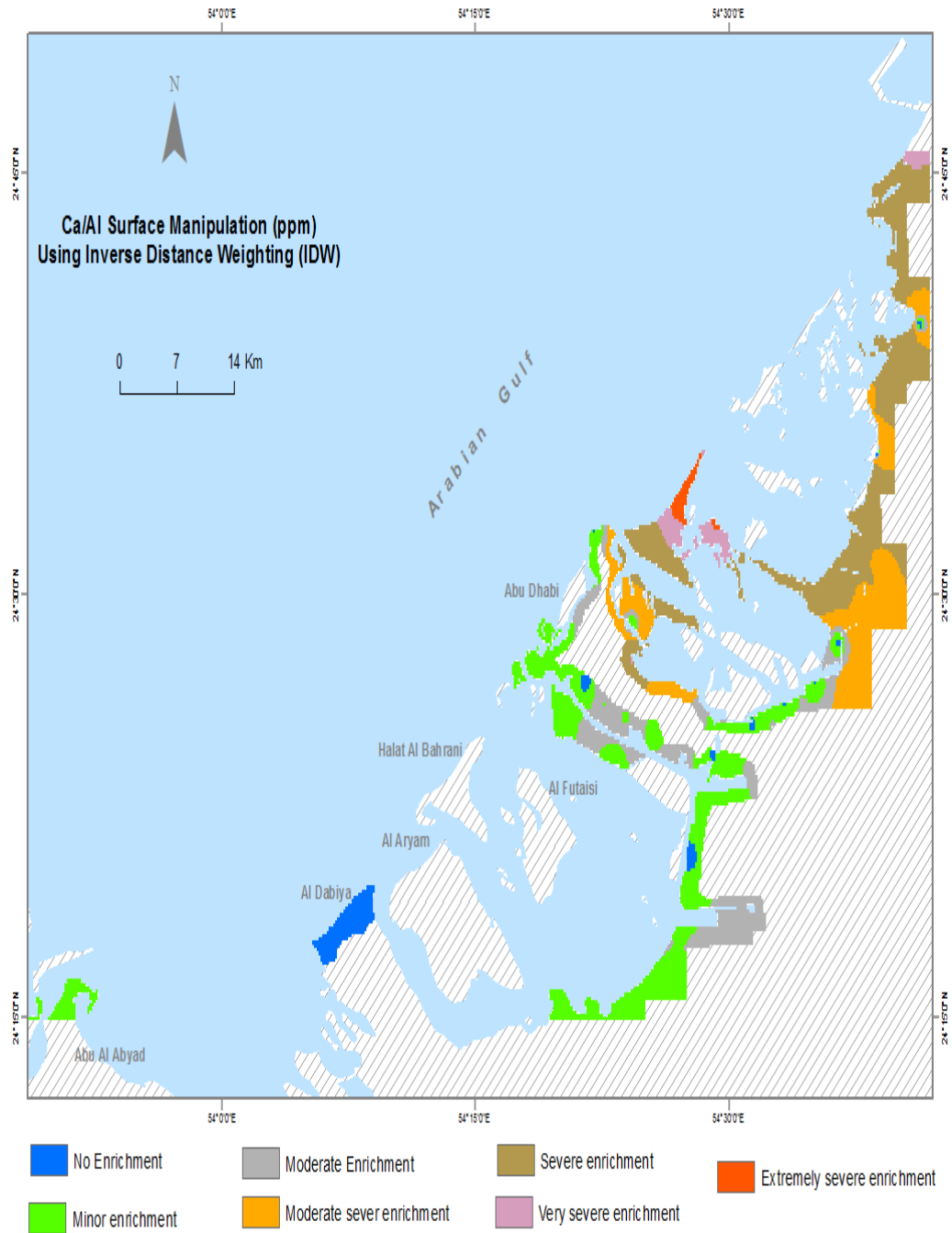


Figure 3.20. Map of Abu Dhabi showing the resulting EF values of Ca/Al of the areas from which the samples were collected.

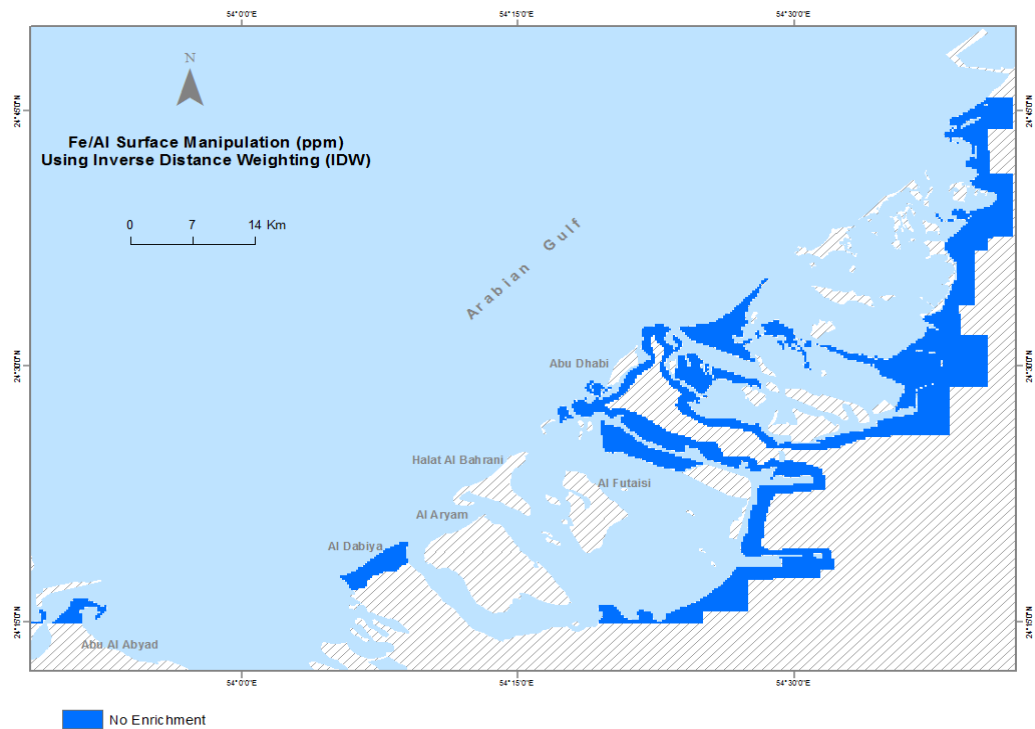


Figure 3.21. Map of Abu Dhabi showing the resulting EF values of Fe/Al of the areas from which the samples were collected.

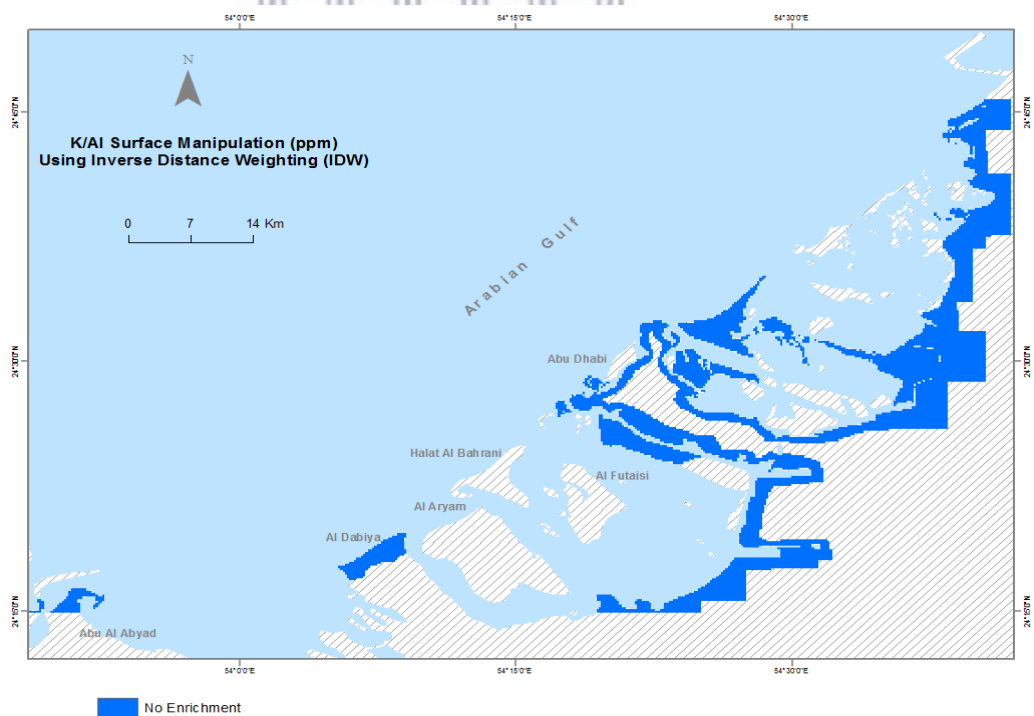


Figure 3.22. Map of Abu Dhabi showing the resulting EF values of K/Al of the areas, from which the samples were collected.

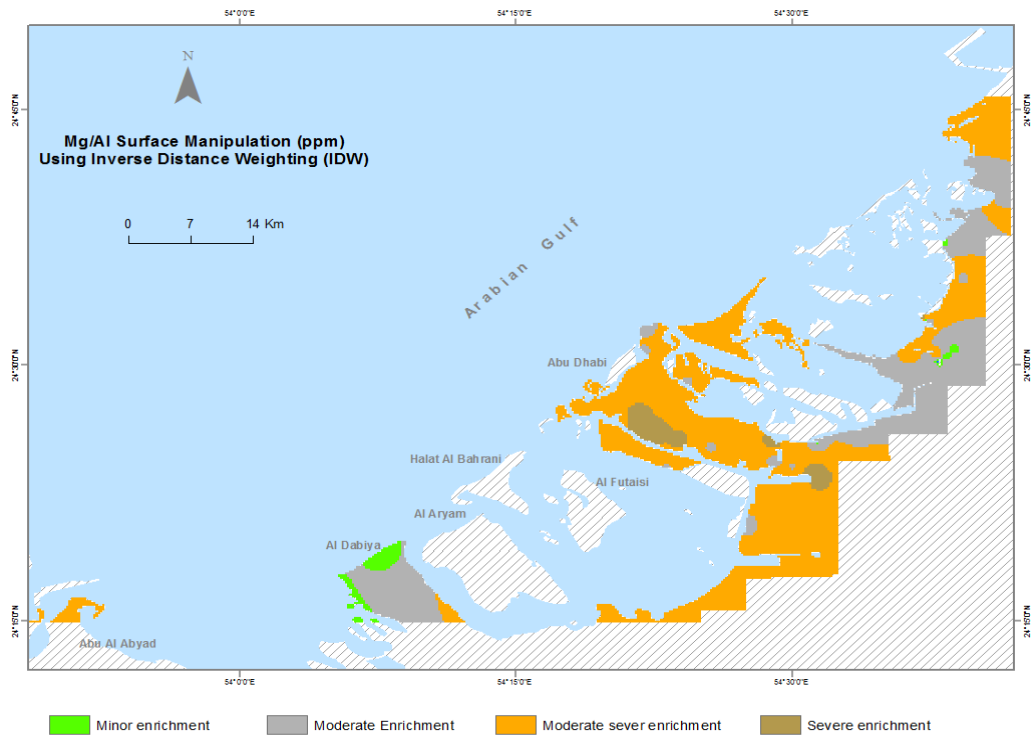


Figure 3.23. Map of Abu Dhabi showing the resulting EF values of Mg/Al of the areas from which the samples were collected.

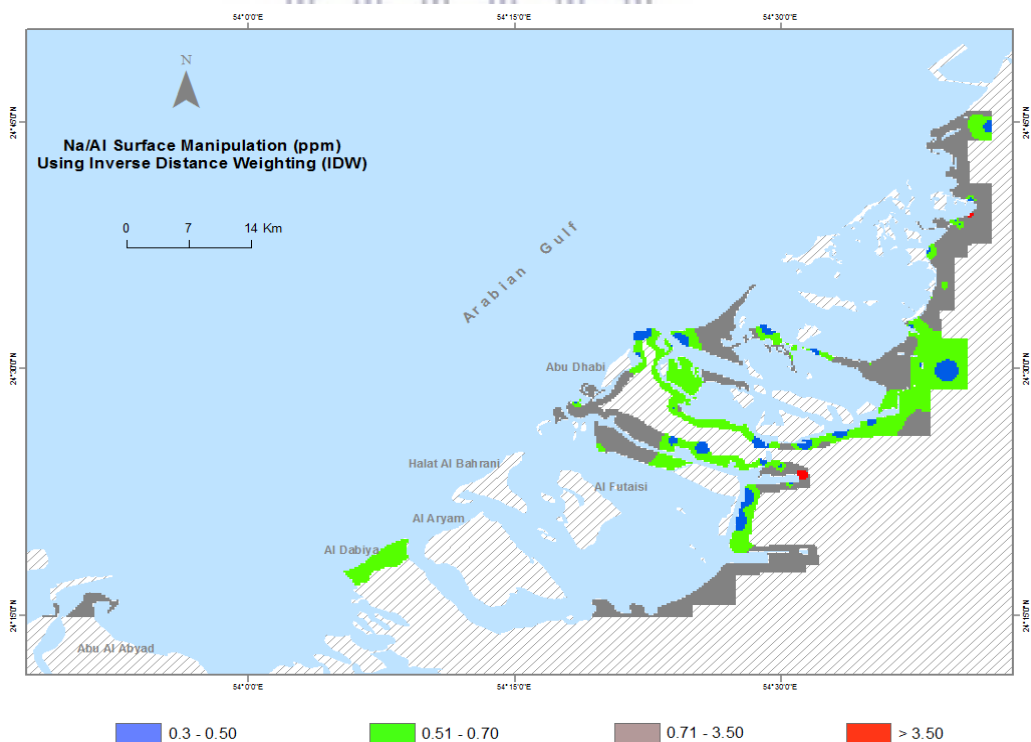


Figure 3.24. Map of Abu Dhabi showing the resulting EF values of Na/Al of the areas from which the samples were collected.

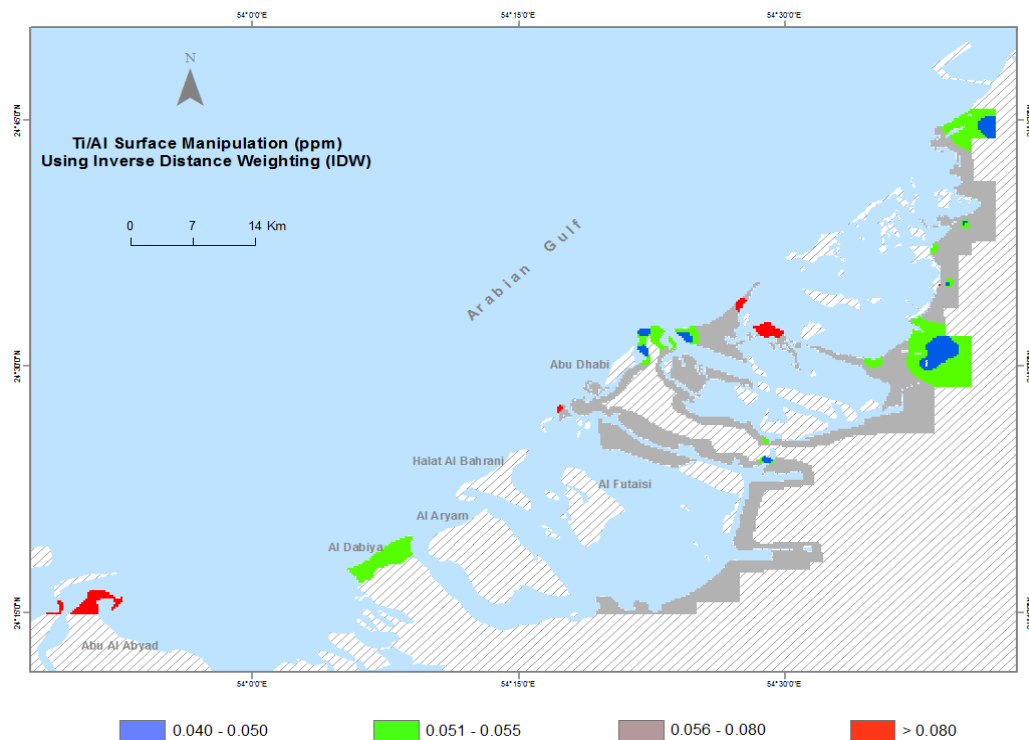


Figure 3.25. Map of Abu Dhabi showing the resulting EF values of Ti/Al of the areas from which the samples were collected.

The extent of enrichment varied spatially. For example, almost 93% of the beach sand samples showed severe to extremely severe Sr enrichment, followed by Cr with 73%; 60% with U; 30% showed severe to extremely severe enrichment. For Sr samples, 54 to 57, with the exception of sample 51, showed extremely severe enrichment. Sample 51 showed very severe enrichment. For As, samples 54 to 57 showed severe to extremely severe enrichment. For U, samples showed moderate severely to very severe enrichment, as shown in Figure 3.7. For Cr, samples 48 to 57 showed severe enrichment to extremely severe enrichment. Moderate to severe enrichment was observed for Zr, Ni, Pb, V and Co. Moderate enrichment was observed with Cu and Th, as shown in Table 3.7. The mean EF values for the studied beach sand samples decreased in the order of Sr>Cr>As>U>Zr>Ni>Pb>Th>V>Co>Cu>Zn, as shown in Table 3.7.

The difference in EF values for the different metals in the beach sediments may be due to the difference in the magnitude of input for each metal in the beach sand and/or the difference in the removal rate of each metal from the beach sand. Metals can be released with the water phase when changes occur in conditions like pH, redox potential, ionic strength, and the concentration of organic complexing agents (Calmano *et al.* 1990).

3.2.4 Index of geoaccumulation (Igeo)

The geoaccumulation index (Igeo) introduced by Muller (1981) was also used as a reference for the extent of metal pollution. The beach sand samples showed no signs of pollution with metals like Co, Cu, Ni, Pb, Th and Zn, as shown in Figures 3.26,3.27,3.28 and 3.29. While elements like As, U and Zr indicate were unpolluted to moderately polluted. The geoaccumulation index results (Table 3.7) indicate that the area is either unpolluted or moderately polluted for most of the metals, except for Cr and Sr. For Sr, 44% of the samples showed moderately to highly polluted quality, while for Cr, 16% of the beach sand samples showed moderately polluted quality. Most of those samples were similar to the ones with severe enrichment factor.

Table 3.7 EF values and geoaccumulation index (Igeo) from Abu Dhabi beach sand samples and minor.

	As	Co	Cr	Cu	Ni	Pb	Sr	Th	U	V	Zr	Zn
EF												
Min	1.84	0.15	0.00	0.25	0.31	0.30	3.41	0.37	1.48	0.27	0.83	0.13
Max	40.64	2.95	25.63	3.78	14.25	10.82	336.72	5.23	33.47	2.37	14.53	4.64
Mean	7.31	0.67	8.0	0.66	1.72	1.26	47.83	1.02	7.46	0.69	3.17	0.57
St. Dev	6.90	0.53	5.66	0.55	2.31	1.67	66.93	0.74	7.24	0.39	2.58	0.70
Igeo												
Min	-1.17	-6.81	-1.16	-5.82	-5.27	-4.10	0.05	-5.49	-1.05	-4.98	-4.07	-5.89
Max	0.70	-1.80	1.84	-2.92	-0.19	-0.53	3.74	-1.85	0.77	-2.60	0.62	-1.76
Mean	-0.20	-3.56	0.11	-4.74	-2.51	-2.93	1.90	-2.85	0.29	-3.38	-1.37	-3.95
St. Dev	0.49	0.80	1.01	0.49	1.00	0.70	0.90	0.68	0.49	0.55	0.90	0.79

According to the Muller scale (Muller, 1981) (Table 3.8), the calculated results of I_{geo} values (Table 3.10) indicated that Sr can be considered a strong pollutant, based on most of the study beach sand samples ($I_{geo} > 1$); 46 out of 57 beach sand samples showed a moderately to highly polluted value. Co, Cu, Ni, Pb, Th and V showed unpolluted status.

Table 3.8 The calculated results of I_{geo} values according to Muller scale (Muller, 1981)

	No Enrichment	Minor enrichment	Moderate Enrichment	Moderate severe enrichment	Severe enrichment	Very severe enrichment	Extremely severe enrichment	Total samples
As	0	0	3	20	26	5	3	57
Co	23	31	1	2	0	0	0	57
Cr	2	0	2	11	24	16	2	57
Cu	47	9	1	0	0	0	0	57
Ni	5	29	13	6	3	1	0	57
Pb	32	18	4	2	1	0	0	57
Sr	0	0	0	4	16	14	23	57
Th	29	26	1	1	0	0	0	57
U	0	11	13	16	13	4	0	57
V	0	40	12	4	1	0	0	57
Zn	40	15	0	2	0	0	0	57
Zr	0	22	20	9	6	0	0	57



UNIVERSITY of the
WESTERN CAPE

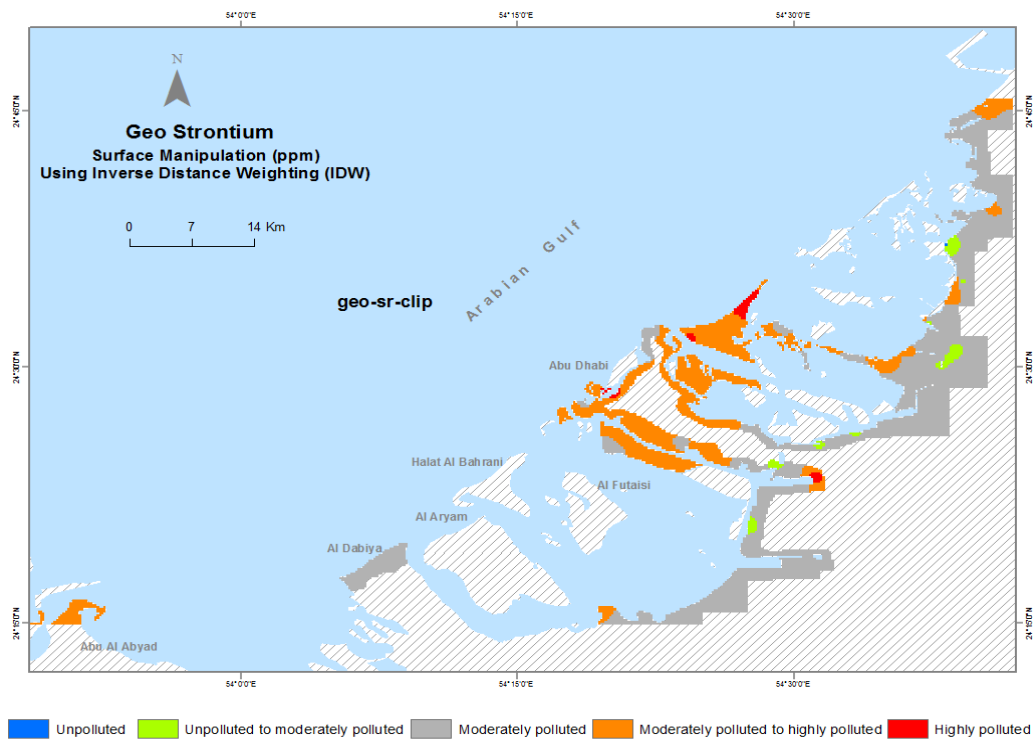


Figure 3.26. GIS map of geoaccumulation index (Igeo) values of strontium in the study area.

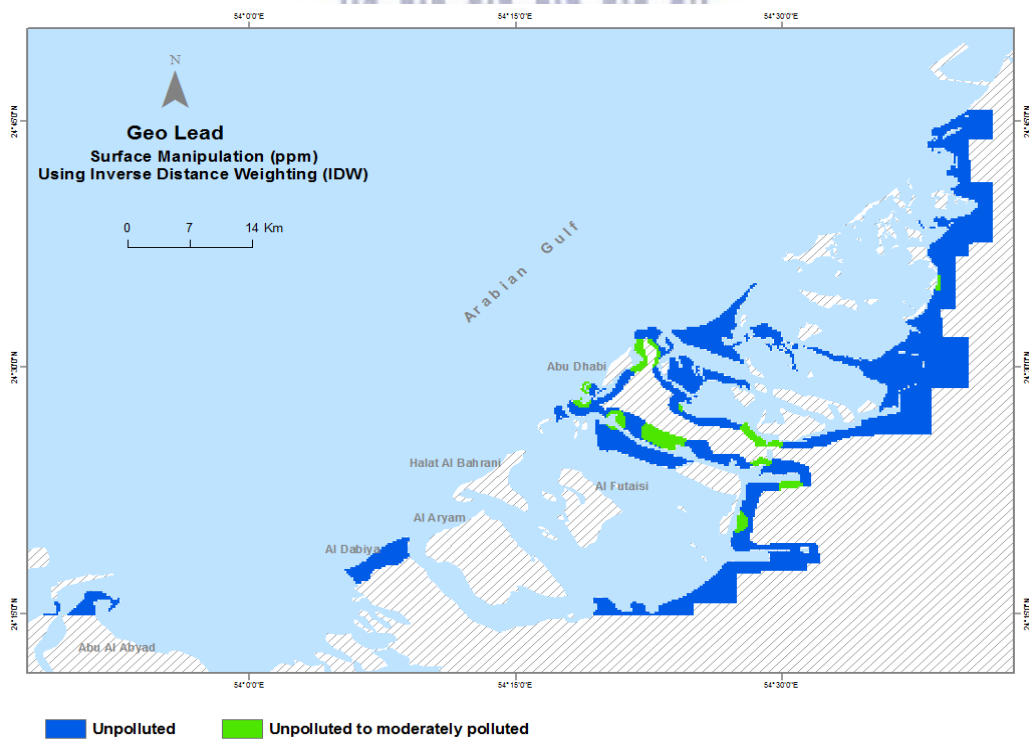


Figure 3.27. GIS map of the geoaccumulation index (Igeo) values of lead in the study area.

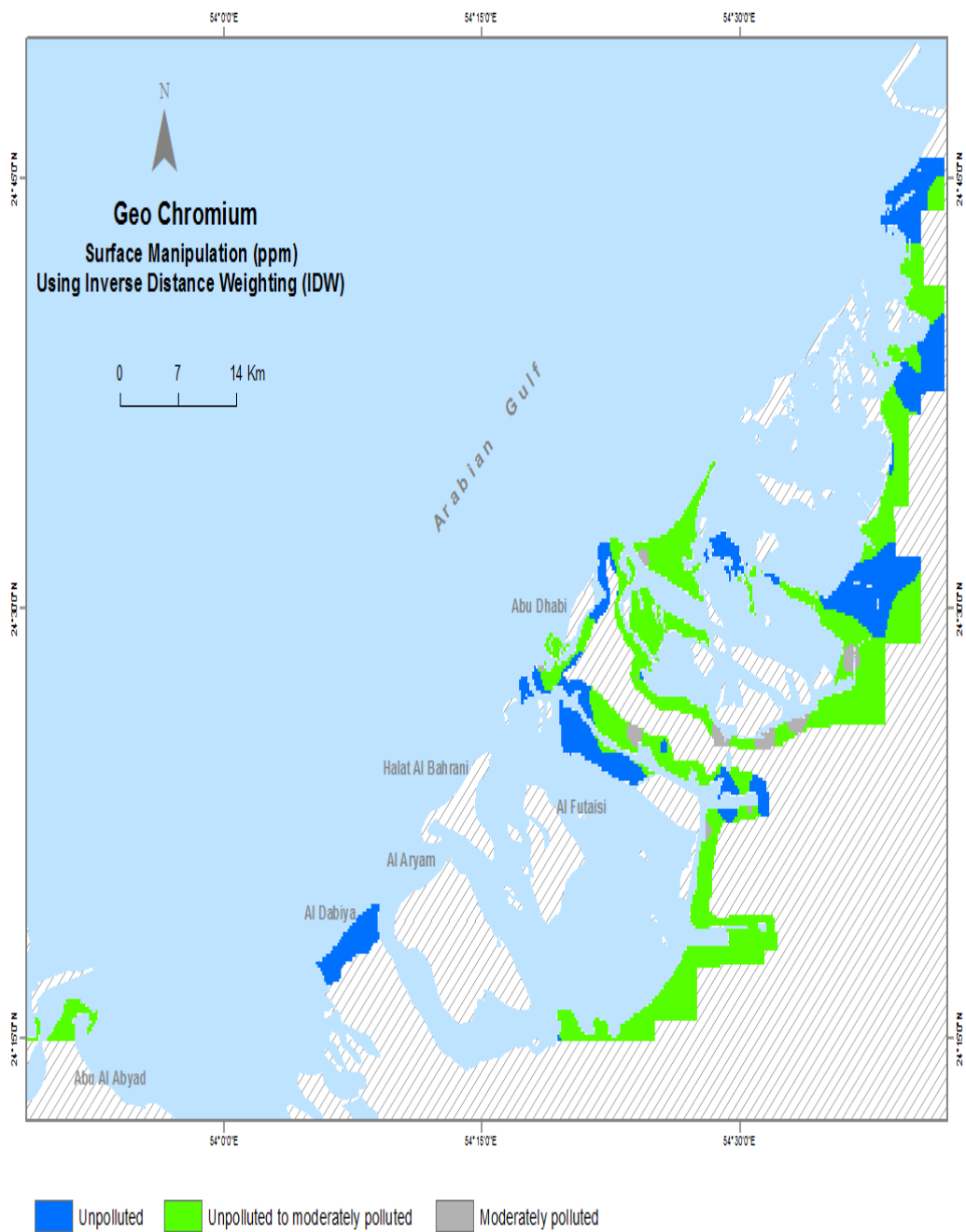


Figure 3.28. GIS map of geo-accumulation index (I_{geo}) values of chromium in the study area.

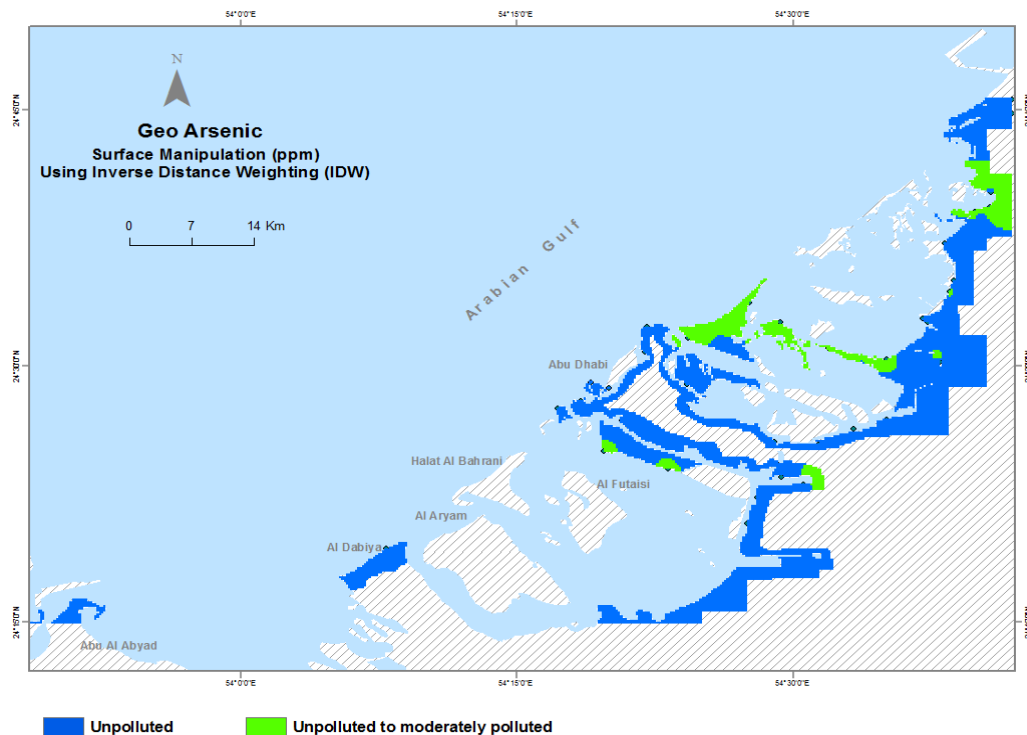


Figure 3.29. GIS map of geoaccumulation index (I_{geo}) values of arsenic in the study area.

3.2.5 Correlation analysis

Significant correlation was found among heavy metals, especially Ni/Co ($r^2=0.76$), Co/Th ($r^2=0.61$), Pb/Zn ($r^2=0.52$), Cu/Zn ($r^2=0.65$), Ni/Zn ($r^2=0.66$), Th/V ($r^2=0.84$), Nb/V ($r^2=0.81$). Cr_2O_3 is mostly positively correlated with Fe_2O_3 , MgO, Co, Nb, V and Zr, indicating possible heavy mineral metals, due to the weathering of chromite-enriched rocks (Table A7; Appendix A). CaO is positively correlated with LOI, Sr, U and As, while it is negatively correlated with almost all the major, minor and trace elements, thus indicating that strontium, uranium and arsenic originate from the sea and not from the continent.

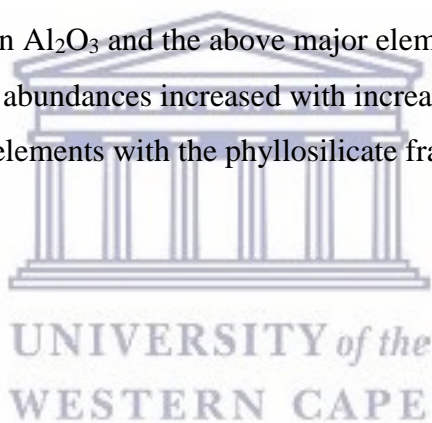
3.2.5.1 Bivariate analysis

Results of the XRF analysis of the major elements, expressed as weight percent oxide, are presented in Table 3.3. As expected, CaO was the most abundant major element, averaging 36.97 wt. %, with a range of 22.81 to 50.97 wt%, followed by LOI (average 33.42 wt%, range 21.44 to 44.80 wt. %). Among the remainder SiO_2 (21.23 wt%, range 2.66 to 48.36 wt%), MgO (2.63, wt%, range 0.32 to 4.90 wt%), Al_2O_3 (2.23 wt%, range 0.36 to 4.42 wt%), Na_2O (1.43 wt%, range 1.83 to 3.50 wt%), Fe_2O_3 (0.89 wt.%, range 0.22 to 2.15), K_2O (0.43 wt%, range

0.09 to 0.93 wt%), TiO₂ (0.13 wt%, range 0.03 to 0.27 wt%). P₂O₅ (average 0.05 wt%), Cr₂O₃ (average 0.04 wt%) and MnO (average 0.02 wt%) were present in small amounts.

Contents of major elements were plotted against CaO contents for all samples in (Figure B3a and Figure B3b; Appendix B). All of the major elements plotted showed broad trends of decreasing abundance with increasing marine carbonate content. The best correlation was shown by LOI. TiO₂, Fe₂O₃, and MgO showed some scatter to higher values above the general detrital trend. Given the association of elements, these occasionally high values were likely caused by sporadic enrichment of heavy minerals, such as magnetite or ilmenite, zircon, chromite and or ferromagnesian minerals, such as biotite or pyroxene. The remaining element, SiO₂, (Fig. 3.31) also showed a well-defined decrease, with increasing CaO. Samples with higher CaO also contained higher LOI values, and hence likely contained a biogenic CaCO₃ component, such as shell material.

The correlation between Al₂O₃ and the above major elements is shown in (Figure 3.30 b). As expected from the above, abundances increased with increasing Al₂O₃, suggesting the association of most of these elements with the phyllosilicate fraction.



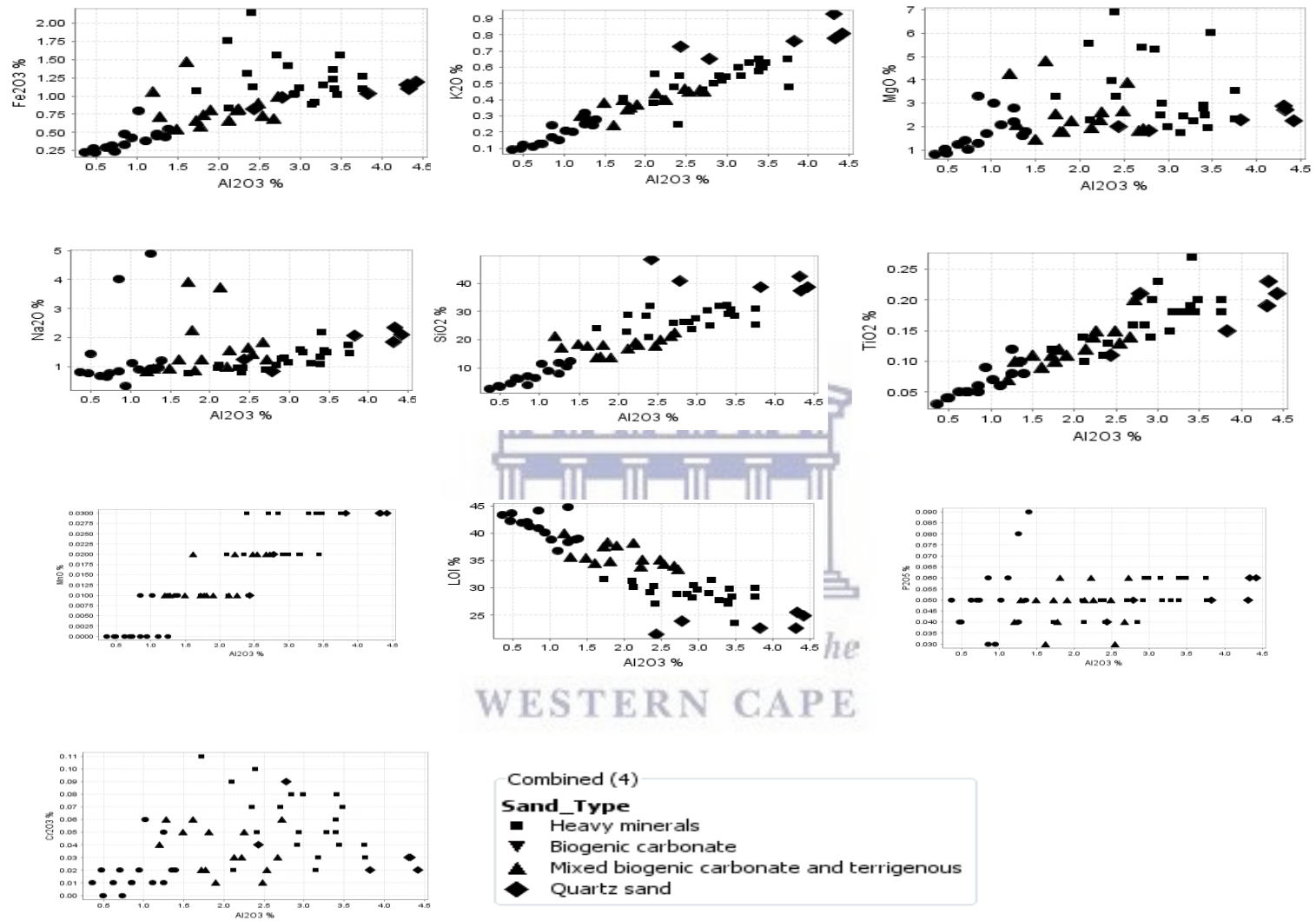


Figure 3.30a. Contents of major elements against Al_2O_3 contents for all samples.

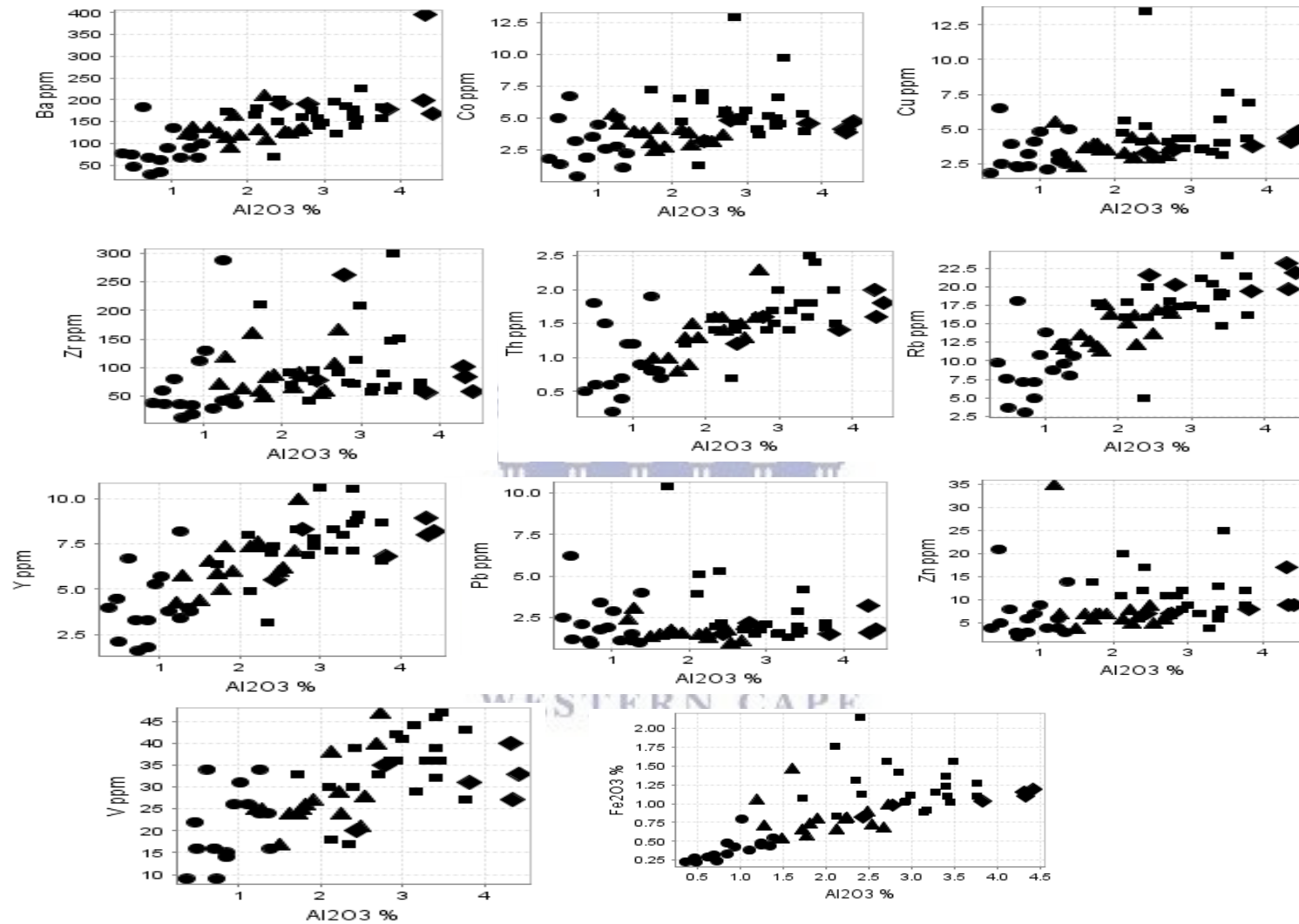


Figure 3.30b. Minor and trace elements – Al₂O₃ variation in beach sand samples from Abu Dhabi, United Arab Emirates.

Overall correlations were somewhat poorer than with CaO, suggesting that biogenic carbonate content is the main control of the chemistry of individual samples. Sodium oxide (Na_2O) and K_2O showed unusual trends. Sodium oxide did not display a strong linear increase with increasing Al_2O_3 . Potassium oxide (K_2O) showed a positive linear relation with Al_2O_3 (Figure 3.30 a). The contrasting pattern in the Abu Dhabi beach sediments was probably due to higher NaCl content in the finer sands (less SiO_2 -rich). The higher NaCl content likely resulted from the presence of K and K-feldspar and phyllosilicates, with the scatter resulting from variable proportions of these two components.

Negative correlations were found between CaO and most of the trace elements, with the exception of Sr, U and As (Table A7), whereas those with Al_2O_3 were positive, suggesting an association with the phyllosilicate fraction, coupled with dilution by quartz. Given the strong linear correlation between Nb and TiO_2 and between Ni and Fe_2O_3 , respectively, (Figure 3.30a, b), these elements were thought to have had the same origin.

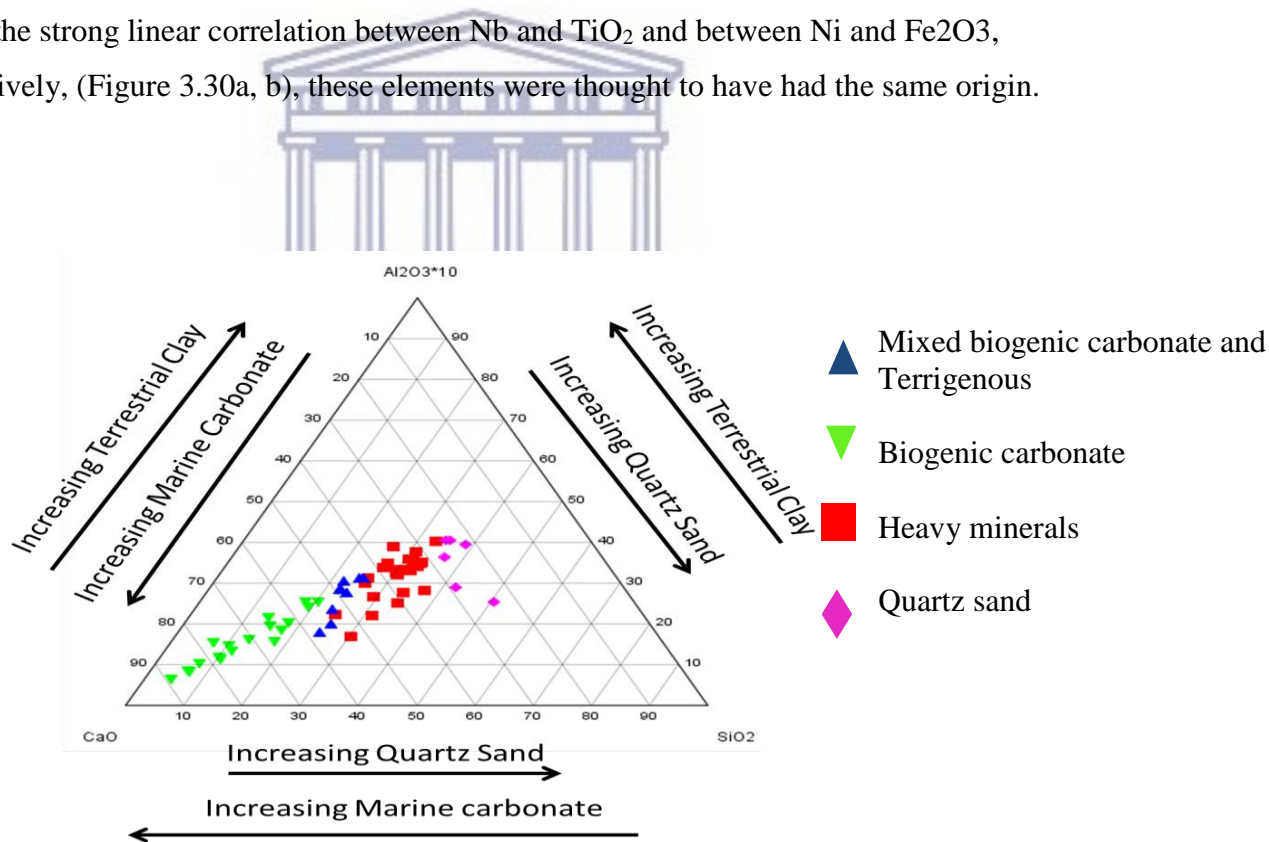


Figure 3.31. The relationship between CaO for biogenic carbonate, SiO_2 for quartz sand, and Al_2O_3 for silt/clay in the beach sediments of Abu Dhabi samples.

3.2.6 Cluster analysis and discriminant analysis

A combination of cluster and discriminant analysis was used in order to classify and characterize the beach sand into geochemically homogenous groups. Cluster analysis (CA) was used to classify the beach sand, while discriminant analysis was used to characterize, in terms of geochemistry, and differentiate the groups created through cluster analysis. Cluster analysis was also used to group the similar sampling sites (spatial variability) and to identify areas of similar geochemical composition or contamination (Casado-Martinez et al., 2009; Chung et al., 2011; Rath et al., 2009; Simeonov et al., 2000; Sundaray et al., 2011; Yang et al., 2009 and AlRashdi and Siad, 2015).

Hierarchical agglomerative cluster analysis was performed on major rock-forming elements using Ward's method, with Euclidean distances used as a measure of similarity. The result was presented as a dendrogram (Figure 3.32), from which four groups containing the 57 beach sand samples were identified. The four beach-sand groups were further characterized geochemically using the linear discriminant analysis technique. From this analysis, the maximum number of discriminant functions is either one less than the number of groups or equal to the number of the predictor variables. A three-group discriminant function was computed using the major rock-forming elements (Table 3.8a). As for the interpretation, a combination of Tables 3.8a and 3.8b was used to pinpoint geochemical elements that characterize each of the beach-sand types.

Function one, highly positively correlated with SiO_2 , K_2O , Al_2O_3 and TiO_2 and negatively correlated with LOI and CaO, separated terrigenous from biogenic marine beach sand. Alumino-silicate and alumino-silicate with heavy mineral beach sediments are characterized by high SiO_2 , K_2O , Al_2O_3 and TiO_2 , indicating a terrigenous source, while biogenic carbonate beach sediments are enriched with CaO and LOI, indicating biogenic marine carbonate.

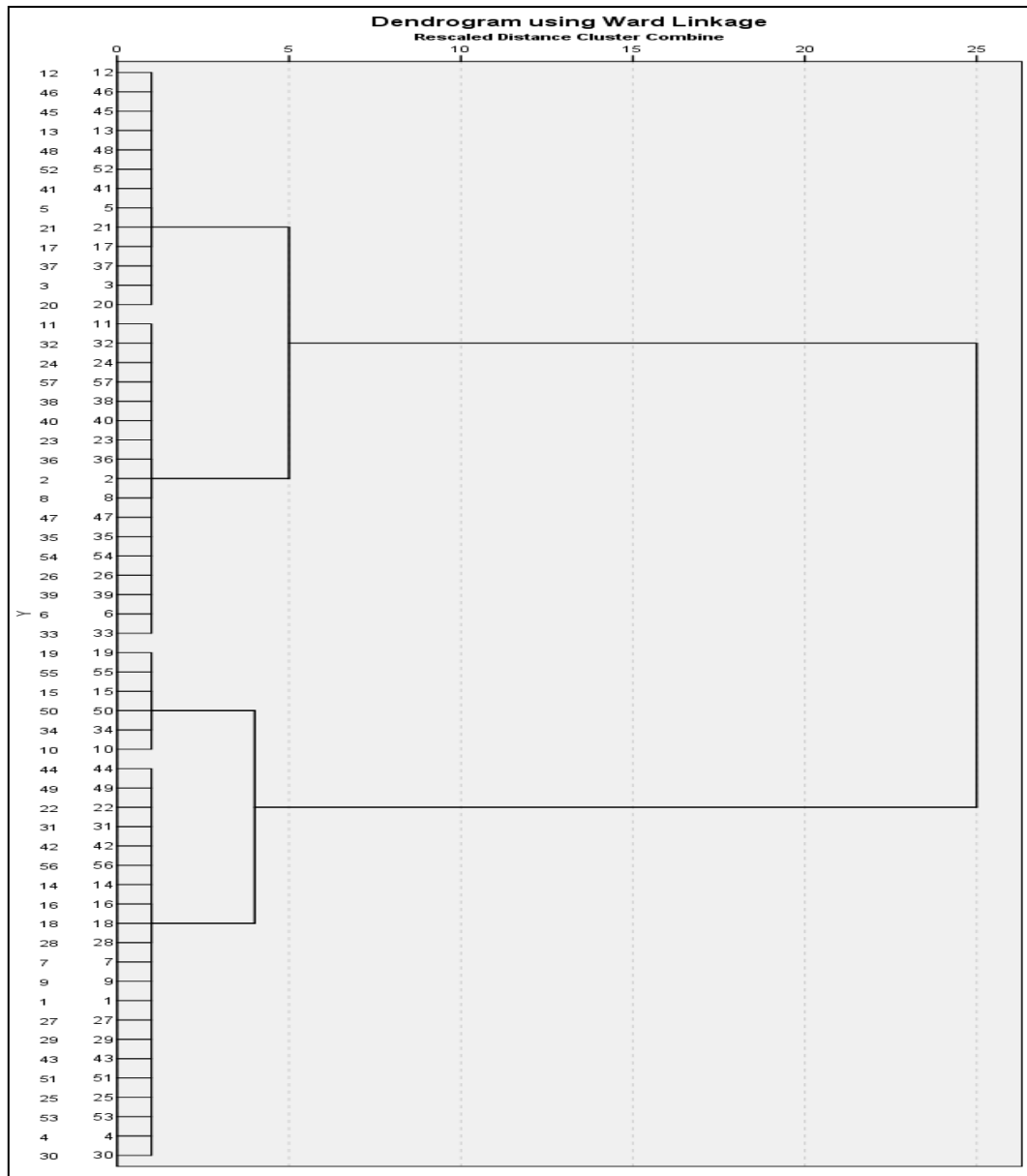


Figure 3.32. Dendrogram showing cluster result for the beach sand of Abu Dhabi, United Arab Emirates.

Function two, highly positively correlated with Fe_2O_3 , Cr_2O_3 , MgO and MnO , categorized as heavy mineral sand types from an ophiolite source, and could be easily differentiated from the silico-feldspathic group.

Function three separated halite's sand type from the other three, with Na_2O . Beach-sand groups classified through cluster analysis are correct by 100%. See Tables 3.8a and

3.8b below. Figure 3.33 is a discriminant plot representing the first two discriminant functions for the beach sand of Abu Dhabi. Since the direct discriminant function method does not show the importance of the individual geochemical variables for the description of classified groups, or their importance in the classification itself, a stepwise discriminant method should be considered (Siad et al., 1994). In this method, variables are selected through a statistical test to determine the order in which they are entered or removed into the analysis. At each step, the element that yielded the best classification was entered. In this process, SiO₂ and Fe₂O₃ were the best discriminating geochemical variables, separating the four beach sands by up to 100%, as shown in Figure 3.34.

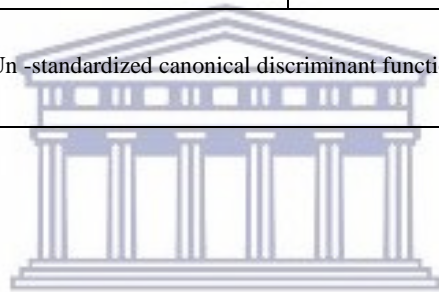
Table 3.9a. Three-discriminant group function

Structure Matrix			
	Function		
	1	2	3
SiO ₂	.747*	.426	-.066
L.O.I	-.671*	-.102	.625
CaO	-.552*	-.038	-.044
K ₂ O	.492*	.342	.158
Al ₂ O ₃	.405*	-.054	.038
TiO ₂	.279*	-.218	.145
Fe ₂ O ₃	.291	-.648*	-.039
Cr ₂ O ₃	.139	-.493*	-.109
MgO	.100	-.457*	-.027
MnO	.302	-.306*	.057
P ₂ O ₅	.010	.004	-.417*
Na ₂ O	.004	.162	.397*

Table 3.9b. Function at group centroid

Functions at Group Centroids			
Beach sand types	Function		
	1	2	3
1	3.184	-.807	-.227
2	-6.065	.406	-.321
3	-1.189	-.123	.661
4	6.991	2.115	-.053

Un-standardized canonical discriminant functions evaluated at group means



UNIVERSITY of the
WESTERN CAPE

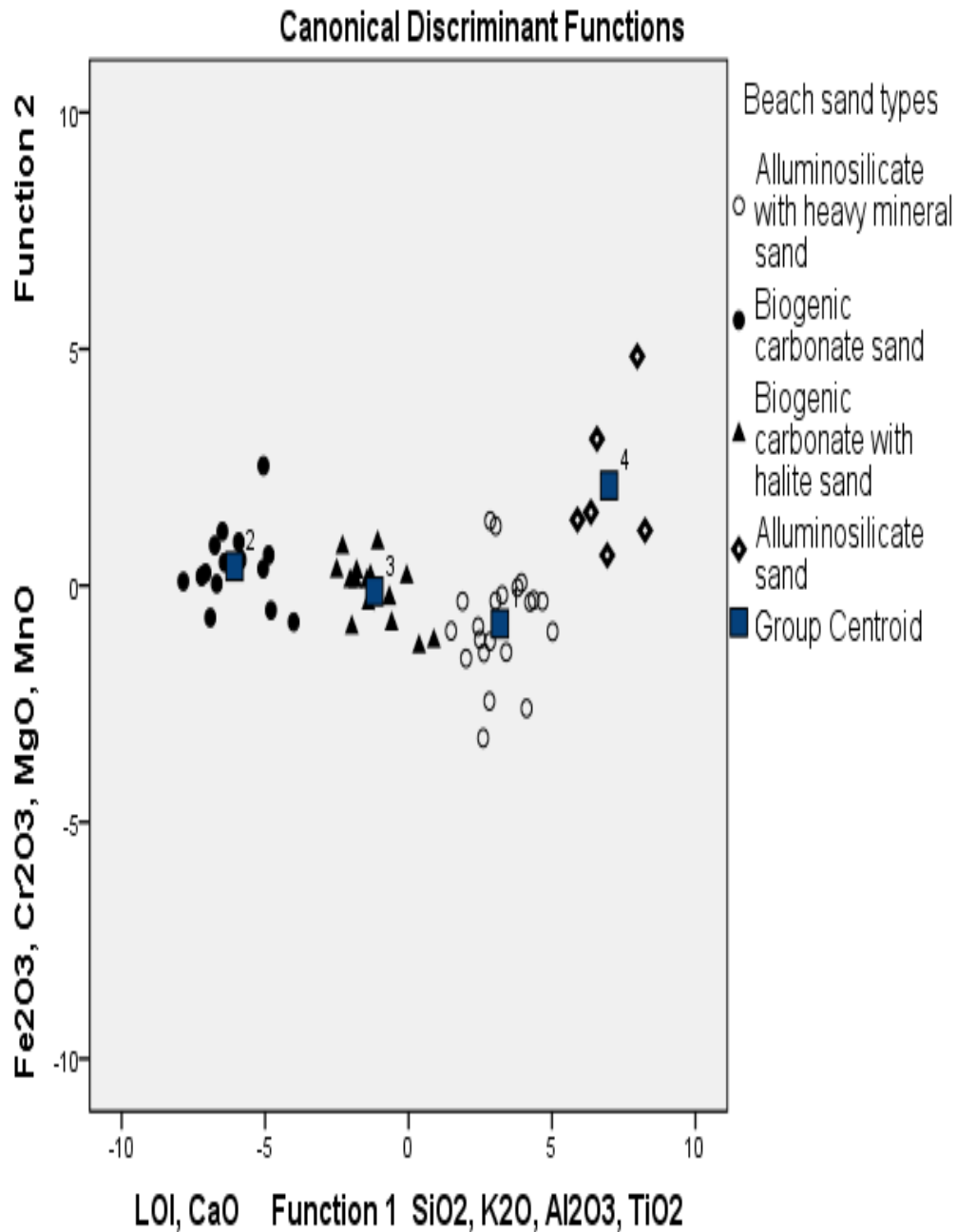


Figure 3.33. Two-function discriminant plot showing the abundance of elements in each beach sand type.

3.2.7 Factor analysis

Factor analysis was performed using 26 variables of the samples analysed. Table 3.9 shows the initial determined factor, their eigen values and the percent of variance contributed by each factor. Only factors with eigen values of 1 or more were taken into consideration, which resulted in five factors that were sufficient in explaining 79.35% of the variance. The total variance explained by these five factors after rotation – factor 1, factor 2, factor 3, factor 4, and factor 5 – are 34.679%, 14.854%, 13.531%, 9.115%, and 7.172%, respectively.

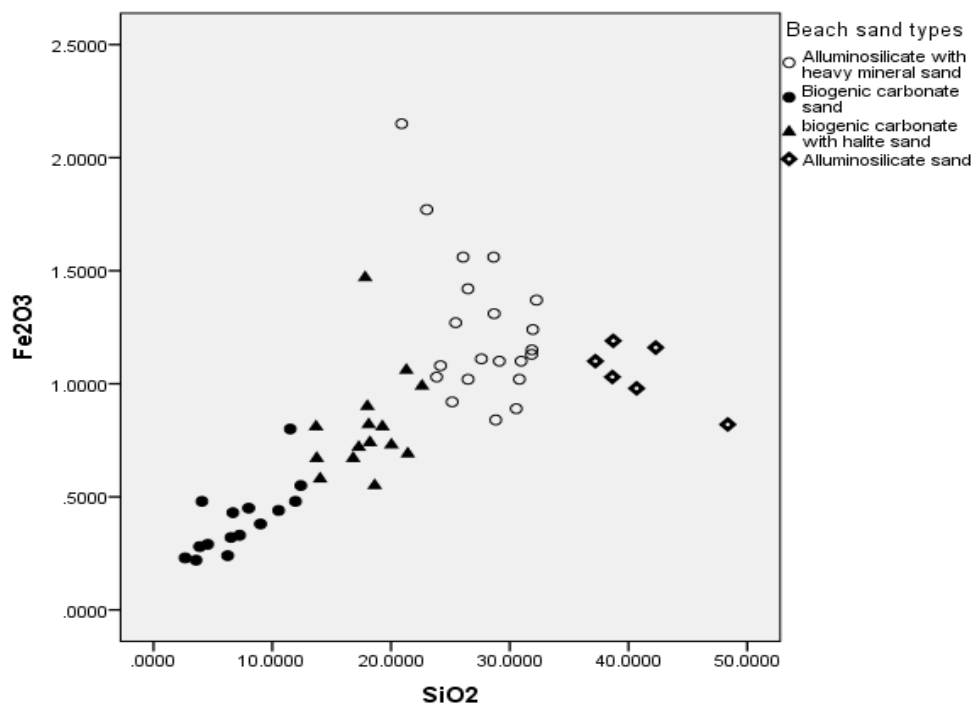


Figure 3.34. Scatter plot of SiO₂ and Fe₂O₃.

The five factors shown in Table 3.11 were found to be dominated by certain variables based on prevailing geochemical processes and land-use practices. These five factors were named “felsic and carbonate beach sand separating factor” for factor 1, “heavy mineral rich

factor” for factor 2, “heavy metals factor” for factor three, “ophiolite originating beach sand factor” for factor 4, and “halite-rich beach sand factor” for factor 5, based on the major contributing variables of the factor loadings. The main positively loaded variables for the terrigenous and biogenic beach sands separating factor are K_2O , Al_2O_3 , SiO_2 , Rb, MnO, TiO_2 , Ba, Nb, V, Th and Fe_2O_3 , characterizing beach sand originating from possible felsic rocks, while CaO, LOI, Sr and U are negatively loaded in this factor, indicating beach sand with a carbonate origin.

Factor two is highly positively with Zr, Nb, V, Th, TiO_2 , Co and Cr_2O_3 . This factor is considered to be beach-sand rich, with heavy metal originating from possible intermediate rock.

Factor three is dominated by heavy metals, including Ni, Zn, Cu, Co and Pb. Although the concentration of these heavy metals is not high, it can be mainly attributed to industrial activities.

The first factor (F1), which is positively correlated with K_2O , Al_2O_3 , SiO_2 , Rb, MnO, TiO_2 , Ba, Nb, V, Th and Fe_2O_3 , and negatively loaded with CaO, LOI, Sr and U (Table 3.10), separates terrigenous beach sand from biogenic marine carbonate sand (Figure B.16). Factor two (F2) is considered to be beach sand rich with heavy metal due to its enrichment with Zr, Nb, V, Th, TiO_2 , Co and Cr_2O_3 (Figure B.17).

Factor three (F3) is dominated by heavy metals, including Ni, Zn, Cu, Co and Pb (Figure B.18). Although the concentration of these heavy metals is not high, it is mainly attributable to industrial activities.

Factor four (F4) is dominated by high loading with MgO, Fe_2O_3 , Cr_2O_3 and MnO (Figure B.19), pointing to heavy mineral beach sand. These elements indicate a possible mafic rock provenance.

Factor five (F5) is positively loaded with As, Na_2O and U and negatively loaded with P_2O_5 (Figure B.20), indicating halite beach sand with high concentrations of arsenic and

uranium. It is negatively loading with P₂O₅, which is interpreted as originating from fertilizing activities or industries.



UNIVERSITY *of the*
WESTERN CAPE

Table 3.10. Factor analysis results: Total variance

Total Variance Explained									
Component	Initial Eigenvalues			Extraction Sums of Squared Loadings			Rotation Sums of Squared Loadings		
	Total	% of Variance	Cumulative %	Total	% of Variance	Cumulative %	Total	% of Variance	Cumulative %
1	12.171	46.810	46.810	12.171	46.810	46.810	9.017	34.679	34.679
2	3.336	12.831	59.641	3.336	12.831	59.641	3.862	14.854	49.533
3	2.058	7.917	67.557	2.058	7.917	67.557	3.518	13.531	63.064
4	1.740	6.693	74.251	1.740	6.693	74.251	2.370	9.115	72.179
5	1.326	5.100	79.351	1.326	5.100	79.351	1.865	7.172	79.351
6	.954	3.671	83.022						
7	.780	3.001	86.023						
8	.744	2.860	88.883						
9	.500	1.925	90.808						
10	.425	1.633	92.440						
11	.369	1.420	93.861						
12	.346	1.330	95.191						
13	.323	1.244	96.435						
14	.231	.888	97.323						
15	.161	.618	97.941						
16	.132	.507	98.447						
17	.118	.454	98.901						
18	.096	.368	99.269						
19	.058	.222	99.490						
20	.054	.209	99.700						
21	.028	.108	99.808						
22	.014	.054	99.862						
23	.013	.050	99.913						
24	.009	.035	99.947						
25	.008	.032	99.979						
26	.005	.021	100.000						

Extraction Method: Principal Component Analysis

Table 3.11. Factor analysis result: Rotated Component Matrix

Rotated Component Matrix					
	Component				
	1	2	3	4	5
K2O	.959				
Al2O3	.936				
SiO2	.922				
CaO	-.903				
L.O.I.	-.899				
Rb	.810				
MnO	.793			.434	
TiO2	.774	.515			
Ba	.749				
Sr	-.719	-.420			
U	-.515				.415
Zr		.832			
Nb	.480	.786			
V	.513	.729			
Th	.560	.725			
Ni			.883		
Zn			.816		
Cu			.729		
Co		.503	.603		
Pb			.550		
MgO				.829	
Fe2O3	.584			.685	
Cr2O3		.498		.677	
As					.794
Na2O					.672
P2O5					-.429

Extraction method: Principal Component Analysis. Rotation method: Varimax with Kaiser normalization: Rotation converged in 7 iterations.

Factor four is dominated by high loading with elements indicating mafic rock, with MgO, Fe₂O₃, Cr₂O₃ and MnO. Factor five is positively loaded with As, Na₂O and U and negatively loaded with P₂O₅, indicating halite beach sand with a high concentration of arsenic and uranium, while negatively loading with P₂O₅, interpreted as originating from fertilizing activities or industries.

3.3 Mineralogy

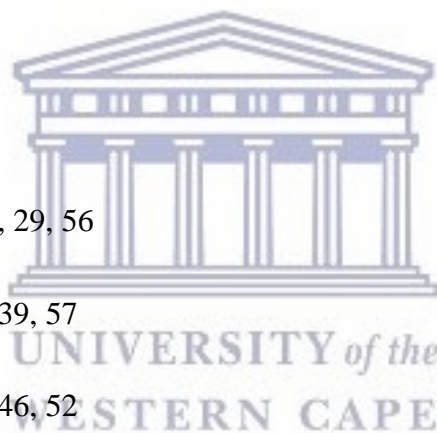
A scatter diagram of the data, based on four groups, was created through cluster analysis. The four groups can be separated with CaO and SiO₂, as per the scatter plot. Three (3) samples were selected from each group. The XRD analysis was conducted for the 12 samples as follows:

Group 1: samples 28, 29, 56

Group 2: samples 8, 39, 57

Group 3: samples 3, 46, 52

Group 4: samples 10, 50, 55



The mineralogical composition of the 12 beach sand samples from Abu Dhabi is shown in Table 3.12. Samples 3, 11, 28, 29, 39, 52, 56, 57 contained halite salt, which could have been formed when the water level increased, and then deposited. Sample 57 contained the highest content of halite. Sample 28 and 29 were of similar mineralogy, and were therefore formed by or underwent similar processes. Sample 3, 11, 39, 46, and 52 contained more limestone (calcite), with a mixture of quartz. Sample 55 and 56 contained the highest content of quartz. Sample 57 contained mostly aragonite. Sample 56 and 57 were still in the

process of forming dolomite, due to the presence of calcite magnesium, which serves as the intermediate mineral between calcite/aragonite and dolomite. Dolomite in the Abu Dhabi beach is formed through a diagenesis process. Sample 50 showed low content of crystalline materials but contained amorphous minerals that the XRD cannot detect. Sample 11, 10, 28, 29, 39, 46 and 50 contained significant oxides of Fe and Mg. The samples were rich in CaO and SiO₂.

Based on the four groups created through the combination of cluster and discriminant analysis, three beach sand samples from each group were selected and analyzed through XRD (Figures B4-B15 in the appendices). Carbonate minerals dominate the mineralogy of the beach sediments, followed by quartz and halite. Some of the samples show a mixture of calcite, halite and quartz. Most of the carbonates are calcite/aragonite and dolomite. Dolomite in the Abu Dhabi beach is formed through diagenesis processes.

Table 3.12. The mineralogical composition of the 12 beach sand samples from Abu Dhabi.

samples	Major mineral	Minor minerals	Trace minerals
3	Calcite* and quartz	Halite	Dolomite, Albite-c, Aragonite
10	Quartz* and calcite	Albite-c	Aragonite, diopside and augite
11	Calcite* and quartz	Aragonite and augite	Albite-c and halite
28	Quartz* and calcite	Albite-c	Diopside, augite, aragonite and halite
29	Quartz* and calcite	Albite-c	Diopside, augite, aragonite and halite
39	Calcite* and quartz	Aragonite and augite	Halite and albite-c
46	Calcite* and quartz	Dolomite and albite-c	Aragonite and augite
50	Quartz* and calcite		Aragonite, dolomite, augite and albite-c
52	Calcite* and quartz	Albite-c	Halite, aragonite and dolomite
55	Quartz*, calcite and aragonite	albite	Dolomite, albite-c
56	Quartz*, calcite and aragonite	Clinochrysotile and Calcite magnesian	Halite and albite-c
57	Aragonite and halite	Calcite, albite-c and quartz	Calcite magnesian

Chapter IV

4.0 Discussion

The major findings of this study, including the grain-size analysis, geochemistry and mineralogy of the coastal sediments of Abu Dhabi, are discussed in the sections below.

4.1 Grain-size distribution

In this section, the results of the study are discussed and compared to the literature regarding beach sediment grain size and its depositional environment in Abu Dhabi, United Arab Emirates.

Most of the beach sediments were identified as gravelly sand (Figure 3.1). Four grain-size statistical parameters (i.e. Mz , σI , Ski and KG ; Folk and Ward, 1957) were calculated using the cumulative curves (Figure 3.3). The mean (Mz) reflects the overall average size of the beach samples and is influenced by sample source, mode of transportation and environment of deposition (Folk, 1966; Udden, 1914). The grain size controls the mode and points the distance of transportation: the finer the size, the greater the distance. Most of the beach sediments are gravel sand to sand (Table A1 in Appendix A), suggesting they were deposited under high energy conditions, as sediments usually become coarser with the increase in energy of the transporting medium (Folk, 1974). The inclusive standard deviation, which measures the uniformity of grain-size distribution within the beach samples, depends on the size range in the source rock, the extent of weathering, the distance of transportation, and the energy variation of the depositing medium (Amaral and Prayor, 1977; Folk and Ward, 1957). The results (Table A1 in Appendix A) show that more than two-thirds of the beach sand have grain-size distributions that are poorly to very poorly to extremely poorly sorted. A poor sorting indicates that little selection of grains has taken place during transport or deposition. This might be explained as the result of highly variable energy, turbulent conditions, and lack of constant energy in any one direction. Table A1 (Appendix A) also shows that almost 90% of the beach samples are coarse- to strongly-coarse-skewed, which indicates the dominance of coarse fraction in Abu Dhabi beach

sediments. The positive values indicate skewness towards the finer grain sizes, while the negative values indicate skewness towards the coarser grain sizes. The analysed samples are skewed towards the coarser grain sizes, indicating marine biogenic sediments. More than half of Abu Dhabi beach sand samples are leptokurtic to very leptokurtic: that is, the central portions are better sorted at the tails. This strongly suggests a fluvial or tidal environment, confirming that the sands are river-deposited.

4.2 Bivariant scatter graphs of grain size parameters

Figure 3.4 shows the relationship between the mean grain size and the sorting of the collected samples, which are mostly medium to coarse sand range. Few samples are within the fine sand range, and most lie in the range of moderately to poorly sorted sediments. Normally mean grain size and sorting are hydraulically controlled, so that all sedimentary environments with the best sorted sediments have mean size in finer fraction. Abu Dhabi beach sediment samples confirm this trend (see Figure 3.5). The relationship between skewness and the sorting of the collected samples ranges mainly from moderately to poorly sorted sediments, and most of the samples have negative skewness values, with few samples near symmetrical (Figure 3.6). The coarse fractions may be due to the presence of shell and rock fragments. Plotting skewness against kurtosis is a powerful tool for interpreting the genesis of sediment, by quantifying the degree of normality of its size distribution (Folk, 1966). It is clear from the plotting relationship between skewness and kurtosis that most of the sediments from the collected samples lay within the negative skewness and kurtosis range of the mesokurtic to leptokurtic field, with few samples lying in the platykurtic range (Figure 3.7). This suggests the dominance of a sand population, with the presence of a subordinate population of coarse-grained particles.

4.3 Determination of the mechanisms and environments of deposition

The process and environment of deposition were decoded using Sahu's (1964) linear discriminate functions of Y1 (Aeolian, beach), Y2 (Beach, shallow agitated water) and Y3

(Shallow marine, fluvial). The scatter plot of Y1 and Y2 shows that the majority of the beach sediments fall within Beach/shallow agitated (Figure 3.8), with few samples falling within Aeolian/shallow agitated. The scatter plot of Y2 and Y3 (Figure 3.9) indicates that almost 50% of the samples are deposited in Shallow marine agitated, while the other 50% are fluvial agitated.

4.4 Pollutant indicators

4.4.1 Trace elements distribution and comparison with Dutch guidelines

In Table 3.6b, Sr is the most abundant element, followed by Cr, Ba and Rb. Among the remaining trace elements, only Ni, Y, Zn, Cu, V, Co, U, Th, Mo, Pb and Nb were present in moderate concentrations. Arsenic and U are relatively high, exceeding the value in the average upper continental crust (see Table 3.6b). All the heavy metals are below the Dutch guidelines (Lijzen et al., 2001), as shown in Table 3.6a and Figure 3. 19.

Antimony and **arsenic** are released from sulphide-ores processing. They are found in realgar (As_4S_4) and stibnite (Sb_2S_3) (Cox, 2004). The level of antimony does not exceed 0.2 ppm in samples no. 3, 21, 22, 31, 39, 46, 47 and 56. The level of Sb, in the rest of the samples, is 60.1 ppm. In all the samples, the level of antimony is well below the safe limit (15 ppm), as specified by the Dutch guidelines (Lijzen et al., 2001).

Arsenic sources include mining, pesticides and power-generating plants (Newton, 2007). Arsenic concentrations in Abu Dhabi are negligible compared to the safe limit, which is 55 ppm. The maximum value is 5.0 ppm, in sample no. 5, from Yas Island. The minimum value of 1.4 ppm, in Abu Dhabi Island (sample 40), greatly agree with the results from De Mora et al. (2004).

Barium concentrations vary from 28 to 227 ppm, with an average of 136 ppm. The highest value in sample 30 (Musaffah Industrial) is only 36% of the safe limit, which is

625 ppm. Fourteen samples have less than 100 ppm of Ba, 38 samples have Ba ranging from 100 to <200 ppm, and three samples have >200 ppm of Ba.

Cadmium sources include mining, industrial wastes, water pipes and electroplating plants (Newton, 2008). Cadmium is used in anti-corrosion coating (Cox, 2004). Half of the samples have Cd concentrations of <0.1 ppm, while the rest do not exceed 0.3 ppm, with the safe limit being 12 ppm. These values are in good agreement with the 0.02 ppm value published by De Mora et al. (2004), but are an order of magnitude smaller than the values reported by Shriadah (1998).

The maximum contamination of **cobalt**, which was found in Musaffah Industrial, is <3% of the safe limit, which is 240 ppm. The values range from 0.4 to 7.2 ppm, with an average of 4.1 ppm, which is an order of magnitude greater than the average reported by De Mora et al. (2004), and almost triple the value reported by Shriadah (1999).

Copper is released from electroplating, mining, and municipal wastes. The maximum contamination of Cu in Abu Dhabi is <3.4% of the safe limit, which is 190 ppm. Cu concentrations range from 1.8 ppm to 6.5 ppm, with an average of 3.8 ppm. The average has doubled since 1999. The minimum values are, however, in good agreement with the 1.99 ppm reported by Shriadah (1999).

Mercury is used in small batteries (Miessler and Tarr, 2003). Mercury concentrations in Abu Dhabi range from <0.01 to 0.04 ppm, which is one-fold greater than the 0.001 ppm value reported in 2004.

Lead is used in drinking-water pipes, paint, batteries and gasoline (Cox, 2004). Lead concentrations in Abu Dhabi range from 0.9 to 4.0 ppm, with an average of 1.9 ppm, i.e. approximately three times greater than the lead contamination of 0.78 ppm reported in 2004.

Industrial wastes are the major source of **molybdenum**. Mo is essential to enzymes in plants, to help catalyse the formation of ammonia (Miessler and Tarr, 2003).

The concentration of molybdenum in Abu Dhabi ranges from <0.1 to 1.7 ppm, well below the safe limit of 200 ppm.

Nickel is commonly used as a catalyst in petroleum and chemical industries (Miessler and Tarr, 2003). It is also used in nickel metal–hydride or nickel–cadmium batteries (P. Atkins 2002). The range of nickel concentrations in Abu Dhabi is 3.5–73.5 ppm, with an average of 25.3 ppm. The highest value reaches only 35% of the safe limit, which is 210 ppm. The average is almost one-fold greater than the value reported in 2004. The Pb and Ni concentrations decreased from 1999 to 2004, but increased from 2004 to 2014.

Zinc is the most important trace element is for the human body, after iron. Zn^{2+} is present in acid-catalysing enzymes, such as carbonic anhydrase (Cox, 2004). The minimum zinc concentration in Abu Dhabi is 2 ppm, which is in good agreement with the average values of 2.463 ± 1.684 ppm reported by Al Hosani and Al Anouti (2014). The maximum zinc concentration in Abu Dhabi is 21 ppm, i.e. well below the Dutch guideline limit of 720 ppm. The range of zinc concentrations is in good agreement with the range 4.59–21.4 ppm reported by Shriadah (1998). The average is 8.2 ppm, which is approximately one third of the average 30.97 ppm reported by F. N. Sadooni, F. Howari and A. El-Saiy, 2010. Figure 3.19 shows that the maximum concentration of each metal does not exceed the Dutch safe limit. The maximum values are relatively negligible, except for barium, nickel and zinc.

4.4.2 Enrichment factor

The enrichment factors were calculated using the following formula:

$$EF = (\text{element}/Al)_{\text{sample}} / (\text{element}/Al)_{\text{background}}$$

Where EF is the enrichment factor, $(\text{element}/Al)_{\text{sample}}$ is the ratio between trace element and aluminium content in a sediment sample, $(\text{element}/Al)_{\text{background}}$ is the ratio

between trace element and aluminium average abundance in the continental crust (Taylor, 1964).

The background concentrations of Fe, Cr, Sr, Cu, Zn, Pb, Hg, Cr, Cd, Th, U and Al in the average crustal abundance obtained from Taylor (1964) are used in this study (see Table 2.1). The EF categories are based on the classifications by Birch (2003), as shown in Table 2.2.

The resulting EF values (Table 3.7) on average show higher enrichment values for As, Cr, Sr and U concentration from Abu Dhabi beach sand samples, and minor or no enrichment for metals such as Co, Cu, Pb, Zn, Ni, V. With the exception of Co, Th and Zn, all the metals show samples with severe enrichment in comparison to their average crustal abundance, as shown in Figures 3.25 to 3.30. The mean EF values decreased as follows: Cu = Zn < Co = Pb = Hg < Ba = Ni = Mo < Cd = Sb < As.

4.4.3 Geo-accumulation index

The geoaccumulation index, originally defined by Muller (1969), was calculated using the following formula:

$$I_{geo} = \log_2 (C_n/1.5*B_n)$$

Where C_n is the measured concentration of element n in the beach sand sample, and B_n is the geochemical background for the element n , which is either directly measured in pre-civilisation sediments of the area or taken from the literature (average crustal abundance).

Muller's (1969) classification of geoaccumulation indices in Table 2.3 was used as the basis for classification. On average, all the elements, with the exception of As, were categorized under "class 0"; therefore, the samples are uncontaminated. With As, samples were uncontaminated to moderately contaminated. 31 samples fell into "class 0", meaning uncontaminated, while 25 samples fell into "class 1", moderately contaminated.

Based on the Dutch guidelines, enrichment factor and geo-accumulation index, the results cumulatively suggest that the Abu Dhabi coastal area is unpolluted. This result stands in good agreement with the relatively modest levels of industrial activity in Abu Dhabi. As of 2009, only 5% of land in Abu Dhabi consists of oil fields, the industrial area accounts for only 2% of Abu Dhabi land, and 92% of land is made up of rangelands (Highlights and Achievements 2014). The areas that had the highest concentrations for most metals were Musaffah Industrial and Abu Dhabi Island. According to the Abu Dhabi Environment Agency, Musaffah Industrial is active with construction, metal, paper, plastic, fiberglass, chemical, food, and petrol-chemical industries.

4.4.4 Geochemical composition: provenance, classification and characterisation

The composition and geochemical variation of beach sediments are controlled by numerous components and processes, including source composition, sorting, climate, relief, long shore drift, and winnowing by wave action (Folk, 1974; Komar, 1976; Ibbeken and Schleyer, 1991). Beaches are exposed to different marine, fluvial, and Aeolian processes, such as wave and tidal regimes, fluvial discharges and wind transport, among other factors. Furthermore, these factors control the grain size and sand composition of the beaches in terms of their mineralogy and geochemistry.

In addition, geomorphological features in the coast may also have control over the grain size, composition and geochemistry of beaches (Le Pera and Critelli, 1997). For instance, some beaches in protected embayment's may have coarse grain sizes as a result of little energy and the removal of finer sizes offshore (Komar, 1976). Furthermore, the provenance of coastal sands may be related to different tectonic settings, as has been documented in several studies (Klitgord and Mammerickx, 1982; Nesbitt and Young, 1982; Carranza Edwards et al., 1994; Kasper-Zubillaga et al., 1999).

Beach sands are generally composed of quartz, feldspar, other silicates, lithic fragments, and biogenic material, such as shells. They are products of weathering, fragmentation and degradation.

In general, the compositions of sediments are mainly controlled by the ratio between carbonate (CaO), quartz (SiO₂), and phyllosilicates and clay minerals (Al₂O₃). The strong negative correlation between CaO and SiO₂ and between CaO and Al₂O₃, the positive correlation between CaO and LOI, and the negative correlation between Al₂O₃ and LOI may indicate the dominance of marine biogenic carbonate. Positive correlations between Al₂O₃ and SiO₂ indicate alumino-silicate minerals. The overall high content of CaO and MgO suggests that the carbonate content of the beach sand sediments is generally high, except in a few samples. Most of the trace elements listed in Table A7 (Appendix A) show a negative correlation with CaO and LOI, with the exception of Sr, U and As. This indicates that Sr, U and As have a marine origin, while the rest of the trace elements have a continental origin. In contrast with Uranium, Thorium is positively correlated with SiO₂ and Al₂O₃, which points to a terrigenous origin.

A combination of cluster and discriminant analysis was used to classify and characterize beach sand into geochemically homogenous groups. Cluster analysis was used to classify the beach sand, while discriminant analysis was used to characterize and differentiate the groups created through cluster analysis.

Hierarchical agglomerative cluster analysis was performed on major rock-forming elements using Ward's method, with Euclidean distances used as a measure of similarity. The result is shown in Figure 3.32 above, from which the 57 beach sand samples were subdivided into four groups. To geochemically characterize and differentiate the four beach sand groups – namely, alumino-silicate, alumino-silicate with heavy minerals, biogenic marine carbonate, and biogenic marine carbonate with halite – a linear discriminant analysis was performed. The results show that SiO₂, K₂O, Al₂O₃ and TiO₂ characterize the alumino-silicate beach; in addition to these elements, alumino-silicate with heavy mineral beach sand shows enrichment with Fe₂O₃, Cr₂O₃, MgO and MnO. Biogenic marine carbonate beach

sand shows CaO and LOI content, while the halite beach sands show high content of Na₂O, in addition to the CaO and LOI content.

A factor analysis of the beach sands' geochemical data was conducted to quantify the contributions of natural chemical processes and the anthropogenic effects of the measured geochemical variables.

The factor analysis was performed by computing the correlation matrix, which involves the correlation coefficient or measure of interrelation. The factor loadings were then estimated and rotated to allow for easy interpretation of the resulting factors. The latter are underlying constructs that influence the expression of observed variables (Suhr, 2005). The factors extracted from the geochemical data reveal geochemical associations that reflect the underlying geochemical processes. Consequently, the factor scores describe the degree to which the geochemical processes are expressed in the composition of the samples (Davis, 1986). Crucially, the spatial distribution of the factor scores allows the expression of geochemical processes, as described by the factors, to be mapped and analysed using GIS technology.

Factor analysis was performed on 26 variables of the beach sand samples analysed. Table 4.9 above shows the initial determined factor, their eigenvalues and the percent of variance contributed by each factor, using the varimax rotation method with Kaiser Normalization and the unrotated factor solution.

Only factors with eigenvalues of 1 or more were taken into consideration, which resulted in five factors being selected that were sufficient in explaining 79.35% of the variance.

The first factor (F1), which is positively correlated with K₂O, Al₂O₃, SiO₂, Rb, MnO, TiO₂, Ba, Nb, V, Th and Fe₂O₃, and negatively loaded with CaO, LOI, Sr and U (Table 3.10), separates terrigenous beach sand from biogenic marine carbonate sand. Factor two (F2) is considered to be beach sand rich with heavy metal due to its enrichment with Zr, Nb, V, Th, TiO₂, Co and Cr₂O₃.

Factor three (F3) is dominated by heavy metals, including Ni, Zn, Cu, Co and Pb. Although the concentration of these heavy metals is not high, it is mainly attributable to industrial activities.

Factor four (F4) is dominated by high loading with MgO, Fe₂O₃, Cr₂O₃ and MnO, pointing to heavy mineral beach sand. These elements indicate a possible mafic rock provenance.

Factor five (F5) is positively loaded with As, Na₂O and U and negatively loaded with P₂O₅, indicating halite beach sand with high concentrations of arsenic and uranium. It is negatively loading with P₂O₅, which is interpreted as originating from fertilizing activities or industries.

4.5 Mineralogical and analysis of the beach sand

Based on the four groups created through the combination of cluster and discriminant analysis, three beach sand samples from each group were selected and analysed through XRD. Carbonate minerals dominate the mineralogy of the beach sediments, followed by quartz and halite. Some of the samples show a mixture of calcite, halite and quartz. Most of the carbonates are calcite/aragonite and dolomite. Dolomite in the Abu Dhabi beach is formed through diagenesis processes.

Chapter V

5.0 Conclusion and Recommendation

5.1 Summary and conclusion

The study describes the sedimentological, geochemical and mineralogical properties of the beach sediments of Abu Dhabi, United Arab Emirates. The sediments are generally coarse grained, poorly sorted, negatively symmetrical and leptokurtic in nature. The energy process discriminant functions of the sediments indicated that they were deposited predominantly by an Aeolian, shallow marine deposition environment, with the influence of fluvial process. Negative correlations were found between CaO and most of the major and trace elements, with the exception of LOI, Sr, U and As, while those with Al₂O₃ and SiO₂ were positively correlated with all the major elements and trace elements, with the exception of CaO, LOI, U, Sr and As. This finding suggests that U, Sr and As are associated with the biogenic sediments and have a marine origin, while the rest of the major and trace elements are terrigenous. Since U is positively correlated with CaO and LOI and Th is positively correlated Al₂O₃ and SiO₂, the two radiogenic elements most likely have different sources. Scatter plots and multivariate statistical techniques, including factor, cluster and discriminant analyses, were used to classify and characterize the beach sediment of the coastal area of Abu Dhabi. The results show two dominant beach sediment types: terrigenous and marine biogenic sediments. The terrigenous sediments were classified intraluminal-silicate and heavy minerals, while the marine biogenic sediments were subdivided into carbon-rich and halite rich sediments. Uranium, arsenic and strontium are enriched in the marine biogenic sediment, while thorium and heavy metals are enriched into alumino-silicate- and heavy-mineral-enriched coastal sediments. The marine carbonate dominates the sediments and makes up almost 50% of the beach sand, while the remaining 50% shows a mixture of the remaining components: quartz silt/sand, terrestrially derived silt-clays, and marine carbonates. The areas that have the highest concentrations for most of the radiogenic elements and heavy metals are Musaffah Industrial and Abu Dhabi Island. Musaffah Industrial is active with construction, metal, paper, plastic, fiberglass, chemical,

food and petro-chemical industries. The Index of Geo-accumulation (Igeo), enrichment factor (EF) and Dutch guidelines were used to study the heavy-metal contamination levels of Abu Dhabi beach sediments. The result of these methods collectively indicate that the coastal area of Abu Dhabi is not polluted by heavy metals and radiogenic elements. Mineralogically, the sediments are dominated by carbonate and quartz. The carbonate are mostly calcite/aragonite and dolomite. Dolomite in the Abu Dhabi beach sediments is formed through diagenesis processes. Some samples show a low content of crystalline materials and contain Amorphous substances that the XRD cannot detect.

5.2 Recommendation

The results of this investigation suggest several areas for future research that will expand our understanding of the concentration distribution of radioactive and heavy metals in the UAE surface environment. Firstly, coverage of the entire UAE surface environment is essential. In addition, it is necessary to conduct a systematic sampling of soil, in particular in the industrial areas, in order to identify the differences between natural concentration and artificial signs of contamination. Finally, the establishment of a soil-to-plant transfer factor for the arid regions is presently missing and is urgently needed.

UNIVERSITY of the
WESTERN CAPE

References

1. Abdel fattah MA, Shahid SA (2007). A comparative characterization and classification of soils in Abu Dhabi coastal area in relation to arid and semiarid conditions using USDA and FAO soil classification systems. *Arid Land Res Manag* 21: PP. 245–271.
2. Abu-Hilal, A.H., Khordagui, H.K (1993). Assessment of tar pollution on the United Arab Emirates beaches. *Environment International*, 19 (6), PP. 589-596.
3. Adejumo, I.B. Obioh, O.J. Ogunsola, F.A. Akeredolu, H.B. Olaniyi, O.I. Asubiojo, A.F. Oluwole, O.A. Akanle, N.M. Spyrou. The atmospheric deposition of major, minor and trace-elements within and around 3 cement factories. *Journal of Radioanalytical and Nuclear Chemistry-Articles*, 179 (1994), PP. 197–199.
4. Adriano, D.C., 1999. *Trace Elements in the Terrestrial Environment*. Springer, New York, PP. 190-210.
5. Adriano DC, Chlopeca A, Kaplan DI, Clijsters H, Van-gronsveld J (1996). Soil contamination and remediation: philosophy, science, and technology. In: Prost R, editor. *Contaminated soils. Third international conference on the bioŽ. geochemistry of trace elements. Paris France. NRA Edition (1997): PP. 465-504.*
6. Afifi, A. A. and Clark, V (1990). *Computer-Aided Multivariate Analysis*. London: Chapman and Hall. PP. 107–111.
7. Ahumada, I., Mendoza, J., Navarrete, E., Ascar, L (1999). Sequential extraction of heavy metals in soils irrigated with wastewater. *Commun. Soil Sci. Plant Anal.* 30, PP. 1507–1519.
8. Al-Asfour, T.A (1982). *Changing Sea-Level Along the North Coast of Kuwait Bay*. Kegan Paul International, London, PP. 186.
9. Al Hosani M, Al Anouti F (2014). A Preliminary Exploration of Heavy Metal Contamination within *Avicennia marina* in the United Arab Emirates. *J Environ Anal Toxicol* 4: PP. 232.

10. Allen, J. R. L (1965). Coastal geomorphology of Eastern Nigeria: Beach-ridge barrier islands and vegetated tidal flats. *Geologie En Mijnbouw*, 44, PP. 1-21.
11. Alperen Ergur, Grigoris Paouris, and J. Maurice Rojas (2016) Probabilistic Condition Number Estimates for Real Polynomial Systems i: A broader Family of Distribution. arXiv: v1 [math.PR]. PP. 215-220.
12. Al Qubaisi, N (2001). Assessment of metals pollution in Sediment of the coastal area, UAE. Unpublished MSc. Thesis UAE university.PP.67-70.
13. AlRashdi, S., Siad, A. (2015). Geochemical classification and characterization of the beach sands of Abu Dhabi, United Arab Emirates: A combination of cluster and discriminant analysis. *Visnyk of Taras Shevchenko National University of Kyiv: Geology*, 4(71), PP. 42-44.
14. AlRashdi, S., Arabi, A. A., Howari, F. M., & Siad, A. (2015). Distribution of heavy metals in the coastal area of Abu Dhabi in the United Arab Emirates. *Marine Pollution Bulletin*, 97(1-2), PP. 494–498.
15. AlRashdi, S., Siad, A (2016 a). Geochemistry of beach sands from Abu Dhabi, United Arab Emirates (UAE). *Visnyk of Taras Shevchenko National University of Kyiv: Geology*, 4(75), PP. 21-23.
16. AlRashdi, S., Siad, A. (2016 b). Grain Size Analysis and Depositional Environment for Beach Sediments Along Abu Dhabi Coast, United Arab Emirates. *International Journal of Scientific and Technology Research*, 5, PP. 2277-8616.
17. Alsharhan, A.S., and Kendall, C.S (2002). Holocene carbonate/evaporites of Abu Dhabi, and their Jurassic ancient analogs. In H. J. Barth, & B. B. Boer (Eds.), *Sabkha ecosystems*. Dordrecht: Kluwer Academic Publishers, PP. 187-202.
18. Alsharhan, A. S., & Kendall, C. G. S. C (2003). Holocene Coastal Carbonates and Evaporites of the Southern Arabian Gulf and Their Ancient Analogues. *Earth Sci. Rev.*, 61(3-4), PP. 191–243.
19. Amaral, E. J., and prayer, W. A (1977) Depositional environment of the St. Peter Sandstone Deducted by Textural Analysis: *Journal of sedimentary research* V.47, no. 1; PP. 32-52.

20. Apps, M.J., Duke, M.J.M., Stephens-New sham, L.G (1988). A study of radionuclides in vegetation on abandoned uranium tailings. *Journal of Radioanalytical and Nuclear Chemistry*, 123 (1), PP. 133-147.
21. Atkins, p., De Paula, Atkins' Physical Chemistry, Oxford University Press, Oxford UK, 7th edition (2002). PP. 120-125.
22. Bakir F., Damluji, S.F., Amin-Zaki L (July 1973). "Methylmercury poisoning in Iraq". *Science* 181 (4096): 230-41.doi:10.1126/science.181.4096.230. PMID 4719063.
23. Baltzer, F., Kenig, F., Boichard, R., Plaziat, J.-C., Purser, B.H (1994). Organic matter distribution, water circulation and dolomitization beneath the Abu Dhabi Sabkha (United Arab Emirates). In: Purser, B., Tucker, M., Zenger, D. (Eds.), *Dolomites, A volume in Honour of Dolomieu*, vol. 21. Blackwell, Oxford, UK, PP. 409– 428. Special Publication.
24. Banat, I.M., Hassan, E.S., El-Shahawi, M.S., Abu-Hilal, A.H (1998). Post-Gulf-War assessment of nutrients, heavy metal ions, hydrocarbons, and bacterial pollution levels in the United Arab Emirates coastal waters. *Environ. Int.* 24, PP. 109–116.
25. Barnhardt, W.A., Belknap, D.F., and Kelley, J.T (1997). Stratigraphic evolution of the inner continental shelf in response to Late Quaternary relative sea-level change, north western Gulf of Maine. *Geological Society of America*, 109, PP. 612–630.
26. BAPTISTA NETO JA, SMITH BJ AND MCALISTER JJ (2000). Heavy metal concentrations in surface sediments in a nearshore environment, Jurujuba Sound, SE Brazil. *Envir Poll* 109: PP. 1-9.
27. Basaham A. and Al-Lihaibi S (1993). Trace Elements in Sediments of the Western Gulf. *Marine Pollution Bulletin*. 27: PP. 103-107.
28. Bathurst, R.G.C (1975). Carbonate sediments and their diagenesis. *Developments in Sedimentology*, vol. 12. Elsevier, Amsterdam. P. 658.
29. Berkovits, D., Feldstein, H., Ghelberg, S., Hershkowitz, A., Navon, E. & Paul, M (2000). ²³⁶U in uranium minerals and standards. *Nuclear Instruments & Methods in Physics Research, Section B: Beam Interactions with Materials and Atoms*, 172(1-4), PP. 372-376.
30. Berry, R.W., Brophy, G.P., Naqash, A (1970). Mineralogy of the suspended sediments in

the Tigris, Euphrates, and Shatt al-Arab rivers of Iraq, and the recent history of the Mesopotamian plain. *Journal of Sedimentary Petrology* 40, PP. 131 –139.

31. Bhuiyan MAH, Islam MA, Dampare SB, Parvez L, Suzuki S (2010) Evaluation of hazardous metal pollution in irrigation and drinking water systems in the vicinity of a coal mine area of north western Bangladesh. *J Hazard Mater* 179: PP. 1065–1077.
32. Birch, G (2003). A Scheme for Assessing Human Impacts on Coastal Aquatic Environments Using sediments.in: Woodcoffe, C. D., Furness, R. A. (Eds.), *Coastal GIS* (2003). Wollongong University Papers in Centre for Maritime Policy, 14, Australia. Woodcoffe CD, Furness RA, PP. 55-57.
33. Bleise, A., Danesi, P. R. & Burkart, W (2003). Properties, use and health effects of depleted uranium (DU): a general overview. *Journal of Environmental Radioactivity*, 64 (2-3), PP. 93-112.
34. Boardman, M.R (1978). Holocene deposition in northwest Providence Channel, Bahamas: a geochemical approach. Chapel Hill, North Carolina: University of North Carolina, Doctoral dissertation. PP. 30–40.
35. Bou-Olayan, A.-H., Al-Mattar, S., Al-Yakoob, S., Al-Hazeem, S (1995). Accumulation of lead, cadmium, copper and nickel by pearl oyster, *Pinctada radiata*, from Kuwait marine environment. *Mar. Pollut. Bull.* 30, PP. 211–214.
36. Boyd, R. and Honig, C.A (1992). Estuarine sedimentation on the eastern shore of Nova Scotia. *Journal of Sedimentary Research*, 62, pp.569–583.
37. Buck, B.J., Brock, A.L., Johnson, W.H. & Ulery, A.L (2004). Corrosion of depleted uranium in an arid environment: Soil-geomorphology, SEM/EDS, XRD, and electron microprobe analyses. *Soil and Sediment Contamination*, 13 (6), PP. 545-561.
38. Butler, G.P (1965). Early diagenesis in the Recent sediments of the Trucial Coast of the Persian Gulf. Unpublished M.Sc. Dissertation, University of London, pp.89–95.
39. Butler, G.P (1969). Modern evaporate deposition and geochemistry of co-existing brines. The Sabkha, Trucial Coast, Arabian Gulf. *Journal of Sedimentary Petrology* 39, PP. 70 – 89.

40. Butler, G.P (1987). Recent evaporates from the Abu Dhabi coastal flats. In G. R. Handford, R. G. Loucks & G. R. Davies (Eds.), *Depositional and diagenetic spectra of evaporates*. SEPM Special Publication, 3rd ed., PP. 33-64.
41. Butler, G.P., Kendall, C.S., Harris, P.M (1982). Recent evaporates from the Abu Dhabi coastal flats. In: Handford, G.R., Loucks, R.G., Davies, G.R. (Eds.), *Depositional and Diagenetic Spectra of Evaporates*. Society of Economic Palaeontologists and Mineralogists Core Workshop, vol. 3, PP. 33 –64.
42. Calmano, W., Ahlf, W., Forstner, U (1990). Exchange of heavy metals between sediment components and water. In: Broekaert, J.A.C., Güçer, Ş., Adams, F. (Eds.), *Metal Speciation in the Environment*. NATO ASI Series, Vol. G 23. Springer-Verlag, Berlin, PP. 503–522.
43. Carranza-Edwards, A., Rosales-Hoz, L., Santiago-Pérez, Sb(1994), Provenance memories and maturity of holocene sands in Northwest Mexico: Canadian. *Journal of. Earth Science*, 31(10), PP.1550-1556.
44. Carter, R.W.G., Orford, J.D., Forbes, D.L., and Taylor, R.B (1990). Morphosedimentary development of drumlin-flank barriers in a zone of rapidly rising sea level, Story Head, Nova Scotia. *Sedimentary Geology* 69(1-2): PP. 117-120.
45. Cattell, R.B (1978), *The Scientific Use of Factor Analysis*, New York: Plenum. PP. 97-112.
46. Çevik, F., M.Z.L. Göksu, O.B. Derici and Ö. Findik (2009). An assessment of metal pollution in surface sediments of Seyhan dam by using enrichment factor, geoaccumulation index and statistical analyses. *Environ. Monit. Assess.*, 152: PP. 309-317.
47. Chlopecka, A., Bacon, J.R., Wilson, M.J., Kay, J (1996). Forms of cadmium, lead, and zinc in contaminated soils from southwest Poland. *Journal of Environmental Quality* 25(1), PP. 69-75.
48. Christopher G. St. C. Kendall, Patrick A. d'E. Skipwith B (1968). Recent algal mats of a Persian Gulf lagoon. *Journal of Sedimentary Research*, 38 (4), PP. 1040– 1058.

49. Clausen, F.L., and O. Harpoth (1983). On the use of discriminant analysis techniques for classifying chemical data from panned heavy—mineral concentrates—Central East Greenland, *Journal of Geochemical Exploration*, 18 (1), PP. 1-24.
50. Conrad C F, Chisholm-Brause C J (2004). Spatial survey of trace metal contaminants in the sediments of the Elizabeth River, Virginia. *Marine Pollution Bulletin*, 49(4): PP. 319–324.
51. Cox P.A (2004). *Inorganic chemistry*, 2nd ed., Bios Scientific, London, P. 27.
52. Crevello, P.D. and Schlager, W., 1980. Carbonate debris sheet sand turbidites, Exuma Sound, Bahamas. *Journal of Sedimentary Petrology*, 50, PP. 1121–1148.
53. Dang, Z., Liu, C., Haigh, M.J (2002). Mobility of heavy metals associated with the natural weathering of coal mine spoils. *Environ. Pollut.* 118, PP. 419–426.
54. Davis J. A (1979). The Davis/Holland/Leinhardt studies: An overview. In P. W. Holland and S. Leinhardt. (eds). *Perspectives on social Network Research*. New York, Academic Press. PP. 62-51.
55. Davis, J.C (1986). *Statistics and data analysis in geology*, 2nd Ed., New York: Wiley, PP. 646.
56. Dawood Y. H (2010). Factors Controlling Uranium and Thorium Isotopic Composition of the Streambed Sediments of the River Nile, Egypt. *Earth Sci.*, Vol. 21, No. 2, pp. 77-103
57. De Laeter, J.R., Böhlke, J.K., De Bièvre, P., Hidaka, H., Peiser, H.S., Rosman, K.J., R. and Taylor, P.D.P (2003). Atomic weights of the elements: Review 2000(IUPAC Technical Report). *Pure and Applied Chemistry*, 75 (6), PP. 683-800.
58. De Mora, S., Sheikholeslami, M.R., Wyse, E., Azemard, S., Cassi, R (2004). An assessment of metal contamination in coastal sediments of the Caspian Sea. *Marine Pollution Bulletin*, 48 (1-2), PP. 61-77.
59. El-Sammak, O.M (2001). Heavy metal pollution in bottom sediment, Dubai, United Arab Emirates. *Bulletin of Environment Contamination and Toxicology*, 67(2), PP. 295–302.
60. Emery, K. O (1956). Sediments and water of Persian Gulf. *American Association of Petroleum Geologists Bulletin*, 40(10), PP. 2354-2383.
61. Environment Agency-Abu Dhabi vector information(EAD), Abu Dhabi Soil Survey (2002), www.ead.ae.

62. Esen F., Tastier Y., Cindoruk S.S (2010). Dry deposition, concentration and gas/particle partitioning of atmospheric carbazole. *Atmospheric Research* 95, PP. 379-385.
63. Evans, G (1970). Coastal and nearshore sedimentation: A comparison of clastic and carbonate deposition. *Proceedings of the Geologists' Association of London*, vol. 81, pp. 493 –508.
64. Evans, G (1994). The Arabian Gulf; a modern carbonate –evaporate factory, a review. In: Arche, A., Lopez-Gomez, J. (Eds.), *Permico y Triasico de la Peninsula Iberica; Permian and Triassic of the Iberian Peninsula*. Cuadernos de Geologia Iberica, vol. 19, PP. 61 –96.
65. Evans, G., Kendall, C. S., and Skipwith, P (1964a). Origin of the coastal flats, the sabkha, of the tracial coast, Persian Gulf. *Nature*, PP. 759-761.
66. Evans, G., Kinsman, D. J., and Shearman, D. J (1964b). A reconnaissance survey of the environment of recent carbonate sedimentation along the tracial coast, Persian Gulf. In L. M. J. U. Van Straaten (Ed.), *Deltaic and shallow marine deposits* Amsterdam: Elsevier. PP. 129-135
67. Evans, G., Schmidt, V., Bush, P., and Nelson, H (1969). Stratigraphy and geologic history of the sabkha, Abu Dhabi, Persian Gulf. *Sedimentology* vol.12, PP. 145 –159.
68. Fairbridge, R.W (1961). Eustatic changes in sea level. *Physics and Chemistry of the Earth* 4, PP. 99 – 105.
69. Finch, R.J. and Ewing, R.C (1992). Corrosion of uraninite under oxidizing conditions. *Journal of Nuclear Materials*, 190, PP. 133-156.
70. Friedman, G.M., Sanders, J.E., and Kopalska-Merkel, D.C (1992). *Principles of Sedimentary Deposits; Stratigraphy and Sedimentology*. New York: McMillan, 717p.
71. Folk, R.L., Ward, M.C (1957). *J Sediment Petrol*, 27, PP. 3-27.
72. Folk, R.L (1966). *Sedimentology*, 6, PP. 73-93.
73. Folk, R.L (1974), *Petrology of Sedimentary Rocks*: Austin, Texas, Hemphill Publishing Co, PP. 182.
74. Fomina, M., Charnock, J.M., Hillier, S., Alvarez, R., Livens, F. and Gadd, G.M (2008). Role of fungi in the biogeochemical fate of depleted uranium. *Current Biology*, pp. 189.
75. Forstner, U. and Wittman, G.T (1983). *Metal Pollution in the Aquatic Environment*.

- Springer, Berlin, Heidelberg, P. 486.
76. Fowler, S.W., Readman, J., Oregioni, B., Villeneuve, J., McKay, K (1993). Petroleum hydrocarbons and trace metals in near shore Gulf sediments and biota before and after the (1991). Gulf war: An assessment of temporal and spatial trends. *Mar. Poll. Bull.* 27, PP. 171-182.
77. Gavrilesco, M., Pavel, L.V., and Cretescu, I (2009). Characterization and remediation of soils contaminated with uranium. *Journal of Hazardous Materials*, 163 (2-3), 475-510.
78. Griffiths, L.C (1967). *Scientific Methods in The Analysis of Sediments*. New York: McGraw-Hill, PP. 352.
79. Godwin, H. and Willis, E. H. (1959) Radiocarbon dating of the late-glacial period in Britain. *Proc. Roy. Soc. B150*, PP. 199-215.
80. Grim, R.E (1968). *Clay Mineralogy* seconded. McGraw-Hill, New York, PP.596.
81. Handley-Sidhu, S., Worsfold, P. J., Boothman, C., Lloyd, J. R., Alvarez, R., Livens, F.R., Vaughan, D.J. and Keith-Roach, M.J (2009). Corrosion and fate of depleted uranium penetrators under progressively anaerobic conditions in estuarine sediment. *Environmental Science and Technology*, vol.43 (2), PP. 350-355.
82. Harbison, P. (1986) Mangrove muds – a sink and a source for Trace Metals. *Marine Pollution Bulletin* Vol 17, No 6, PP. 246-250.
83. Hartmann, M., Lange, H., Seibold, E., and Walger, E (1971). Oberflächen-sedimente in persischen golf and golf von oman. I. geologisch-hydrologischer rahmen und erste sedimentologische ergebnisse. *Meteor For schungsergebnisse*, C, 4, PP.1-76.
84. Highlights and Achievements (2014). International Centre for Bioscience Agriculture. Dubai. United Arab Emirates. PP. 20-25.
85. Houbolt, J.J.H.C (1957). Surface Sediments of the Persian Gulf near the Qatar Peninsula. Ph.D. Thesis, University of Albright, Des Haal Montana Co. PP. 30-35.
86. Howari, F.M., Banat, K.M (2001). Assessment of Fe, Zn, Cd, Hg, and Pb in the Jordan and Yarmouk River sediments in relation to their physicochemical properties and sequential extraction characterization. *Water Air Soil Pollute.* 132 (1–2), PP.43–59.

87. Hugo Raguét, Jalal M. Fadili, Gabriel Peyré. (2013). A Generalized Forward-Backward Splitting. *SIAM Journal on Imaging Sciences*, Society for Industrial and Applied Mathematics, 6 (13), pp.1199-1226.
88. Hunter, J.R (1986). The physical oceanography of the Arabian Gulf: A review and theoretical interpretation of previous observations. In: Halwagy, Clayton, and Bebehabi, eds., *Proceedings of the 1st Gulf Conference on Environment and Pollution*, KISR, Kuwait. (KISR is the Kuwait Institute for Scientific Research), PP. 1–23.
89. IAEA (1999). Technical options for the remediation of contaminated groundwater. International Atomic Energy Agency, Vienna. P.132.
90. IAEA (2003). Radiological Conditions in Areas of Kuwait with Residues of Depleted Uranium. International Atomic Energy Agency, Vienna, Report STI/PUB/pp. 116.
91. IAEA (2004). The long-term stabilization of uranium mill tailings. International Atomic Energy Agency, Vienna, Final report of a coordinated research project (2000–2004), P. 76.
92. Ibe, K.K. S. I. Ibeneme, Y. E. Obioha, I. O. Eze, I. L. Ibeneme, H. O. Israe, B. O. Ubechu, C. O. Nlemadim (2013). Foundation Studies in A Rapidly Urbanising Area: Case Study of Naze, Owerri Southeastern Nigeria. *International Journal of Advanced Scientific and Technical Research* Issue 3 volume 6, ISSN 2249-9954 R S, <http://www.rspublication.com/ijst/index.html>. PP.128-129.
93. Jansseeens-Maenhout, G., ed. *Nuclear Safeguards and Non-Proliferation Course Syllabus* (2008). Office for Official Publications of the European Communities: Luxembourg. PP. 89-91.
94. Jesus T., Arvalho C., Aguiar W., Aleluia F. and Jesus S (2003). Effects of Nickel Mining in the Heavy Metal Distribution in Sediments of a Tropical River, Ne, Brazil. *Proceedings of 15th International Conference on Heavy Metals in the Environment*. Gdansk, Poland PP. 76-81.
95. Kamon, M., Katsumi, T., Watanabe, K (2000). Heavy-metal leaching from cement stabilized waste sludge. *Geotech. High Water Content Mater. ASTM STP 1374*, PP. 113–116.

96. Kasper-Zubillaga, J.J., Carranza-Edwards, A., Rosales-Hoz, L(1999), Petrography and geochemistry of Holocene sands in the western Gulf of México: implications of provenance and tectonic setting: *Journal of Sedimentary Research*, 69(5), PP. 1004-1008.
97. Kessler, P (1973). The structural and geomorphic evolution of the Persian Gulf. In B. H. Purser (Ed.), *The Persian Gulf – Holocene carbonate sedimentation and diagenesis in a shallow Epicontinental sea* New York: Springer, PP. 11-32.
98. Kelley, J.T (1987). An inventory of coastal environments and classification of Maine's glaciated shoreline. In: Fitzgerald, D.M. and Rosen, P.S. (eds.), *Glaciated Coasts*. New York: Academic Press, PP. 151–176.
99. Kendall, C. G. S. C., & Skipwith, P (1968). Recent algal mats of a Persian Gulf lagoon. *Journal of Sedimentary Petrology*, 38(4), PP. 1040-1058.
100. Kendall, C. G. S. C., & Skipwith, S. P (1969a). Geomorphology of a recent shallow-water carbonate province: Khor al bazam, tracial coast, south-west Persian Gulf. *Geological Society of America Bulletin*, 80, PP. 865-891.
101. Kendall, C. G. S. C., & Skipwith, S. P (1969b). Holocene shallow-water carbonate and evaporate sediments of khor al bazam, Abu Dhabi, southwest Persian Gulf. *American Association of Petroleum Geologists Bulletin*, 53(4), PP 841-869.
102. Kendall, C. G. S. C., & Warren, J. K (1987). A review of the origin and setting of tepees and their associated fabrics. *Sedimentology*, 34(6), PP. 1007-1028.
103. Kendall, C. G. S. S. C., Sadd, J. L., & Alsharhan, A. S (1994). Holocene marine cement coatings on beach-rocks of the Abu Dhabi coastline (UAE); analogy for cement fabrics in ancient limestones. *Carbonates and Evaporates*, 9(2), P. 119-131.
104. Kenig, F., Huc, A. Y., Purser, B. H., & Oudin, J (1989). Sedimentation, distribution and diagenesis of organic matter in a recent carbonate environment, Abu Dhabi, UAE. *Organic Geochemistry*, 16(4), PP. 735-745.
105. Kersten M, Forstner U (1989). Specification of trace elements in sediments. In: Batley, G.E. (Ed.), *Trace Element Specification, Analytical Methods and Problems*. CRC Press, Boca Raton, PP. 245–318.

106. Kinsman, D. J. J., & Park, R. K (1976). Algal belt and coastal sabkha evolution, tracial coast, Persian Gulf. In M. R. Walter (Ed.), *Stromatolites*. Amsterdam: Elsevier, PP. 421-433.
107. Kinsman, D.J. J (1964). Recent carbonate sedimentation near Abu Dhabi, Trucial Coast, Persian Gulf. Unpublished Ph.D. Thesis, University of London, PP. 96-99
108. Kirkham, A (1997). Shoreline evolution, Aeolian deflation and anhydrite distribution of the holocene, Abu Dhabi. *Geo Arabia*, 2(4), PP. 403-416.
109. Kirkham, A (1998a). A quaternary proximal foreland ramp and its continental fringe, Arabian Gulf, U.A.E. In: Wright, V.P., Burchette, T.P. (Eds.), *Geological Society Special Publication*, vol. 149, PP. 15 –42.
110. Kirkham, A (1998b). Pleistocene seif dunes and their role in the development of complex past and present coastlines of the UAE. *Geo Arabia*, Vol. 3(1), Gulf Petro Link, Bahrain. PP. 49-55.
111. Klitgord, K.D., Mammerrickx, J (1982), Northern East Pacific Rise: magnetic anomaly and bathymetric framework: *Journal of Geophysical Research*, 87(B8), PP.6725-6750.
112. Komar, P.D (1976), *Beach Processes and Sedimentation*: New Jersey, Prentice-Hall, PP. 429.
113. Krupka, K.M., Parkhurst, M.A., Gold, K., Arey, B.W., Jenson, E.D. & Guilmette, R.A (2009). Physicochemical characterization of Capstone depleted uranium aerosols III: morphologic and chemical oxide analyses. *Health Physics*, 96 (3), PP. 276-291.
114. Kureishy T. W (1993). Concentration of heavy metals in marine organisms around Qatar before and after the Gulf War oil spill. *Mar. Pollut. Bull.*, 27, pp. 183–186.
115. Larsen, B (1975). Marine geophysical survey of the East Greenland Shelf south of Angmagssalik. *Rep, Geol. Surv. Of Greenland*. 75, PP. 87-88.
116. Leal-Acosta, M.L., Shumilin, E., Mirlean, N (2013), Sediment geochemistry of shallow submarine hydrothermal vents in Mapachitos, Bahía Concepción, Baja California peninsula, Mexico: *Revista Mexicana de Ciencias Geológicas*, v. 30, núm. 1, PP. 233-245.

117. Le Pera, E., Critelli, S (1997), Sourceland controls on the composition of beach and fluvial sand of the northern Tyrrhenian coast of Calabria, Italy: implications for actualistic petrofacies: *Journal of Sedimentary Research*, 110(1-2), PP. 81-97.
118. Lijzen, J. P. A., Baars, A. J., Otte, P. F., Rikken, M. G. J., Swartjes, F. A., & Verbruggen, A. P. E. M. J. and van Wezel (2001). Technical evaluation of the Intervention Values for Soil/sediment and Groundwater. Human and ecotoxicological risk assessment and derivation of risk limits for soil, aquatic sediment and groundwater. National Institute of Public Health and the Environment, PP. 201-207.
119. Lind, O. C., Salbu, B., Skipperud, L., Janssens, K., Jaroszewicz, J. & De Nolf, W (2009). Solid state speciation and potential bioavailability of depleted uranium particles from Kosovo and Kuwait. *Journal of Environmental Radioactivity*, 100 (4), PP.301-307.
120. Lokier, F., Knaf, A., and Kimiagar, S (2013). A quantitative analysis of Recent arid coastal sedimentary facies from the Arabian Gulf Coastline of Abu Dhabi, United Arab Emirates. *Marine Geology* 346: PP.141-152.
121. Mahur, A.K., Kumar, R., Mishra, M., Sengupta, D., Prasad, R (2008). An investigation of radon exhalation rate and estimation of radiation doses in coal and fly ash samples. *Appl. Radiat. Isot.* 66, PP. 401-406.
122. Matalas, N., C. and Barbara J. Reiher, B., J (1967). Some comments on the use of factor analyses. *Water resources research*. 3, PP.213-223.
123. McEachern, R. J. & Taylor, P (1998). A review of the oxidation of uranium dioxide at temperatures below 400 °C. *Journal of Nuclear Materials*, 254 (2-3), PP. 87-90.
124. Melville, F. and M. Burchett (2002). Genetic variation in *Avicennia marina* in three estuaries of Sydney (Australia) and implications for rehabilitation and management. *Mar. Pollut. Bull.*, 44: PP. 469-479.
125. Meza-Figueroa, D., Maier, R. M., de la O-Villanueva, M., Gónez-Alvarez, A., Moreno-Zazueta, A., Rivera, J., Palafox-Reyes, J (2009). The Impact of unconfined mine tailings in residential areas from a mining town in a semi-arid environment: Nacozari, Sonora, Mexico. *Chemosphere*, 77, PP. 140-147.
126. Miessler G. and Tarr D (2003). *Inorganic Chemistry* (3rd Edition). Prentice Hall. New Jersey, USA, PP. 229-232.

127. Mortimer, E.F (2000) Microgenetic analysis and the dynamic of explanation in science classrooms. Proceedings of the III Conference for Sociocultural Research, <http://www.fae.unicamp.br/br2000>. PP. 106–109.
128. Mucha, A.P., Vasconcelos, M.T.S.D., Bordalo, A.A (2003). Macro benthic community in the Douro Estuary: relations with trace metals and natural sediment characteristics. *Environmental Pollution* 121, PP. 169–180.
129. Muller, G (1969). Index of geoaccumulation in sediments of the Rhine River, *J. Geol.*, 2: PP. 108-118.
130. Namasivayan, C (1994). Conditioning of soil polluted by cement dust using polymer flocculants. *Toxicol. Environ. Chem.* 42 (1–2), PP. 65–70.
131. Nesbitt, H.W., Young, G.M (1982). Early Proterozoic climates and plate motions inferred from major elements of lutites. *Nature*, 299, PP. 715-717.
132. Newell, N. D., Rigby, J. K., Whiteman, A. J., & Bradley, J. S (1951). Shoal-water geology and environments, eastern Andros island, Bahamas. *Bulletin of the American Museum of Natural History*, 97(1), PP. 7-26.
133. Newton DE. *Forensic Chemistry*. New York, NY: Info base Publishing (2007), PP. 107-112.
134. Oliver, I.W., Graham, M.C., Mac Kenzie, A.B., Ellam, R.M. & Farmer, J. G (2008b). Distribution and partitioning of depleted uranium (DU) in soils at weapons test ranges – Investigations combining the BCR extraction scheme and isotopic analysis. *Chemosphere*, 72 (6), PP. 932-939.
135. Parkhurst, M.A., Daxon, E.G., Lodde, G.M., Szrom, F., Guilmette, R. A., Roszell, L.M., Falo, G. A. & McKee, C. B (2004). *Capstone Aerosols: Depleted Uranium Aerosol Doses and Risks*. Battelle for U.S. Army. Volume 11, PP. 58-65.
136. Paul B. Tchounwou, Clement G. Yedjou, Anita K. Patlolla, and Dwayne J. Sutton (2012). *Heavy Metals Toxicity and the Environment*. US National Library of Medicine, National Institutes of Health, 101: PP.133–164. doi: 10.1007/978-3-7643-8340-4_6, PMID: PMC4144270.
137. Pekey, H (2006): Heavy Metals Pollution Assessment in Sediments of the Izmit Bay, Turkey. *Environmental Monitoring and Assessment*. 123, PP. 219-231.

138. Plant, J.A. & Saunders, A.D (1996). The radioactive earth. *Radiation Protection Dosimetry*, 68 (1-2), PP. 25-36.
139. Prangea J.A. and Dennison W.C (2000). Physiological Responses of Five Seagrass Species to Trace Metals. *Marine Pollution Bulletin*. Volume 41, Issues 7–12, PP. 327–336
140. Pray, L. C (1966). Hurricane Betsy (1965). Near shore carbonate sediments of the Florida Keys. Geological Society of America Annual Meeting, San Francisco, Program with Abstracts, PP. 168-169.
141. Priest, N.D (2001). Toxicity of depleted uranium. *Lancet*, 357 (9252), PP. 244-246.
142. Privett, D. W (1959). Monthly charts of evaporation from the N. Indian ocean (including the red sea and the Persian Gulf). *Quarterly Journal of the Royal Meteorological Society*, 85(366), PP. 424-478.
143. Pickrill, R.A (1986). Sediment pathways and transport rates through a tide-dominated entrance, Rangaunu Harbor, New Zealand. *Sedimentology*, vol.33, PP. 887–898.
144. Pirkle, F., J. Howell, G. Wecksong, B. Duran, and N. Stablein (1984). An example of Cluster Analysis Applied to a Large Geologic Data Set: Aerial Radiometric Data from Copper Mountain, Wyoming, PP. 202-215.
145. Plumb, Jr., R.H (1981). Procedures for Handling and Chemical Analysis of Sediment and Water Samples. Technical Report EPA/CE Contract No. EP-4805572010. U.S. EPA, Environmental Laboratory. Vicksburg, MS, pp.112–120.
146. Purser, B.H., and Evans, G (1973). Regional sedimentation along the Trucial Coast, SE Persian Gulf. In: Purser, B.H. (Ed.), *The Persian Gulf, Holocene Carbonate Sedimentation in a Shallow Epeiric Continental Sea*. Springer, New York, PP. 211 –232.
147. Purser, B.H., and Seibold, E (1973). The principal environmental factors influencing Holocene sedimentation and diagenesis. In: Purser, B.H. (Ed.), *The Persian Gulf— Holocene Carbonate Sedimentation and Diagenesis in a Shallow Epicontinental Sea*. Springer, New York, PP. 1 –9.
148. Ract, P.G., Espinosa, C.R., Teno´ rio, J.A.S (2003). Determination of Cu and Ni incorporation ratios in Portl and cement clinker. *Waste Manage.* 23 (3), PP. 281–285.
149. Reimann, C., and Filzmoser, P (2000). Normal and lognormal data distribution in geochemistry: death of a myth. *Consequences for the statistical treatment of geochemical*

- and environmental data. *Environ Geol.* 39/9: PP. 1001 – 14.
150. Reinson, G.E (1992). Transgressive barrier island and estuarine systems. In: Walker, R.G. and James, N.P. (eds.), *Facies Models: Response to Sea Level Change*. Canada: Geological Association of Canada, PP. 179–194.
151. Richter, S., Alonso, A., De Bolle, W., Wellum, R. & Taylor, P.D.P (1999). Isotopic 'fingerprints' for natural uranium ore samples. *International Journal of Mass Spectrometry*, 193 (1), PP. 9-14.
152. Sadooni, F. N., Howari, F. and A. El-Saiy (2010). Microbial dolomites from the carbonate-evaporate sediments of the coastal sabkha of Abu Dhabi and their exploration implications *Journal of Petroleum Geology*, Vol. 33(4), October 2010, PP. 289-298.
153. Sahu, B.K (1964). Depositional mechanisms from the size analysis of clastic sediments. *Journal of Sedimentary Research*, 34(1), PP. 73– 83.
154. Salomons, W. and Forstner, U (1984). *Metals in the hydro cycle*. Springer-Verlag, Berlin, Heidelberg, New York, PP. 43-46.
155. Sarnthein, M. (1972). covered areas of southwestern and central nigeria. *ITC Journal*, (1), PP. 7-Sediments and history of the postglacial transgression in the Persian Gulf and north-west Gulf of Oman. *Marine Geology*. 12, PP.45-66.
156. Schiff, K. C. and Weisberg, S. B (1999). Iron as a reference element for determining trace metal enrichment in Southern California coastal shelf sediments. *Marine Environmental Research* 48: PP. 161-176.
157. Schimmack, W., Gerstmann, U., Schultz, W. & Geipel, G (2007). Long-term corrosion and leaching of depleted uranium (DU) in soil. *Radiation and Environmental Biophysics*, 46 (3), PP. 221-227.
158. Scientific Opinion of the Panel on Contaminants in the Food Chain on a request from the European Commission on cadmium in food. *The EFSA Journal* (2009) 980, PP. 1-139.
159. Searle, M.P. and Malpas, J (1980). Structure and metamorphism of rocks beneath the Semail Ophiolite of Oman and their significance in ophiolite obduction. *Transactions of the Royal Society of Edinburgh, Earth Sciences*, v. 71, part 4, PP. 247-26.

160. Sheppard, C., Price, A., & Roberts, C. (1992). Marine ecology of the Arabian region: Patterns and processes in extreme tropical environments. London: Academic Press, PP. 359-367.
161. Shriadah, M. A (1998). Heavy metals in mangrove sediments of the United Arab Emirates Shoreline (Arabian Gulf). *Water, Air and Soil Poll.* 116: PP. 523-534.
162. Siad, A. M., Matheis, G., Utke, A., & Burger, H. (1994). Discriminant analysis as a geochemical mapping technique for lateritic covered areas of southwestern and central Nigeria. *ITC Journal* 1994-1, Special CODATA Issue, 7-12, Enschede".
163. Singh M, Ansari AA, Muller G, Singh I B (1997). Heavy metals in freshly deposited sediments of the Gomati River (a tributary of the Ganga River): effects of human activities. *Environ Geol*, 29(3): PP. 246–252.
164. Steiger, R. H. & Jäger, E (1977). Sub commission on geochronology: Convention on the use of decay constants in geo- and Cosmo chronology. *Earth and Planetary Science Letters*, 36 (3), PP. 359-362.
165. Steve, M., Richard, E., Jason, M., Andrew, F., & Leon, L (2012). Engineering geological characterisation of the Barzaman Formation, with reference to coastal Dubai, UAE. *Bulletin of Engineering Geology and Environment*, 71 (1), PP.1-19.
166. Soldic-Aleksic, J. (2012). IJAR Combined Approach of the Kohonen SOM and CHAID Decision Tree Model to Clustering Problem: a market segmentation example, *Journal of Economics and Engineering*, Vol.3, No.1, April 2012. PP. 20-28.
167. Storlazzi, C.D. and Field, M.E (2000). Sediment distribution and transport along a rocky, embayed coast: Monterey Peninsula and Carmel Bay, California. *Marine Geology*, 170, PP. 289–316.
168. Sugden, W (1963). Some aspects of sedimentation in the Persian Gulf. *Journal of Sedimentary Petrology*, 33(2), PP. 355-364.
169. Suk, H., and K.-K. Lee (1999), Characterization of a ground water hydrochemical system through multivariate analysis: Clustering into ground water zones, *Ground Water*, 37, PP. 358–366.
170. Sutherland, R.A., AND Lee, C.T (1994). Discrimination between coastal sub environments using textural characteristics. *Sedimentology*, 41: PP. 1133-1143.

171. Taylor, R.N., Croudace, I.W., Warwick, P.E. & Dee, S.J (1998). Precise and rapid determination of $^{238}\text{U}/^{235}\text{U}$ and uranium concentration in soil samples using thermal ionisation mass spectrometry. *Chemical Geology*, 144 (1-2), PP. 73-80.
172. Taylor, S.R (1964). Abundance of chemical elements in the continental crust: a new table. *Geochimica et Cosmochimica Acta*, 28 (8), PP. 1273-1285.
173. Temple DH, Auerbach BM, Nakatsukasa M, Sciulli PW, Larsen CS (2008). Variation in limb proportions between Jomon foragers and Yayoi agriculturalists from prehistoric Japan. *Am J Phys Anthropol* 137: PP. 164–174.
174. Tessier, A., Campbell, P.G., Bisson, M (1979). Sequential extraction procedure for the speciation of particulate trace metals. *Anal. Chem.* 51, PP. 844–851.
175. Thurman, H.V. and Trujillo, A.P (1999). *Essentials of Oceanography*. Prentice Hall College Div, U.S.A. PP. 150-162.
176. Török, S., Osán, J., Vincze, L., Kurunczi, S., Tamborini, G. & Betti, M (2004). Characterization and speciation of depleted uranium in individual soil particles using microanalytical methods. *Spectrochimica Acta – Part B Atomic Spectroscopy*, 59 (5), PP. 689-699.
177. Tucker, M., (1990). *Techniques in sedimentology*. Blackwell Scientific Publications, PP 63-86.
178. Udden, J. A. (1914). Mechanical composition of clastic sediments. *Geological Society of America Bulletin*, 25(1), 655–744. doi:10.1130/gsab-25- P. 655.
179. Vallee, B. L., and Wacker, W. E. C (1970), *Metalloproteins*, v. 5 of Neurath, Hans, ed., *The Proteins-Composition, structure and function*: New York, Academic Press, 192 p.
180. Vaughan, T. W (1909). Geology of the Florida Keys and the marine bottom deposits and holocene corals of southern Florida. *Carnegie Institute of Washington Yearbook*, 7, PP. 131-136.
181. Wagner, C., & Van der Togt, C (1973). Holocene sediment types and their distribution in the southern Persian Gulf. In B. H. Purser (Ed.), *The Persian Gulf*. New York: Springer, PP. 123-156.

182. Walkden, G., & Williams, A (1998). Carbonate ramps and the pleistocene-recent depositional systems of the Arabian gulf. In V. P. Wright, & T. P. Burchette (Eds.), Geological society of London, special publication 149, pp. 45-54.
183. Wei, W., Liu, M. & Jordan, F (2002) Solvent kinetic isotope effects monitor changes in hydrogen bonding at the active centre of yeast pyruvate decarboxylase concomitant with substrate activation: the substituent at position 221 can control the state of activation. *Biochemistry* 41(2): PP. 451-61.
184. Weijermars, R. (1999). Quaternary evolution of dawahat zulum (half moon bay) region of eastern province, Saudi Arabia. *Geo Arabia*, 4(1), PP. 71-90.
185. Weyer, S., Anbar, A.D., Gerdes, A., Gordon, G.W., Algeo, T.J. & Boyle, E. A (2008). Natural fractionation of $^{238}\text{U}/^{235}\text{U}$. *Geochimica et Cosmochimica Acta*, 72 (2), PP. 345-359.
186. White, C., Sharman, A.K., Gadd, G.M (1998). An integrated microbial process for the bioremediation of soil contaminated with toxic metals. *Nat. Biotechnol.*, 16, PP. 572-575.
187. Whittle, G. L., Alsharhan, A. S., & Kendall, C. G. S. C (1998). Petrography of holocene beach rock and hardgrounds, Abu Dhabi, United Ara (b Emirates. In A. S. Alsharhan, K. W. Glennie, G. L. Whittle & C. G. Kendall (Eds.), *Quaternary deserts and climatic change*. Rotterdam, The Netherlands: Balkema. PP. 57-70.
188. Wolf, S.E (1999). Analytical Methods for Determination of Uranium in Geological and Environmental Materials. In: P.C. Burns & R. Finch (eds) *Uranium: Mineralogy, Geochemistry and the Environment*. Mineralogical Society of America, Washington, DC. PP. 623-652.
189. World Health Organization (W.H.O.) (2008). Guidelines for drinking-water quality (electronic resource): incorporating 1st and 2nd addenda, Vol.1, Recommendations, 3rd ed. World Health Organization, Geneva. PP. 62-65.

Appendices

Appendix A: Laboratory chemical analysis results

Table A.1 Shows the cumulative percent of the collected samples from the study area.

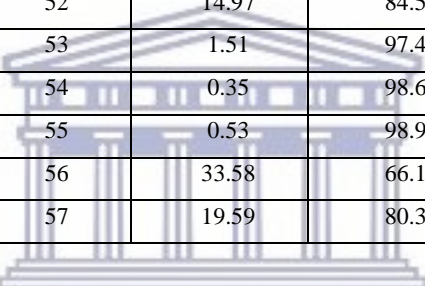
Mesh	5	10	18	35	60	120	4	pan
Phi (Ø)	-2.0	-1.0	0.0	1.0	2.0	3.0	4.0	>4
mm	4	2	1	0.5	0.25	0.125	0.062	<0.062
1	0.56	0.98	1.77	8.49	39.67	87.06	99.37	100.00
2	0.5	1.07	2.05	8.89	42.30	93.56	99.00	100.00
3	11.51	16.62	22.27	31.83	48.39	88.60	99.65	99.98
4	3.63	5.58	7.46	14.38	28.97	77.24	99.04	99.98
5	1.18	4.12	7.90	29.15	75.69	96.36	99.95	99.95
6	3.39	8.52	13.51	22.15	50.02	87.88	98.50	99.90
7	1.27	2.41	3.16	5.64	19.46	71.94	99.01	99.94
8	18.05	26.70	33.93	42.76	62.27	91.24	99.14	99.97
9	0.96	1.82	2.31	4.39	10.25	59.22	99.51	99.96
10	3.04	5.06	7.92	12.42	44.36	90.70	99.73	100.00
11	4.09	4.78	6.46	44.59	91.37	99.52	100.00	100.00
12	1.47	5.80	10.64	27.03	46.46	77.29	97.63	99.97
13	12.1	21.23	27.48	39.76	68.07	94.49	99.72	99.98
14	0	0.15	0.95	3.71	18.28	75.37	99.80	100.00
15	0	0.55	2.53	6.74	14.16	65.39	98.64	99.98
16	0	0.00	0.20	0.78	19.83	77.99	99.65	99.93
17	10.8	18.75	24.72	31.27	41.18	81.93	99.81	99.81
18	2.61	4.40	5.69	8.70	19.86	75.28	97.32	99.87
19	12.29	25.81	34.24	43.47	56.63	84.94	94.37	99.91
20	10.3	17.47	24.70	36.77	51.77	82.54	99.14	99.94
21	23.68	34.43	42.69	48.75	59.25	83.19	97.74	99.95
22	6.18	15.90	23.16	29.72	40.11	72.61	98.38	99.94
23	26.56	46.37	54.78	63.10	75.95	89.79	97.54	99.93
24	0.44	4.00	10.66	19.73	66.49	96.88	99.06	99.91

Mesh	5	10	18	35	60	120	4	pan
Phi (Ø)	-2.0	-1.0	0.0	1.0	2.0	3.0	4.0	>4
mm	4	2	1	0.5	0.25	0.125	0.062	<0.062
25	4.67	7.02	11.77	24.54	62.41	94.07	98.86	100.00
26	20.88	29.65	39.37	48.35	66.90	89.61	97.71	99.95
27	26.31	42.74	52.32	59.84	68.18	87.13	98.47	99.89
28	18.84	21.44	24.75	30.41	46.14	76.75	98.92	99.99
29	31.4	36.24	39.71	45.65	59.30	85.60	99.25	100.00
30	21.91	40.84	52.10	59.42	66.97	80.26	96.15	99.96
31	22.62	38.09	48.39	58.41	68.56	90.93	99.83	99.99
32	2.54	5.54	9.35	22.75	51.79	86.64	99.35	100.00
33	38.33	43.05	46.25	49.87	61.62	86.62	98.53	99.83
34	0.82	2.28	4.40	8.85	14.80	56.05	99.15	99.93
35	35.87	41.59	47.09	59.46	82.07	94.55	98.98	99.80
36	13.57	19.66	25.80	40.52	71.37	91.40	98.25	99.85
37	12.23	15.48	20.59	36.85	69.87	91.82	98.83	99.91
38	3.52	6.01	9.11	24.76	71.58	96.84	99.62	99.89
39	8.49	10.15	12.20	17.31	41.66	85.10	98.54	99.92
40	0	0.12	0.78	10.36	57.29	96.71	99.73	99.99
41	0.15	0.93	7.02	49.49	94.86	99.48	99.98	99.98
42	15.48	19.34	22.97	27.96	40.87	77.67	98.59	99.92
43	16.31	22.53	27.83	34.78	50.64	83.09	97.54	100.00
44	37.31	45.83	52.01	60.41	71.81	89.98	99.19	99.94
45	17.3	22.56	30.51	49.86	64.96	80.80	98.53	99.98
46	19.88	33.44	43.88	49.33	53.72	78.71	98.53	99.92
47	33.99	43.74	50.12	54.04	58.57	82.77	98.76	99.98
48	1.27	2.69	4.10	11.33	45.04	91.09	99.69	99.96
49	28.1	37.70	44.57	57.90	76.00	92.42	99.43	99.95
50	1.16	2.61	3.26	5.56	25.07	81.87	99.58	99.94
51	3.67	5.19	8.02	14.98	32.20	81.20	99.40	99.85
52	10.49	14.97	18.58	29.95	56.59	91.48	99.53	99.93
53	1.05	1.51	2.31	2.99	4.99	57.31	98.95	99.84
54	0	0.35	2.08	21.51	69.23	92.39	98.97	99.95
55	0	0.53	1.42	2.61	6.27	61.15	99.51	99.98
56	22.68	33.58	44.01	55.93	70.83	95.11	99.68	99.88
57	19.06	19.59	20.74	36.35	94.69	99.11	99.96	99.99

Table A.2 Shows the texture of the collected samples from the study area.

Sample no.	Gravel%	Sand%	mud%	Texture
1	0.98	98.39	0.63	Sand
2	1.07	97.93	1.00	Sand
3	16.62	83.03	0.33	Gravelly Sand
4	5.58	93.46	0.94	Gravelly Sand
5	2.94	96.93	0.00	Sand
6	8.52	89.98	1.40	Gravelly Sand
7	2.41	96.60	0.93	Sand
8	26.70	72.44	0.83	Gravelly Sand
9	1.82	97.69	0.45	Sand
10	5.06	94.67	0.27	Gravelly Sand
11	4.78	95.22	0.00	Sand
12	5.80	91.83	2.34	Gravelly Sand
13	21.23	78.49	0.26	Gravelly Sand
14	0.15	99.65	0.20	Sand
15	0.55	98.09	1.34	Sand
16	0.00	99.65	0.28	Sand
17	18.75	81.06	0.00	Gravelly Sand
18	4.40	92.92	2.55	Sand
19	25.81	68.56	5.54	Gravelly Sand
20	17.47	81.67	0.80	Gravelly Sand
21	23.68	59.51	14.55	Gravelly Sand
22	15.90	82.48	1.56	Gravelly Sand
23	46.37	51.17	2.39	Sandy Gravel
24	4.00	95.06	0.85	Sand
25	7.02	91.84	1.14	Gravelly Sand
26	29.65	68.06	2.24	Gravelly Sand
27	42.74	55.73	1.42	Sandy Gravel
28	21.44	77.48	1.07	Gravelly Sand
29	36.24	63.01	0.75	Sandy Gravel
30	40.84	55.31	3.81	Sandy Gravel
31	25.77	61.74	0.16	Gravelly Sand
32	5.54	93.81	0.65	Gravelly Sand
33	43.05	55.48	1.30	Sandy Gravel
34	2.28	96.87	0.78	Sand
35	41.59	57.39	0.82	Sandy Gravel
36	19.66	78.59	1.60	Gravelly Sand

37	15.48	83.35	1.08	Gravelly Sand
38	6.01	93.61	0.27	Gravelly Sand
39	10.15	88.39	1.38	Gravelly Sand
40	0.12	99.61	0.26	Sand
41	0.15	99.33	0.50	Sand
42	19.34	79.25	1.33	Gravelly Sand
43	22.53	75.01	2.46	Gravelly Sand
44	45.83	53.36	0.75	Sandy Gravel
45	22.56	75.97	1.45	Gravelly Sand
46	33.44	65.09	1.39	Sandy Gravel
47	43.74	55.02	1.22	Sandy Gravel
48	2.69	97.00	0.27	Sand
49	37.70	61.73	0.52	Sandy Gravel
50	2.61	96.97	0.36	Sand
51	5.19	94.21	0.45	Gravelly Sand
52	14.97	84.56	0.40	Gravelly Sand
53	1.51	97.44	0.89	Sand
54	0.35	98.62	0.98	Sand
55	0.53	98.98	0.47	Sand
56	33.58	66.10	0.20	Sandy Gravel
57	19.59	80.37	0.03	Gravelly Sand



UNIVERSITY of the
WESTERN CAPE

Table A3 Shows the Size parameter values of the collected samples from the study area.

S.No.	Median	Mean(Mz)	Sorting(σ_1)	Skewness(SkI)	Kurtosis(KG)
1	1.70	1.65	0.80	-0.11	1.07
2	1.62	1.55	0.74	-0.17	1.14
3	1.54	0.77	2.12	-0.62	1.37
4	1.94	1.75	1.22	-0.40	1.64
5	0.96	0.92	0.98	-0.13	1.27
6	1.50	1.24	1.45	-0.38	1.52
7	2.11	2.06	0.77	-0.18	1.20
8	0.88	-0.11	2.83	-0.57	1.07
9	2.36	2.29	0.65	-0.28	1.26
10	1.60	1.52	1.05	-0.31	1.59
11	0.60	0.58	0.80	-0.14	1.32
12	1.62	1.42	1.45	-0.28	1.00
13	0.87	0.18	2.26	-0.53	1.27
14	2.07	2.04	0.65	-0.16	1.10
15	2.23	2.21	0.77	-0.21	1.38
16	2.03	2.02	0.60	-0.04	0.95
17	1.71	0.75	2.38	-0.67	1.22
18	2.06	2.02	1.03	-0.25	1.97
19	1.02	0.21	2.71	-0.45	1.00
20	1.41	0.75	2.17	-0.52	1.11
21	0.62	-0.31	3.20	-0.46	0.86
22	1.81	1.05	2.14	-0.58	1.08
23	-1.04	-1.52	3.66	-0.24	0.85
24	1.17	1.08	0.99	-0.25	1.43
25	1.20	1.05	1.25	-0.29	1.52
26	0.59	-0.11	2.62	-0.41	0.92
27	-0.72	-1.09	3.40	-0.23	0.80
28	1.62	0.32	3.40	-0.71	1.78
29	0.85	-1.92	5.85	-0.76	1.09
30	-0.68	-0.69	3.15	-0.08	0.78
31	1.46	1.32	1.26	-0.26	1.24
32	-0.24	-1.85	4.28	-0.58	0.98

33	0.55	-2.63	6.53	-0.75	0.95
34	2.37	2.27	0.86	-0.39	1.54
35	-0.24	-1.85	4.28	-0.58	0.98
36	0.81	0.25	2.27	-0.45	1.47
37	0.90	0.55	2.01	-0.41	1.68
38	1.05	0.98	1.10	-0.26	1.63
39	1.68	1.49	1.70	-0.46	2.35
40	1.38	1.36	0.66	-0.08	1.01
41	1.51	1.49	0.66	-0.06	1.03
42	1.74	0.59	3.09	-0.71	1.94
43	1.50	0.43	2.80	-0.63	1.27
44	-0.81	-1.78	4.22	-0.39	0.84
45	0.54	0.26	2.47	-0.27	1.03
46	0.75	-0.08	2.98	-0.44	0.79
47	-0.50	-1.46	4.26	-0.40	0.81
48	1.59	1.53	0.85	-0.19	1.18
49	-0.05	-1.13	3.55	-0.49	0.96
50	1.93	1.88	0.73	-0.16	1.22
51	1.85	1.68	1.17	-0.38	1.51
52	1.28	0.80	2.05	-0.54	1.83
53	2.41	2.39	0.51	-0.06	0.98
54	1.12	1.17	0.87	0.10	1.08
55	2.35	2.32	0.53	-0.13	1.06
56	0.02	-0.52	2.62	-0.35	0.85
57	0.68	-0.81	4.44	-0.86	6.75

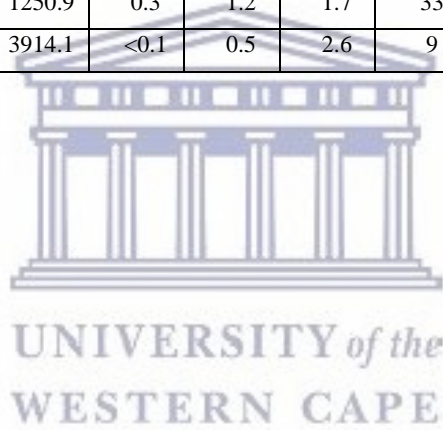
Table A.4 Sampling name and the trace elements concentration, which has been done by Inductively Coupled Plasma (ICP) Analyses for the 57 samples .

	Analyte	Ba	Be	Co	Cs	Ga	Hf	Nb	Rb
	Unit	PPM	PPM	PPM	PPM	PPM	PPM	PPM	PPM
Sample	Type								
1	Soil	201	<1	6.4	0.4	3.1	2.1	3.9	20.0
2	Soil	68	<1	2.6	0.2	1.7	0.8	2.5	8.7
3	Soil	134	<1	4.1	0.4	2.5	1.7	3.8	15.1
4	Soil	157	<1	4.7	0.5	3.6	2.1	3.7	17.3
5	Soil	136	<1	5.5	0.5	3.3	4.6	4.9	16.4
6	Soil	90	<1	2.8	0.4	0.9	0.8	1.5	9.6
7	Soil	185	<1	5.2	0.6	2.9	2.2	2.9	20.4
8	Soil	92	<1	2.5	0.2	1.6	1.0	2.0	11.3
9	Soil	159	<1	5.3	0.9	3.7	2.1	4.1	21.4
10	Soil	190	<1	3.2	0.6	2.8	1.9	2.1	21.5
11	Soil	74	<1	5.0	0.2	1.3	1.1	0.9	7.6
12	Soil	109	<1	2.9	0.4	2.5	2.8	2.0	12.3
13	Soil	125	<1	3.9	0.4	2.1	4.3	3.5	12.7
14	Soil	156	<1	4.6	0.5	3.3	2.1	4.0	19.1
15	Soil	179	<1	4.6	0.5	2.9	1.5	3.4	19.4
16	Soil	197	<1	4.1	0.6	2.9	1.3	2.8	21.1
17	Soil	124	<1	3.2	0.3	2.2	1.3	2.7	16.9
18	Soil	161	<1	5.0	0.5	3.3	1.6	3.3	19.2
19	Soil	168	1	4.7	0.6	4.0	1.7	4.0	21.9
20	Soil	115	<1	3.1	0.3	1.6	1.5	2.2	11.9
21	Soil	131	2	3.7	0.5	2.9	2.3	3.4	17.2
22	Soil	123	<1	3.7	0.5	2.7	1.5	4.0	17.1
23	Soil	89	<1	3.5	0.3	1.3	2.6	2.6	10.8
24	Soil	46	<1	1.4	<0.1	<0.5	0.6	1.4	3.7
25	Soil	70	<1	1.3	0.1	<0.5	1.0	1.1	4.9
26	Soil	99	<1	2.2	0.3	1.1	0.9	1.3	10.7
27	Soil	176	<1	12.9	0.7	2.6	1.9	3.0	17.3
28	Soil	179	1	4.4	0.7	3.0	3.9	3.2	18.6
29	Soil	161	<1	5.6	0.4	3.2	2.6	3.0	18.1
30	Soil	227	<1	9.7	0.9	4.0	3.7	4.6	24.2

31	Soil	141	<1	5.1	0.5	2.8	2.9	3.0	17.4
32	Soil	184	<1	6.7	0.5	2.8	2.0	2.6	18.1
33	Soil	35	<1	1.9	0.2	<0.5	0.4	0.7	4.9
34	Soil	199	<1	4.1	0.5	3.6	2.5	3.7	23.1
35	Soil	136	<1	4.5	0.3	1.6	3.0	3.0	13.8
36	Soil	62	<1	1.9	0.2	0.7	0.9	1.1	7.1
37	Soil	122	<1	5.3	0.3	2.5	1.7	2.5	12.3
38	Soil	68	<1	3.2	0.1	1.4	1.0	1.6	7.1
39	Soil	68	<1	1.1	<0.1	1.6	1.2	1.9	8.0
40	Soil	28	<1	0.4	<0.1	<0.5	0.1	0.7	3.0
41	Soil	139	<1	4.6	0.2	2.1	2.7	2.4	11.7
42	Soil	183	<1	4.0	0.5	3.3	1.6	3.2	16.2
43	Soil	180	<1	4.7	0.5	2.8	2.1	2.4	17.9
44	Soil	166	2	6.5	0.5	3.3	2.2	4.1	15.9
45	Soil	210	<1	3.9	0.5	3.3	2.1	3.7	16.1
46	Soil	128	<1	3.2	0.5	2.7	1.3	2.9	13.7
47	Soil	120	1	2.8	0.5	2.8	2.1	3.5	16.3
48	Soil	139	<1	4.0	0.2	2.0	1.7	2.4	13.6
49	Soil	150	1	7.0	0.4	3.2	2.3	3.9	15.9
50	Soil	190	<1	4.8	0.3	3.5	6.7	4.6	20.2
51	Soil	149	<1	5.6	0.6	3.7	4.7	6.0	17.5
52	Soil	165	<1	4.2	0.6	3.1	2.0	2.8	17.7
53	Soil	141	2	6.6	0.4	3.6	7.1	6.1	14.7
54	Soil	117	<1	5.0	0.3	2.5	7.5	4.4	12.4
55	Soil	396	1	3.9	0.5	3.5	2.5	3.6	19.6
56	Soil	173	<1	7.2	0.4	2.5	4.8	4.0	17.8
57	Soil	77	<1	1.8	0.2	1.2	1.0	1.8	9.7

	Analyte	Sn	Sr	Ta	Th	U	V	W	Zr	Y	La
	Unit	PPM	PPM	PPM	PPM	PPM	PPM	PPM	PPM	PPM	PPM
Sample	Type										
1	Soil	<1	1702.5	0.3	1.4	1.7	39	<0.5	76.7	7.4	6.7
2	Soil	<1	4163.2	0.2	0.9	3.0	26	<0.5	29.1	3.8	4.9
3	Soil	<1	2027.5	0.2	1.6	3.2	38	<0.5	65.7	7.4	6.9
4	Soil	<1	1430.3	0.2	1.7	1.6	42	0.5	72.2	7.4	9.2
5	Soil	<1	1079.6	0.3	2.3	1.9	47	<0.5	166.1	10.0	11.3
6	Soil	<1	3653.2	0.1	0.8	2.9	24	<0.5	42.2	3.4	3.8
7	Soil	<1	1273.0	0.3	1.8	1.6	36	<0.5	88.9	8.0	9.9
8	Soil	3	1647.1	0.2	0.9	2.5	25	<0.5	50.0	5.0	5.9
9	Soil	<1	560.9	0.3	2.0	1.4	43	0.5	74.7	8.7	9.9
10	Soil	3	870.8	0.1	1.2	1.4	20	<0.5	78.3	5.5	6.0
11	Soil	2	3916.1	<0.1	1.8	2.5	22	<0.5	59.4	4.5	6.9
12	Soil	1	3399.7	0.2	1.4	3.1	24	<0.5	86.3	7.4	7.2
13	Soil	<1	3521.9	0.2	0.8	3.0	24	<0.5	161.9	6.6	3.6
14	Soil	<1	880.8	0.3	1.8	1.3	36	<0.5	68.9	8.8	8.7
15	Soil	<1	915.3	0.2	1.4	1.5	31	<0.5	56.5	6.8	8.3
16	Soil	<1	908.8	0.2	1.4	1.4	44	<0.5	58.3	7.1	7.0
17	Soil	<1	2131.9	0.2	1.3	4.6	28	0.6	61.0	6.2	7.8
18	Soil	<1	1446.5	0.3	1.6	1.7	32	<0.5	60.7	7.1	7.4
19	Soil	<1	875.1	0.2	1.8	1.9	33	0.5	58.4	8.2	8.3
20	Soil	<1	2330.9	<0.1	1.3	2.6	24	<0.5	60.4	5.9	6.5
21	Soil	<1	3159.4	0.3	1.6	2.9	40	0.5	107.5	7.1	8.5
22	Soil	<1	2328.1	0.3	1.7	3.2	29	<0.5	66.9	8.3	8.7
23	Soil	<1	1997.1	0.2	1.2	1.8	26	<0.5	112.5	5.3	5.5
24	Soil	<1	7243.6	0.1	0.6	3.6	16	<0.5	37.0	2.1	3.4
25	Soil	<1	4643.7	<0.1	0.7	4.0	17	<0.5	41.7	3.2	3.8
26	Soil	<1	4444.1	<0.1	0.7	3.1	16	<0.5	36.0	3.8	4.2
27	Soil	<1	2188.0	0.2	1.4	2.0	36	<0.5	74.7	6.9	7.3
28	Soil	<1	923.3	0.2	1.8	1.9	39	<0.5	147.4	8.6	7.5
29	Soil	<1	1254.8	0.2	1.6	1.7	33	<0.5	92.7	8.3	8.8
30	Soil	<1	1789.3	0.3	2.4	2.2	47	1.1	150.9	9.1	10.2
31	Soil	<1	1956.0	0.3	1.5	3.0	36	<0.5	113.7	7.8	8.2
32	Soil	<1	2019.8	0.2	1.5	1.9	34	<0.5	80.7	6.7	9.2
33	Soil	<1	6851.6	<0.1	0.4	4.0	14	<0.5	18.6	1.8	2.4
34	Soil	<1	682.3	0.2	2.0	1.4	40	0.6	102.1	8.9	9.6
35	Soil	<1	3199.7	0.2	1.2	2.7	31	<0.5	130.4	5.7	5.9
36	Soil	<1	4148.8	<0.1	0.7	3.6	15	<0.5	34.2	3.3	3.1
37	Soil	1	3208.5	0.1	0.9	1.6	25	<0.5	71.7	4.3	6.8
38	Soil	<1	4277.3	<0.1	0.6	2.5	16	<0.5	35.5	3.3	4.2
39	Soil	<1	2033.4	<0.1	0.8	4.6	24	<0.5	45.4	4.0	6.0
40	Soil	<1	6855.0	<0.1	0.2	2.4	9	<0.5	11.6	1.6	2.0

41	Soil	<1	3091.4	0.1	1.0	1.7	25	<0.5	119.1	5.8	6.1
42	Soil	<1	1781.3	0.2	1.5	2.8	27	<0.5	61.0	6.6	10.2
43	Soil	<1	1852.8	0.2	1.4	1.5	18	<0.5	69.2	4.9	8.8
44	Soil	<1	1884.3	0.3	1.6	2.2	30	<0.5	91.9	8.0	9.6
45	Soil	<1	3148.5	0.3	1.6	1.8	29	<0.5	91.5	7.6	10.6
46	Soil	<1	2330.8	0.2	1.5	2.3	21	<0.5	55.3	6.0	7.7
47	Soil	<1	1098.9	0.2	1.3	2.0	27	<0.5	87.5	6.0	8.7
48	Soil	<1	3363.8	0.2	1.0	1.9	17	<0.5	63.2	4.4	5.9
49	Soil	<1	1829.4	0.2	1.5	2.0	30	<0.5	95.1	7.0	10.2
50	Soil	<1	974.3	0.3	1.6	1.3	35	<0.5	262.5	8.3	10.7
51	Soil	<1	993.7	0.4	2.0	1.7	41	<0.5	208.1	10.6	13.3
52	Soil	<1	1207.6	0.2	1.5	1.5	26	<0.5	82.9	7.4	9.5
53	Soil	<1	1168.7	0.5	2.5	2.3	46	<0.5	300.1	10.5	12.7
54	Soil	<1	3678.5	0.3	1.9	3.4	34	<0.5	288.0	8.2	8.9
55	Soil	<1	1231.0	0.2	1.6	1.8	27	<0.5	84.2	8.0	10.0
56	Soil	<1	1250.9	0.3	1.2	1.7	33	<0.5	210.7	6.4	7.3
57	Soil	<1	3914.1	<0.1	0.5	2.6	9	<0.5	37.5	4.0	3.5



	Analyte	Ce	Pr	Nd	Sm	Eu	Gd	Tb	Dy	Ho	Er	Tm	Yb	Lu
	Unit	PPM												
Sample	Type													
1	Soil	11.7	1.49	5.9	1.37	0.38	1.47	0.27	1.47	0.32	0.78	0.11	0.67	0.11
2	Soil	9.3	1.01	3.4	0.69	0.24	0.72	0.14	0.66	0.15	0.37	0.06	0.35	0.08
3	Soil	12.2	1.56	6.0	1.09	0.33	1.16	0.22	1.23	0.25	0.74	0.11	0.57	0.11
4	Soil	16.5	2.00	8.4	1.46	0.38	1.45	0.23	1.25	0.30	0.77	0.12	0.93	0.14
5	Soil	20.8	2.55	10.1	1.82	0.48	1.75	0.31	1.76	0.40	1.09	0.15	1.08	0.17
6	Soil	6.5	0.80	3.6	0.69	0.18	0.64	0.11	0.60	0.17	0.39	0.05	0.50	0.07
7	Soil	17.4	2.12	6.7	1.48	0.43	1.55	0.25	1.42	0.27	0.86	0.11	0.75	0.13
8	Soil	9.9	1.31	6.2	1.02	0.25	1.03	0.14	0.79	0.16	0.48	0.06	0.44	0.07
9	Soil	18.9	2.30	10.5	1.73	0.47	1.66	0.26	1.53	0.30	0.85	0.11	0.93	0.15
10	Soil	11.4	1.43	5.5	1.03	0.30	1.14	0.14	0.98	0.18	0.50	0.06	0.51	0.06
11	Soil	13.4	1.60	8.1	0.89	0.16	0.73	0.09	0.83	0.11	0.27	0.05	0.44	0.04
12	Soil	12.9	1.56	5.3	1.40	0.31	1.12	0.14	1.07	0.18	0.45	0.08	0.57	0.09
13	Soil	7.0	0.94	3.9	0.82	0.28	0.98	0.10	0.90	0.16	0.35	0.06	0.63	0.08
14	Soil	15.4	1.84	7.9	1.50	0.41	1.45	0.23	1.27	0.31	0.83	0.11	0.82	0.14
15	Soil	13.7	1.72	6.6	1.15	0.35	1.23	0.20	1.31	0.27	0.68	0.09	0.66	0.10
16	Soil	12.8	1.64	6.3	1.18	0.34	1.28	0.21	1.27	0.23	0.66	0.10	0.87	0.10
17	Soil	12.2	1.54	5.3	1.06	0.32	1.19	0.17	1.08	0.24	0.68	0.08	0.50	0.09
18	Soil	12.4	1.74	8.2	1.42	0.37	1.34	0.20	1.17	0.20	0.70	0.10	0.79	0.11
19	Soil	14.7	1.84	7.7	1.39	0.39	1.53	0.21	1.40	0.26	0.85	0.11	0.78	0.11
20	Soil	10.8	1.33	6.3	1.01	0.28	1.02	0.16	1.09	0.22	0.63	0.07	0.67	0.09
21	Soil	15.2	1.89	8.1	1.48	0.35	1.48	0.22	1.22	0.24	0.74	0.10	0.67	0.11
22	Soil	15.9	1.87	6.2	1.38	0.35	1.50	0.22	1.33	0.25	0.80	0.08	0.62	0.09

23	Soil	10.1	1.21	5.0	0.79	0.24	1.03	0.13	0.94	0.17	0.62	0.07	0.59	0.09
24	Soil	6.0	0.66	3.0	0.40	0.09	0.42	0.05	0.29	0.04	0.17	0.02	0.24	0.03
25	Soil	7.1	0.85	3.4	0.66	0.15	0.59	0.09	0.59	0.12	0.35	0.03	0.26	0.05
26	Soil	6.7	0.81	4.0	0.62	0.17	0.62	0.09	0.53	0.12	0.41	0.04	0.38	0.05
27	Soil	11.5	1.54	6.6	1.11	0.30	1.22	0.17	1.12	0.28	0.65	0.09	0.76	0.13
28	Soil	14.2	1.79	8.0	1.55	0.42	1.56	0.22	1.72	0.29	0.86	0.12	0.91	0.14
29	Soil	15.7	1.86	7.1	1.47	0.37	1.59	0.22	1.29	0.26	0.79	0.10	0.82	0.12
30	Soil	18.9	2.29	8.3	1.73	0.41	1.70	0.25	1.54	0.29	1.08	0.13	0.94	0.12
31	Soil	14.9	1.86	8.3	1.45	0.39	1.43	0.22	1.31	0.29	0.81	0.10	0.81	0.12
32	Soil	16.0	1.99	7.9	1.53	0.39	1.34	0.19	1.20	0.23	0.59	0.09	0.65	0.09
33	Soil	4.3	0.47	2.4	0.36	0.08	0.37	0.04	0.33	0.05	0.16	0.01	0.20	0.03
34	Soil	17.8	2.23	8.2	1.61	0.42	1.52	0.23	1.50	0.31	0.90	0.11	0.84	0.13
35	Soil	9.2	1.21	4.5	0.92	0.28	0.93	0.14	0.81	0.19	0.66	0.07	0.66	0.08
36	Soil	6.6	0.75	3.3	0.56	0.13	0.57	0.08	0.51	0.10	0.26	0.02	0.25	0.03
37	Soil	11.3	1.15	4.3	0.77	0.25	0.76	0.15	0.93	0.21	0.56	0.07	0.39	0.10
38	Soil	6.2	0.84	2.8	0.51	0.19	0.53	0.13	0.48	0.13	0.39	0.06	0.34	0.06
39	Soil	10.4	1.12	4.7	0.77	0.23	0.71	0.15	0.63	0.21	0.49	0.08	0.39	0.09
40	Soil	3.0	0.37	1.2	0.21	0.08	0.24	0.04	0.17	0.06	0.17	0.01	0.12	0.03
41	Soil	10.3	1.22	4.8	0.88	0.26	0.92	0.19	0.93	0.25	0.63	0.09	0.63	0.11
42	Soil	16.8	1.82	7.1	1.38	0.34	1.29	0.23	1.24	0.25	0.83	0.11	0.66	0.12
43	Soil	15.1	1.64	7.3	1.01	0.29	0.97	0.17	0.86	0.23	0.58	0.06	0.50	0.08
44	Soil	16.8	1.86	7.3	1.27	0.35	1.32	0.24	1.21	0.29	0.97	0.12	0.72	0.12
45	Soil	18.8	1.93	8.0	1.47	0.38	1.36	0.26	1.32	0.33	0.93	0.11	0.74	0.14
46	Soil	14.6	1.60	6.0	1.10	0.32	1.12	0.22	1.12	0.26	0.76	0.09	0.64	0.12
47	Soil	14.8	1.63	5.7	1.18	0.34	1.26	0.21	1.12	0.25	0.81	0.09	0.59	0.11
48	Soil	9.5	1.08	3.9	0.80	0.22	0.79	0.14	0.70	0.17	0.51	0.05	0.47	0.07
49	Soil	18.5	1.95	6.9	1.28	0.34	1.26	0.24	1.28	0.35	0.95	0.11	0.84	0.14
50	Soil	18.5	1.99	7.2	1.54	0.37	1.33	0.26	1.32	0.35	1.01	0.14	0.86	0.15

51	Soil	25.5	2.72	9.7	2.01	0.47	1.97	0.34	1.79	0.42	1.24	0.15	0.97	0.19
52	Soil	15.2	1.70	6.1	1.26	0.35	1.27	0.22	1.22	0.30	0.98	0.11	0.71	0.13
53	Soil	23.7	2.57	10.3	1.85	0.41	1.79	0.34	1.64	0.47	1.36	0.17	1.14	0.23
54	Soil	15.7	1.71	6.6	1.28	0.31	1.27	0.25	1.39	0.33	1.05	0.15	1.06	0.20
55	Soil	16.3	1.78	7.1	1.32	0.33	1.34	0.25	1.28	0.31	0.99	0.12	0.82	0.13
56	Soil	14.0	1.57	6.6	1.27	0.32	1.07	0.20	1.00	0.26	0.73	0.09	0.74	0.12
57	Soil	6.2	0.73	2.7	0.59	0.15	0.56	0.11	0.59	0.16	0.42	0.05	0.43	0.04



	Analyte	Mo	Cu	Pb	Zn	Ag	Ni	As	Au	Cd	Sb	Bi	Hg	Tl	Se
	Unit	PPM	PPM	PPM	PPM	PPM	PPM	PPM	PPB	PPM	PPM	PPM	PPM	PPM	PPM
Sample	Type														
1	Soil	0.5	13.5	2.2	17	<0.1	86.8	2.9	1.5	<0.1	0.1	<0.1	<0.01	<0.1	<0.5
2	Soil	0.8	2.1	1.1	4	<0.1	8.5	2.5	2.4	<0.1	<0.1	<0.1	0.01	<0.1	<0.5
3	Soil	2.6	3.3	1.5	6	<0.1	24.6	3.2	2.2	<0.1	0.2	<0.1	0.02	<0.1	<0.5
4	Soil	0.6	3.6	1.9	12	<0.1	29.8	2.7	<0.5	0.1	<0.1	<0.1	<0.01	<0.1	<0.5
5	Soil	0.3	3.7	2.1	7	<0.1	19.3	5.0	<0.5	0.1	0.1	<0.1	<0.01	<0.1	<0.5
6	Soil	6.2	3.2	1.1	4	<0.1	20.9	4.0	2.1	<0.1	<0.1	<0.1	0.01	<0.1	<0.5
7	Soil	5.0	3.4	1.3	4	<0.1	15.0	3.1	<0.5	0.1	0.1	<0.1	0.02	0.2	<0.5
8	Soil	0.4	3.9	1.8	7	<0.1	27.5	2.3	0.5	0.1	0.1	<0.1	<0.01	<0.1	<0.5
9	Soil	0.3	4.3	1.9	9	<0.1	22.6	2.6	<0.5	<0.1	<0.1	<0.1	<0.01	<0.1	<0.5
10	Soil	0.5	3.3	1.5	7	<0.1	42.5	2.3	<0.5	<0.1	0.1	<0.1	0.02	<0.1	<0.5
11	Soil	0.2	6.5	6.2	21	<0.1	73.5	2.8	1.1	<0.1	<0.1	<0.1	0.01	<0.1	<0.5
12	Soil	0.5	3.0	1.3	5	<0.1	25.3	3.3	0.6	<0.1	<0.1	<0.1	0.01	<0.1	<0.5
13	Soil	0.2	3.7	1.5	7	<0.1	37.3	2.8	<0.5	<0.1	<0.1	<0.1	0.02	<0.1	<0.5
14	Soil	0.2	4.0	1.7	8	<0.1	20.5	2.7	<0.5	<0.1	0.1	<0.1	<0.01	<0.1	<0.5
15	Soil	0.8	3.8	1.5	8	<0.1	34.5	1.8	<0.5	<0.1	<0.1	<0.1	0.01	<0.1	<0.5
16	Soil	0.6	3.5	1.5	7	<0.1	19.0	2.5	<0.5	<0.1	<0.1	<0.1	<0.01	<0.1	<0.5
17	Soil	0.2	3.0	1.0	5	<0.1	18.3	3.7	0.6	<0.1	0.1	<0.1	<0.01	<0.1	<0.5
18	Soil	0.6	4.0	2.0	7	<0.1	38.7	2.8	<0.5	0.1	<0.1	<0.1	<0.01	<0.1	<0.5
19	Soil	0.5	4.8	1.8	9	<0.1	25.2	2.6	<0.5	0.1	<0.1	<0.1	0.01	<0.1	<0.5
20	Soil	4.2	3.9	1.6	6	<0.1	14.8	2.7	<0.5	0.2	0.1	<0.1	<0.01	<0.1	<0.5
21	Soil	1.1	3.1	1.1	6	<0.1	17.3	3.7	<0.5	0.3	0.2	<0.1	0.04	0.2	<0.5
22	Soil	0.6	3.6	1.6	7	<0.1	21.6	4.4	<0.5	<0.1	0.2	<0.1	0.02	<0.1	<0.5
23	Soil	0.3	4.1	1.9	7	<0.1	18.4	3.5	2.1	<0.1	<0.1	<0.1	<0.01	<0.1	<0.5
24	Soil	0.3	2.5	1.2	5	<0.1	9.6	5.1	1.0	<0.1	0.1	<0.1	0.04	<0.1	<0.5
25	Soil	0.3	4.1	2.0	6	<0.1	18.6	4.0	<0.5	0.1	<0.1	<0.1	<0.01	<0.1	<0.5
26	Soil	0.6	5.0	4.0	14	<0.1	26.5	2.4	<0.5	<0.1	<0.1	<0.1	0.03	<0.1	<0.5
27	Soil	1.0	4.3	1.5	11	<0.1	118.2	2.2	<0.5	0.1	<0.1	<0.1	0.02	<0.1	<0.5
28	Soil	0.9	5.7	2.9	13	<0.1	23.7	2.6	<0.5	0.1	0.1	<0.1	<0.01	<0.1	<0.5
29	Soil	0.5	4.1	1.8	11	<0.1	34.3	2.2	<0.5	<0.1	0.1	<0.1	<0.01	<0.1	<0.5
30	Soil	2.7	7.6	4.2	25	<0.1	82.2	2.8	<0.5	<0.1	0.1	<0.1	0.02	<0.1	<0.5

31	Soil	1.7	4.3	1.8	8	<0.1	30.6	3.1	<0.5	0.2	0.2	<0.1	0.02	<0.1	<0.5
32	Soil	0.7	3.9	2.1	8	<0.1	66.4	3.1	<0.5	0.1	<0.1	<0.1	<0.01	<0.1	<0.5
33	Soil	1.1	2.3	1.8	3	<0.1	13.1	4.2	<0.5	<0.1	0.1	<0.1	0.02	<0.1	<0.5
34	Soil	0.6	4.3	3.2	17	<0.1	26.3	2.9	<0.5	0.2	<0.1	<0.1	0.02	<0.1	<0.5
35	Soil	0.5	4.8	2.9	9	<0.1	31.3	1.9	<0.5	<0.1	<0.1	<0.1	0.02	<0.1	<0.5
36	Soil	0.4	3.2	3.4	6	<0.1	13.9	2.3	0.9	<0.1	0.1	<0.1	0.03	<0.1	<0.5
37	Soil	0.2	5.5	2.4	35	<0.1	78.1	2.6	<0.5	<0.1	<0.1	<0.1	<0.01	<0.1	<0.5
38	Soil	0.2	2.3	1.1	3	<0.1	37.1	3.2	<0.5	<0.1	<0.1	<0.1	0.02	<0.1	<0.5
39	Soil	0.4	2.5	1.0	3	<0.1	6.1	2.7	<0.5	<0.1	0.2	<0.1	<0.01	<0.1	<0.5
40	Soil	<0.1	2.2	0.9	2	<0.1	3.5	1.4	<0.5	<0.1	<0.1	<0.1	<0.01	<0.1	<0.5
41	Soil	0.5	3.2	3.1	7	<0.1	33.2	2.3	<0.5	<0.1	<0.1	<0.1	<0.01	<0.1	<0.5
42	Soil	1.4	6.9	2.2	12	<0.1	19.1	2.9	<0.5	0.1	0.1	<0.1	<0.01	<0.1	<0.5
43	Soil	0.7	5.6	5.1	20	<0.1	45.3	2.3	<0.5	0.1	0.1	<0.1	<0.01	<0.1	<0.5
44	Soil	0.6	4.7	3.9	11	<0.1	57.1	2.1	0.5	<0.1	0.1	<0.1	0.02	<0.1	<0.5
45	Soil	0.5	4.4	1.6	8	<0.1	18.0	2.6	<0.5	0.1	0.1	<0.1	<0.01	<0.1	<0.5
46	Soil	0.9	4.3	1.8	9	<0.1	15.8	3.9	0.5	0.1	0.2	<0.1	0.02	<0.1	<0.5
47	Soil	0.2	3.5	1.6	7	<0.1	11.4	4.0	<0.5	<0.1	0.2	<0.1	<0.01	<0.1	<0.5
48	Soil	0.1	2.3	1.4	4	<0.1	17.3	2.2	<0.5	<0.1	<0.1	<0.1	<0.01	<0.1	<0.5
49	Soil	0.5	5.2	5.3	12	<0.1	44.9	2.5	1.4	0.1	0.1	<0.1	0.02	<0.1	<0.5
50	Soil	0.3	3.5	2.2	7	<0.1	17.8	2.9	<0.5	0.1	<0.1	<0.1	0.01	<0.1	<0.5
51	Soil	0.4	4.3	2.1	9	<0.1	21.9	1.6	<0.5	0.1	0.1	<0.1	<0.01	<0.1	<0.5
52	Soil	0.4	3.5	1.6	7	<0.1	19.3	2.3	0.9	0.1	<0.1	<0.1	<0.01	<0.1	<0.5
53	Soil	0.3	3.1	1.5	6	<0.1	11.6	3.0	0.7	<0.1	0.1	<0.1	<0.01	<0.1	<0.5
54	Soil	0.3	2.7	1.5	6	<0.1	9.3	1.8	<0.5	<0.1	<0.1	<0.1	<0.01	<0.1	<0.5
55	Soil	0.3	4.1	1.6	9	<0.1	15.9	2.2	1.6	<0.1	0.1	<0.1	<0.01	<0.1	<0.5
56	Soil	0.3	3.5	10.4	14	<0.1	61.6	2.6	1.6	0.1	0.2	<0.1	0.02	<0.1	<0.5
57	Soil	0.2	1.8	2.5	4	<0.1	5.4	2.4	0.7	<0.1	<0.1	<0.1	<0.01	<0.1	<0.5

Table A.5 XRF analysis of the major elements, expressed as weight percent oxide

Sample	Al ₂ O ₃	CaO	Fe ₂ O ₃	K ₂ O	MgO	MnO	Na ₂ O	P ₂ O ₅	SiO ₂	TiO ₂	L.OI
1	2.41	29.37	1.13	0.55	3.30	0.01	0.95	0.04	31.84	0.11	27.13
2	1.11	48.63	0.38	0.20	2.07	0.00	0.91	0.06	9.01	0.06	36.83
3	2.13	36.82	0.67	0.44	1.94	0.01	3.73	0.05	16.81	0.12	38.25
4	2.91	31.71	1.02	0.55	2.49	0.02	1.27	0.05	26.49	0.14	28.22
5	2.72	37.37	0.99	0.45	1.92	0.02	1.25	0.06	22.61	0.20	33.33
6	1.25	37.79	0.45	0.32	2.79	0.00	4.90	0.04	8.01	0.08	44.80
7	3.28	31.72	1.15	0.63	2.23	0.03	1.13	0.05	31.86	0.18	27.71
8	1.77	41.34	0.58	0.34	1.79	0.01	2.24	0.04	14.03	0.10	38.30
9	3.75	31.20	1.10	0.65	2.33	0.03	1.75	0.06	30.96	0.20	28.40
10	2.43	23.09	0.82	0.73	2.01	0.01	1.24	0.04	48.36	0.11	21.44
11	0.47	48.89	0.28	0.10	1.05	0.00	0.76	0.04	3.89	0.04	42.29
12	2.25	38.64	0.82	0.40	2.64	0.01	1.56	0.05	18.12	0.15	35.22
13	1.61	38.14	1.47	0.24	4.83	0.02	1.25	0.03	17.82	0.09	34.47
14	3.44	32.19	1.02	0.60	1.94	0.02	1.57	0.06	30.81	0.18	28.42
15	3.82	28.39	1.03	0.76	2.27	0.03	2.08	0.05	38.64	0.15	22.70
16	3.14	32.82	0.89	0.60	1.73	0.02	1.58	0.06	30.55	0.15	28.99
17	2.54	36.08	0.73	0.45	3.87	0.02	1.43	0.03	20.03	0.13	34.34
18	3.39	30.87	1.37	0.58	2.93	0.03	1.08	0.05	32.25	0.18	27.06
19	4.42	26.11	1.19	0.81	2.25	0.03	2.11	0.06	38.71	0.21	24.92
20	1.72	36.79	0.67	0.40	2.56	0.01	3.92	0.05	13.74	0.11	37.55
21	2.67	37.04	0.69	0.46	1.81	0.02	1.83	0.04	21.41	0.14	34.05
22	3.17	34.30	0.92	0.55	2.46	0.02	1.50	0.05	25.15	0.18	31.39
23	0.94	48.52	0.43	0.15	1.70	0.00	0.32	0.03	6.68	0.09	40.07
24	0.49	48.71	0.22	0.12	0.85	0.00	1.45	0.04	3.58	0.04	43.59
25	2.35	32.70	1.31	0.48	3.97	0.02	0.96	0.05	28.68	0.11	29.23
26	1.39	42.71	0.55	0.28	1.80	0.01	1.20	0.09	12.40	0.08	39.02
27	2.84	30.45	1.42	0.50	5.33	0.03	1.05	0.04	26.48	0.16	28.86

28	3.39	30.45	1.24	0.65	2.81	0.03	1.35	0.06	31.94	0.19	27.69
29	2.70	31.51	1.56	0.46	5.41	0.03	0.91	0.05	26.07	0.16	28.97
30	3.48	22.81	1.56	0.63	6.04	0.03	1.50	0.06	28.64	0.20	23.66
31	2.93	33.73	1.03	0.52	3.00	0.02	1.30	0.06	23.84	0.20	30.57
32	0.62	49.65	0.29	0.11	1.22	0.00	0.67	0.05	4.56	0.05	41.96
33	0.85	42.49	0.48	0.24	3.32	0.01	4.03	0.03	4.07	0.05	44.14
34	4.31	23.84	1.16	0.93	2.90	0.03	1.86	0.05	42.29	0.19	22.58
35	1.02	43.13	0.80	0.21	3.00	0.01	1.13	0.05	11.51	0.07	38.78
36	0.85	47.58	0.33	0.17	1.30	0.00	0.84	0.06	7.25	0.06	40.92
37	1.20	37.28	1.06	0.30	4.28	0.01	0.84	0.04	21.29	0.07	40.00
38	0.70	48.23	0.32	0.13	1.40	0.00	0.65	0.05	6.52	0.05	42.02
39	1.35	45.53	0.44	0.24	1.60	0.01	0.97	0.05	10.53	0.10	38.90
40	0.73	48.65	0.24	0.13	1.01	0.00	0.76	0.05	6.24	0.05	41.26
41	1.28	41.19	0.72	0.29	2.09	0.01	0.93	0.05	17.28	0.10	35.65
42	3.76	33.42	1.27	0.48	3.54	0.03	1.48	0.05	25.44	0.18	30.00
43	2.12	34.18	0.84	0.56	2.28	0.01	1.05	0.04	28.82	0.10	30.19
44	2.10	34.62	1.77	0.38	5.58	0.02	0.95	0.05	23.01	0.14	31.37
45	2.22	38.50	0.81	0.40	2.30	0.02	0.99	0.06	19.27	0.14	33.83
46	2.48	38.33	0.90	0.47	2.66	0.02	1.64	0.05	18.01	0.15	35.17
47	1.90	42.33	0.81	0.37	2.25	0.01	1.25	0.05	13.68	0.11	37.71
48	1.49	40.53	0.55	0.38	1.47	0.01	0.93	0.05	18.62	0.11	35.41
49	2.39	35.02	2.15	0.25	6.92	0.03	0.81	0.05	20.89	0.13	30.33
50	2.78	27.72	0.98	0.65	1.81	0.02	0.83	0.05	40.68	0.21	23.93
51	2.99	34.32	1.11	0.54	2.01	0.02	1.14	0.06	27.61	0.23	29.63
52	1.81	40.77	0.74	0.35	1.78	0.01	0.86	0.06	18.22	0.12	34.77
53	3.41	31.79	1.10	0.61	2.48	0.03	2.19	0.06	29.12	0.27	29.85
54	1.25	43.70	0.48	0.25	2.22	0.01	0.94	0.08	11.95	0.12	38.38
55	4.33	26.53	1.10	0.78	2.73	0.03	2.34	0.06	37.21	0.23	25.53
56	1.72	36.28	1.08	0.41	3.30	0.01	0.78	0.04	24.17	0.12	31.70
57	0.36	50.97	0.23	0.09	0.80	0.00	0.82	0.05	2.66	0.03	43.35

Table A.6 Correlation coefficient matrix of different geochemical variables for the beach sands of Abu Dhabi.

	Al2O3	CaO	Cr2O3	Fe2O3	K2O	MgO	MnO	Na2O	P2O5	SiO2	TiO2	LOI	As	Ba	Co	Cu	Nb	Ni	Pb	Rb	Sr	Th	U	V	Zn	Zr
Al2O3	1																									
CaO	-0.88	1																								
Cr2O3	0.31*	-0.46	1																							
Fe2O3	0.67	-0.74	0.72	1																						
K2O	0.93	-0.93	0.26	0.56	1																					
MgO	0.30*	-0.47	0.59	0.82	0.19	1																				
MnO	0.90	-0.81	0.48	0.82	0.78	0.54	1																			
Na2O	0.16	-0.20	-0.27*	-0.09	0.22	0.01	0.07	1																		
P2O5	0.23	-0.07	0.07	0.03	0.16	-0.17	0.19	-0.12	1																	
SiO2	0.87	-0.94	0.44	0.66	0.94	0.28*	0.76	-0.01	0.12	1																
TiO2	0.90	-0.78	0.48	0.63	0.82	0.26	0.84	0.10	0.33*	0.76	1															
LOI	-0.88	0.92	-0.50	-0.72	-0.90	-0.36	-0.81	0.10	-0.16	-0.96	-0.78	1														
As	-0.05	0.10	-0.23	-0.14	-0.08	-0.07	-0.09	0.27*	-0.30*	-0.19	-0.03	0.23	1													
Ba	0.69	-0.71	0.35	0.70	0.70	0.28*	0.62	-0.02	0.19	0.71	0.63	-0.72	-0.27*	1												
Co	0.37	-0.46	0.65	0.31*	0.31*	0.55	0.48	-0.17	0.02	0.38	0.44	-0.46	-0.22	0.52	1											
Cu	0.27	-0.38	0.21	0.26	0.26	0.36	0.24	-0.12	-0.02	0.31*	0.17	-0.35	-0.09	0.29*	0.42	1										
Nb	0.63	-0.55	0.58	0.54	0.54	0.28*	0.61	-0.05	0.27*	0.55	0.78	-0.59	-0.09	0.56	0.58	0.23	1									
Ni	0.03	-0.26	0.39	0.06	0.06	0.50	0.11	-0.22	-0.26	0.17	-0.04	-0.21	-0.18	0.28*	0.76	0.58	0.10	1								
Pb	-0.09	-0.03	0.41	-0.06	-0.06	0.24	-0.03	-0.24	0.03	0.02	-0.08	-0.07	-0.18	0.12	0.33*	0.29*	0.06	0.42	1							
Rb	0.78	-0.78	0.38	0.80	0.80	0.28*	0.69	-0.04	0.16	0.80	0.71	-0.81	-0.19	0.82	0.59	0.37*	0.69	0.29*	0.10	1						
Sr	-0.71	0.66	-0.39	-0.70	-0.70	-0.19	0.60	0.05	-0.14	-0.71	-0.71	0.71	0.20	-0.68	-0.49	-0.28*	-0.68	-0.18	-0.11	-0.86	1					
Th	0.70	-0.59	0.43	0.62	0.62	0.20	0.65	0.003	0.31*	0.57	0.80	-0.61	-0.01	0.59	0.61	0.32*	0.81	0.17	0.10	0.74	-0.72	1				
U	-0.39	0.44	-0.30*	-0.46	-0.46	-0.02	-0.31*	0.22	-0.09	-0.54	-0.37	-0.53	0.36*	-0.59	-0.47	-0.27*	-0.42	-0.30*	-0.20	-0.64	0.60	-0.44	1			
V	0.65	-0.58	0.47	0.54	0.57	0.26	0.61	0.06	0.23	0.54	0.72	-0.58	0.01	-0.53	-0.64	0.31*	0.81	0.23	0.02	0.73	-0.70	0.84	-0.40	1		
Zn	0.16	-0.32*	0.22	0.19	0.19	0.41	0.19	-0.20	-0.03	0.26	0.08	0.08	-0.17	0.31*	0.47	0.65	0.17	0.66	0.52**	0.31*	-0.22	0.29*	-0.35*	0.23	1	
Zr	0.22	-0.26	0.65	0.22	0.22	0.14	0.28*	-0.16	0.22	0.28*	0.50	0.50	0.12	0.29*	0.44	0.04	0.72	0.03	0.21	0.34*	-0.36*	0.57	-0.22	0.55	0.10	1

UNIVERSITY of the
WESTERN CAPE

Table A.7 Shows the determined factor.

Sample name	FAC1_1	FAC2_1	FAC3_1	FAC4_1	FAC5_1
1	0,64068	3,16069	-0,66698	-0,68962	0,64148
2	-1,02055	-0,93357	-0,37662	-0,51321	-0,63675
3	-0,05680	-0,18418	0,52152	-0,69831	1,75159
4	0,70717	0,18833	0,13871	-0,41794	-0,02316
5	-0,00857	-0,25111	2,59858	-0,50932	1,37214
6	-0,71379	-0,10748	-0,54448	-0,46738	2,71602
7	1,11123	-0,65498	0,29219	-0,04778	-0,00725
8	-0,30781	-0,05167	-0,73285	-0,59133	0,23379
9	1,29389	-0,19022	0,52268	-0,60947	0,04920
10	1,50284	0,00057	-1,67243	-0,51249	-0,92666
11	-1,84164	2,57903	0,36715	-1,39203	0,02117
12	-0,32234	-0,76216	0,06384	0,47105	0,44197
13	-0,69728	-0,17263	-0,40636	2,23657	0,21272
14	1,08189	-0,30314	0,18559	-0,75936	-0,26236
15	1,74866	-0,24286	-1,24388	-0,41382	-0,46689
16	1,18568	-0,29846	-0,05069	-1,24391	-0,32329
17	-0,00473	-0,56870	-0,48475	0,83044	1,72271

18	1,00611	-0,19051	-0,29902	0,61471	-0,26590
19	1,89758	-0,32545	-0,56804	-0,51617	0,21206
20	-0,08915	-0,32490	-0,41933	-0,44574	1,12389
21	0,09648	-0,44632	0,61924	-0,36103	1,38925
22	0,43154	-0,49113	0,17529	0,03964	1,43306
23	-1,19963	0,42122	0,51173	-1,02028	0,21929
24	-1,78623	-0,56542	-0,54917	-0,42926	1,67939
25	-0,21147	-1,16909	-1,48163	2,50359	0,39947
26	-0,74258	-0,18140	-0,69658	-0,51998	-1,44107
27	0,19054	1,70369	0,08050	1,95423	0,07881
28	1,00623	0,02711	0,54535	0,01596	-0,26928
29	0,54537	0,01806	-0,13000	1,61234	-0,61787
30	0,84223	2,29079	1,13297	1,08383	0,59486
31	0,33690	-0,40379	0,64912	0,40988	0,27766
32	-1,16317	1,46665	1,10685	-2,06598	-0,01735
33	-1,37291	-0,66164	-1,40654	1,02623	2,60459
34	1,97336	0,35579	-0,29228	-0,54646	0,33571
35	-1,01686	0,29340	0,48798	0,34667	-0,77620
36	-1,31813	-0,59780	-0,71029	-0,46916	-0,97809
37	-0,67234	2,61770	-1,01586	0,21151	-0,15036

38	-1,40596	-0,33992	-0,55385	-0,49138	-0,39754
39	-0,86248	-1,35068	-0,39034	0,04987	0,04245
40	-1,27107	-1,35682	-1,92877	-0,32511	-1,68507
41	-0,67517	-0,04258	0,16496	0,09254	-1,17520
42	0,83408	0,14543	-0,69705	0,48084	0,45351
43	0,41363	1,65861	-1,14213	-0,88965	-0,74946
44	-0,14983	0,67146	0,07760	2,12999	-0,81006
45	0,22881	-0,24678	0,12310	-0,57812	-0,60745
46	0,19044	-0,16598	-0,38281	-0,33685	0,90880
47	-0,20825	-0,16267	0,24686	-0,93092	0,63837
48	-0,25379	-0,74576	-0,54595	-0,23064	-1,21684
49	-0,30102	0,72802	0,12148	3,14180	-0,77396
50	0,84670	-0,72938	1,34421	0,20224	-0,90290
51	0,45905	-0,53756	1,69231	0,06137	-1,14257
52	-0,00856	-0,25923	0,32477	-0,83723	-1,19091
53	0,41385	-1,25401	3,05412	0,59923	0,56812
54	-1,20987	-1,32551	2,60320	-0,04649	-1,27248
55	2,18938	-0,58491	-0,89644	-0,46914	-0,46719
56	-0,85754	1,58156	1,39738	1,12192	-1,38207
57	-1,42482	-0,70771	-0,86413	-0,86089	-1,18588

Table A.8 EF values from Abu Dhabi beach sand samples and minor.

	No Enrichment	Minor enrichment	Moderate Enrichment	Moderate sever enrichment	Severe enrichment	Very severe enrichment	Extremely severe enrichment	Total
As	0	0	3	20	26	5	3	57 samples
Co	23	31	1	2	0	0	0	57 samples
Cr	2	0	2	11	24	16	2	57 samples
Cu	47	9	1	0	0	0	0	57 samples
Ni	5	29	13	6	3	1		57 samples
Pb	32	18	4	2	1			57 samples
Sr	0	0	0	4	16	14	23	57 samples
Th	29	26	1	1	0	0	0	57 samples
U	0	11	13	16	13	4	0	57 samples
V	0	40	12	4	1	0	0	57 samples
Zn	40	15	0	2	0	0	0	57 samples
Zr	0	22	20	9	6	0	0	57 samples

UNIVERSITY of the
WESTERN CAPE

Table A.9 The Min., Max., Average and St. Dev of the EF values and geo accumulation index (Igeo) from Abu Dhabi beach sand samples and minor.

	As	Co	Cr	Cu	Ni	Pb	Sr	Th	U	V	Zr	Zn
EF												
Min	1.84	0.15	0.00	0.25	0.31	0.30	3.41	0.37	1.48	0.27	0.83	0.13
Max	40.64	2.95	25.63	3.78	14.25	10.82	336.72	5.23	33.47	2.37	14.53	4.64
Average	7.31	0.67	8.0	0.66	1.72	1.26	47.83	1.02	7.46	0.69	3.17	0.57
St. Dev	6.90	0.53	5.66	0.55	2.31	1.67	66.93	0.74	7.24	0.39	2.58	0.70
Igeo												
Min	-1.17	-6.81	-1.16	-5.82	-5.27	-4.10	0.05	-5.49	-1.05	-4.98	-4.07	-5.89
Max	0.70	-1.80	1.84	-2.92	-0.19	-0.53	3.74	-1.85	0.77	-2.60	0.62	-1.76
Average	-0.20	-3.56	0.11	-4.74	-2.51	-2.93	1.90	-2.85	0.29	-3.38	-1.37	-3.95
St. Dev	0.49	0.80	1.01	0.49	1.00	0.70	0.90	0.68	0.49	0.55	0.90	0.79

UNIVERSITY of the
WESTERN CAPE

Table A.10. The mineralogical composition of the 12 beach sand samples from Abu Dhabi.

sample	Minerals											
	Dolomite - CaMg(CO ₃) ₂	Halite - NaCl	Albite, calcian, ordered - (Na,Ca)Al(Si,Al) ₃ O ₈	Calcite, syn - CaCO ₃	Aragonite - CaCO ₃	Quartz, syn - SiO ₂	Augite - (Ca.818Mg.792Fe.183Fe.086Al.151Al.269Si.1.751)O ₆	Diopside - CaMg(Si ₂ O ₆)	Albite, high (K-bearing) (K _{0.22} Na _{0.78})(AlSi ₃ O ₈)	Albite, ordered (NaAlSi ₃ O ₈)	Clinochrysolite - 2Mg ₃ Si ₂ O ₅ (OH) ₄	Calcite magnesium - Mg _{0.1} Ca _{0.9} CO ₃
3	2.85%	8.20%	5.50%	66.11%	6.02%	37.36%						
11		3.33%	2.96%	63.79%	13.11%	40.54%	10.67%					
10			3.12%	24.74%	1.04%	73.02%	0.70%	1.15%				
28		2.44%	17.92%	47.27%	5.99%	69.76%	5.87%	6.60%				
29		2.44%	17.92%	47.27%	5.99%	69.76%	5.38%	6.60%				
39		3.33%	2.96%	63.79%	13.11%	40.54%	10.67%					
46	7.43%			47.61%	4.29%	25.22%	3.06%		5.20%			
50	1.51%		1.09%	15.69%	1.29%	20.68%	1.19%					
52	1.57%	2.10%	5.03%	62.21%	1.81%	42.10%						
55	3.86%		2.08%	25.85%	21.18%	53.24%			19.22%			
56		1.33%	1.11%	49.63%	20.82%	93.45%					3.44%	3.59%
57		26.95%	18.64%	18.64%	93.74%	16.08%						7.92%

Appendix B: Figures.

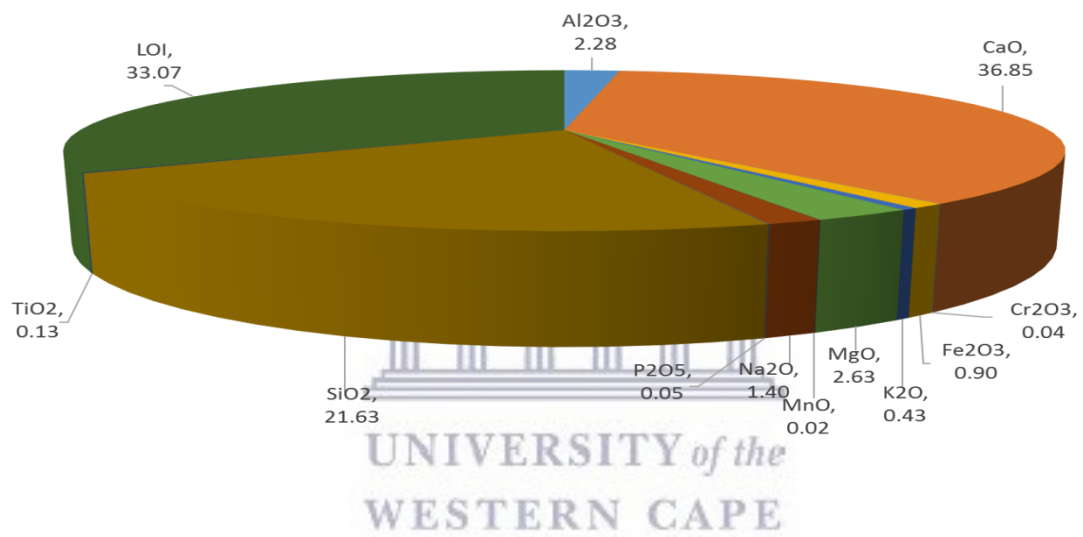


Figure B.1. Average percent distribution of all oxides in the studied samples.

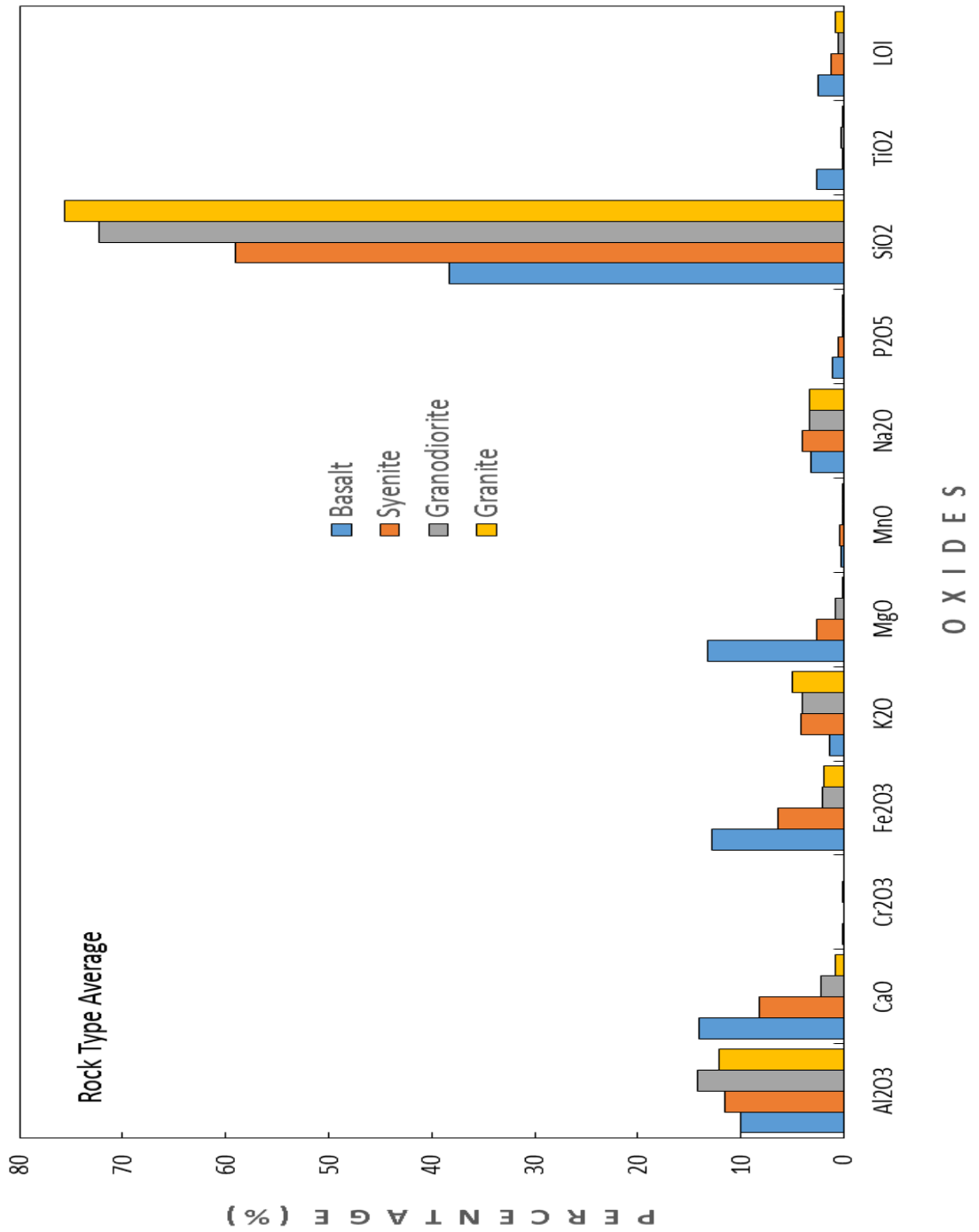


Figure B.2. Average percent distribution of oxides in basalt, syenite, granodiorite and granite

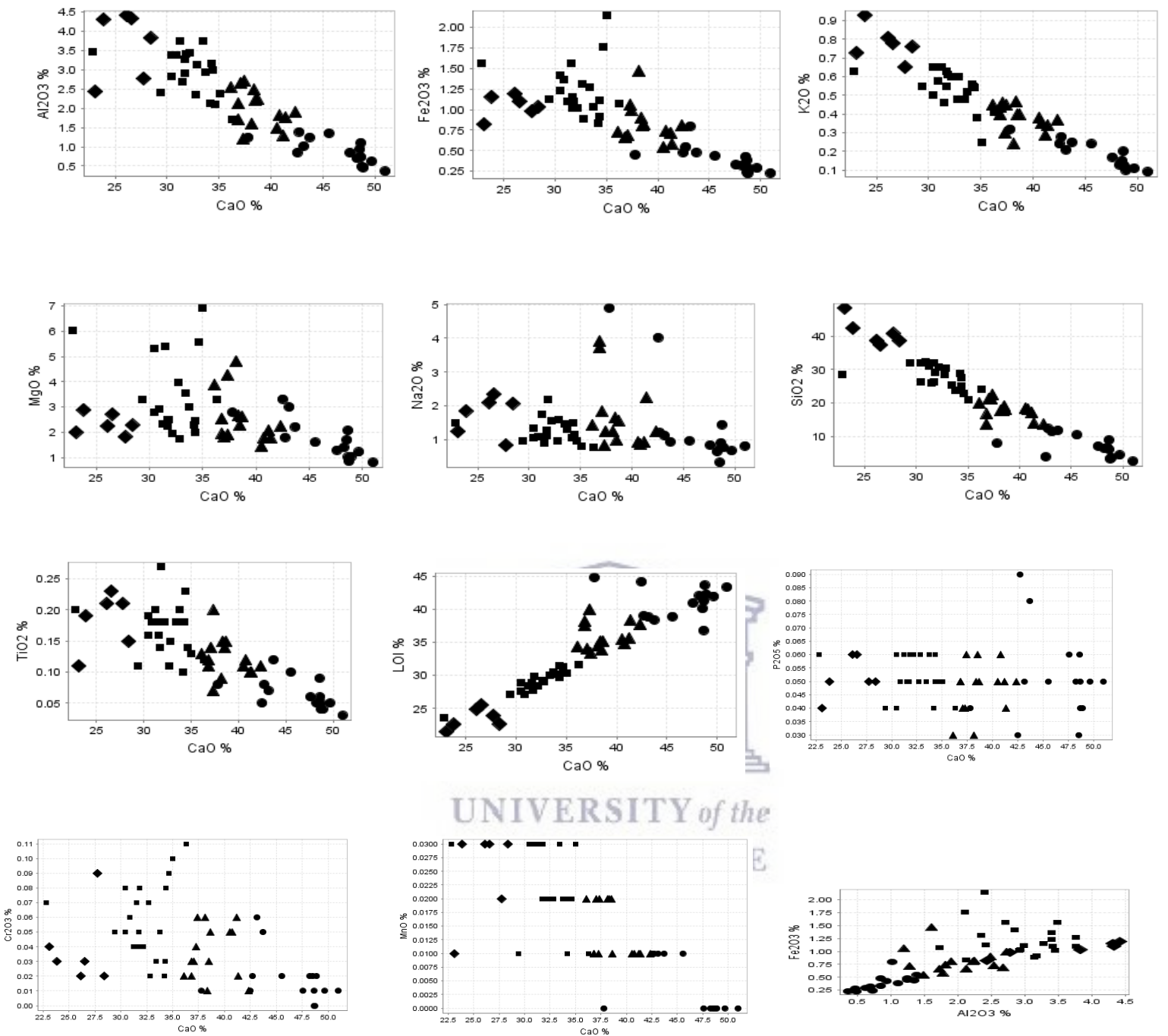


Figure B.3a. Contents of major elements against CaO contents for all samples.

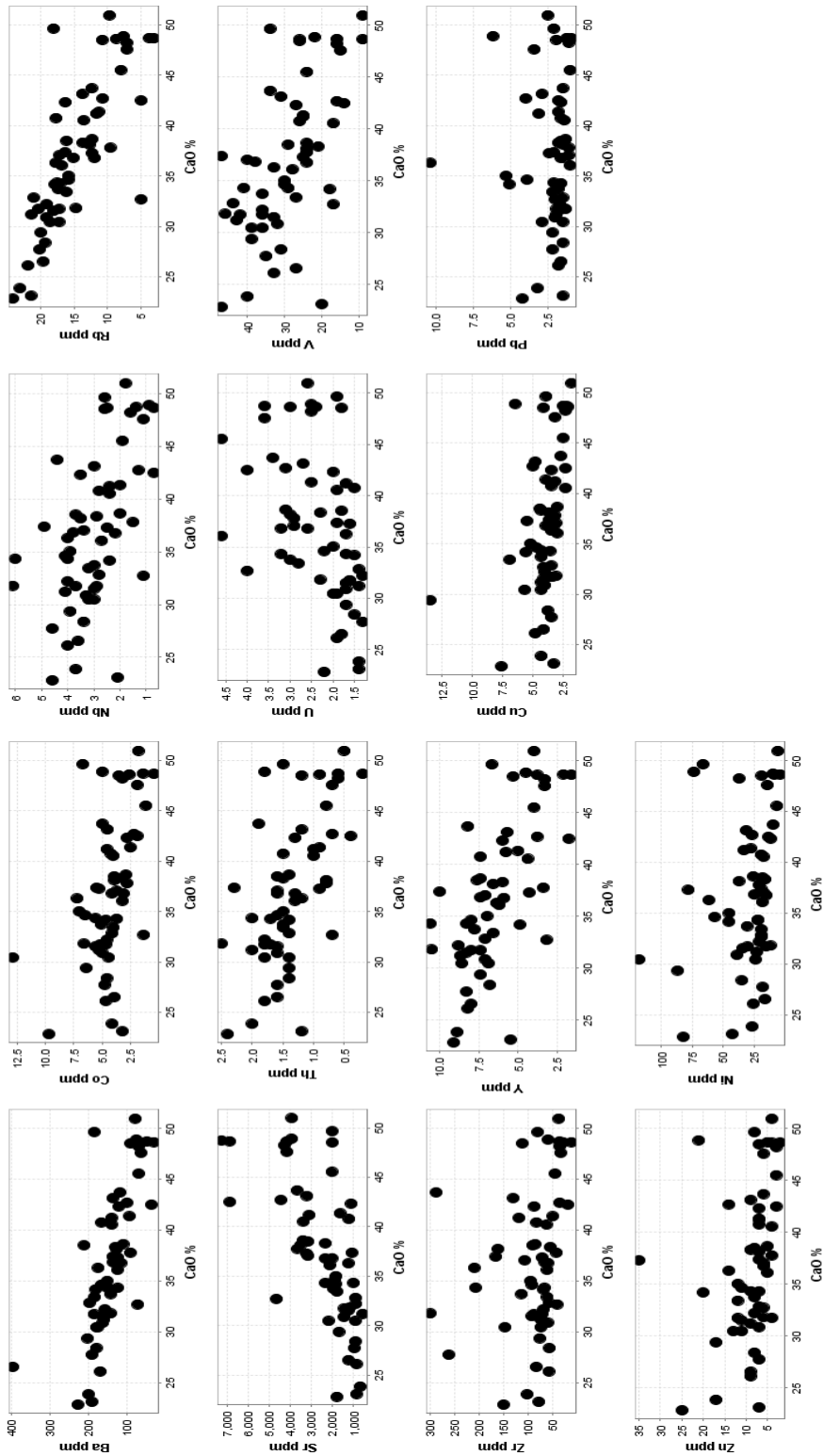


Figure B.3b. Minor and trace elements – CaO variation in beach sand samples from Abu Dhabi, United Arab Emirates.

Quartz, syn

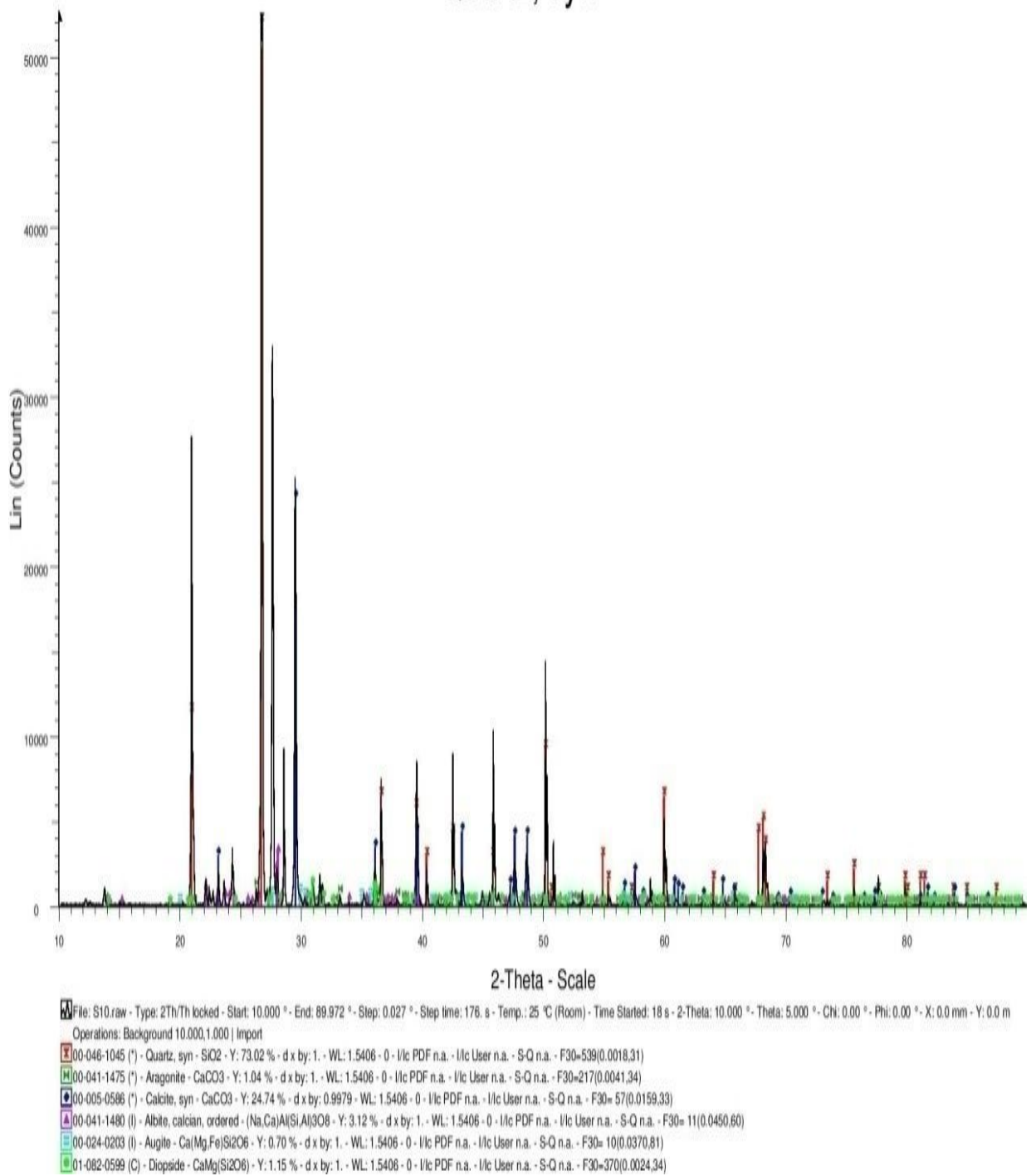
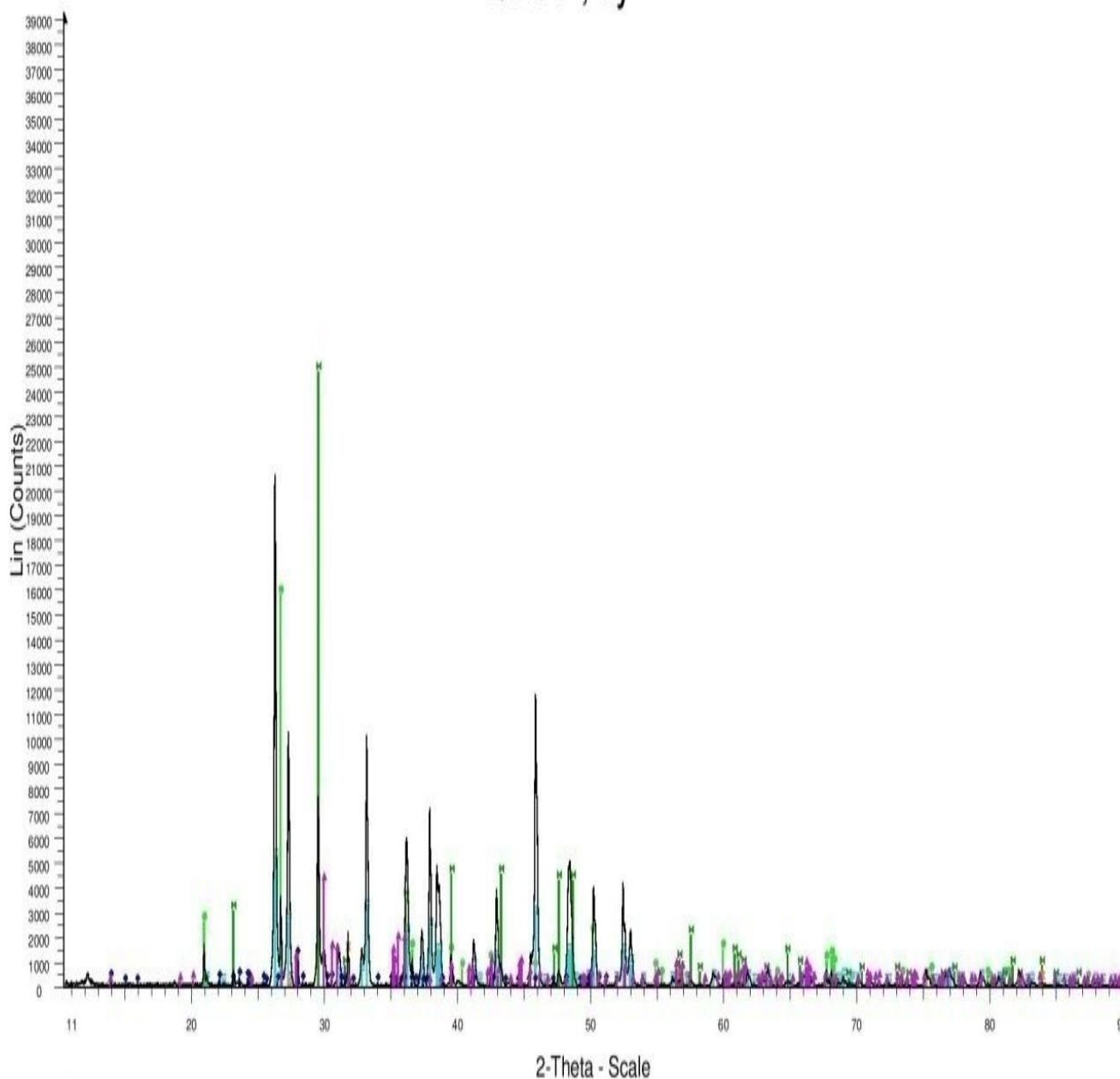


Figure B.4. X-Ray Diffraction showing the mineralogical composition of the sample 10 from study area.

Quartz, syn



File: S11.raw - Type: 2Th/Th locked - Start: 10.000 ° - End: 89.972 ° - Step: 0.027 ° - Step time: 176. s - Temp.: 25 °C (Room) - Time Started: 18 s - 2-Theta: 10.000 ° - Theta: 5.000 ° - Chi: 0.00 ° - Phi: 0.00 ° - X: 0.0 mm - Y: 0.0 m
Operations: Background 10.000,1.000 | Import

- 00-046-1045 (*) - Quartz, syn - SiO₂ - Y: 40.54 % - d x by: 1. - WL: 1.5406 - 0 - I/Ic PDF n.a. - I/Ic User n.a. - S-Q n.a. - F30=539(0.0018,31)
- 00-041-1475 (*) - Aragonite - CaCO₃ - Y: 13.11 % - d x by: 1. - WL: 1.5406 - 0 - I/Ic PDF n.a. - I/Ic User n.a. - S-Q n.a. - F30=217(0.0041,34)
- 00-005-0586 (*) - Calcite, syn - CaCO₃ - Y: 63.79 % - d x by: 0.9979 - WL: 1.5406 - 0 - I/Ic PDF n.a. - I/Ic User n.a. - S-Q n.a. - F30=57(0.0159,33)
- 01-075-0306 (C) - Halite - NaCl - Y: 3.33 % - d x by: 1. - WL: 1.5406 - 0 - I/Ic PDF n.a. - I/Ic User n.a. - S-Q n.a. - F9=1000(0.0001,9)
- 01-071-0721 (C) - Augite - (Ca₈18Mg₇92Fe₁₈₃Fe₀₈₆Al₁₅₁Al₂₆₉Si₁₇₅₁)O₆ - Y: 10.67 % - d x by: 1. - WL: 1.5406 - 0 - I/Ic PDF n.a. - I/Ic User n.a. - S-Q n.a. - F30=229(0.0036,36)
- 00-009-0466 (*) - Albite, ordered - NaAlSi₃O₈ - Y: 2.96 % - d x by: 1. - WL: 1.5406 - 0 - I/Ic PDF n.a. - I/Ic User n.a. - S-Q n.a. - F30=36(0.0138,60)

Figure B.5. X-Ray Diffraction showing the mineralogical composition of the sample 11 from study area.

Quartz, syn

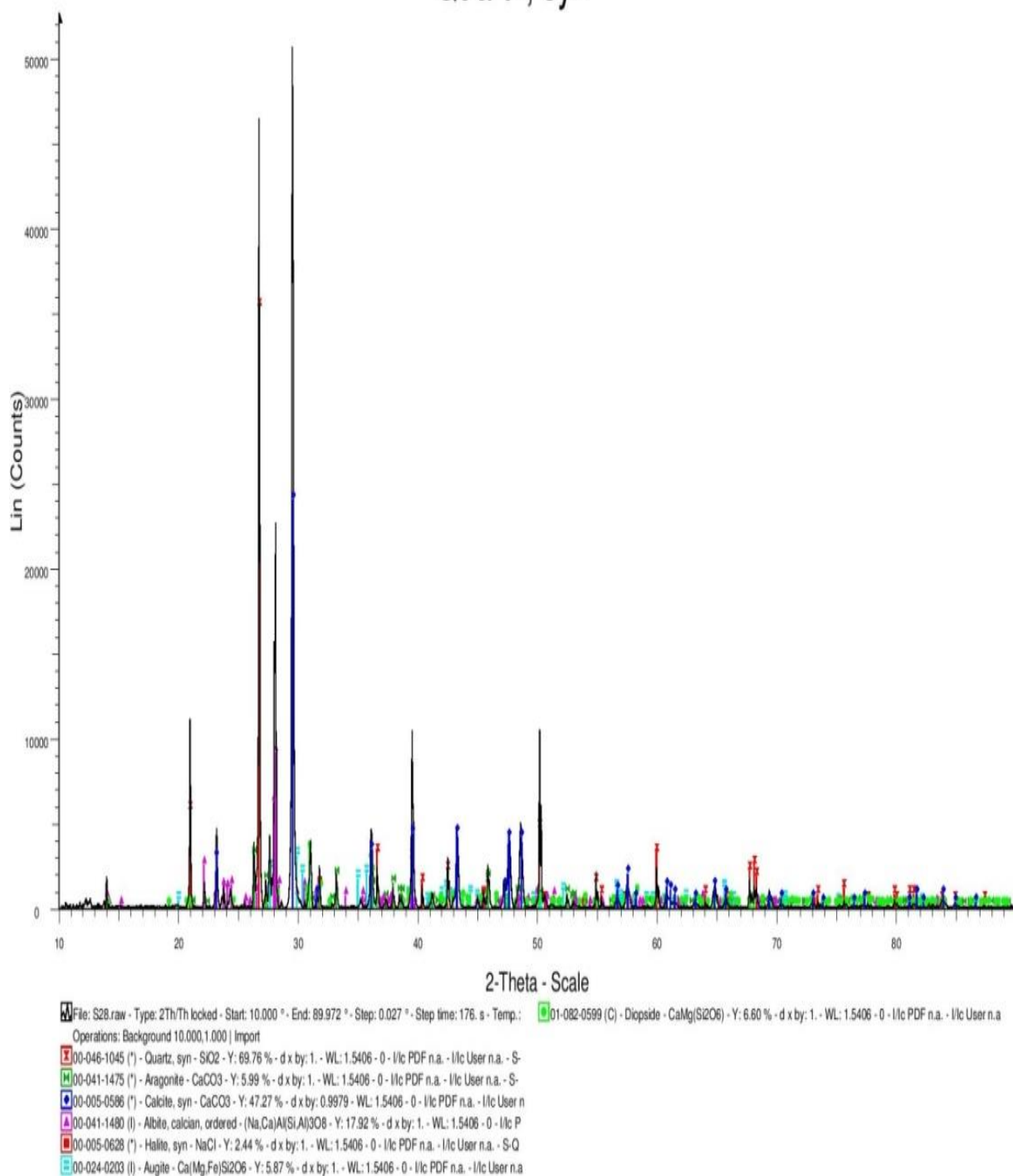


Figure B.6. X-Ray Diffraction showing the mineralogic composition of the sample 28 from study area.

Quartz, syn

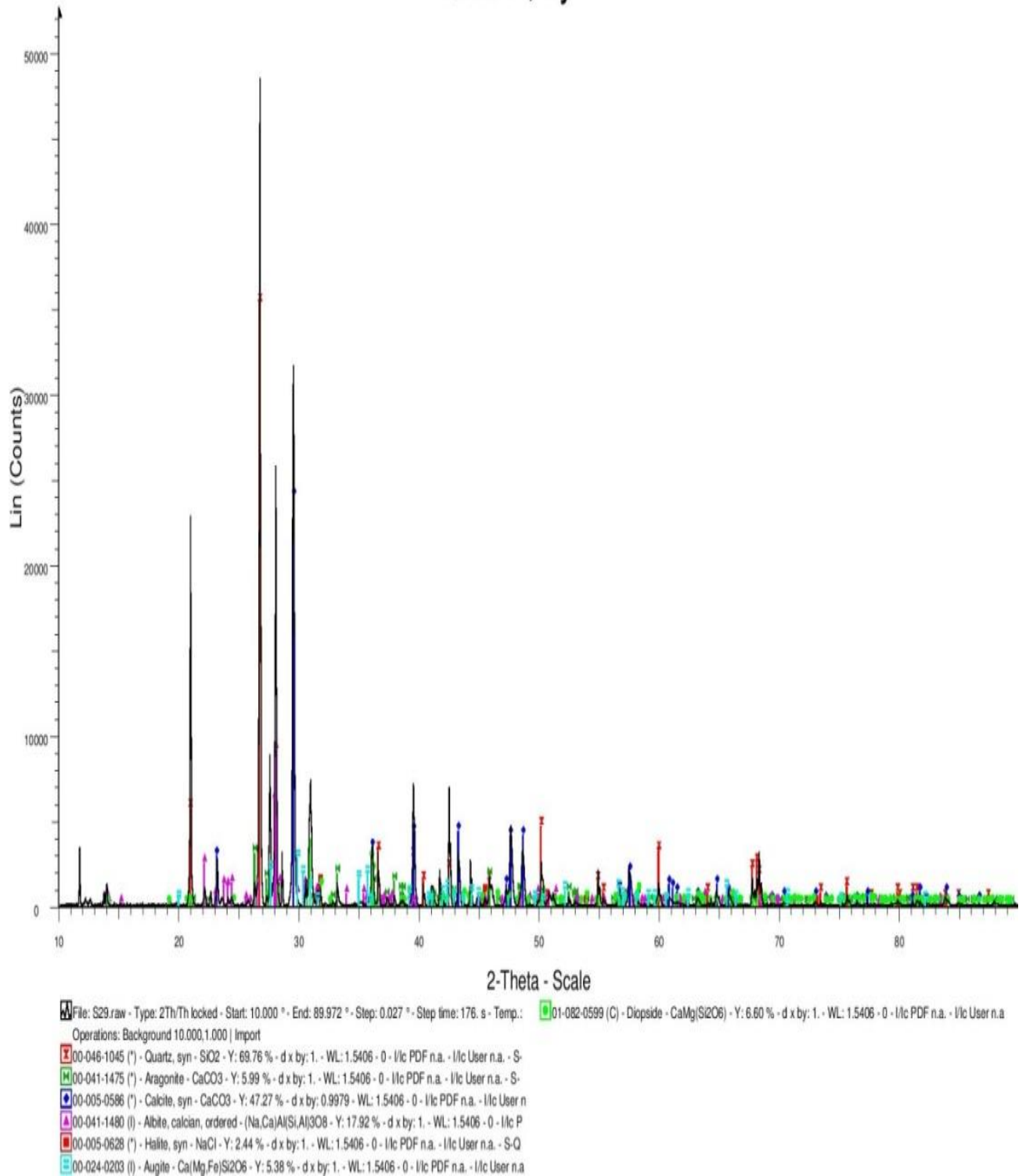


Figure B.7. X-Ray Diffraction showing the mineralogic composition of the sample 29 from study area.

Quartz, syn

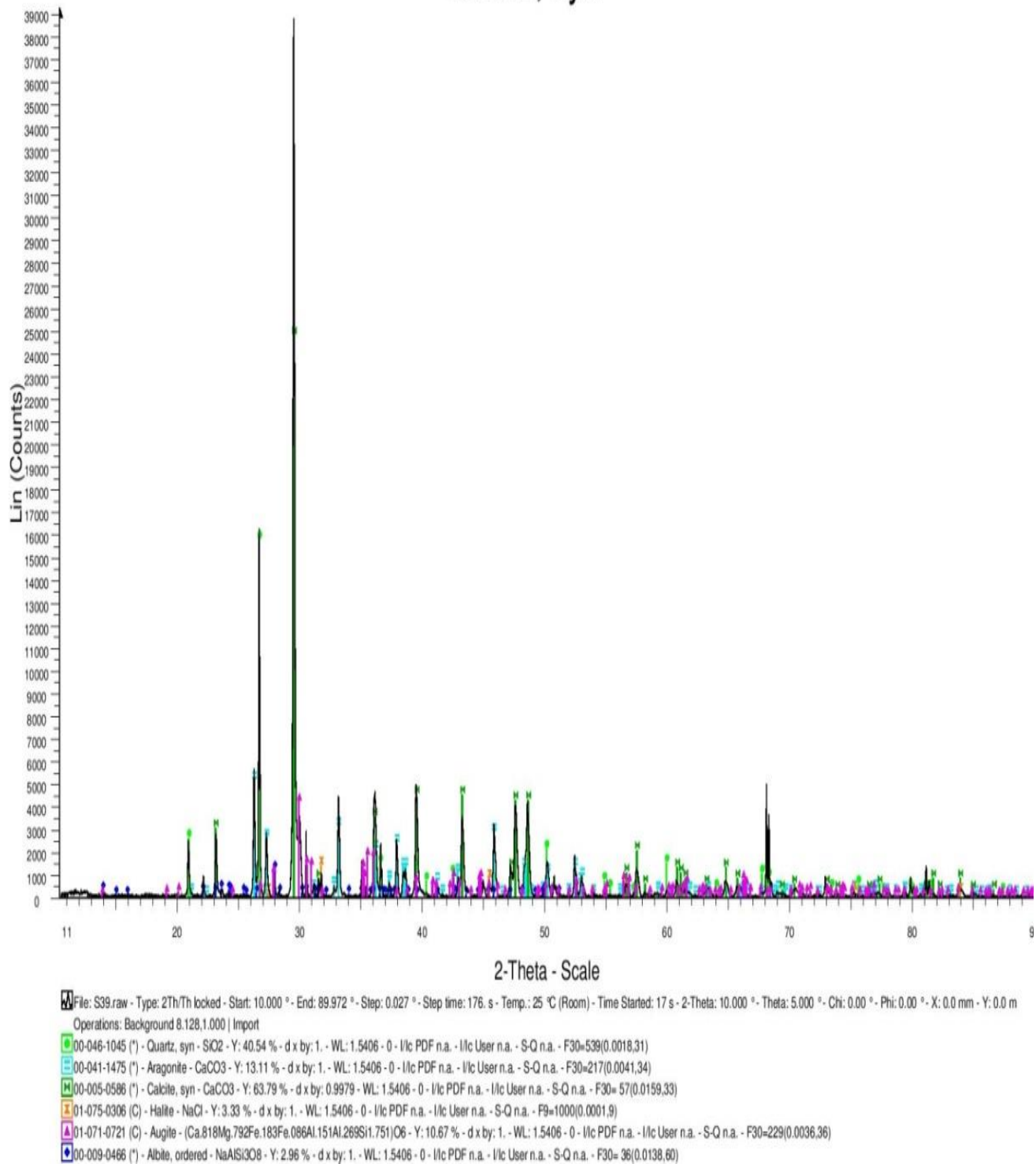
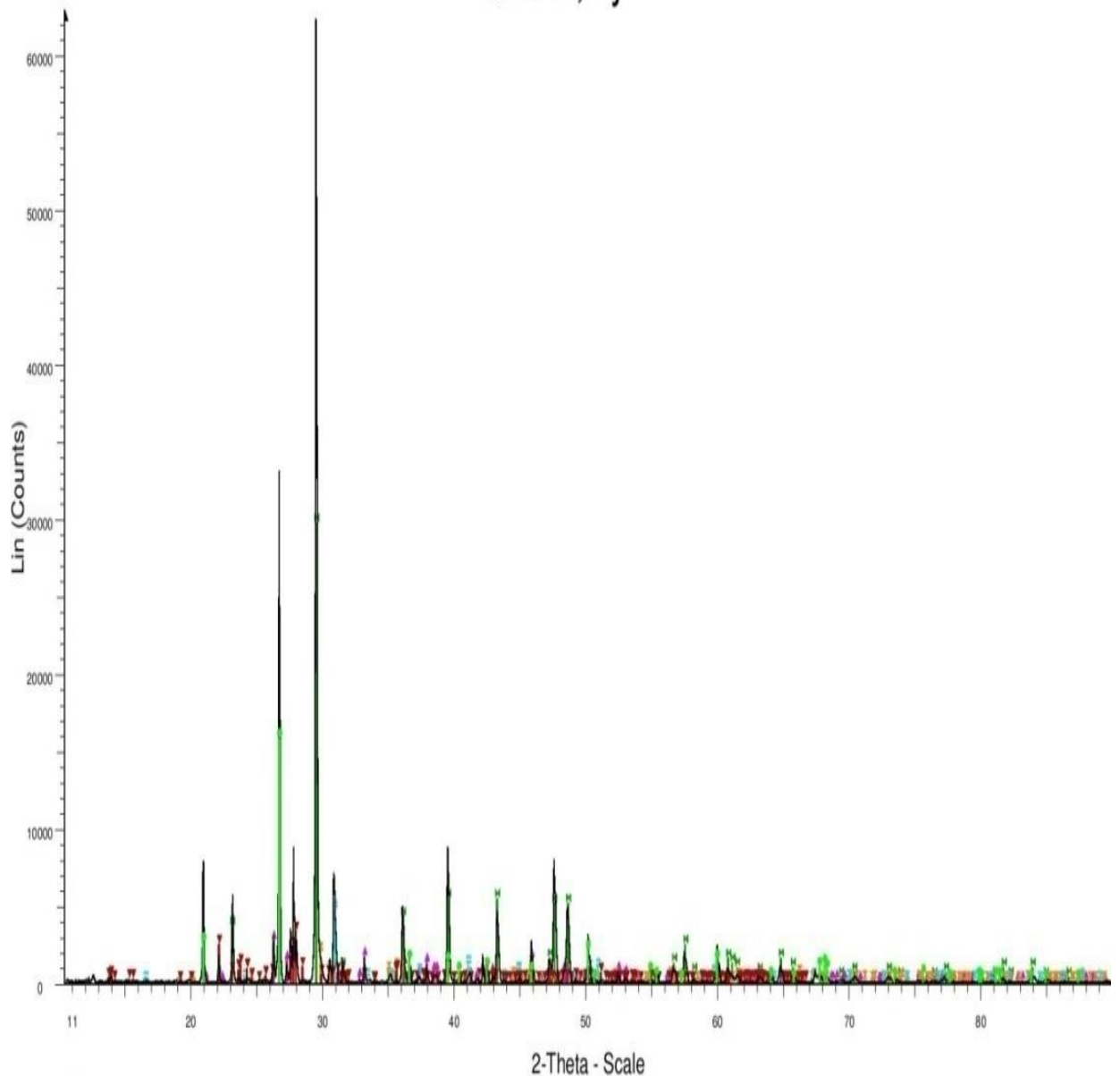


Figure B.8. X-Ray Diffraction showing the mineralogic composition of the sample 39 from study area.

Quartz, syn

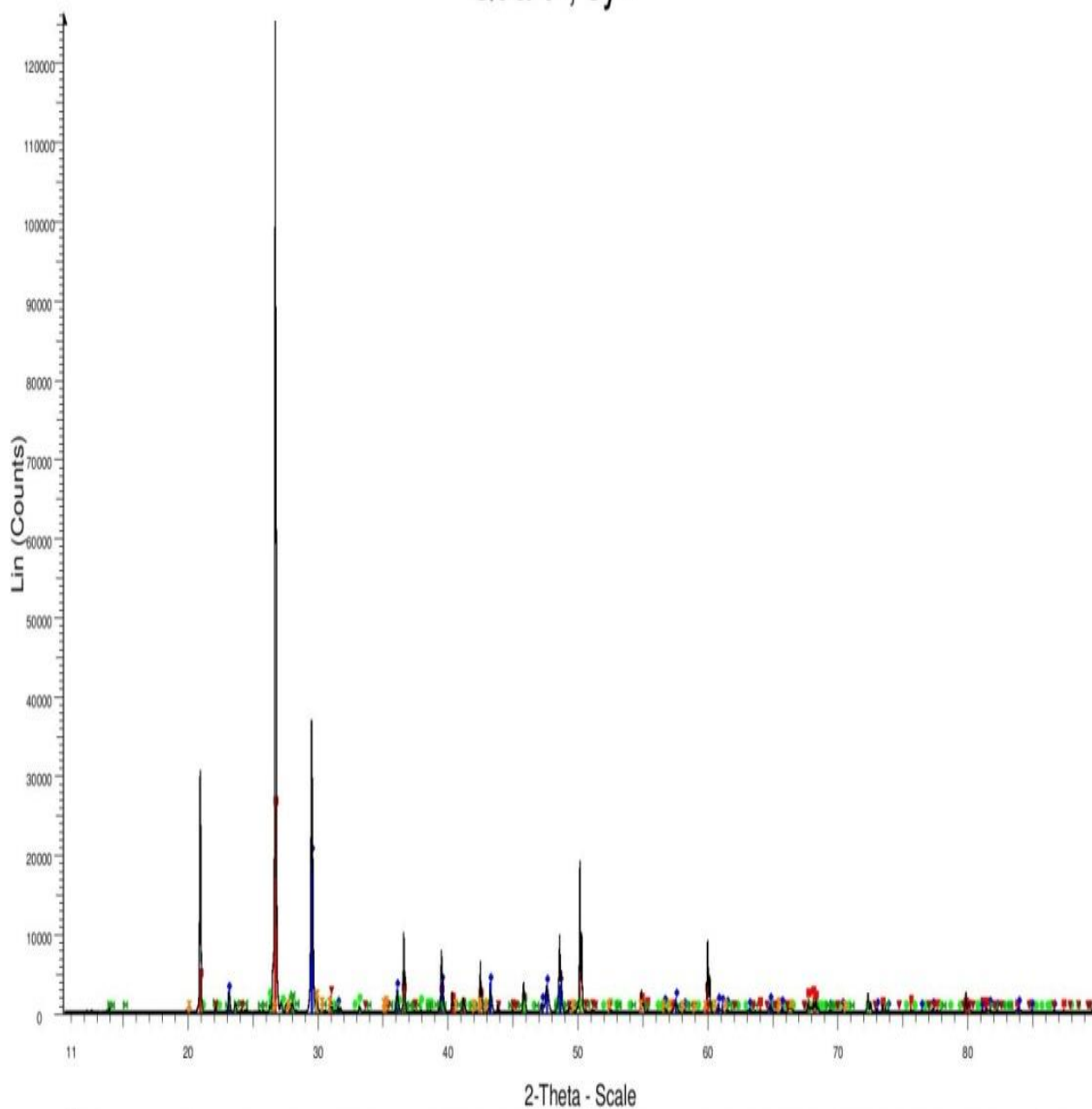


File: S46.raw - Type: 2Th/Th locked - Start: 10.000 ° - End: 89.972 ° - Step: 0.027 ° - Step time: 176. s - Temp.: 25 °C (Room) - Time Started: 8 s - 2-Theta: 10.000 ° - Theta: 5.000 ° - Chi: 0.00 ° - Phi: 0.00 ° - X: 0.0 mm - Y: 0.0 mm
Operations: Background 10.000,1.000 | Import

- 00-046-1045 (*) - Quartz, syn - SiO2 - Y: 25.22 % - d x by: 1. - WL: 1.5406 - 0 - I/Ic PDF n.a. - I/Ic User n.a. - S-Q n.a. - F30=539(0.0018,31)
- 00-041-1475 (*) - Aragonite - CaCO3 - Y: 4.29 % - d x by: 1. - WL: 1.5406 - 0 - I/Ic PDF n.a. - I/Ic User n.a. - S-Q n.a. - F30=217(0.0041,34)
- 00-005-0586 (*) - Calcite, syn - CaCO3 - Y: 47.61 % - d x by: 0.9979 - WL: 1.5406 - 0 - I/Ic PDF n.a. - I/Ic User n.a. - S-Q n.a. - F30= 57(0.0159,33)
- 01-076-0544 (C) - Augite - Ca0.61Mg0.78Fe0.49(SiO3)2 - Y: 3.06 % - d x by: 1. - WL: 1.5406 - 0 - I/Ic PDF n.a. - I/Ic User n.a. - S-Q n.a. - F30=471(0.0020,32)
- 01-074-1687 (C) - Dolomite - CaMg(CO3)2 - Y: 7.43 % - d x by: 1. - WL: 1.5406 - 0 - I/Ic PDF n.a. - I/Ic User n.a. - S-Q n.a. - F30=160(0.0054,35)
- 01-083-1658 (C) - Albite high (K-bearing) - from Rabb Canyon Pegmatite, Grant - (K0.22Na0.78)(AlSi3O8) - Y: 5.20 % - d x by: 0.998 - WL: 1.5406 - 0 - I/Ic PDF n.a. - I/Ic User n.a. - S-Q n.a. - F30=197(0.0044,35)

Figure B.9. X-Ray Diffraction showing the mineralogical composition of the sample 46 from study area.

Quartz, syn



File: S50.raw - Type: 2Th/Th locked - Start: 10.000 ° - End: 89.972 ° - Step: 0.027 ° - Step time: 176. s - Temp.: 25 °C (Room) - Time Started: 17 s - 2-Theta: 10.000 ° - Theta: 5.000 ° - Chi: 0.00 ° - Phi: 0.00 ° - X: 0.0 mm - Y: 0.0 m
Operations: Background 10.000,1.000 | Import

- 00-046-1045 (*) - Quartz, syn - SiO₂ - Y: 20.68 % - d x by: 1. - WL: 1.5406 - 0 - I/Ic PDF n.a. - I/Ic User n.a. - S-Q n.a. - F30=539(0.0018,31)
- 00-041-1475 (*) - Aragonite - CaCO₃ - Y: 1.29 % - d x by: 1. - WL: 1.5406 - 0 - I/Ic PDF n.a. - I/Ic User n.a. - S-Q n.a. - F30=217(0.0041,34)
- 00-005-0586 (*) - Calcite, syn - CaCO₃ - Y: 15.89 % - d x by: 0.9979 - WL: 1.5406 - 0 - I/Ic PDF n.a. - I/Ic User n.a. - S-Q n.a. - F30= 57(0.0159,33)
- 00-041-1480 (I) - Albite, calcian, ordered - (Na,Ca)Al(Si,Al)3O₈ - Y: 1.09 % - d x by: 1.0021 - WL: 1.5406 - 0 - I/Ic PDF n.a. - I/Ic User n.a. - S-Q n.a. - F30= 11(0.0450,60)
- 00-036-0426 (*) - Dolomite - CaMg(CO₃)₂ - Y: 1.51 % - d x by: 1. - WL: 1.5406 - 0 - I/Ic PDF n.a. - I/Ic User n.a. - S-Q n.a. - F30=148(0.0063,32)
- 00-024-0202 (D) - Augite, aluminian - Ca(Mg,Al,Fe)Si₂O₆ - Y: 1.19 % - d x by: 1. - WL: 1.5406 - 0 - I/Ic PDF n.a. - I/Ic User n.a. - S-Q n.a. - F26= 4(0.0390,191)

Figure B.10. X-Ray Diffraction showing the mineralogical composition of the sample 50 from study area.

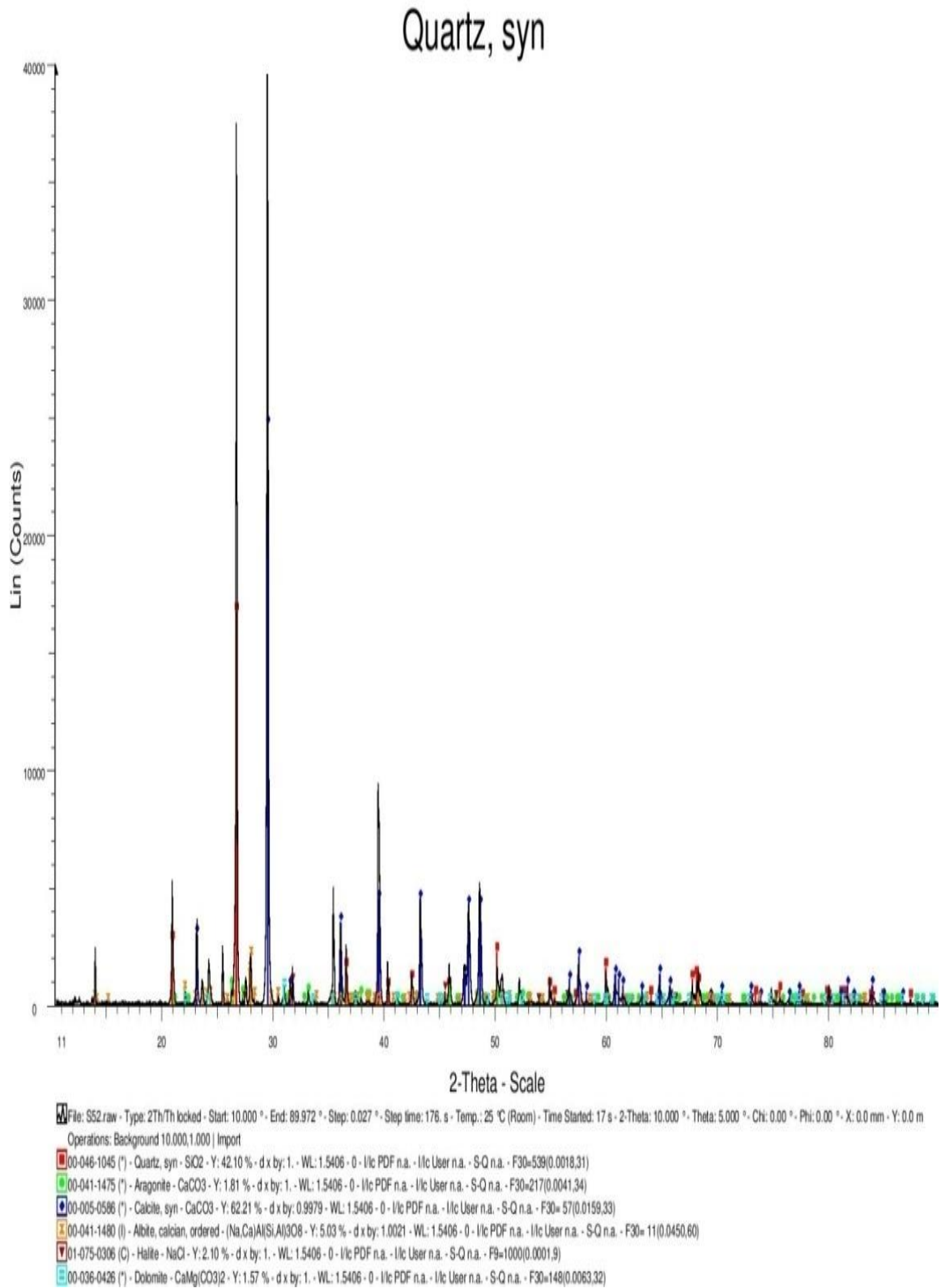


Figure B.11. X-Ray Diffraction showing the mineralogical composition of the sample 52 from study area.

Quartz, syn

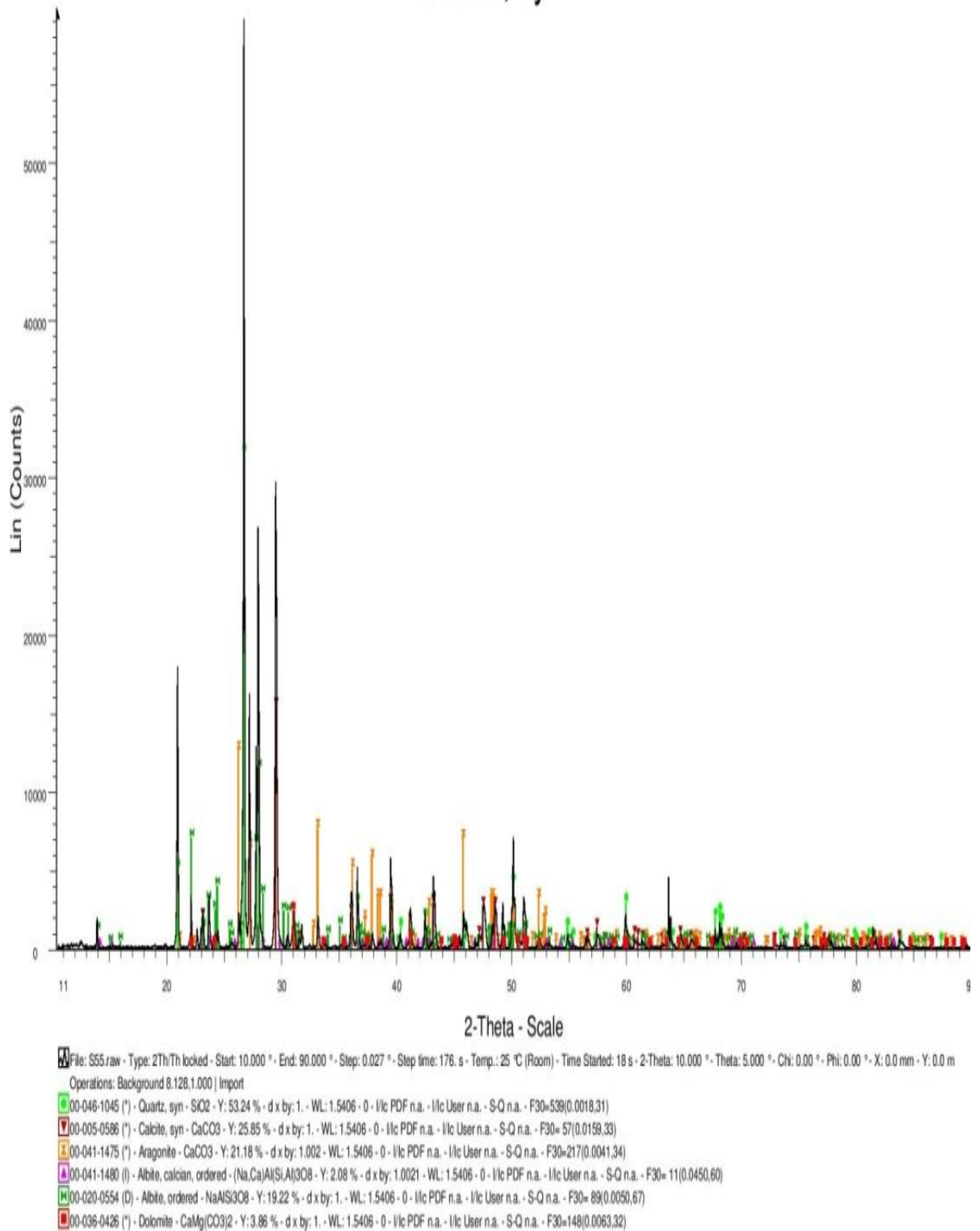
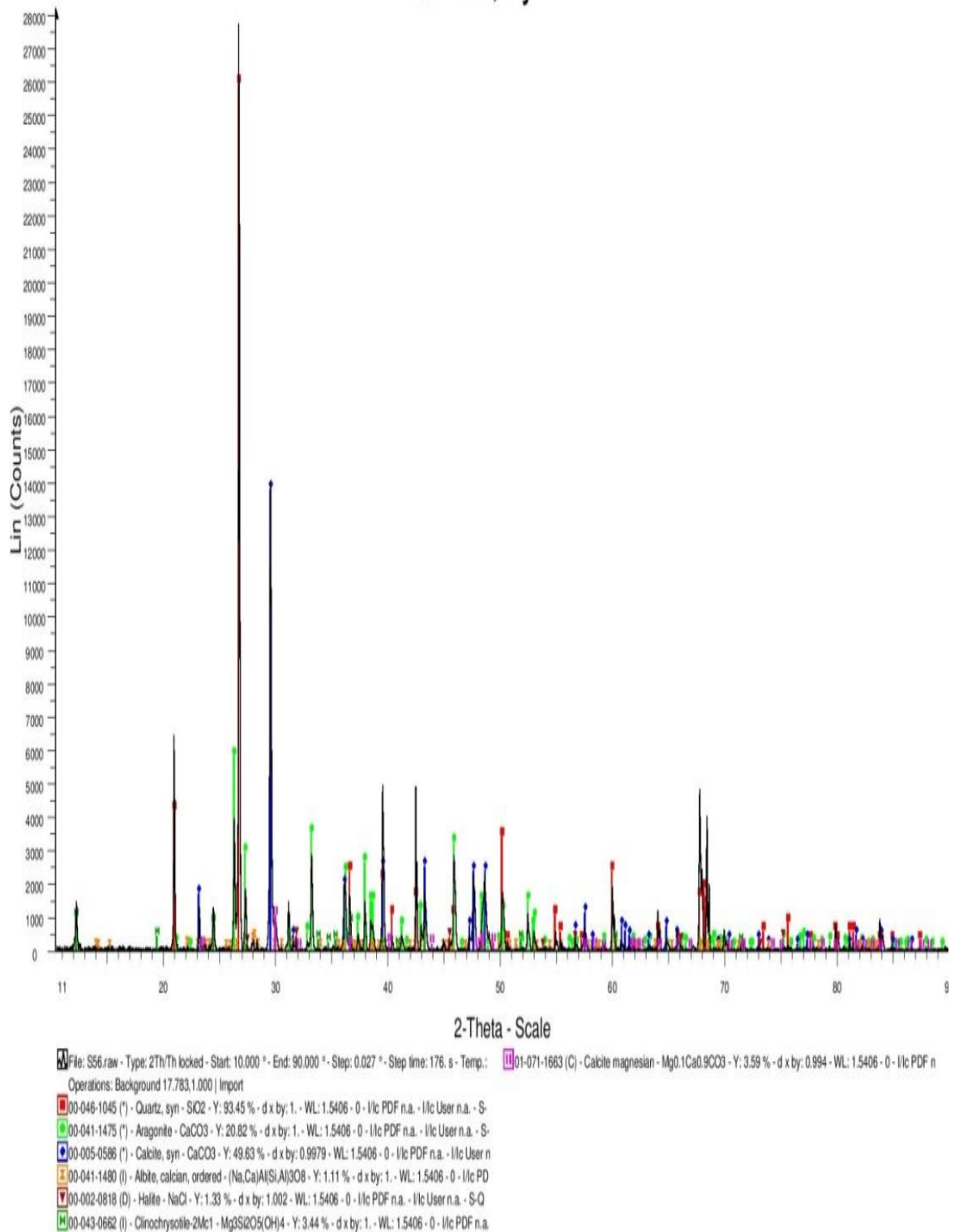


Figure B.12. X-Ray Diffraction showing the mineralogical composition of the sample 55 from study area.

Quartz, syn



Quartz, syn

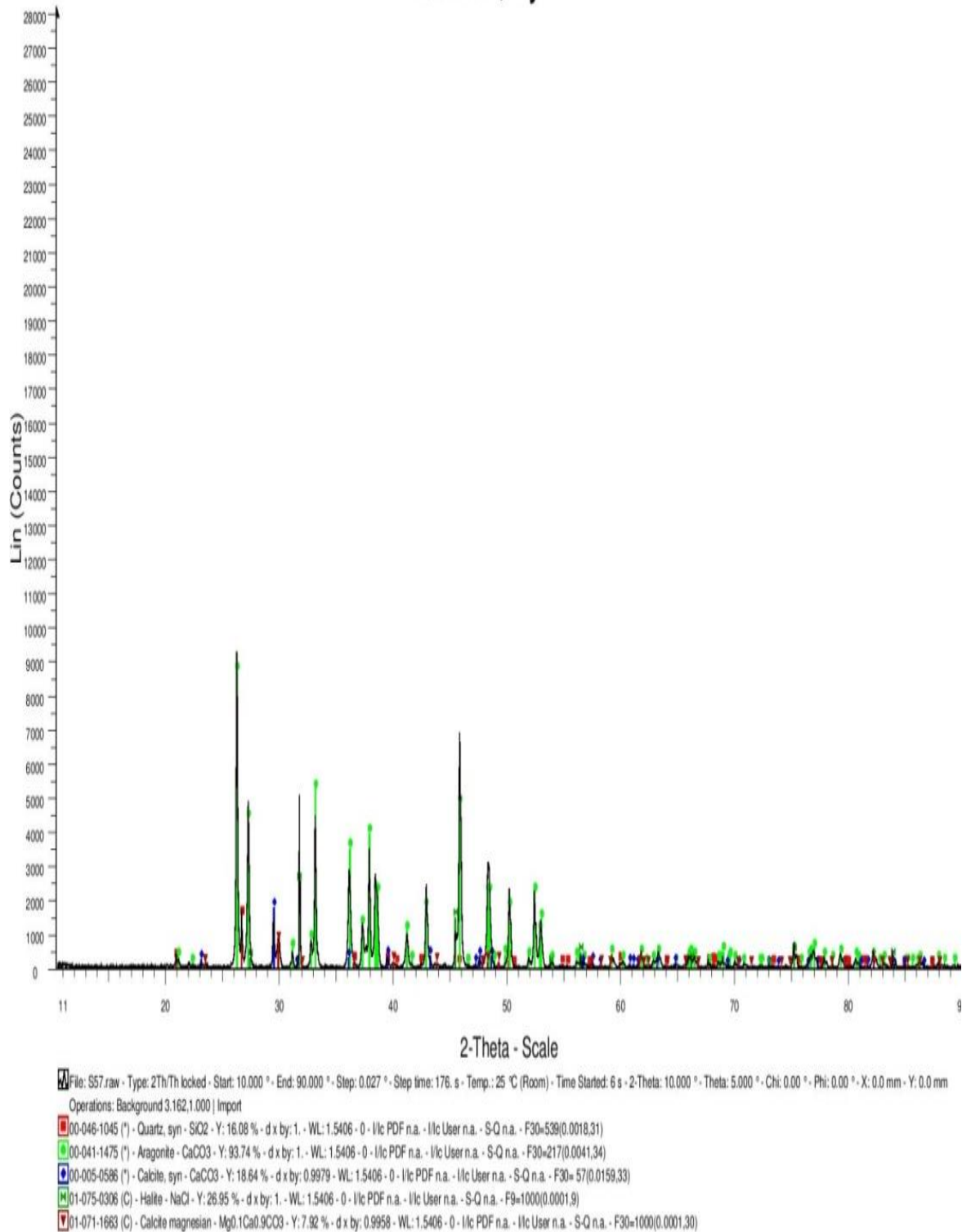


Figure B.14. X-Ray Diffraction showing the mineralogical composition of the sample 57 from study area.

Quartz, syn

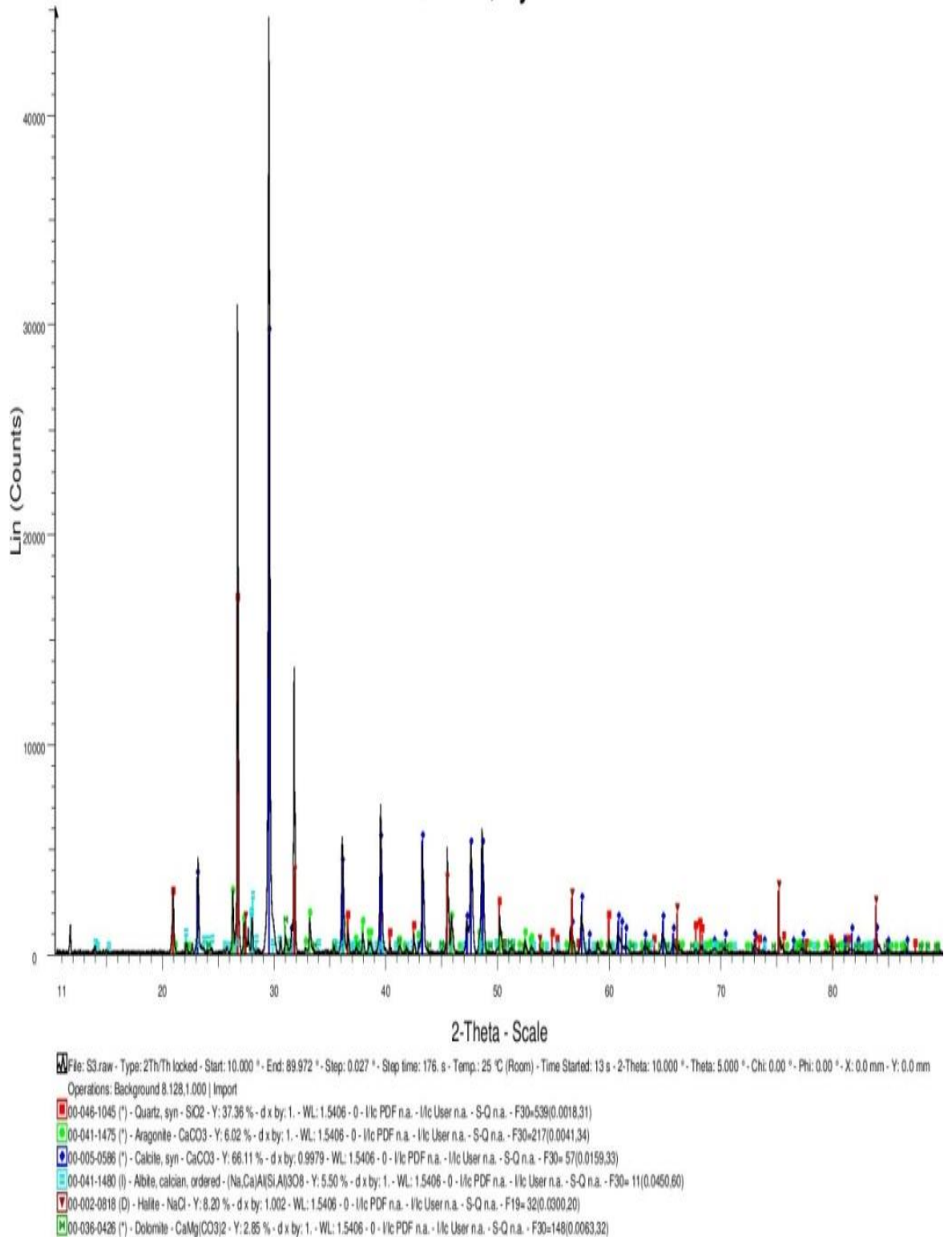


Figure B.15. X-Ray Diffraction showing the mineralogical composition of the sample 3 from study area.

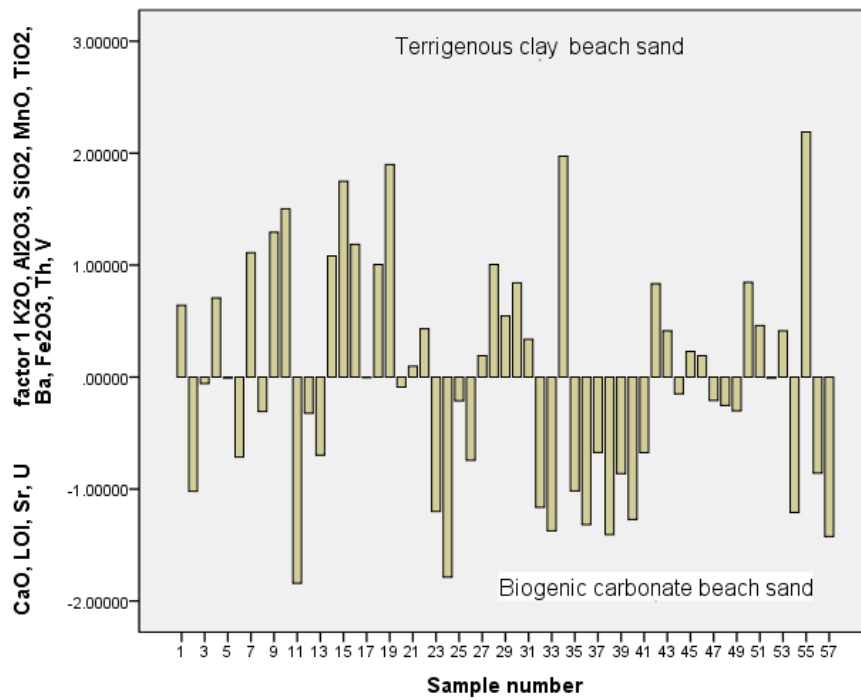


Figure B.16. Factor 1 (FAC1_1) map of beach samples in study area.

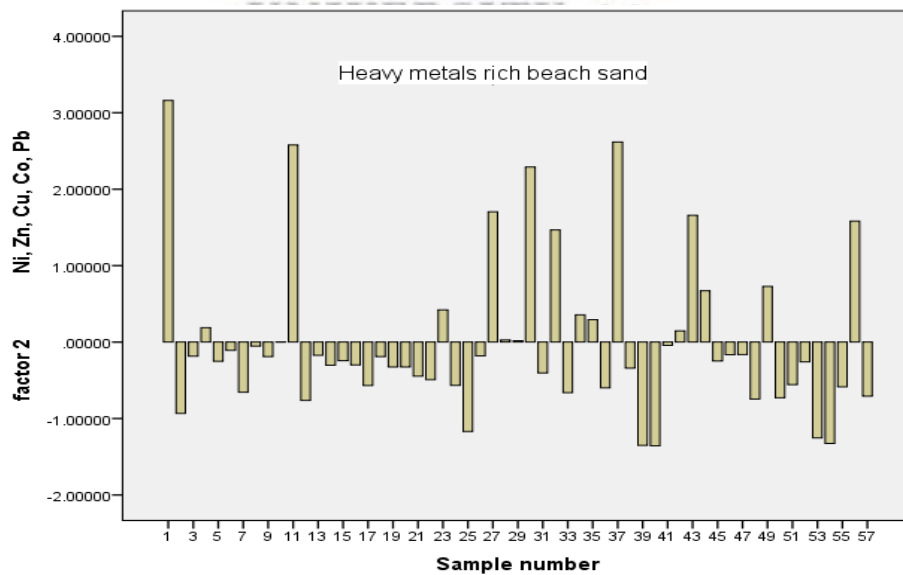


Figure B.17. Factor (FAC2_1) map of beach samples in study area.

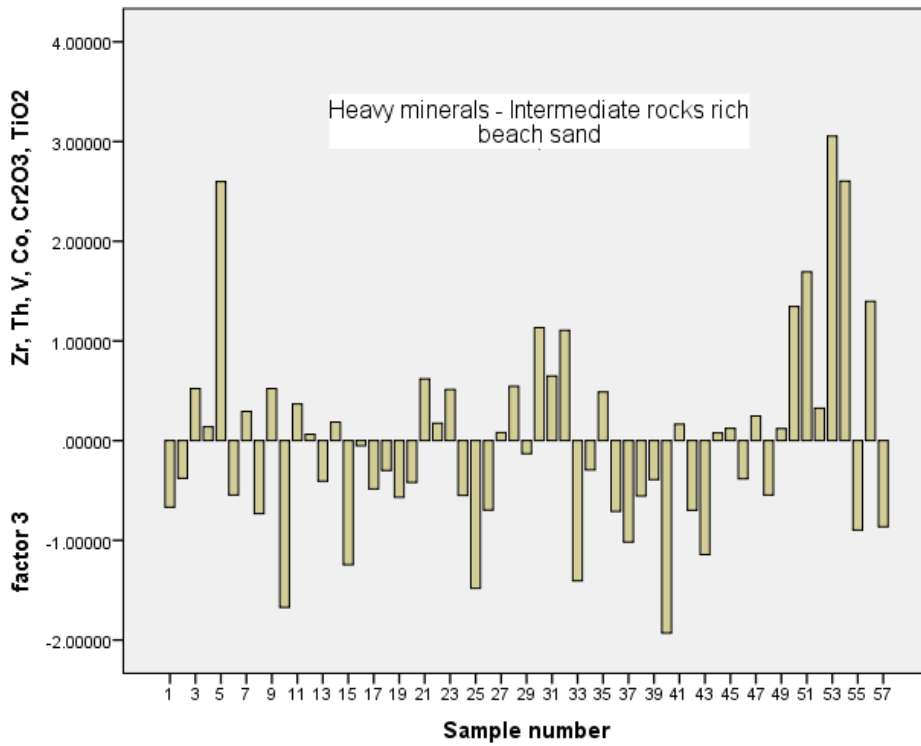


Figure B.18. Factor 3 (FAC3_1) map of beach samples in study area.

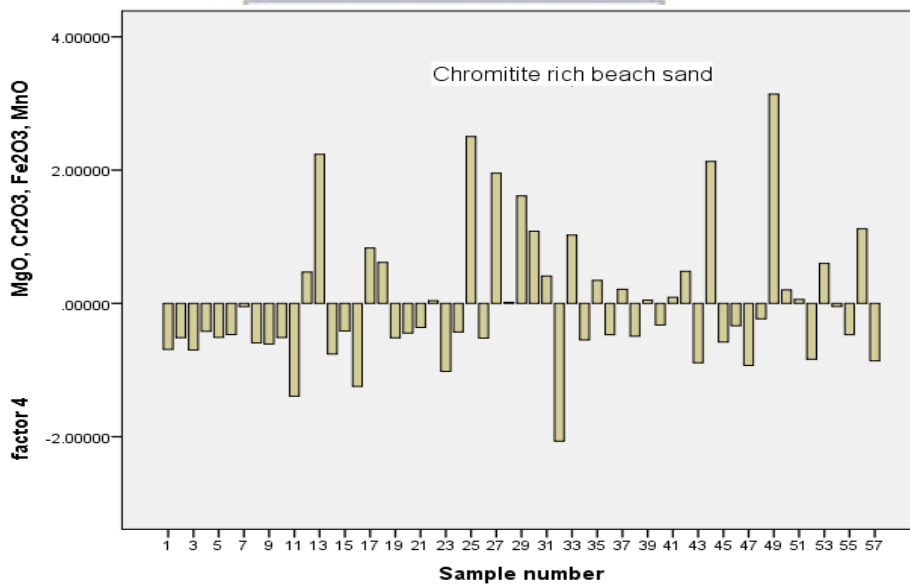
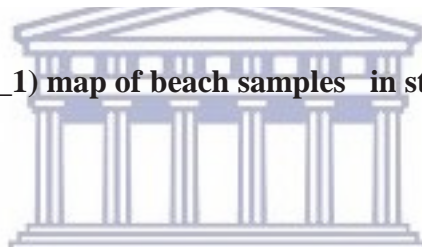


Figure B.19. Factor 4 (FAC4_1) map of beach samples in study area.

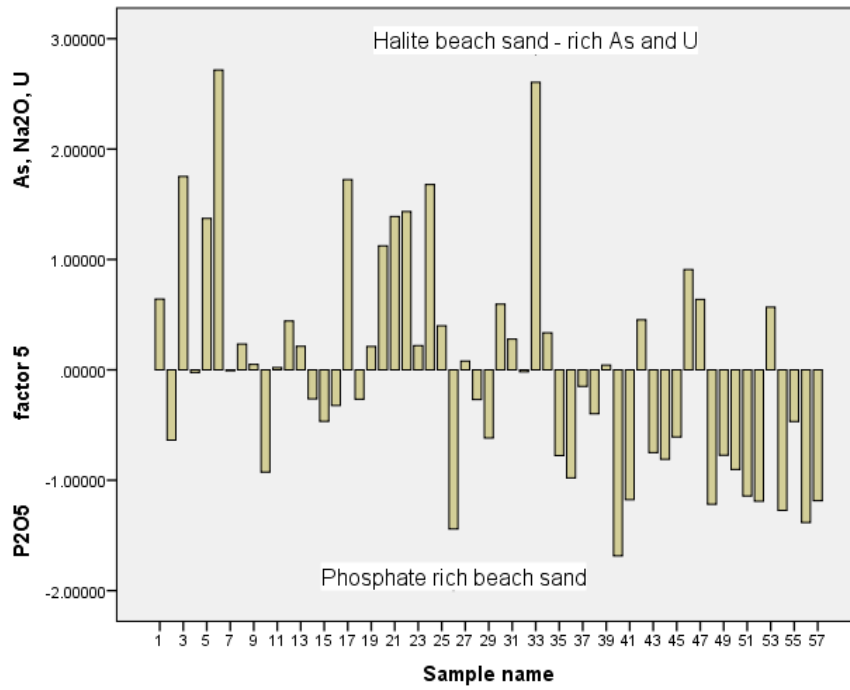
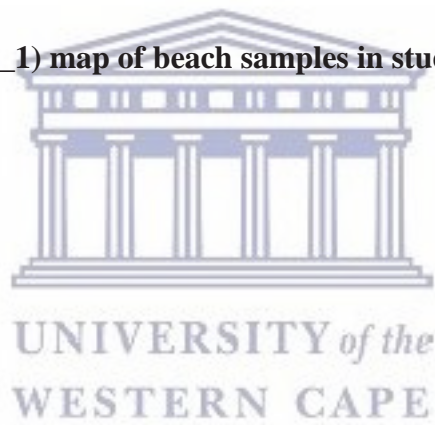


Figure B.20. Factor 5 (FAC5_1) map of beach samples in study area.



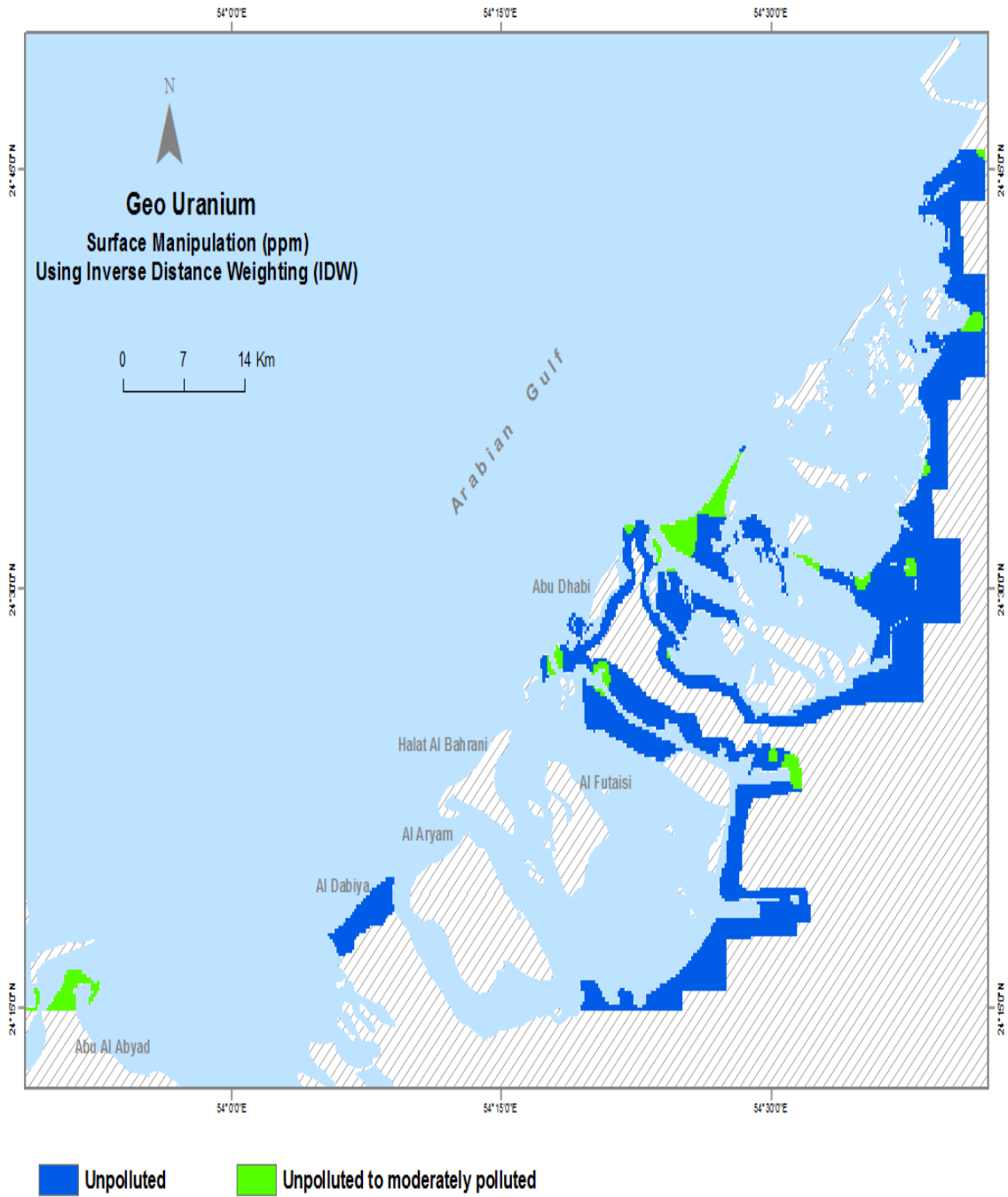


Figure B.21. GIS map of Geo-accumulation index (I_{geo}) values of Uranium in study area.

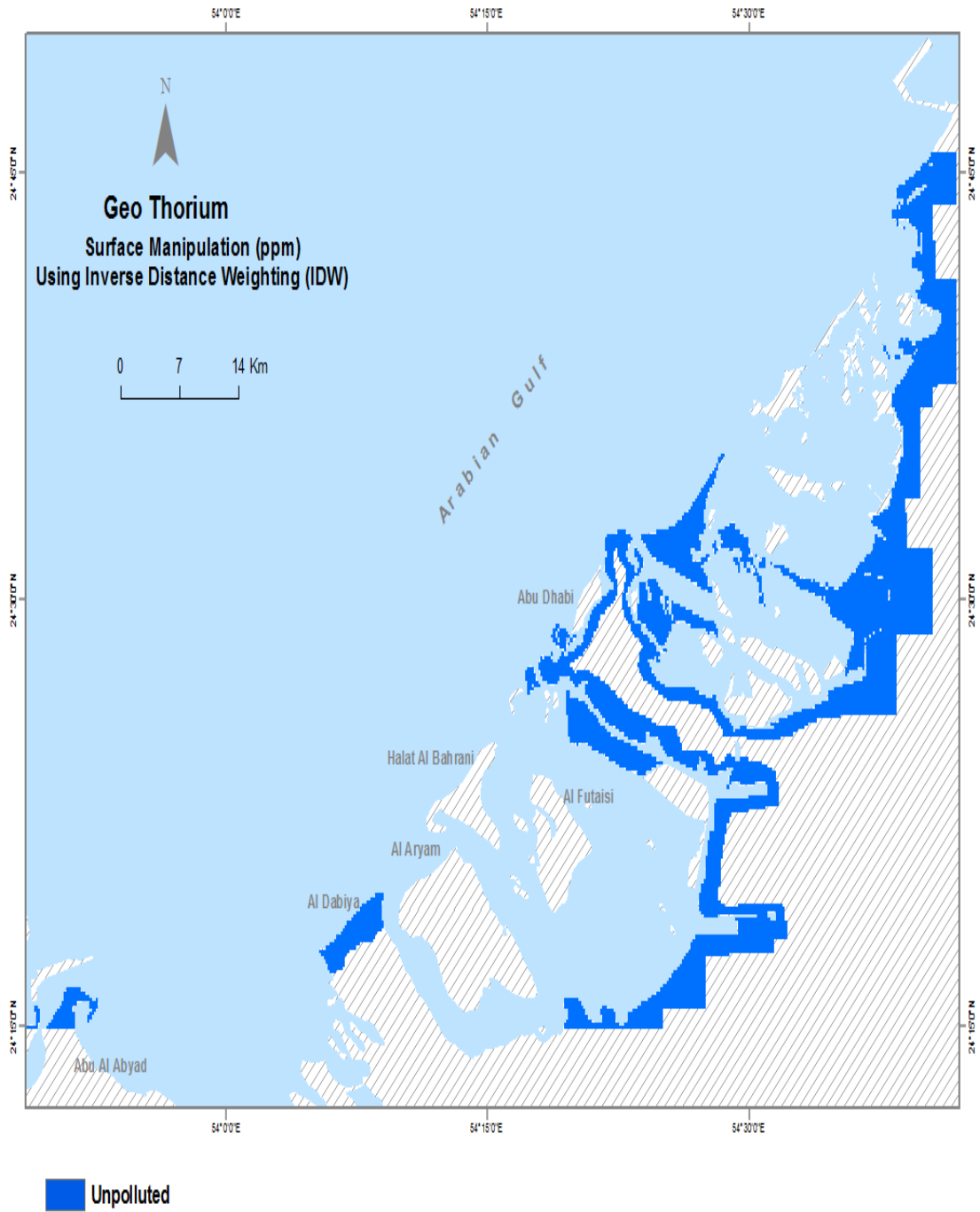
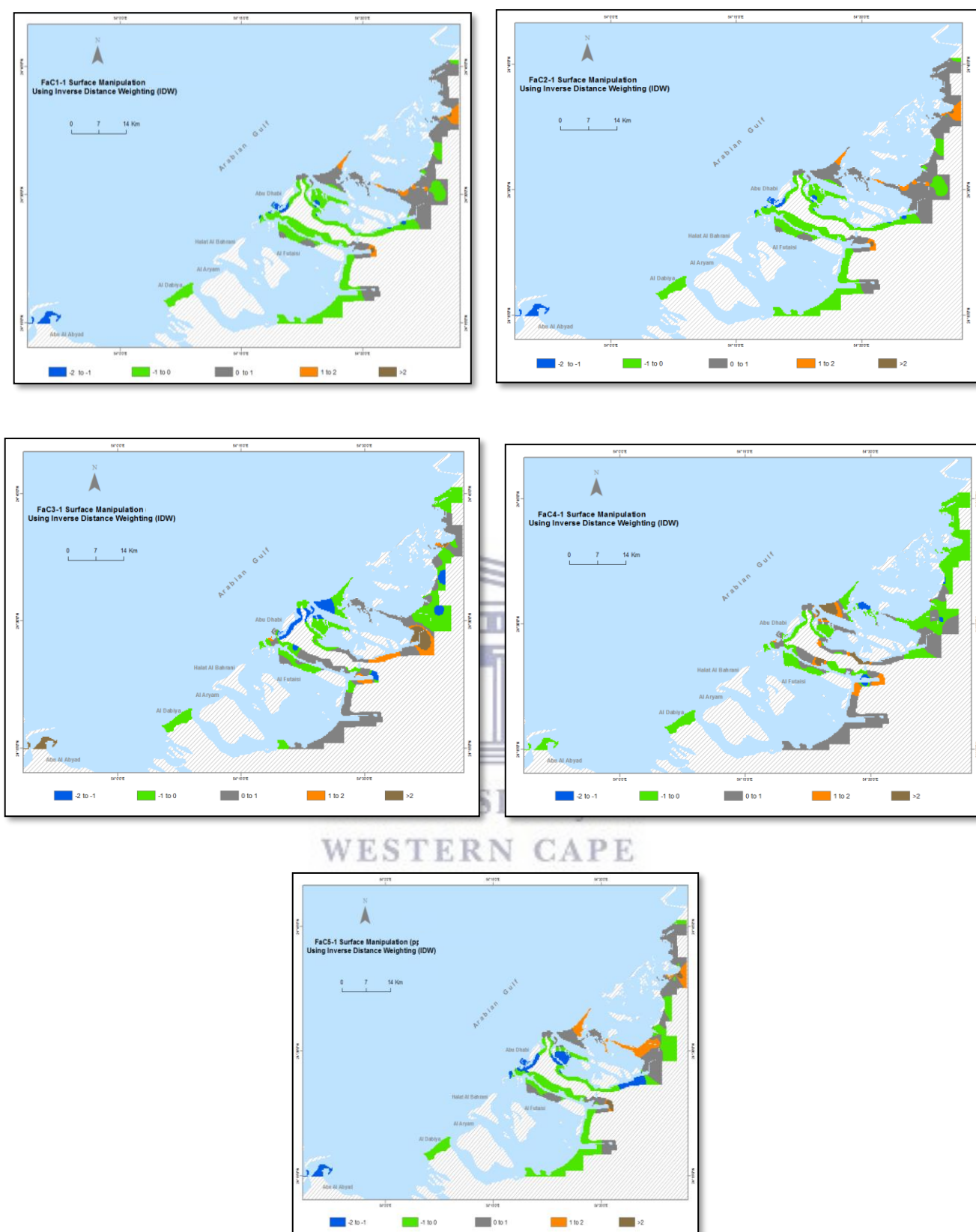


Figure B.22. GIS map of Geo-accumulation index (Igeo) values of Thorium.



WESTERN CAPE

Figure B.23. FaC1) factor 1, FaC2) Factor 2 ,FaC3) Factor 3 ,FaC4) Factor 4 and FaC5) Factor 5 distribution map of Abu Dhabi Coastal area in study area.

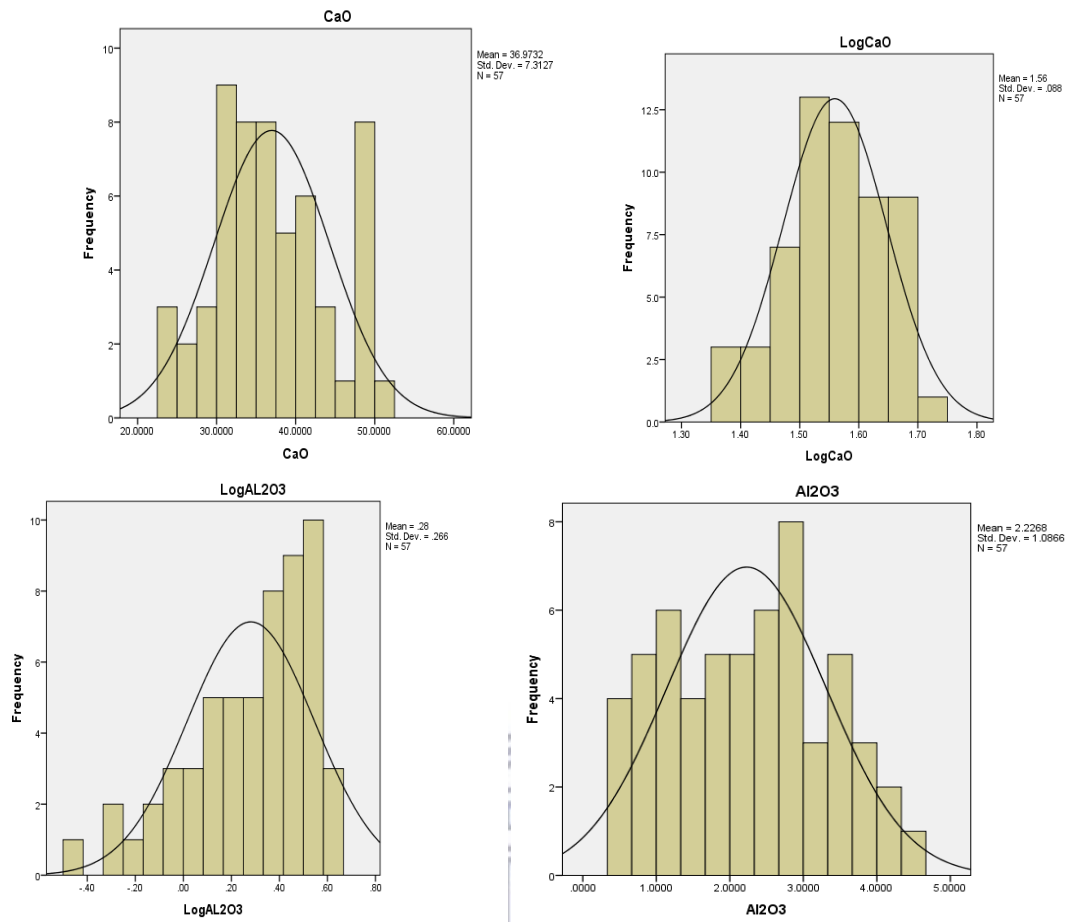
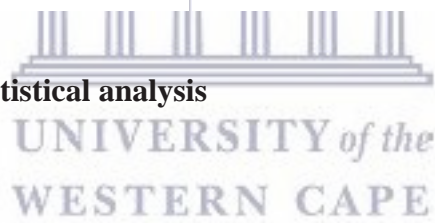


Figure B.24. multivariate statistical analysis



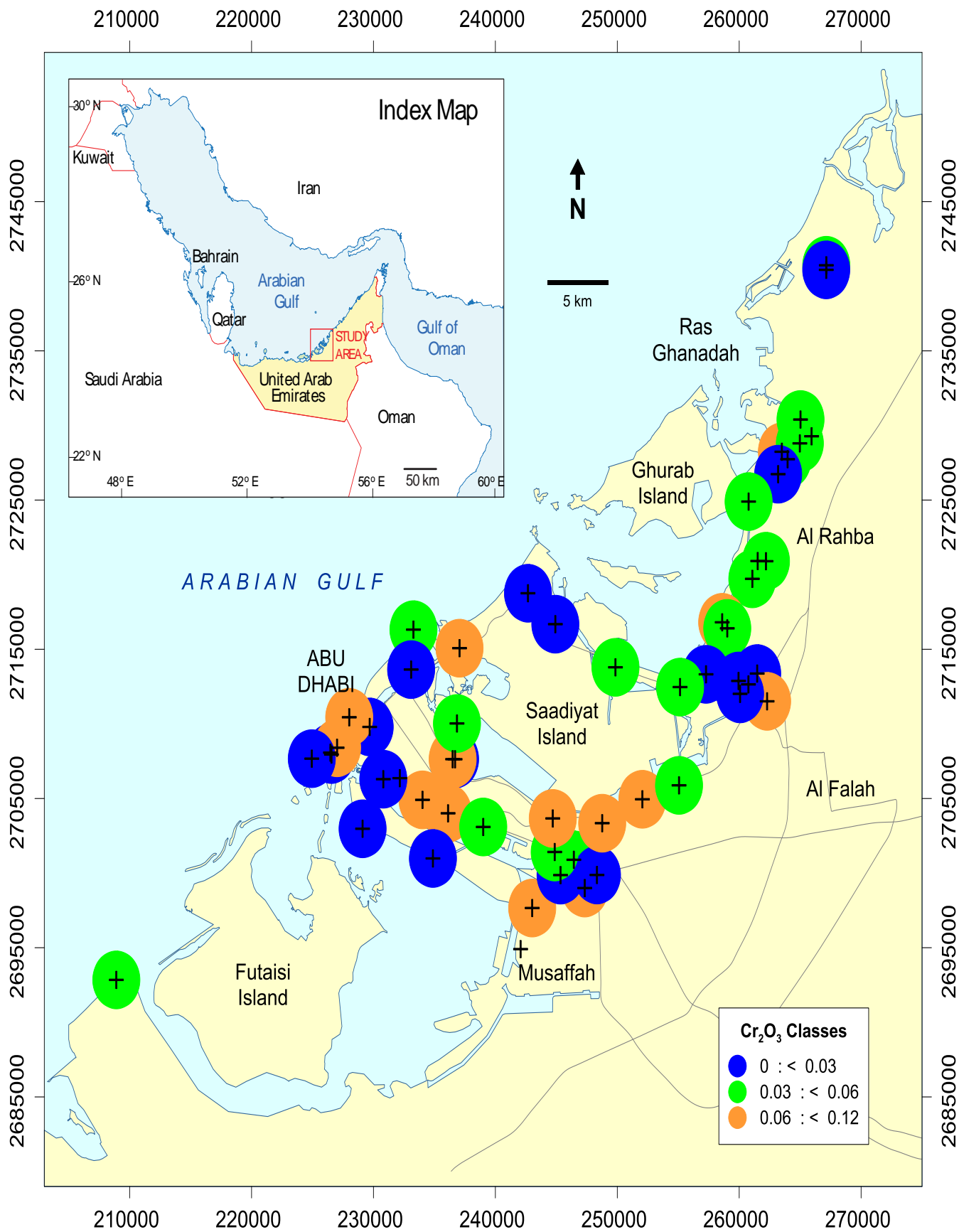


Figure B.25. Chromium oxides (Cr₂O₃) class distribution in the study area.

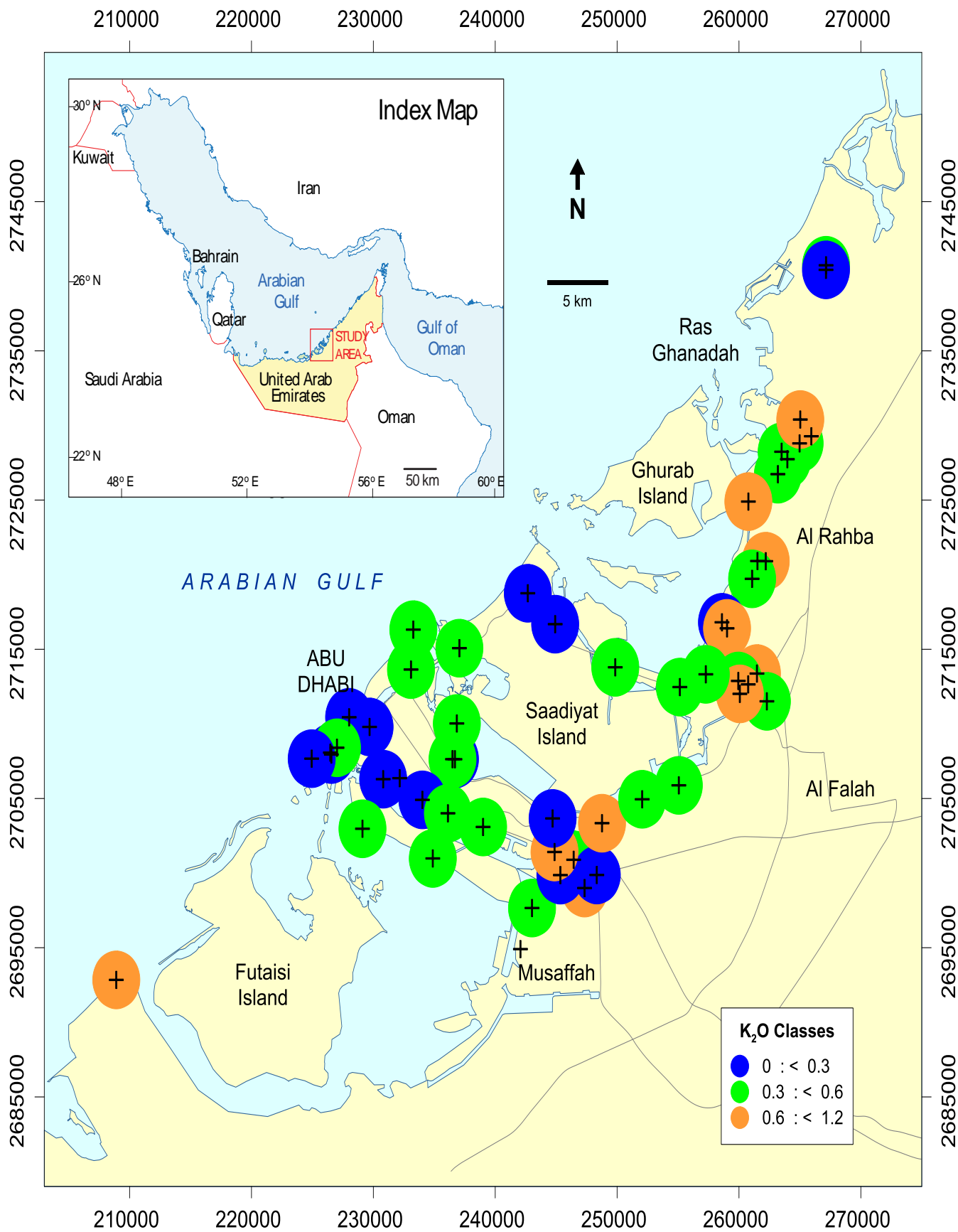


Figure B.26. Potassium oxides (K_2O) class distribution in the study area.

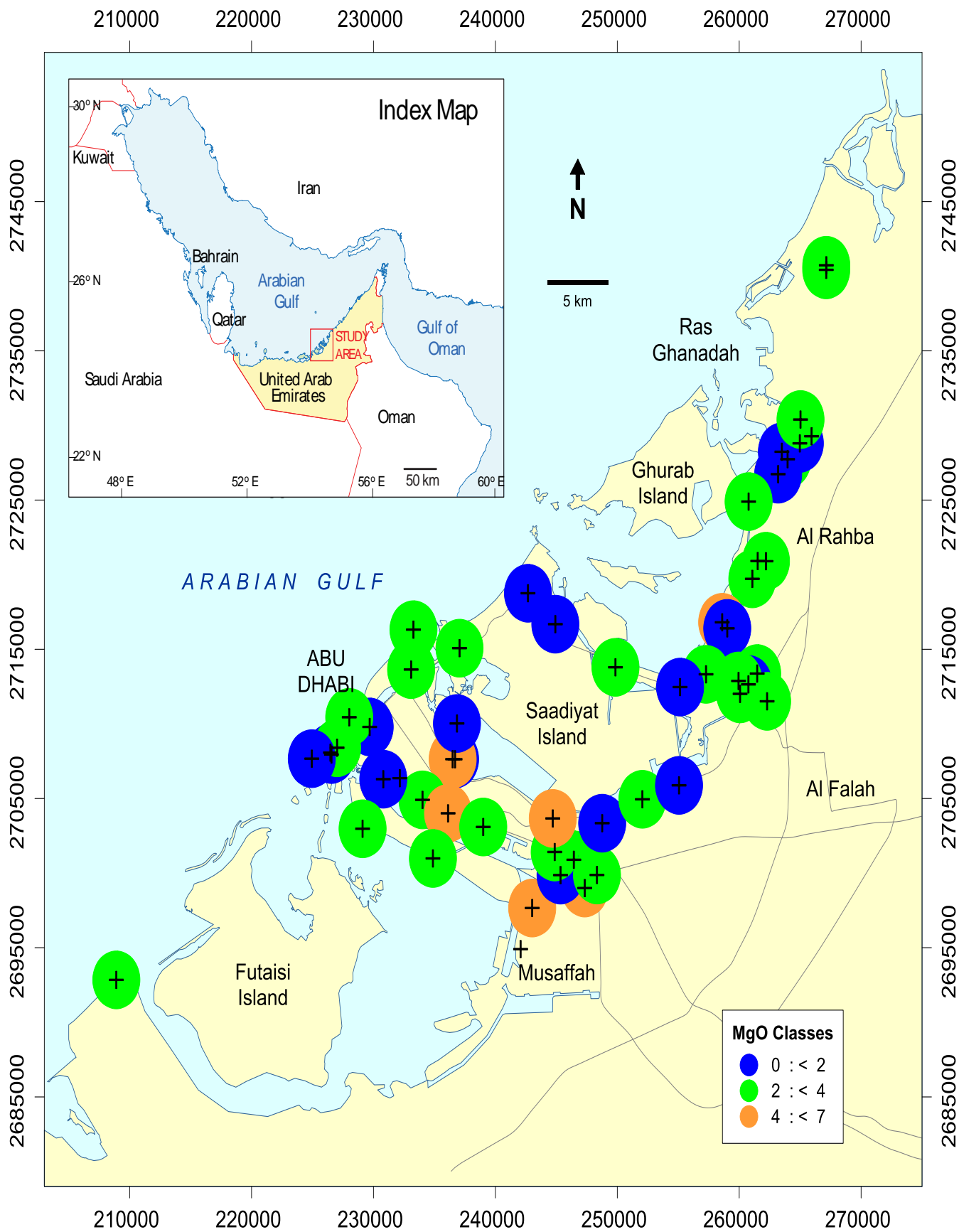


Figure B.27. Magnesium oxides (MgO) class distribution in the study area.

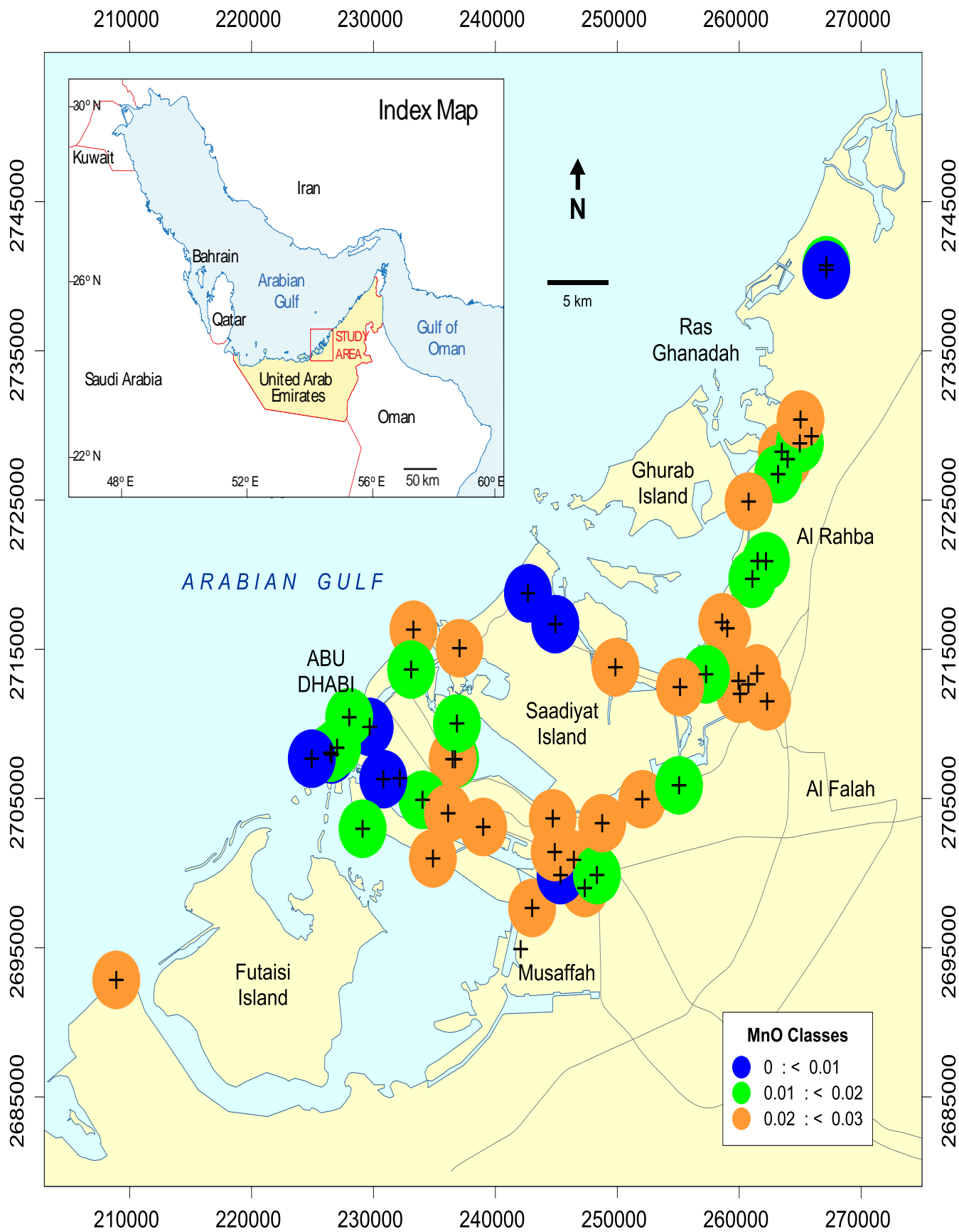


Figure B.28. Manganese oxides (MnO) class distribution in the study area.

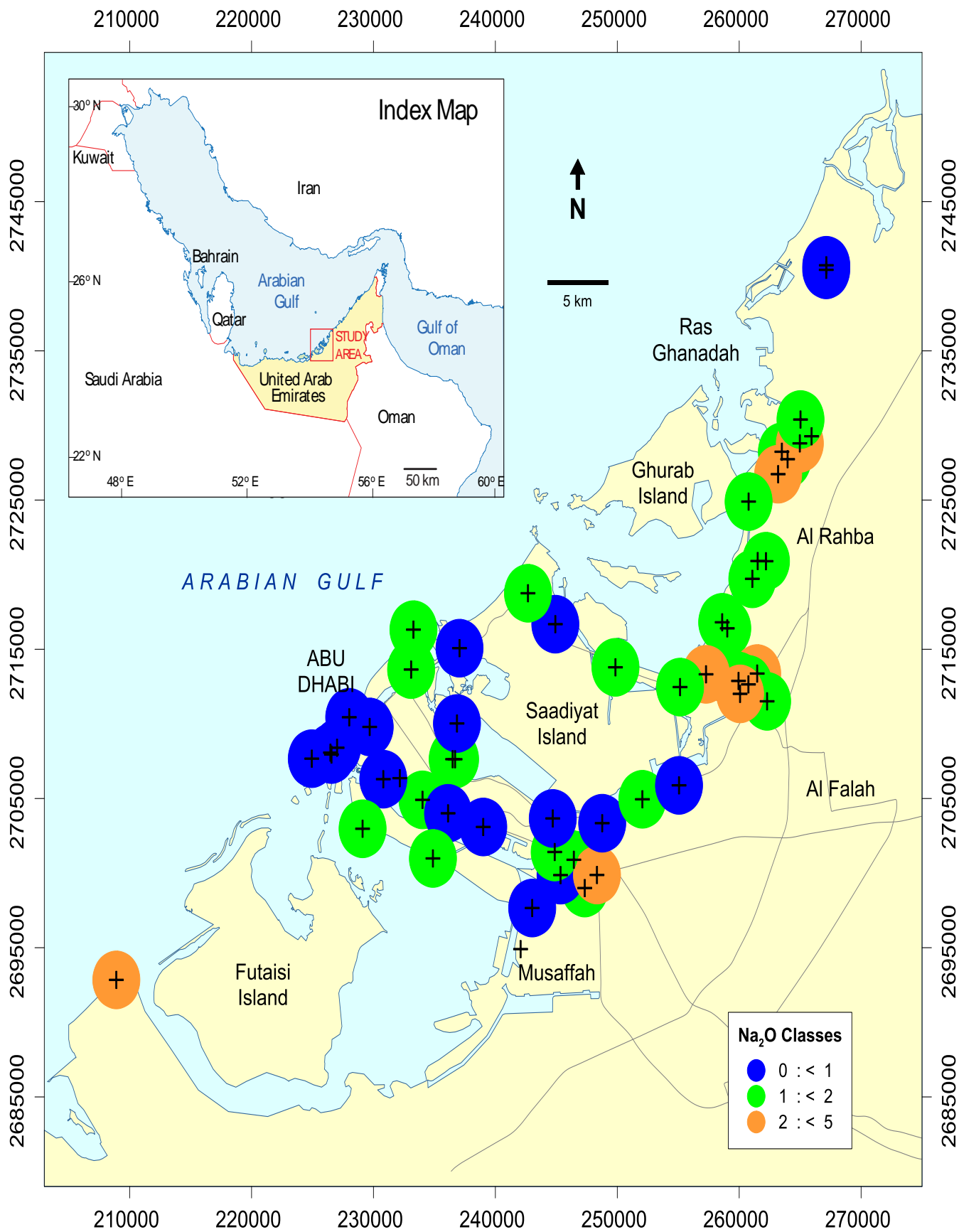


Figure B.29. Sodium oxides (Na_2O) class distribution in the study area.

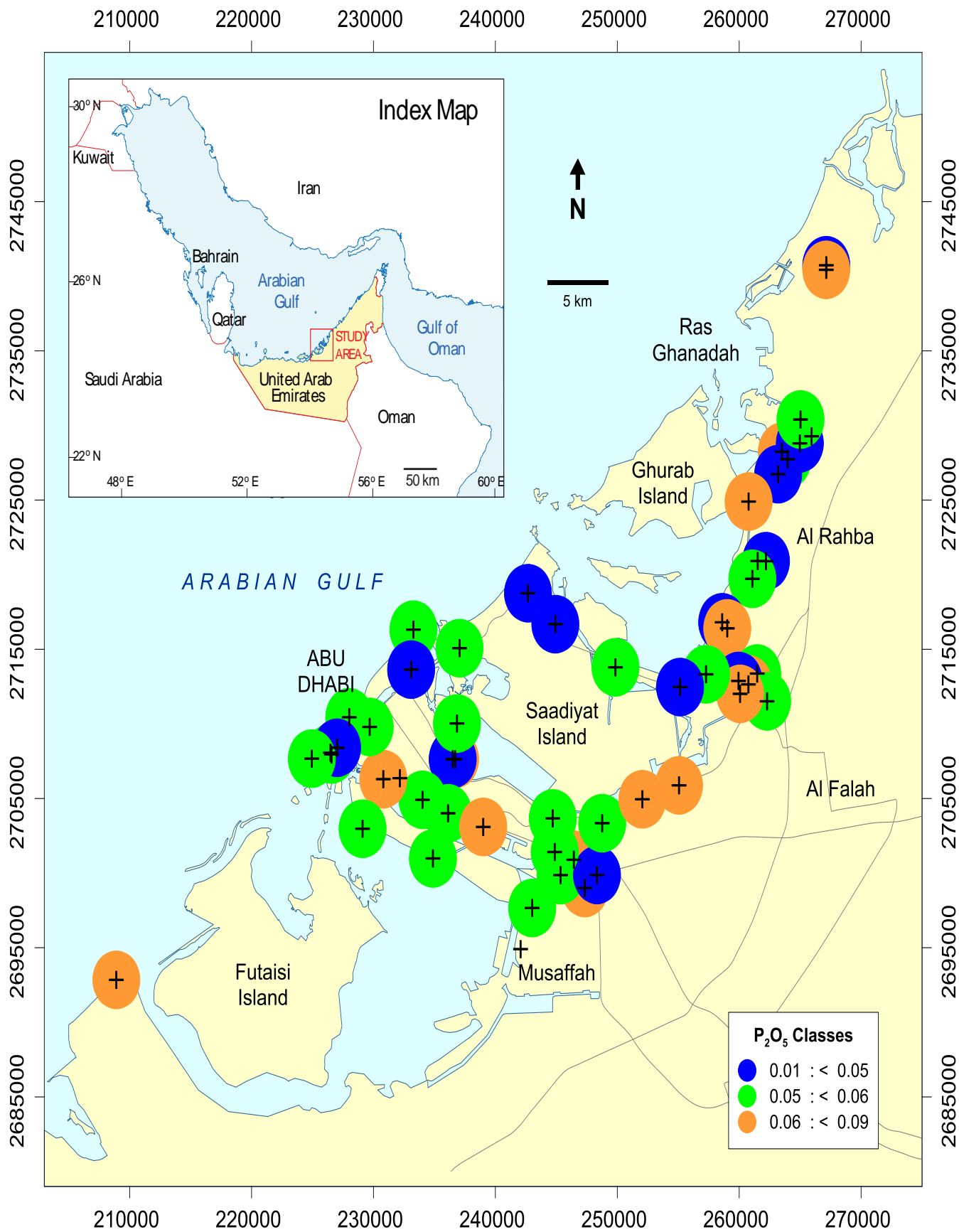


Figure B.30. Phosphorus oxides (P_2O_5) class distribution in the study area.

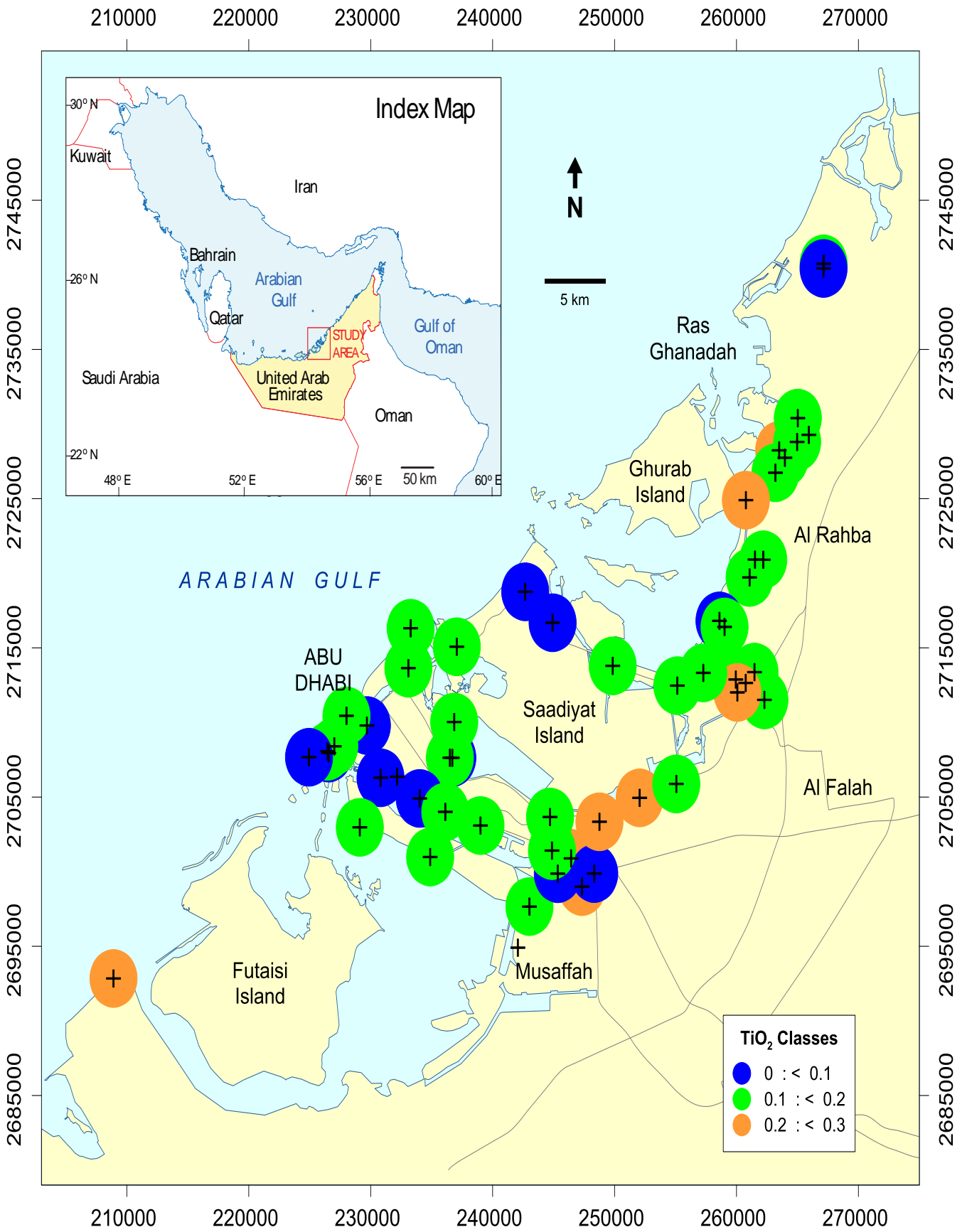


Figure B.31. Titanium oxides (TiO₂) class distribution in the study area.

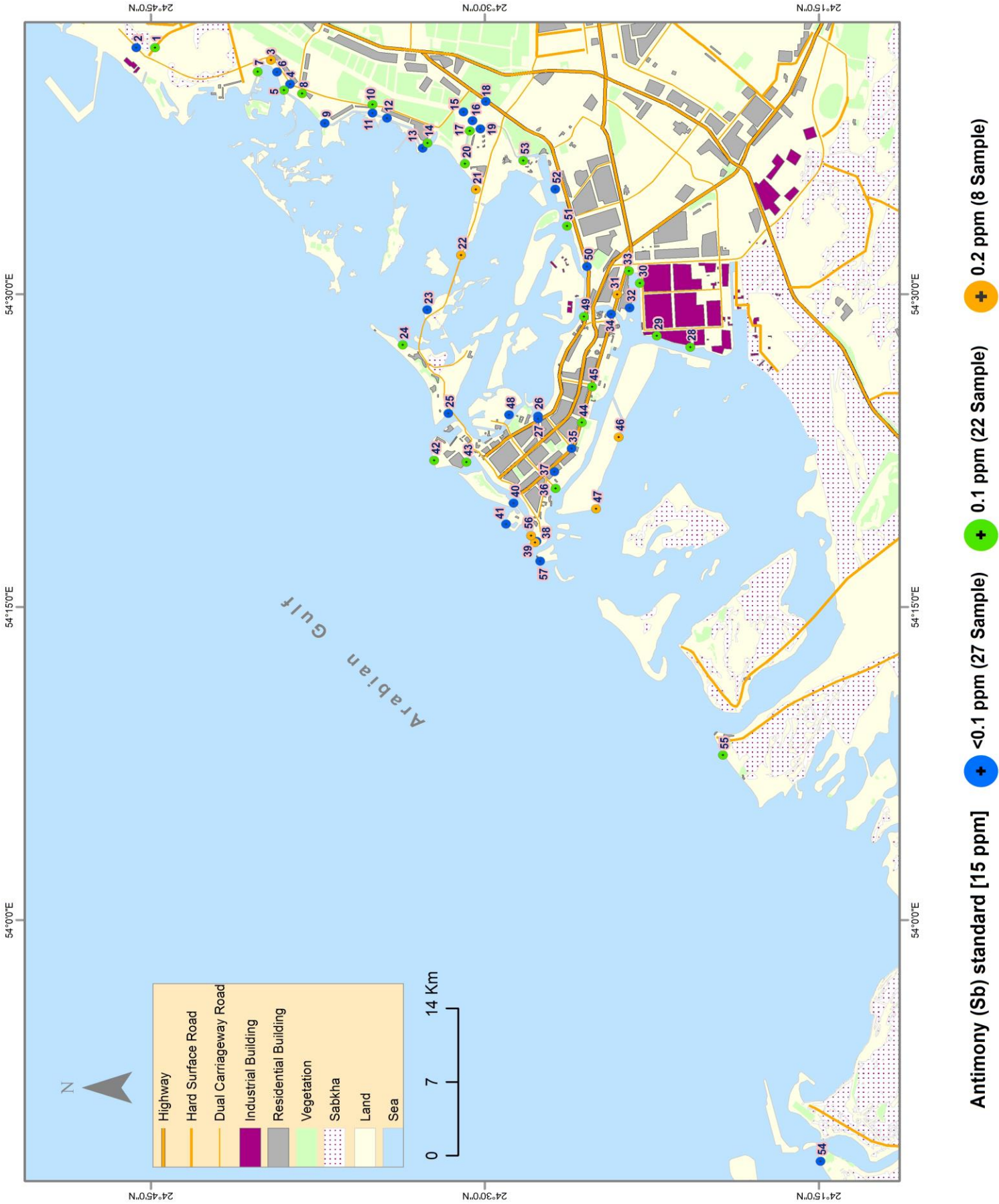


Figure B.32. Map of Abu Dhabi showing the Antimony (Sb) concentration of the areas from which the samples were collected, as indicated with dots, along with their numbers.

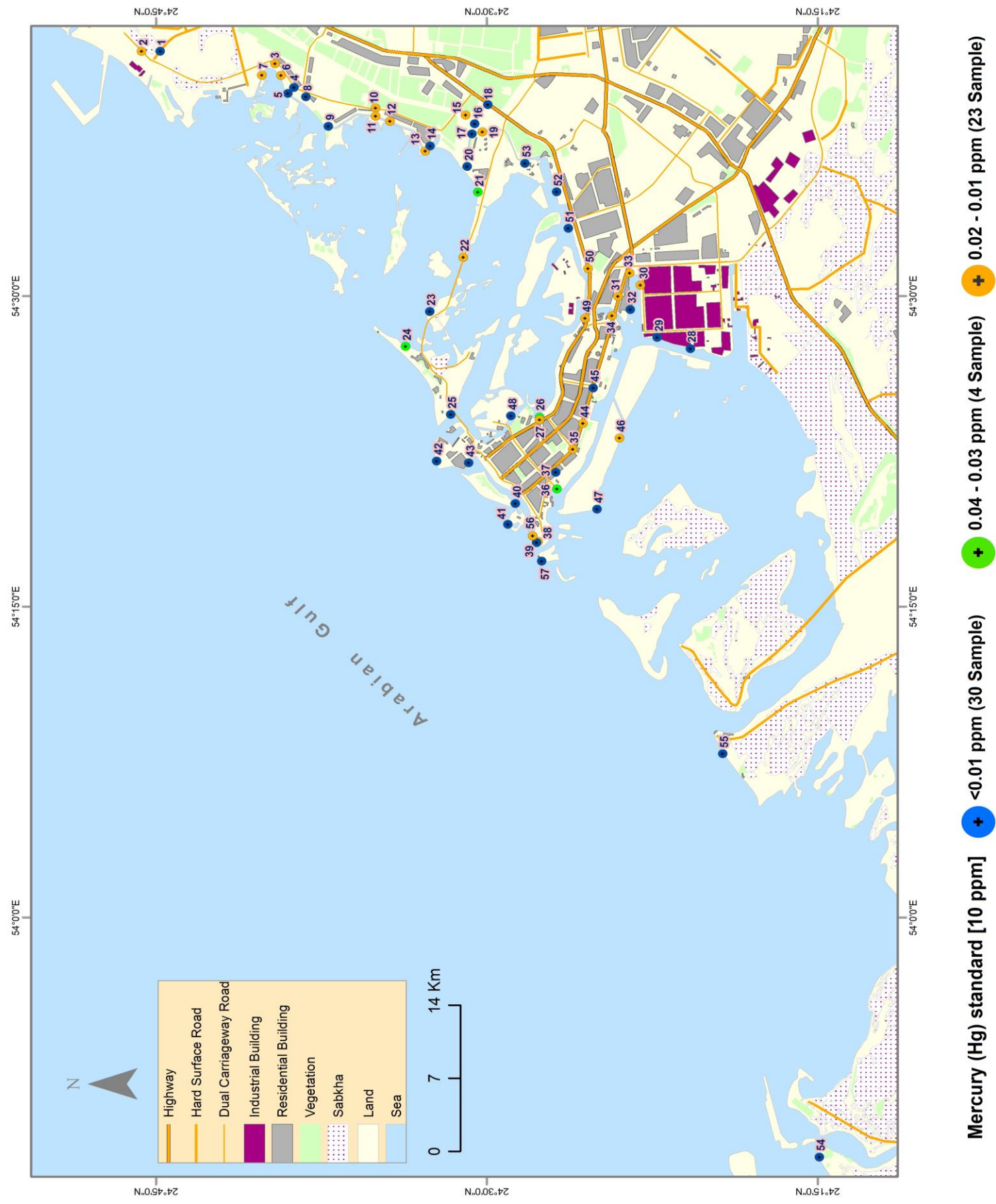


Figure B.33. Map of Abu Dhabi showing the mercury (Hg) concentration of the areas from which the samples were collected, as indicated with dots, along with their numbers.

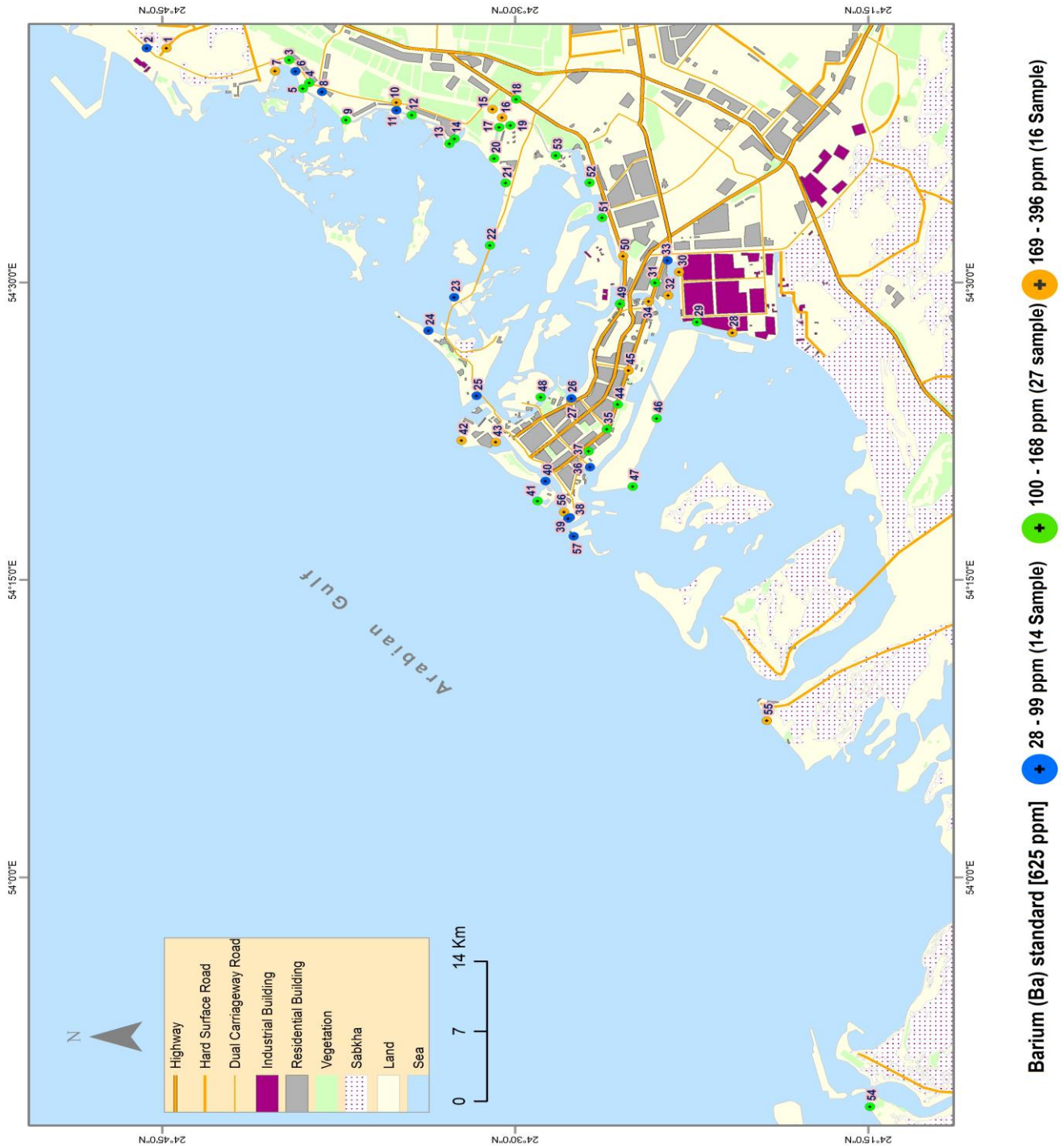


Figure B.34. Map of Abu Dhabi showing the barium (Ba) concentration of the areas from which the samples were collected, as indicated with dots, along with their numbers.

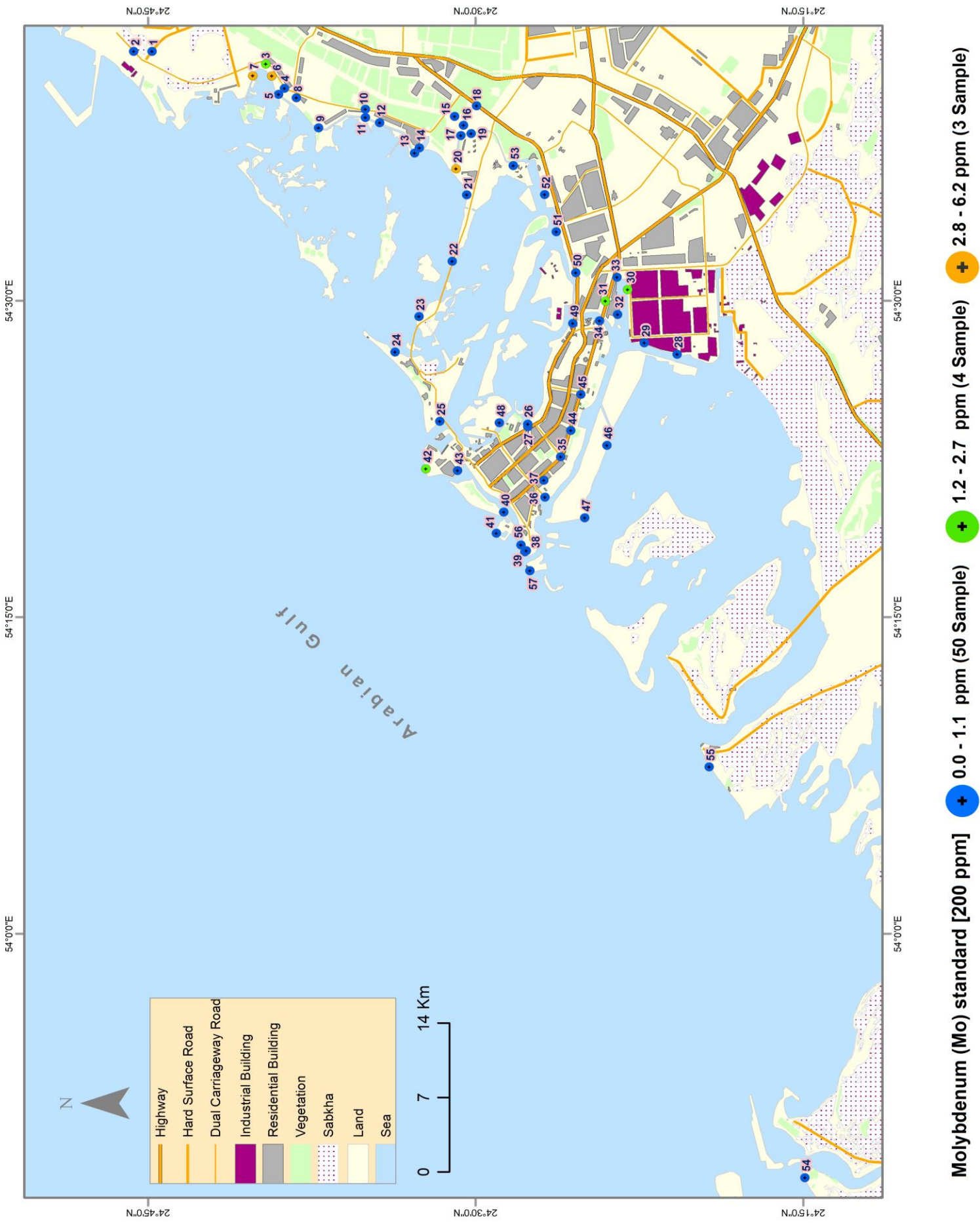


Figure B.35. Map of Abu Dhabi showing the molybdenum (Mo) concentration of the areas from which the samples were collected, as indicated with dots, along with their numbers.

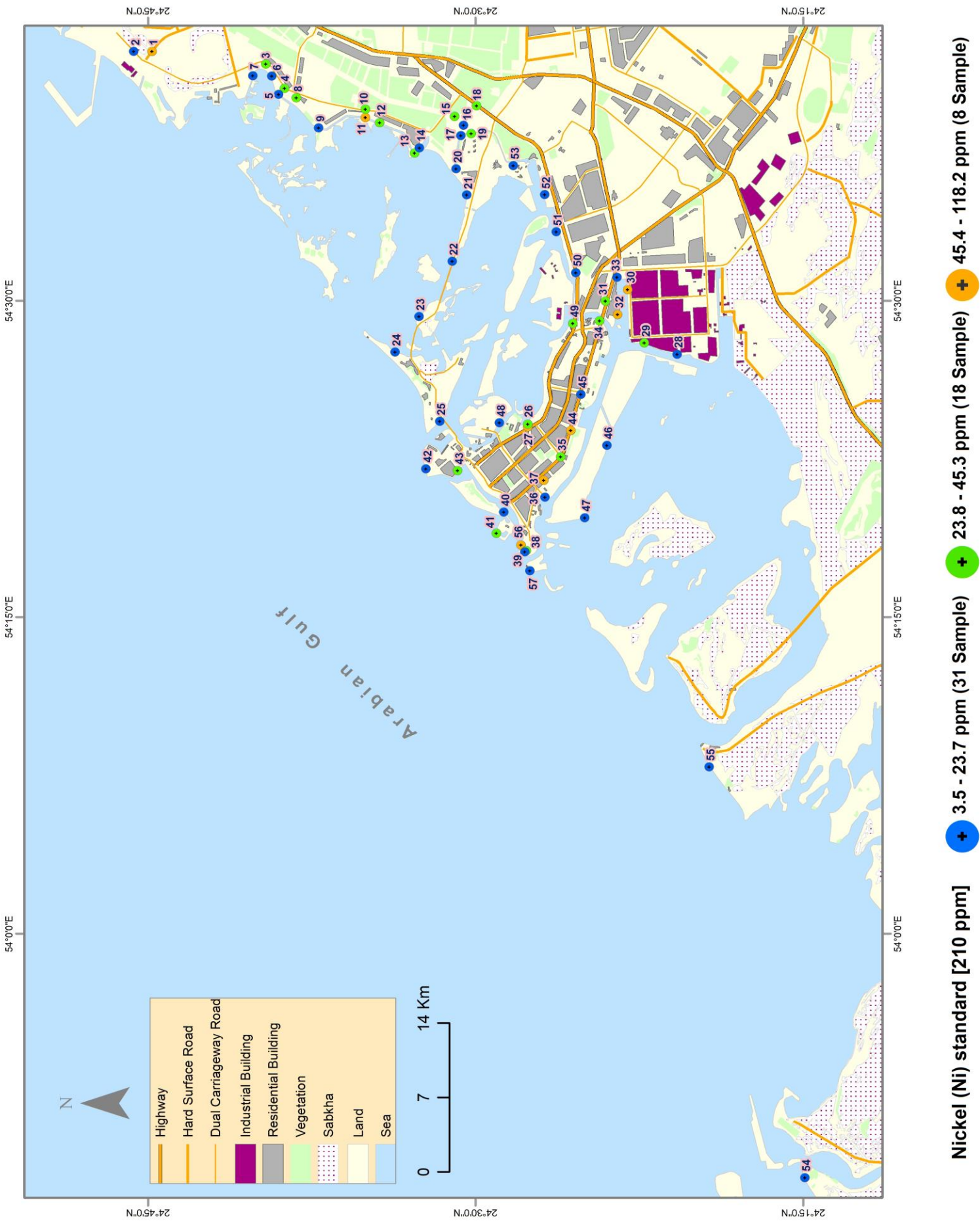


Figure B.36. Map of Abu Dhabi showing the nickel (Ni) concentration of the areas from which the samples were collected, as indicated with dots, along with their numbers.

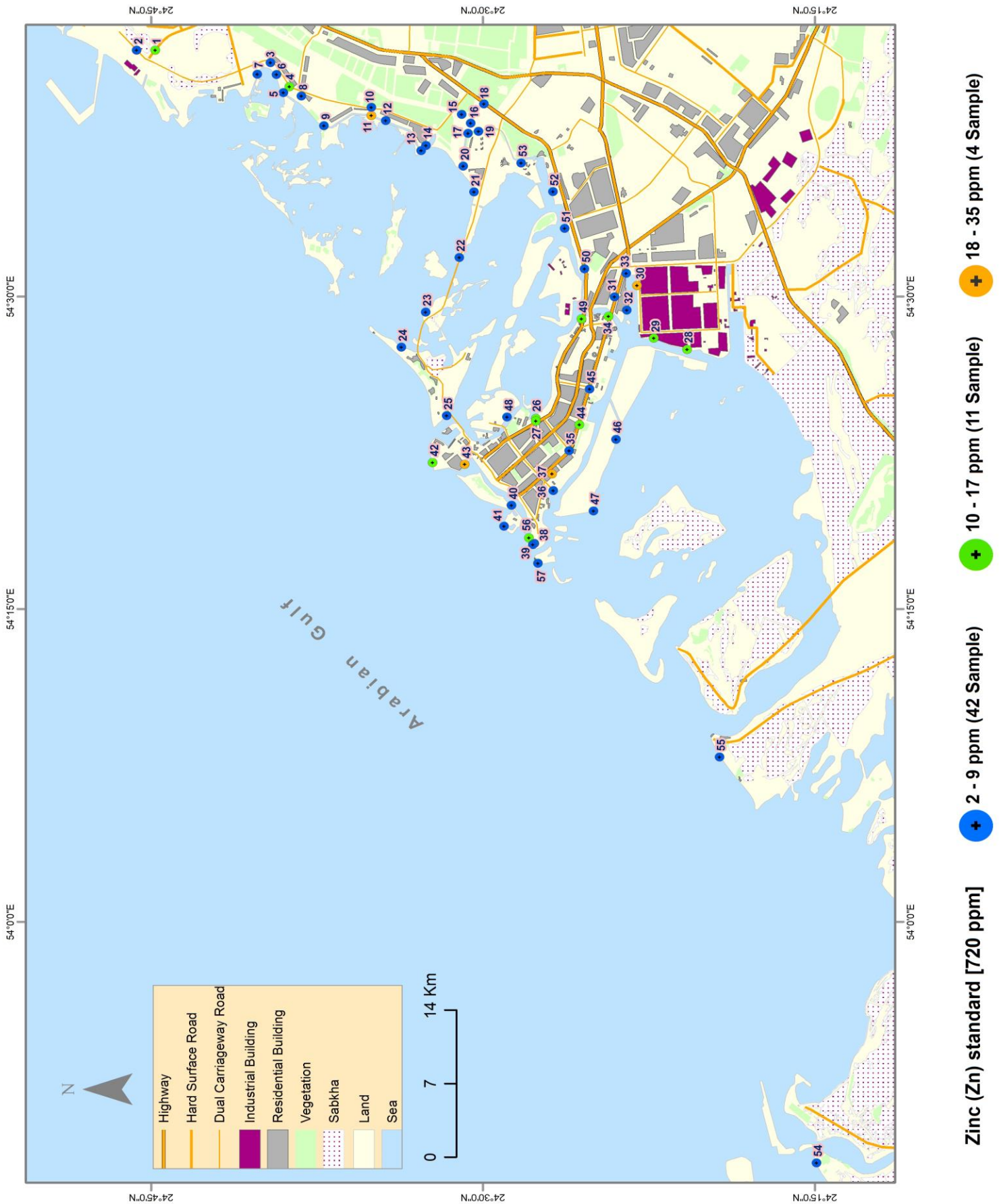


Figure B.37. Map of Abu Dhabi showing the zinc (Zn) concentration of the areas from which samples were collected, as indicated with dots, along with their numbers